Optimisation of high-speed automated layup of thermoset carbon-fibre preimpregnates

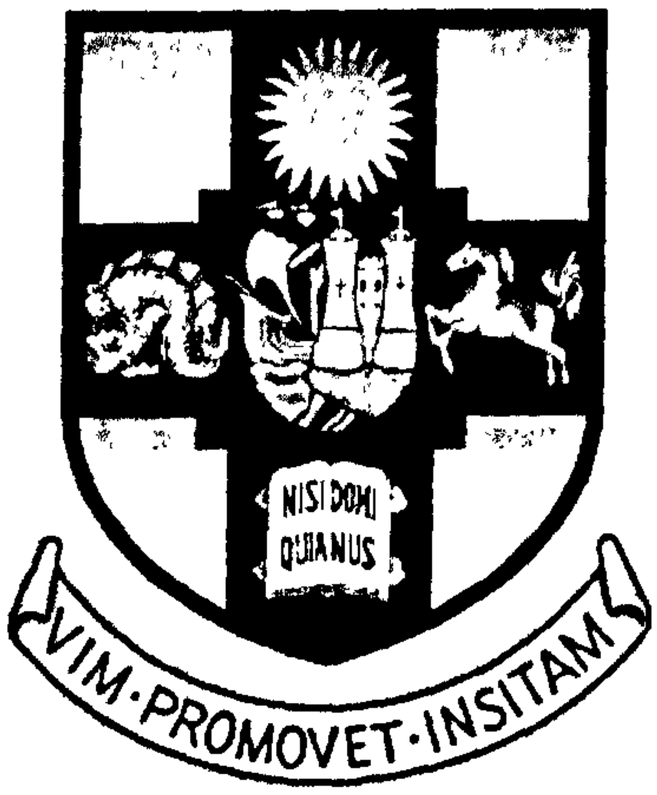

Dirk Hans-Joachim Adrian Lukaszewicz

A dissertation submitted to the University of Bristol in accordance with the requirements of the degree of Doctor of Philosophy in the Faculty of Engineering, Department of Aerospace Engineering; April 2011.

Number of words: 51094

AUTHOR'S DECLARATION

"I declare that the work in this dissertation was carried out in accordance with the Regulations of the University of Bristol. The work is original, except where indicated by special reference in the text, and no part of the dissertation has been submitted for any other academic award. Any views expressed in the dissertation are those of the author.

SIGNED: ..... DATE: 27/6/2011....."

Abstract

Automated layup of prepreg is slowly replacing manual layup during the production of composite parts for aerospace, automotive and renewable energy applications. This is driven by a need for higher manufacturing rates from aerospace manufacturers and a need for high quality manufacture for wind and tidal power blades. The main methods for automated layup are Automated Tape Laying (ATL) and Automated Fibre Placement (AFP). However, despite its industrial importance the amount of research into both processes is limited, in particular with respect to productivity and process reliability.

The study outlined in this presentation aims to investigate feasible processing conditions for automated layup that may improve laminate quality and productivity both analytically and experimentally whilst curing out-of-autoclave. Prepreg properties relevant to automated processing are identified. Lastly, requirements for an optimised layup system are proposed.

A detailed study of the resin content of automation grade prepreg shows a significant variability of resin content that may affect tack and lead to unsuccessful layup. High product quality is governed by the amount of voidage entrapped in the uncured plies. A study of the surface roughness of uncured prepreg shows the potential for significant entrapment of air during layup. Since debulking is commonly omitted for continuous processing a large amount of voidage is entrapped in the uncured laminate and may have detrimental impact on mechanical performance.

A model was developed that takes into account the prepreg interface and forming behaviour during automated processing to predict the amount of entrapped air and allow optimisation of processing conditions. A two-stage layup model was implemented in Abaqus/Implicit to study the process in detail. First, the interaction between ply and layup system was studied in detail, the results were then used to predict the forming behaviour of uncured prepreg on a microscopic scale.

To understand the effect of processing conditions in more detail a laboratory layup system was built that enables layup at conditions currently not achievable with industrial equipment. The interaction between layup temperature and pressure was studied experimentally to validate previously developed models.

Previous Publications

Journals

Lukaszewicz D.H.-J.A. and Potter K. *Through-thickness compression response of uncured prepreg during manufacture by automated layup*, IMechE Part B, doi: 10.1177/0954405411411817.

Lukaszewicz D.H.-J.A. and Potter K. *The internal structure and conformation of prepreg with respect to reliable automated processing.* Composites Part A 2011; 42 (3): 283-292.

Invited Papers

Lukaszewicz D.H.-J.A. and Potter K, *Optimised automated layup of thermoset prepreg*, JEC Magazine, (unpublished).

Conferences

Lukaszewicz D.H.-J.A, Weaver P.M. and Potter K. *An automated ply collation system for material and process development.* In SAMPE Seico 10, Paris, 12th – 14th April 2010.

Lukaszewicz D.H.-J.A, Winter D., Evans S., Buckley M., Weaver P.M. and Potter K. *An empirical model for the automated deposition of thermoset composite.* In ACS 24th Annual Technical Conference, Delaware, 10th - 13th September 2009.

Lukaszewicz D.H.-J.A, Weaver P.M. and Potter K. *The Impact of processing conditions on the final part quality in automated tape deposition technologies.* In SAMPE Seico 09, Paris, 23rd- 25th March 2009.

ACKNOWLEDGEMENTS

I would like to express my gratitude and appreciation to Airbus who have provided my scholarship for this PhD for the past three years. The input from Airbus into the project has been an invaluable and I hope that this work will help Airbus strengthen its production system and market position in the future.

There are many people that I need to thank. Firstly, Marcel Buckley from Airbus UK who organised my PhD scholarship, provided the initial research program, and mentored me throughout my studies. Further, I would like to thank my supervisors Professor Paul Weaver and Professor Kevin Potter. Paul was always there when I needed support and advice. Kevin has been an unwavering support and has mentored me throughout my PhD with patience and subtle advice.

Thanks are also due to the many colleagues who have supported me throughout my studies, mainly Dr. Julie Etches, Dr. Carwyn Ward, and Dr. Kalyan Hazra. I am also indebted to my fellow PhD's Dr. Alberto Pirrera, Dr. Stephen Jones, Dr. Yusuf Mahadik, Dr. Greg McCombe, Michael Russ, Delphin Carrella-Payan, Adam Pickard, Thomas Gorochowski, Charlotte Szostek and Matt O'Donnell for their help and friendship.

It is with great pleasure that I would also like to acknowledge the support of the technical staff at the University of Bristol, including Ian Chorley, Mike Jones, Guy Pearn, Dave Hooper, John Morrison, Mark Fitzgerald and many more.

A special thanks goes to my mother Liane and father Wolfgang for their support and trust in me throughout my PhD. Lastly I would like to thank my brother Jan for being a constant challenge throughout my live upon which I could improve and nurture my aspiration.

CONTENTS

List of Figures

List of Tables

Symbols

α; Angle [°]; Angular acceleration [rad/s^2]

a; Acceleration [m/s^2]

A; Area [m^2]; Strain hardening coefficient

c; Specific Heat Capacity [Jkg^{-1}K^{-1}]

d *and* D; Diameter [mm]

l; Length [m]

ε; Strain [mm/mm]; Emissivity [-]

E; Elastic Modulus [MPa]

F; Force [N]; Line Load [N/mm]

h: Height [mm]

I; Second moment of inertia [m^4]; Electrical current [A]

j; Integer counter [-]

J; Moment of Inertia [kgm^2]

K; Safety factor [-]

m; Mass [kg]; Number of Prony series coefficients; Strain hardening coefficient

M; Bending moment [Nm]

ν; Poisson's ratio [-]

n; Number of plies in a course [-]; Angular speed [rpm]

p; Productivity [kg/h]; Pressure [bar, MPa]

P; Power [W]

R; Radius [mm]

π; Pi with a numerical value of 3.14159

ρ; Density [kg/m^3]

s; Distance [m]

σ; Stress [MPa]

t ; Ply thickness [mm]; Time [s]

T; Temperature [°C]

U; Electrical Voltage [V]

v ; Speed [m/s]

V; Volume [m^3]; Volume fraction [-]

w; Width [m]; Deflection [mm]

ω; Angular speed [rps]

ABBREVIATIONS

AC; Alternating Current

ATL; Automated Tape Layer or Automated Tape Laying

AFP; Advanced Fibre Placement

CCD; Central Composite Design

CFRP; Carbon-fibre reinforced plastic(s)

CNC; Computer Numeric control

CTE; Coefficient of thermal expansion

CTLM; Contour Tape Laying machine(s)

DC; Direct current

FE; Finite Element

FEM; Finite Elements Method

FFD; Full-Factorial Design

FRP; Fibre reinforced plastic(s)

FTLM; Flat Tape Laying machine(s)

GFRP; Glass-fibre reinforced plastic(s)

ISO; International Organization for Standardization

PC; Personal Computer

PID; Proportional-Integral-Differential controller

PLC; Programmable Logic Controller

PEEK; Poly-ether-ether-ketone

PEKK; Poly-ether-ketone-ketone

Prepreg; Fibres pre-impregnated with resin

RVE; Representative Volume Element

R&D system; Research and Development Layup system from Chapter 4

RMSE; Root Mean Square Error

TRL; Technology readiness level

UD; Unidirectional

WLF; Williams-Landel-Ferry

1 Introduction

1.1 Preamble

Composite materials are some of the oldest construction materials known to man. Wood and straw reinforced clay bricks have been used for more than 3000 years in buildings and structures. The increase in composite materials usage in the last century was driven by the development of novel advanced matrix materials, e.g. plastics and ceramics, and the advent of high-performance continuous fibres, e.g. glass, carbon or organic fibre [1].

Advanced composite materials are used in a number of diverse applications and industries such as aerospace, renewable energy, automotive and consumer goods. Fibre-reinforced-plastic (FRP) composite materials can be advantageous compared to metallic materials due to improved mechanical properties, possible weight reductions, tailorable properties, functional integration and improved corrosion resistance, but the potential numerous advantages of composites must be considered against the challenges in their manufacture such as geometric fidelity, imperfections or defects [2]. FRP manufacture has to achieve desirable material properties and product geometries in the same process. This generally requires accurate knowledge and control of both the micro- and macro-structure of the part to be manufactured. To alleviate this issue composites are often manufactured from semi-finished products called prepregs (for Pre-impregnates) [3].

High performance applications in aerospace, automotive and renewable energy industries mostly employ unidirectional (UD) glass- (GFRP) or carbon-fibre reinforced plastics (CFRP). These have historically been manufactured from prepreg using manual layup. However, composites are increasingly considered for mass-market applications and very large

structures. This requires improvements in the consistency, reliability and productivity of layup that may be achieved through automation. The main automated processes for prepreg layup are Automated Tape Laying (ATL) and Automated Fibre Placement (AFP).

1.2 An introduction to Composite Manufacturing

Composite components were initially used in military and civil aircraft programs due to the potential for weight savings. Weight reductions were achieved by substituting metallic components with composite components having superior mechanical performance, for example fatigue. Weight savings are still a strong driver for composite adoption in a number of fields, e.g. renewable energy and automotive. However, to replace metallic structures in these areas composites additionally need to be cost effective in manufacture when compared to their metallic counter-parts.

Historically, advanced composite components have been manufactured by manual layup of either dry fibre or prepreg. Here we are solely concerned with the prepreg manufacturing routes as they are chiefly used for primary aircraft structures. During prepreg layup the component is built up iteratively, by manually laying pre-cut prepreg plies into a mould. This process is often described as inverse machining, since the part is built up by adding material, as opposed to material removal during machining. The entire process of ply cutting, layup and preparation for cure is often termed "ply collation" [4], see Figure 1. This figure illustrates a composite manufacturing system for components made from thermoset prepreg with a detailed breakdown of the ply collation process for manual, ATL and AFP layup. During manual layup plies are cut in a separate operation, either manually or in an automated process. The plies are then laid up into a mould with regular vacuum void removal (debulking) operations. Both during and after layup, plies are inspected for layup quality,

mostly by visual inspection. In some circumstances the plies are initially laid up on a flat mould and then subsequently formed into the tooling for cure in a separate operation. ATL integrates ply cutting and layup into a single automated operation. Additionally, vacuum void removal is omitted to enable continuous layup. To consolidate the plies they are laid up at elevated temperatures and under pressure. Quality inspection is then mostly done visually, but in some cases automated systems are in use [5]. Since ATL is most productive for flat laminates it is sometimes more productive to manufacture a flat laminate, which is then formed into a mould for curing. AFP layup extends the approach from ATL layup further by enabling direct layup into complex moulds, making subsequent forming unnecessary. Furthermore, quality inspection is increasingly being automated during AFP layup.

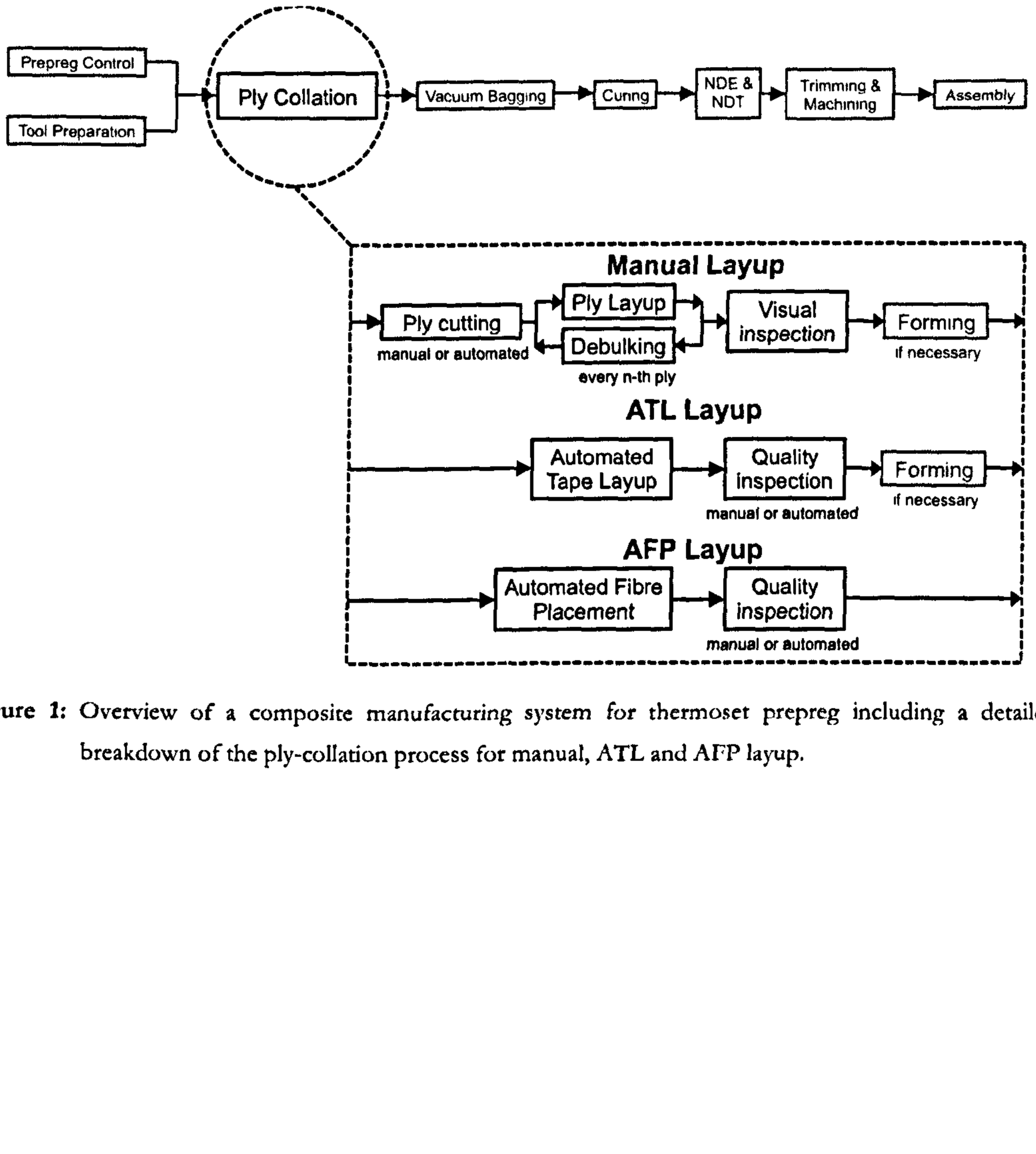

Figure 1: Overview of a composite manufacturing system for thermoset prepreg including a detailed breakdown of the ply-collation process for manual, ATL and AFP layup.

1.3 Automated composite manufacturing requirements

ATL and AFP have become relatively mature manufacturing processes since their developments in the 1970's (for ATL and AFP respectively) [6, 7]. Both processes have also seen significant extensions of their capabilities. ATL productivity increased gradually with higher layup speeds, improved layup control and improved materials [8] from the 1980's onwards. AFP has seen similar development in a much shorter timeframe and is now at a comparable maturity level to ATL. Additionally, AFP possesses process characteristics that may be beneficial for future applications, e.g. simplified thermoplastic layup and capability to steer material during layup. Both manufacturing processes are now used to manufacture aircraft flight components. It is therefore often argued that the technology readiness level (TRL) [9] for both processes is 9, the highest possible ranking, however this stands in contrast to the unresolved issues that still affect productivity during automated layup.

Currently, automated layup processes are found to achieve a productivity of approximately 8.6kg/h [10] for typical aerospace components. To meet future aircraft program requirements, machine productivity needs to be increased by at least a factor of two [11], but much higher values are likely required to meet requirements for renewable energy and automotive industries. Due to the past focus of automated layup on general process capability it is unclear how this can be achieved. A clear understanding of process capabilities for ATL and AFP and recommendations for their improvement is therefore required. Additionally, the impact of part-complexity needs to be considered to translate process capability estimates into component specific productivity estimates.

The introduction of automated layup makes a critical re-evaluation of the production system shown in Figure 1 necessary. Further details are given in chapter 3. Prepreg has traditionally been manufactured for manual layup and was then adapted for automated layup. It

is, however, unclear which prepreg properties are necessary for high quality and high rate automated layup. This is evaluated in more detail in chapter 4.

The most significant and time-consuming process step after layup is the cure cycle. Any productivity increase during layup cannot translate to an overall productivity increase if this step and all subsequent operations are not considered. With potential limitations in existing autoclave capacity, improvements in this area can be achieved by moving the curing process to vacuum-bag only, out-of-autoclave, curing. Another important aspect of the curing process is its impact on final product quality. Currently, out-of autoclave curing can be less robust than autoclave curing and may lead to higher variability of the final part properties. For very large components, vacuum void removal can be ineffective, as the voids in the laminate are not directly connected to the vacuum, leading to higher porosity for large part sizes. Automated layup claims to control layup pressure and tape temperature and may thus be used to achieve consolidation during layup and allow a subsequent cure out-of-autoclave whilst achieving comparable mechanical performance.

Chapter 2 will attempt to cover the progress that has been made regarding automated layup capability and robustness. This work is thus not focused on the feasibility or demonstrating basic capability of automated layup, but to identify and address remaining questions regarding both layup processes in the context of a composite component production system, and to identify whether layup can be enhanced to allow accurate laminate control during layup. The questions that will be addressed in this context are:

- What is the current manufacturing capability of the processes and what are their limitations?

- What is the current degree of control during layup and how critical is it for successful layup? Furthermore, how can "successful layup" be defined consistently?
- What are desirable material properties for the prepreg used in automated layup, by comparison to prepreg for manual layup?
- Can the impact of the interaction between layup system, prepreg material, and mould, on final part properties be predicted by modelling?
- Is it possible to improve the stability of both processes by enhancing the degree of control?
- Can automated layup be enhanced to enable out-of-autoclave cure of high performance components?

By singling out one of these questions a deep understanding may lead to small improvements, but by addressing as many systematic questions as possible, larger improvements may be achieved. This is also justified because automated layup has to be considered as part of a manufacturing system and changes to one element of such a system will always have implications for subsequent operations. An example would be a simple change of prepreg material that may lead to complications during subsequent operations. Recommendations for improvement at any stage during component manufacture will therefore have to consider the implications for all subsequent operations.

Finally, the two primary aims of this work are; 1. to improve manufacturing rates by providing a better understanding of the layup systems and; 2. to identify the wider implications of automated layup for a composite component manufacturing system, i.e. the possibility to enhance quality control during layup.

1.4 Thesis Outline

This thesis aims to cover many diverse aspects of automated layup technology. As a result the dissertation consist of nine chapters, including this introduction, and is structured as follows:

Chapter 2 discusses the past research in the area of automated prepreg layup, and prepreg processing is reviewed. The development of automated layup regarding productivity and process control is explored to gain an understanding of the limitations of current processes.

Chapter 3 reviews the current state of the art in automated layup in some detail. Productivity drivers for automated layup processes are identified and ways in which automated layup productivity can be improved significantly by addressing layup strategy are discussed. The current degree of process control is then studied with respect to high-speed layup to identify possible improvements in layup control.

Chapter 4 introduces a laboratory layup system to overcome the shortcomings of industrial scale layup systems identified in chapter three. The laboratory layup system is designed to allow layup with processing conditions currently not achievable with industrial scale layup systems.

Chapter 5 studies the current standard of prepreg materials for automated manufacture. Recommendations for improving prepreg for automated layup are made.

Chapter 6 provides material properties for uncured prepreg. Some observations regarding the mechanical properties of uncured prepreg are made and the data are evaluated with respect to their use in numerical modelling.

Chapter 7 combines the results from the two previous chapters into a numerical model to describe the interaction between prepreg and layup system for various processing

conditions. The model is then used to test various modifications to the laboratory layup system and to predict the quality of an uncured laminate as a function of the processing conditions during automated layup.

Chapter 8 illustrates the benefits of improved layup by comparing the compressive strength of laminates from various manufacturing methods and layup conditions.

Chapter 9 provides a discussion and some conclusions of this work. Further research directions for improving the capability of automated layup are outlined.

2 Literature review

2.1 Automated Tape Laying

2.1.1 A Description of the Automated Tape Laying Process

ATL can be interpreted as a form of additive manufacturing or inverse machining, since the part is built up by adding material, as opposed to material removal during machining [12]. The ATL head handles the prepreg tape, which is typically 75mm, 150mm, or 300mm wide and supplied on a paper core [8], similar to prepreg for manual layup. Most ATL systems store the prepreg material directly on the layup head and a schematic of an ATL head according to Ästrøm [13] is shown in Figure 2. Due to the mass of both the head and material, as well as the size of the parts typically manufactured, the ATL system is normally mounted on a horizontal gantry, see Figure 3, or a vertical column system, see Figure 4 [14]. This strongly affects the initial capital expenditure which is around 3.5M$ for the most basic systems [15]. The majority of aerospace structure laminates consist of ramps and valleys as well as ply terminations, resulting in a complex surface topology. These components are typically manufactured using systems, that have three linear degrees of freedom and two rotational degrees of freedom, so called Contour Tape Laying Machines (CTLM), to enable layup over changing thicknesses, tapered laminates and geometries with single curvature. Other variants are Flat Tape Laying machines (FTLM), which have only linear degrees of freedom.

Computer Numeric Control (CNC) allows automated layup systems to follow a predefined program accurately and reproducibly to eliminate possible layup errors that could occur in manual layup. During the layup of each ply, a tape is placed next to one other with a gap between of 0.5 - 1mm. This gap is required to accommodate variations in placement due to

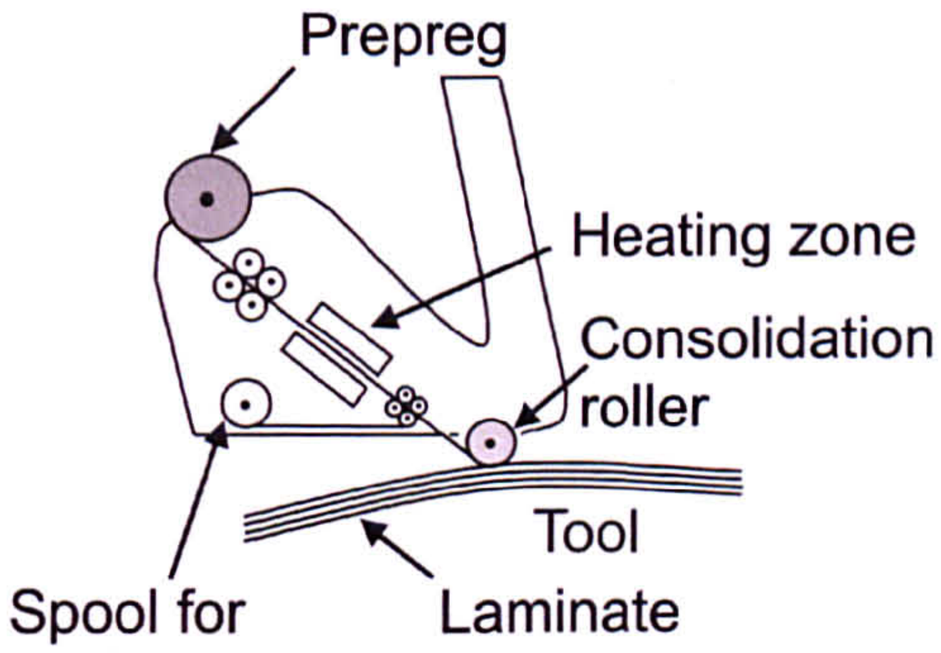

Figure 2: Schematic of an ATL layup head, according to Astrøm [13].

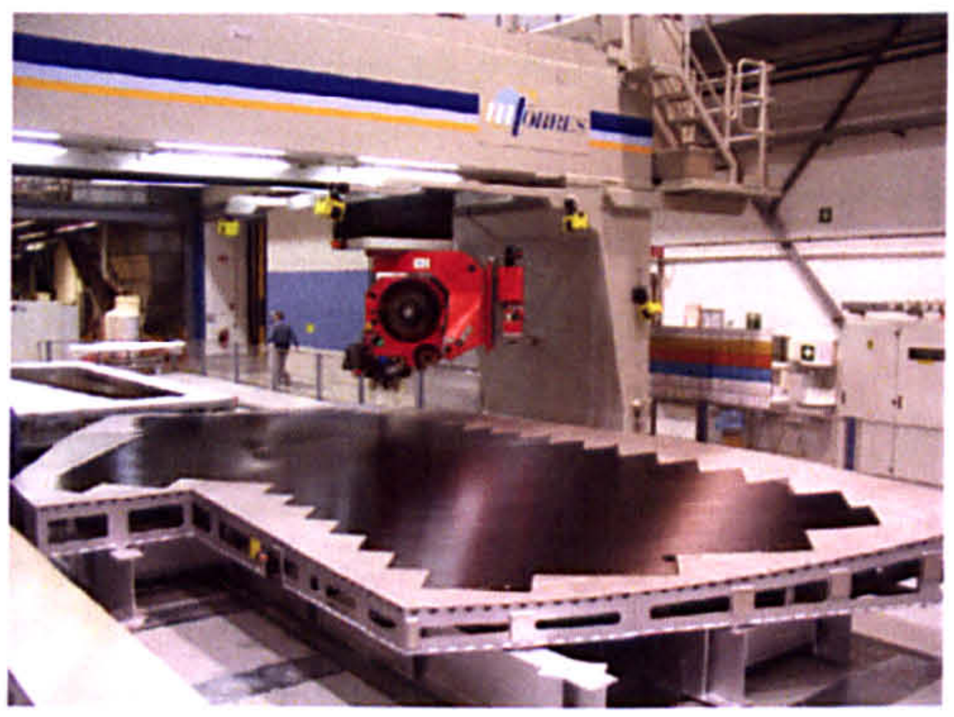

Figure 3: Example of a gantry type ATL laying onto a female tool.

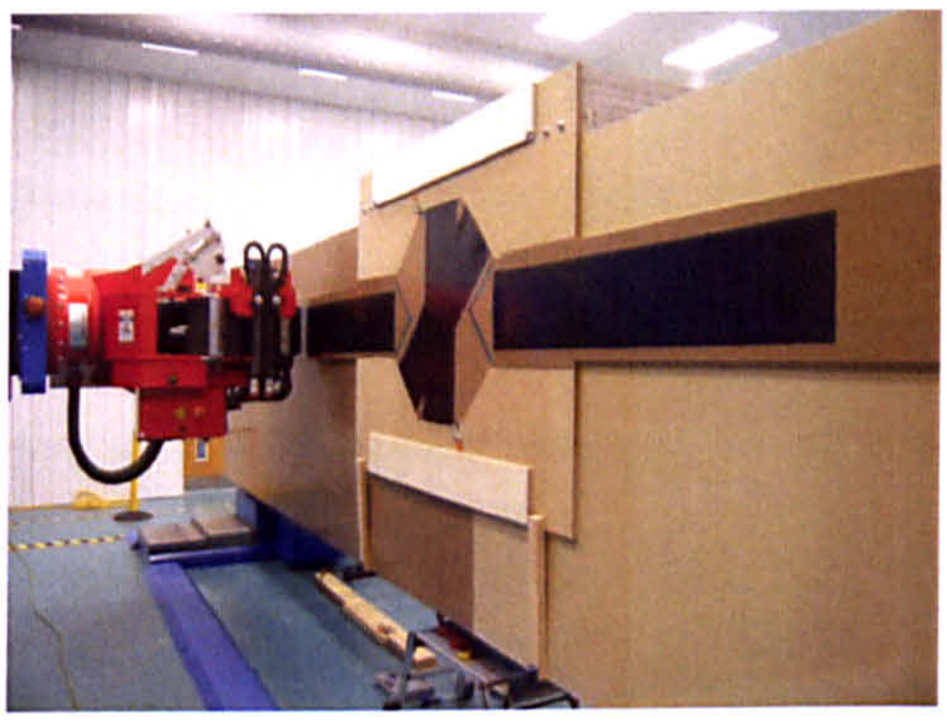

Figure 4: Column Type ATL laying 300mm wide tape onto a vertical tool.

machine control and tape tolerances. During ATL layup, tolerances are normally sufficiently small to minimise the impact of gaps on mechanical performance. During AFP layup, smaller material and steering enhance this effect significantly, which will be discussed later.

At the start of the sequence the ATL system attaches a pre-determined length of tape slowly onto the tool using a soft roller. After the beginning of the course has been applied the system accelerates and delivers the remaining ply course using a second soft or a stiff curved end-effector [16-18]. The reason for having separate layup elements is the relative difficulty of attaching the first ply to the tool, which will be discussed later. Most automated layup systems achieve maximum linear layup speeds between $v = 0.83$ to $v = 1 ms^{-1}$ and accelerate at $a =$

0.5ms^{-2}. Performance for the rotational axes in CTLM is more varied and therefore not quoted. During layup the material is attached to the mould using additional force transferred through the end-effector. The end-effector can again be a flexible silicone roller, but more sophisticated methods have been developed to control the pressure distribution over complex surfaces, e.g. segmented laying shoes [18, 19]. Typical layup systems deliver between F = 445N for 75mm wide thermoset tape [20] to 1000N for 300mm wide thermoset tape. For thermoplastic layup Colton [21] has quoted a necessary pressure of p = 1.4 MPa for APC-2 layup at T = 316°C, while pressures up to p = 3.6 MPa have been reported elsewhere [22]. During layup, the ATL head controls the tension on the plies and ply backing and allows heating of the prepreg prior to layup. To control the temperature during layup the material can be heated either in front of the layup head or on the layup system during delivery and both methods are used in industrial application.

At the end of the ply course the head decelerates prior to finishing and cuts the tape automatically using rotating or pinching blades. The distance between the blade position and the roller contact point is called "minimal course length" and it is a lower bound on the part sizes that can be manufactured. This value is around l = 0.1m for most systems. After severing the tape the remaining, or minimal course length, is delivered at low speeds to finish the ply course. This process is repeated until the part is finalised, the system is stopped by either the program or user intervention or if an automated fault detection system has identified a layup error.

2.1.2 History of Automated Tape Laying

Automated layup systems were developed from the end of the 1960's onwards [23]. By the middle of the 1970's research ATL systems were developed and used in applications which

enabled force controlled material delivery, layup of 300mm wide tape or tape heating. For example, a patent assigned to Goldsworthy et al. [7] in 1974 describes an automated system to deliver 76mm wide tape over a curved surface, including facilities for automated ply backing removal, and cutting plies at the end of a ply course, for example Figure 5. Aerospace manufacturers and research institutions built most of these early automated layup systems in-house, and they were normally part of a component centred production system for a given aircraft program [24], for example Figure 6. Commercial ATL systems became available at the beginning of the 1980's, supplied by Cincinnati Milacron (now MagCincinnati) who acquired a patent for an automated layup system from Vought Aerospace [25]. Competing concepts for prepreg material delivery existed from a number of suppliers [26, 27] with some of them being reintroduced for dry fibre layup a decade later. Initially, improvements regarding layup reliability and material utilisation over manual layup were desired as manual layup productivity at the beginning of 1980 was around 1kg/h [28] and scrap rates were high (50-100 %), due to the lack of automated ply cutters and optimised consumables and prepreg. Automated ATL layup at that time was capable to achieve a 65% [29] reduction in layup time and an additional reduction in scrap rates for certain components.

Reduction of layup errors due to CNC together with reduced scrap rates resulted in an improved material utilization, which made automated layup a viable process for some aerospace applications using cost intensive materials. For example, Grimshaw [30] calculated the layup waste generation of an ATL layup as a function of part size. ATL generates between 15% (for 150mm wide tap) and 30% (for 300mm wide tape) waste for a part smaller than 0.25m^2. As part size increased to about 6.25m^2 waste generation decreased rapidly to 2-4%. Similar results have been reported elsewhere [8]. Furthermore, Krolewski and Gutowski [28, 31] and Foley [32] published economic assessments of various manufacturing methods

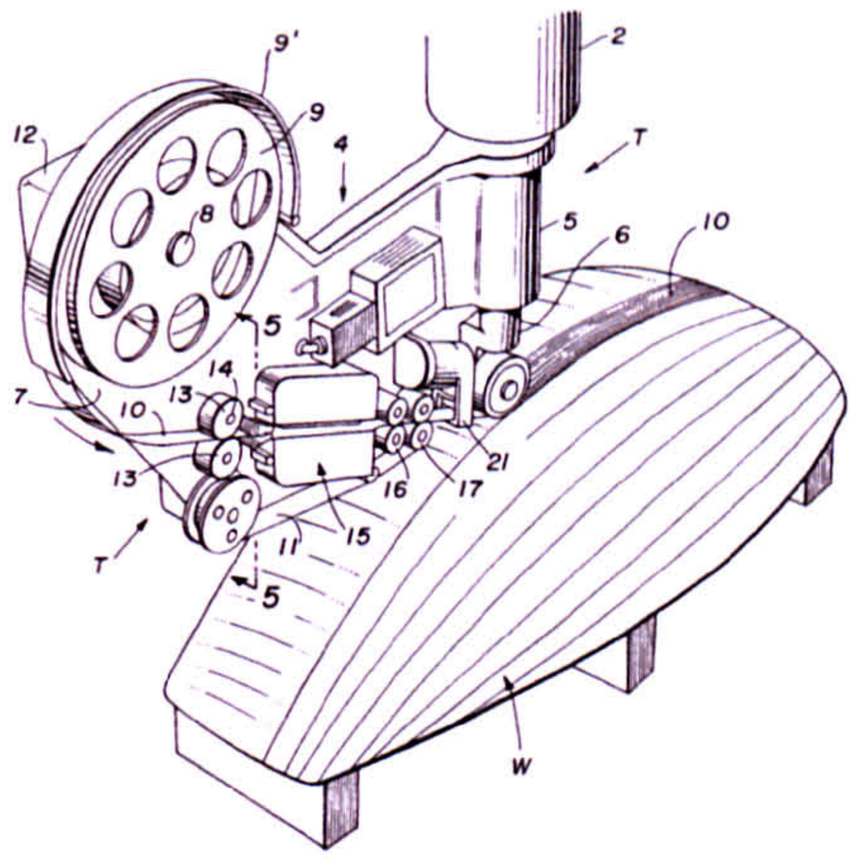

Figure 5: Drawing from Goldsworthy's early patent application [7] of an ATL delivering slit tape over a curved surface.

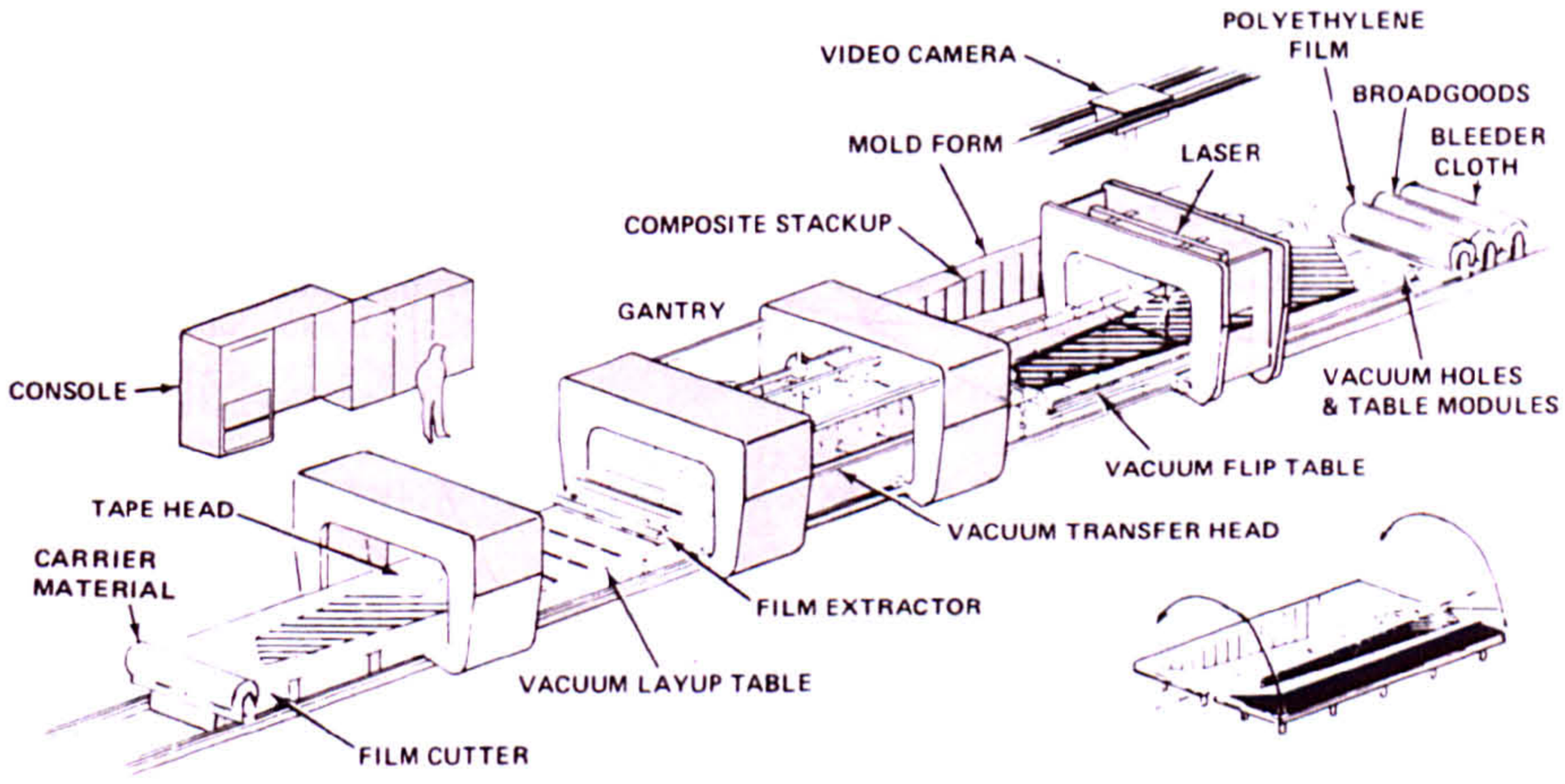

Figure 6: Drawing of an early automated composite components manufacturing system from [24]. The material is moved from left to right and material is applied to a mould using a bespoke tape layup head.

available at the end of the 1980's in terms of productivity and part cost. They show that at that time automated layup offered no appreciable increase in productivity over manual layup. Considering the additional capital investment for layup systems, the recurring part cost increased for automated layup, however the authors conclude that automation was still

desirable due to effects that were not accounted for in their early study, including improved reliability, consistency, and reduction of scrap.

Problems that occurred during ATL layup were the attachment of the first ply to a tool [18], the start of a ply course, as well as accurate control of compaction pressure. To address the first issue ATL heads using two separate elements to attach the material were developed [18]. Improvement to pressure control for layup over complex geometries was achieved by highly accurate force-feedback control of the z-axis that allowed mapping the composite material onto a tooling surface [33, 34] and by using differentiated layup elements. The aim was to reduce debulking operations, which affected productivity detrimentally, but it is unclear whether current layup systems can achieve this in practice. The effective pressure transferred from the head onto the laminate has to be higher than during vacuum pressing due to the fact that it is applied over a much shorter time frame. The pressure on the laminate depends on the machine capability, the roller geometry and roller material and the shape of the mould the material is applied onto. Alternative methods for consolidation during layup have been studied as well. Instead of using a flexible roller and heating the tape, ultrasonic consolidation has been demonstrated as a feasible alternative [35-37] to remove voids and form a bulk laminate.

Ply tension control during layup may improve layup for complex geometries, as the tension keeps the plies aligned [38]. Initially, prepreg systems with high tack were used for automated manufacture, which complicated removal of the ply backing, affected layup quality due to uneven tension and lay-down speeds [39]. By contrast, systems with low tack are used presently and the ply backing is normally coated or laminated to reduce the transferable load between the ply backing and composite material. In some circumstances, the prepreg delivered from the ATL head may contain defective areas, which must not be applied onto the part. This can either be addressed by providing additional technology on the head [40] to reroute the

defective material, or by laying the defective material down outside the part area. Some systems cut the ply ends on the tape without severing the backing, e.g. to enable automated removal of defective areas on the delivery head. The appropriate tack level during automated layup is thus a careful balancing of conflicting requirements. To improve this situation with respect to layup quality, most ATL systems are equipped with heating elements to control tack and formability, hot air fans are commonplace but more recent systems use irradiation by infrared light. Calawa and Nancarrow [41] argue that the optimal temperature for thermoset deposition is around T = 35°C. It seems that the optimal temperature for layup depends on properties like tack, which varies between materials [42-44]. Tack describes the transferable force normal to prepreg plies and has been linked to the bulk properties and viscosity of the resin. Furthermore, tack is rate-sensitive, meaning that tack force during high-speed layup may differ from tack test results. Tack scales with layup temperature and reaches a maximum around a temperature of 20-25°C above the instantaneous glass transition temperature. It should be noted that tack is still a prepreg property that is not fully explored and cannot be accounted for in process models despite some past research in this area [42-47]. While the prepreg material needs to be relatively soft at the point of lay-down, to exhibit optimum tack it has to be slightly stiff and non-tacky throughout most of the delivery head to avoid resin build-up in the delivery system or during cutting.

ATL development since the 1990's focused on increasing layup rates, improving error detection and developing improved layup software. Off-line programming software was developed to optimise layup programs and increase the proportion of time spent on component manufacture. To improve productivity for aerospace applications the lay-down speeds were increased. Usage of higher areal weight materials also allowed for higher productivity for the marine and renewable energy industries. To bridge a gap that currently

exists between AFP and ATL layup with respect to material width and layup dexterity, at least two rolls of either 75mm, 150mm or 300 wide material can be combined on one ATL head to potentially improve both productivity and dexterity [48]. Lastly, nesting technology was developed for ATL layup to improve productivity for large parts with small features. The ply patches are pre-cut in a separate operation, stored on ply-backing and wound back onto a roll. Some ATL systems employ two separate heads to deliver either the continuous ply course or small pre-cut prepreg patches [49, 50].

To maintain the desired fibre orientation of a ply over a curved shape the ply needs to be laid down along a curved path. This is commonly referred to as steering. The amount of steering available in ATL is inherently limited by the width of the material and narrower tape can be steered more easily including around smaller steering radii. Recently, the focus has shifted towards AFP systems due to increases in the productivity, reliability and the potential for tailoring mechanical properties by steering the tows during layup [51, 52].

Today, ATL is a highly productive process, which is in widespread use in aerospace and renewable energy industries. Advantages are high layup rates, high mechanical properties due to the use of prepreg, capability to manufacture large parts, capability to handle high areal weight materials and simplified offline machine programming. Disadvantages are high initial capital expenditure, limited geometric complexity and higher waste rates than AFP layup. Despite the potential limitations of ATL manufacture it has recently received new interest due to the high productivity achievable for flat laminates. After layup, flat laminates can be formed into the desired shape by hot forming, though in practice this can be limited. For large composite components and material with high prepreg areal weight this offers a cost competitive manufacturing route.

ATL systems are used for manufacture of a variety of parts, e.g. tail planes, wing skins [53] and the centre wing box of the A380. The main manufacturers of aerospace ATL equipment are MAG-Cincinnati (USA), MTorres (Spain), and Forest Liné (France). GFM (Germany) and ATK (USA) supply ATL systems as well, but do not have a comparable number of installed systems. Ingersoll has stopped supplying ATL systems in favour of AFP.

2.2 Automated Fibre Placement

2.2.1 A Description of the Automated Fibre Placement Process

AFP systems differ from ATL in the width of the material that is laid down with typical material widths' of 3.2mm, 6.4mm, and 12.7mm, however, AFP will normally deliver several [54] tows in a single sequence. Today, AFP systems deliver up to 32 tows in parallel at linear speeds up to 1m/s [54]. In addition AFP systems tend to have higher acceleration in the linear axes, typical values are around $a = 2m/s^2$. Again, rotational speeds and accelerations are more varied and therefore not quoted. However, it is important to note that rotational speed and acceleration can have a much higher impact on layup productivity for complex components and are therefore more relevant to AFP layup than to ATL. The width and number of tows delivered depends strongly on the complexity and local geometry of the part that the course is to be laid over, and material width and tow count affect productivity. Each tow is normally driven individually, can be clamped, cut and restarted during manufacture [54, 55], which makes it possible to deliver each tow at individual speeds, enabling layup over complex geometries and some tow steering, see Figure 7. This feature is beneficial for complex structures such as fuselage sections with window cut-outs or wing skins with pad-ups and valleys. While steering was initially conceived to improve layup over surfaces with double-

Figure 7: AFP layup of steered tows onto a flat mould, from [56].

curvature [7], the individual tow payout improves productivity and also reduces waste [31]. The quality of the cut "on-the-fly" normally decreases with increasing speed during cutting and secondary operations are still necessary to remove crenulations around a geometric feature, e.g. window cut-outs. For this reason AFP systems tend to have lower "minimal course length"' than ATL, typically around $l = 0.05$m (compared to $l = 0.1$m for ATL).

Productivity for AFP layup is typically lower than ATL because it is generally employed for more complex parts. Productivity for layup of a complex fuselage section is currently around 8.6kg/h [10], about half of ATL layup rates for flat laminates. While the material is delivered with controlled tension during ATL, during AFP layup tension is negligible or controlled to be very low, to enable steering for layup into convex geometries and features. The composite material for AFP layup can either be impregnated tows or slit prepreg tape. Slit prepreg tape is more expensive but offers clear advantages with respect to productivity, reliability and product quality [8] and is therefore preferred for AFP layup. Slit tape and impregnated tows are normally wound onto paper bobbins and supplied with an interleaf film to reduce tack and friction in the material supply. The small diameter of the bobbin additionally enables accurate tension control during unwinding. The main differences between ATL and AFP can thus be found in the material form and material supply to the layup head. Otherwise,

layup operation during AFP layup is similar to ATL. The material is delivered to a compaction roller, where additional heat and force are applied to compact the material in an attempt to eliminate vacuum void removal. AFP systems use flexible rollers to compress the material and reduce debulking though the same reservations as previously for ATL, regarding the effectiveness of this procedure, apply. To heat the tape, AFP systems employ hot torches, laser, and infrared irradiation. The prepreg tape or tows are either delivered to the head from a creel cabinet, for example Coriolis composite's AFP, see Figure 8, or are stored directly on the head, for example used by Electroimpact [57], see Figure 9 and Figure 10. The first allows use of simple industrial robots due to the reduced head weight; the latter requires column or gantry type AFP systems, see Figure 11.

Robotic systems improve the affordability of AFP since industrial robots are significantly cheaper than the gantry units employed previously for ATL, and today robotic AFP systems are generally cheaper than comparable gantry AFP or ATL systems.

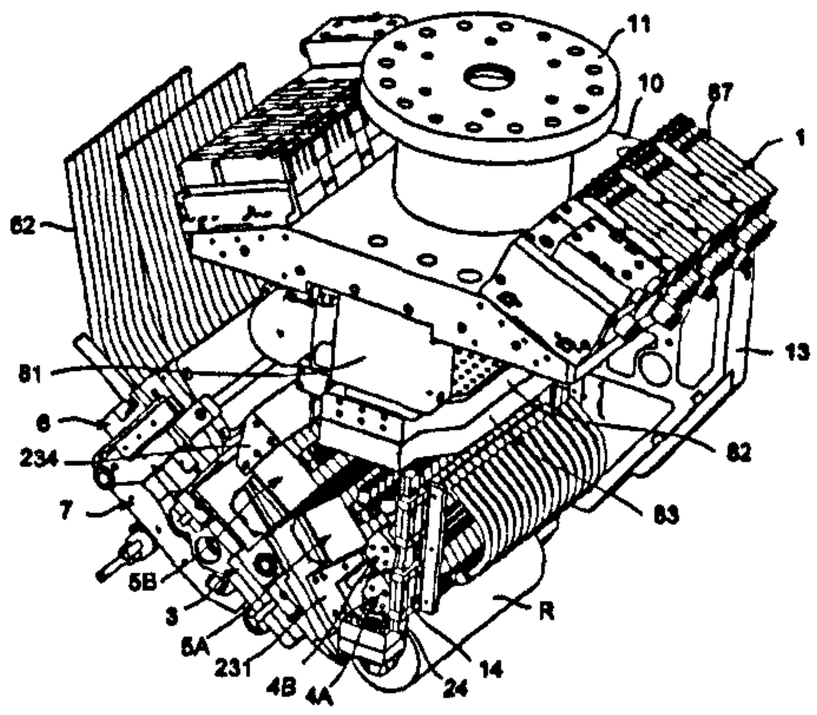

Figure 8: Drawing of an AFP head with external material storage, from [58].

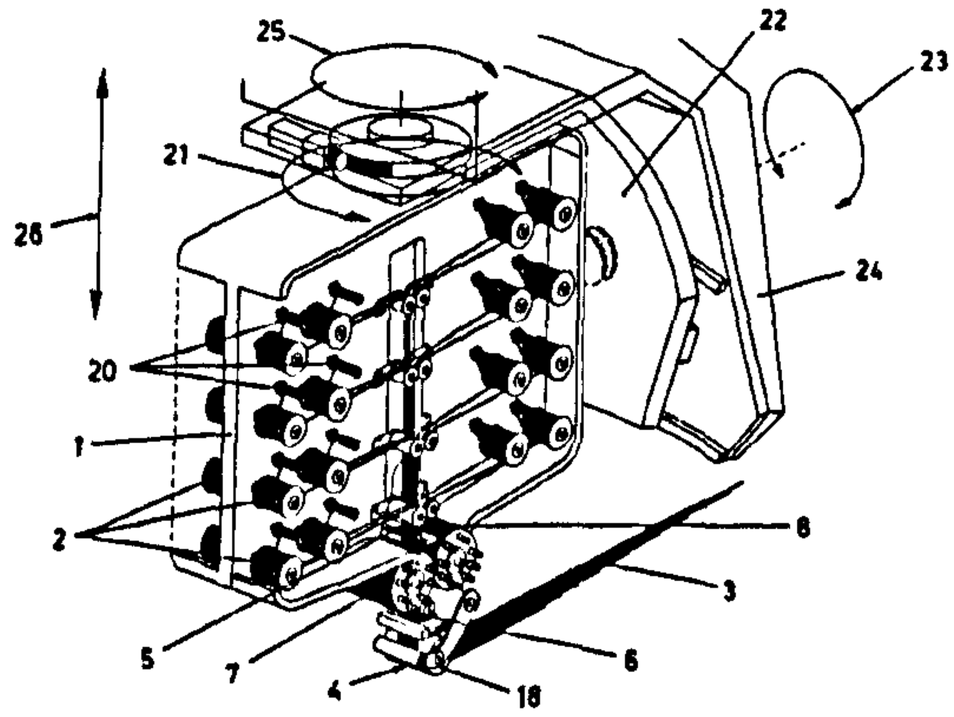

Figure 9: AFP head with internal material storage: capable of delivering up to 32 tows at the same time, from [59].

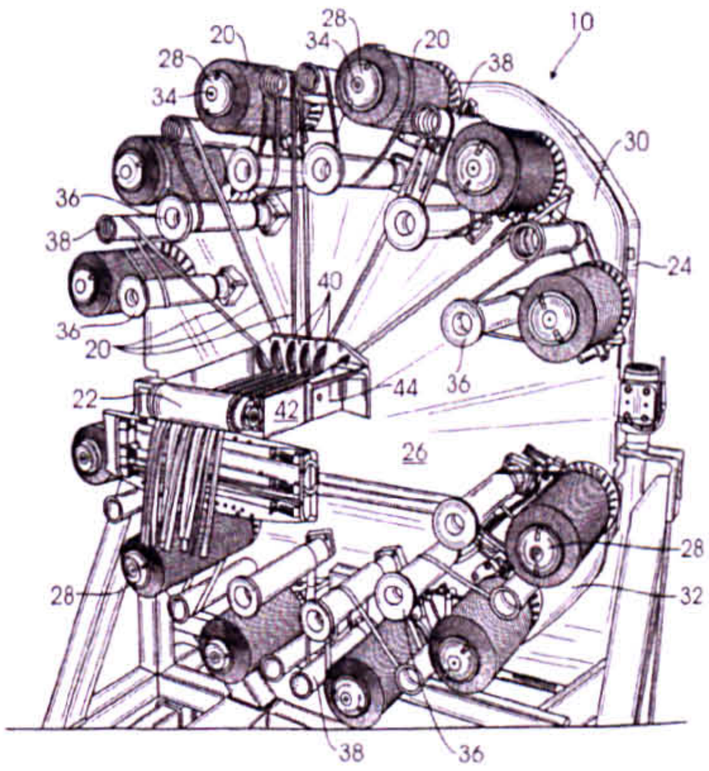

Figure 10: Schematic of an AFP system with material storage on the head, from [57].

Figure 11: Ingersoll gantry-type AFP laying into a female mould, from [5].

2.2.2 History of Automated Fibre Placement

AFP was initially developed as a combination of filament winding and ATL [60] from the late 1970's onwards. By combining the characteristics of these two processes significant productivity and quality improvements were expected and in particular, for the layup over complex geometries. Consequently, some of the first AFP systems were filament winding systems [61, 62] that were simply converted for prepreg layup, see Figure 12, by adding a compaction element. Due to the use of prepreg, mechanical performance of AFP manufactured components could be higher than filament wound parts [63]. Commenting on Figure 5, it is interesting to note that this represents an early AFP system as well as an ATL. A detailed view of element 15 in Figure 5 can be seen in Figure 13, which shows an integrated slitting device that cuts the tape down into 3.2mm wide strips to improve the layup over complex geometries. However, the slit tow was delivered at the same speed, presumably leading to buckled tows and inaccurate layup as the tows were not individually tensioned.

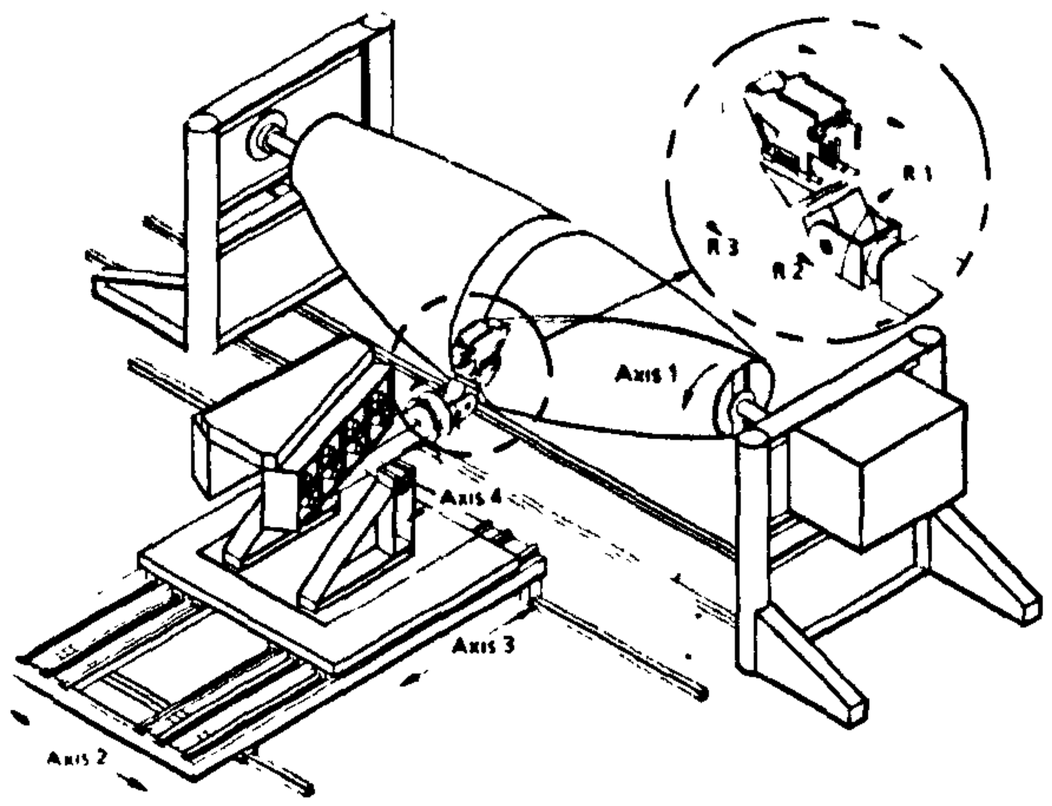

Figure 12: An early AFP layup system by Hercules from [63]. The commonalities between Filament winding and ATL are clearly visible from the machine layout. Material is mounted directly on the head and the head carries up to 16 creels of prepreg.

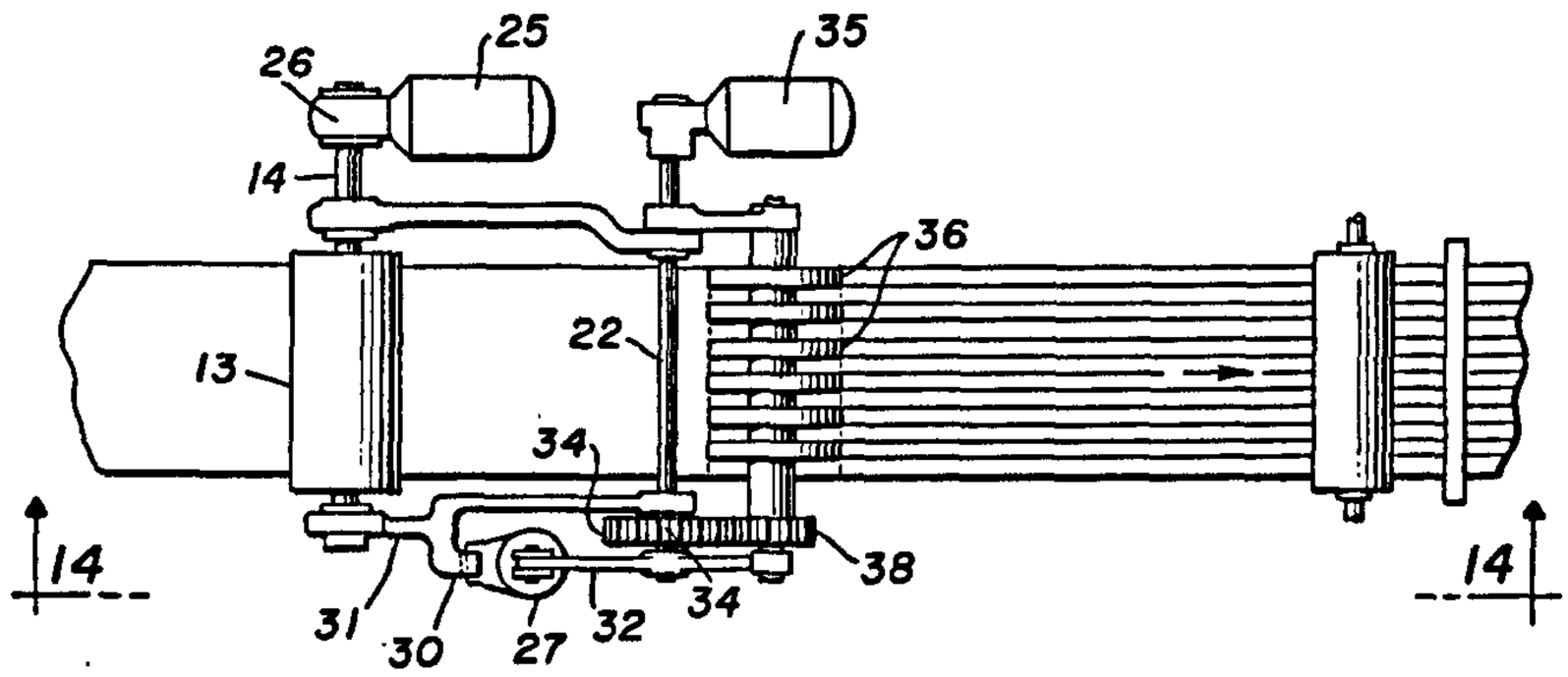

Figure 13: Integrated slitting unit with individual tow pay-out from [7]. This can be interpreted as the first AFP concept.

AFP systems became commercially available from the end of 1980's [60] with the first suppliers being MAG-Cincinnati and Ingersoll Tools. AFP systems were at the time significantly more expensive than ATL systems and their uptake was therefore a lot slower. Large scale ATL systems cost between $2.5-3.5M, while AFP systems can cost up to $6M [15]. Today, prices for AFP systems have decreased and simple robotic AFP systems can be cheaper than most ATL layup systems. Some very simple AFP systems are a combination of an end-

effector mounted onto an industrial robot and a creel cabinet for storing the prepreg material. This reduces the inertia of the system and improves manufacturing rates for smaller and more complex parts. Reducing the size enables the head to reach into more complex geometries, e.g. a wing spar or a fuselage section. AFP systems are also supplied as column (e.g. by MAG-Cincinnati) and gantry systems (e.g. by Ingersoll). Initially, AFP systems were only able to handle a small number of tows and did not deliver them reliably. This translated into a much lower productivity for AFP, which was therefore mostly found in military and space applications where the high material cost and complex geometries made them more viable as processes [62], see Table 1. Typical material waste values for AFP are around 7% for parts smaller than $w < 0.5m$ and decrease with increasing part size. AFP thus results in less waste during layup than ATL for all part sizes and significantly reduces scrap over manual layup.

Further improvements in robotic control were also necessary in the 1980's to allow accurate synchronisation of all axes (each tow is an axis during AFP layup) and to improve accuracy and productivity of AFP systems [64]. AFP manufacturers have invested significant resources into the material delivery stage to improve its reliability [65, 66]. As a result the creel cabinets can be cooled to reduce tack and unwind the material with a defined and low force. From there they are delivered to the end-effector using plastic tubes [65] or guide roller systems, e.g. Ingersoll or MTorres respectively.

Table 1: Overview of AFP applications in 2000, from [67]. AFP was used for military applications only.

Aircraft program	Components made by AFP
F-18 E/F	Inlet Duct, Aft Center Side Skins, Stabilator Skins
C-17 Globemaster	Fan Cowl Doors, Landing Gear Pods
Bell Agusta 609	Fuselage Panels
V-22 Osprey	Aft fuselage, Side Skins, Drag Angle, Sponsons, Grips
Premier I	Fuselage Sections
Hawker Horizon	Fuselage Sections
F22 Raptor	Stabilator Pivot Shaft
Sea Launch	Payload Fairing

Most systems tend to bend or twist the tows, but aim to avoid any yaw. Barth [63] first demonstrated AFP layup on a rotating mandrel to produce complex composite wing-ribs, spars and fuselage sections with similar mechanical performance to manual layup. Enders and Hopkins [68] introduced a 24 tow AFP system with feed error detection systems. Material was delivered in a cooled head and heated prior to layup to control tack. Lastly, a detailed demonstration of fibre steering was made. An overview of the state of the art of AFP in the 1990's is presented by Evans in [39, 69].

AFP development in the 1990's was not focused on affordability and rate but rather on new materials and applications, for example in-situ thermoplastic layup [70]. This need for in-situ consolidation and curing arose from the requirement to produce very large submarine- or rocket shells and fuselage sections that exceed most autoclaves diameters. The main limiting factor for thermoplastic layup is the amount of time required to heat the material above its melting point [71]. Thus, maximum speed of layup is currently between $v = 3.6 mmin^{-1}$ [72] to $v = 5 mmin^{-1}$ [73], resulting in considerably lower productivity than thermoset layup. Some of the earlier publications by Springer and coworkers [74-76] focus on the heat transfer into the material, the interfacial healing between the plies after layup, and the development of voids and residual stresses during in-situ thermoplastic layup to improve laminate quality after deposition. Their work was picked up by Gillespie Jr. et al. [77-80] to predict optimal processing conditions for reduced void growth, and maximised speed and interfacial bonding to improve layup speeds further. Similar models were developed to predict the transient temperature distribution during layup of thermoset material [81]. For thermoset materials, electron beam curable prepregs were mainly investigated [82, 83] for in situ curing. Additional methods investigated for in-situ curing were laser [84, 85] and induction heating [86]. Good mechanical performance

for these composite parts was demonstrated, but adoption of the process has stopped. This is likely due to the need for specially developed prepregs, which can be cured by irradiation.

The focus of automation from the 1990's for new materials and processes was shifted to improved rate and affordability from 2000 [87]. This was achieved by increasing the number of tows that could be laid simultaneously, increasing the linear speeds of the layup system and improving the cutting operations to allow cut-stop-restart of each tape at full speed. While initially used for layup on rotating mandrels, AFP systems were being employed for flat layup as well, in order to achieve good tolerances for aerodynamic surfaces [88] and thus competed directly with ATL processing. Splicing errors, dropped tows and material changes were the main reasons for unscheduled downtime and decrease in productivity. Automated splicing units [89], error detection systems [5] and interchangeable heads [90] were developed to address these issues and increase productivity further. Lastly, novel methods for tool path optimisation have been developed for AFP to address issues during layup of complex geometries and to increase productivity [91].

Steering and AFP layup control are currently an area of ongoing research [92, 93]. Due to the smaller tape width that is used for AFP layup, smaller steering radii can be achieved. Additionally, it allows manufacture of unsymmetrical laminates that can have locally changing fibre orientations. AFP is therefore a driver for future developments in the area of smart and tailored structures and their application. The available amount of steering is often reported as the smallest possible radius that the fibres can be laid into without significant layup flaws. Wiehn and Hale [94] have reported successful layup for steering radii as small as $r_{AFP} = 50.8$ cm compared to $r_{ATL} = 610$ cm for ATL layup of 150 mm wide tape. Moon, Johnson and Hale [95] reported that the number of defects is a function of the smallest steering radius. Steering defects include tow gaps, twisted tows, buckled tows, steering overlaps and gaps. The impact of

these defects on the mechanical performance of laminates has not been studied extensively. Blom et.al. [56] have reported numerical modelling results showing significant (up to 32%) strength reductions arising from tow drop areas. Croft et.al. [96] conducted a number of mechanical tests on AFP laminates containing all the aforementioned defects and found significantly lower (3-15%) strength reductions than predicted previously. The impact of AFP layup on mechanical performance may thus warrant further research.

Main manufacturers of AFP systems are Automated Dynamics (USA), Accudyne (USA), MAGCincinatti (USA), Coriolis (France), Electroimpact (USA), Foster Miller / ATK (USA), Ingersoll (USA) and MTorres (Spain). Automated Dynamics, Accudyne, Coriolis and Electroimpact supply their systems on industrial robots and horizontal or column type gantries. Cincinnati, Foster Miller, Ingersoll and MTorres use either column type or horizontal gantries and robots. Robotic layup systems tend to have a lower initial capital expenditure and can be tailored for specific applications. Gantry layup systems offer improved general productivity and reliability by handling more tows.

2.3 Future research needs

Process development with respect to ATL and AFP can be grouped into three areas; Processing and Control, Material research, and Virtual development and optimisation. For all three areas further improvements are necessary and they will be discussed below.

2.3.1 Processing and control

Returning to Figure 2 it is important to note, that automated layup derives possible increases in productivity not only from automating manual operations, but also from

combining several serial tasks into a single operation or parallel operations. Future layup systems will thus likely automate and integrate more functions on the head as well as exhibit higher productivity by controlling more tows, having less downtime or allowing layup of high areal weight prepreg materials. A second route for enhancing productivity, however, might be a reduction of head functions if significant speed increases can be achieved. Additional functions that are feasible for integration on the manufacturing process are tooling preparation and online inspection systems [97]. Systems that allow inline quality control by optical means are already in use or further development, e.g. by Ingersoll. Multiple robot interaction and synchronization, improved layup kinematics and optimised CNC post-processing can deliver further gains in productivity for both ATL and AFP. Synchronisation of multiple robots can greatly improve the layup of large parts as several robots can work on different part areas and different stages of a ply sequence. The recent work by Debout [91] on optimisation of AFP layup paths' has demonstrated a reduction of 33% of layup time, and further improvements are likely. To allow high-rate thermoplastic layup significant heating beyond the material melting point is required. This requires accurate control and high power density for robust manufacture and continued research in this area is therefore necessary. Induction heated moulds and laser heating seem to be a viable option as they reduce the mass of the head and allow high heating rates and accurate temperature control. Lastly, AFP layup is currently limited to low areal weight prepregs, which limits its use to aerospace applications. Future AFP systems need to be able to deliver higher areal weight materials for renewable and automotive industry applications.

2.3.2 Material research

Prepreg materials have historically been developed with mechanical performance in mind and optimized for manual layup. They were then adapted for automated layup by developing specific ply backing films or slitting prepreg tape for AFP layup. Research on thermoplastic tape has illustrated the importance of tape uniformity, porosity and interface properties on the quality of the final product in in-situ layup. Increasing amounts of composite automation currently coincide with the more widespread use of out-of-autoclave curing prepregs and modified prepregs. This opens up a unique possibility to re-evaluate the entire production system for composite components and to develop specific material solutions for effective automated manufacture. Figure 14 shows slit tape for AFP layup with fuzzy edges. This is a health and safety concern, leads to unscheduled downtime for AFP layup and may result in excessive voidage in the dry, fuzzy areas. Slit tape needs to be prepared with high degrees of impregnation to avoid fuzziness after slitting. Additionally, the material variability needs to be reduced to achieve uniform properties on slit-tape level, which is typically only 6.4mm wide. In most cases the tolerances between manual and automated layup are the same and only the backing and tack specification are changed [60, 69, 98] which consequently leads to an unreliable automated layup. Figure 15 shows a defect in a roll of ATL tape. This area is typically removed and laid outside the part. Removing scrap during layup is very time consuming and affects productivity detrimentally. These examples illustrate the improvements that are possible with regards to prepreg material for automated layup.

Vacuum debulking is employed in manual layup to reduce voids and create a solid stack of prepreg. Vacuum debulking may be ineffective for large parts due to the low permeability and limited time [99]. It is omitted in automated layup due to productivity requirements and replaced by the aforementioned consolidation pressure exerted by a roller.

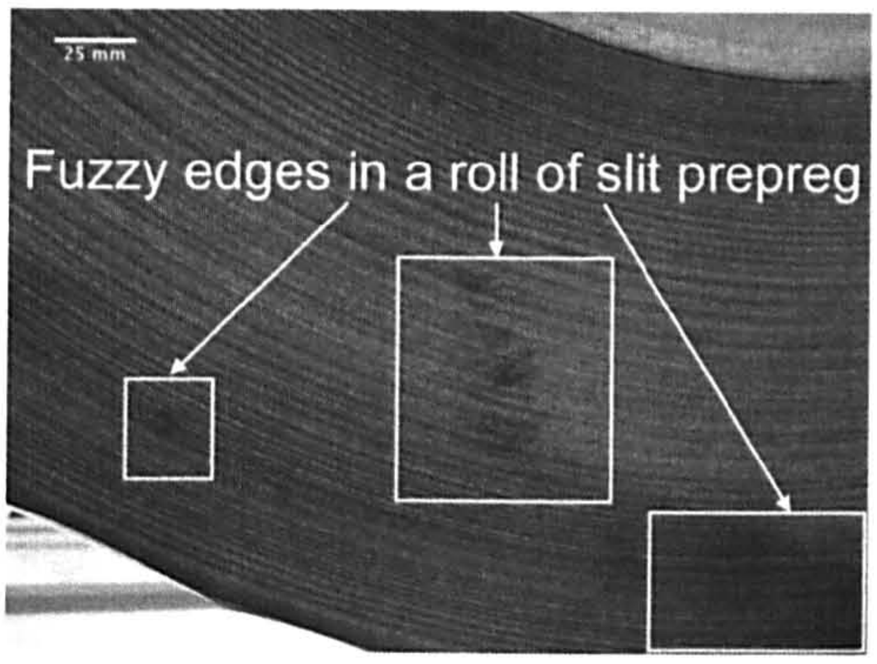

Figure 14: Example of fuzzy edges at the edge of a roll of slit tape (Scale top left).

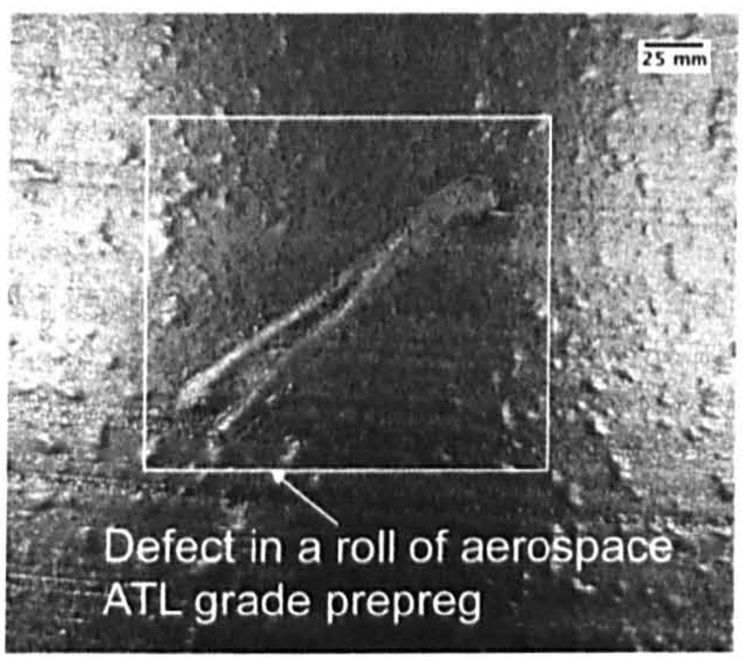

Figure 15: Example of a common defect in ATL grade prepreg.

Depending on pressure, temperature and contact time some flow can occur between the plies during layup, which may reduce interply-voidage and improve laminate quality prior cure [100]. Currently this interaction is not well understood and it is likely that further improvements in this area can be made. A time-temperature-pressure relationship is required to describe this interaction in more detail and to enable direct layup with high quality and effectively reduce debulking [38]. Prior work by MAG Cincinnati [17, 19] on segmented laying shoes illustrates the importance of this interaction. Improved rollers will deliver more pressure to the laminate while also having greater dexterity and thus improve laminate quality and productivity.

New developments in sustainable manufacture will see increasing amounts of natural fibre and plastics derived from natural and renewable sources. While automated manufacture is not likely to be employed for these applications in the immediate future the potential applications in automotive, renewable energy and consumer goods markets are significant. Currently sustainable fibres and resins rely mostly on liquid composite moulding techniques since high quality prepregs are not available. Developing sustainable prepregs suited for automated layup would greatly improve product consistency, reduce costs and thus open up new markets for composites.

2.3.3 Virtual development and optimisation

Currently, engineering guidelines and expensive and time consuming manufacturing trials are necessary to identify robust processing conditions for a given geometry and material. In ATL layup the limitations of the process are often described by phenomenological engineering design rules and are not rooted in a physical understanding of the process. Currently, software packages enable a coherent manufacturing modelling process to avoid collisions and improve layup accuracy and rate. It would also be desirable to create process models, which exist for thermoplastic manufacture [101] for thermoset deposition. Integrating these into the offline programming software for the ply sequences would allow the user to optimize the geometry and path of the head as well as the settings for the layup to achieve optimal laminate quality over complex geometries by locally varying the layup conditions, e.g. speed, pressure or temperature and ultimately, reduce the number of manufacturing trials and guidelines.

Novel applications for composites will make increasing use of the heterogeneity of the material to embed added functionality into the structure, e.g. self-sensing or self-healing. By tailoring the material to an application, e.g. by morphing structures and aero-elastic-tailoring, additional performance advantages and weight reductions can be achieved. All these applications lend themselves to the use of prepreg as the embedded functionality and tailoring can be easily achieved. AFP in particular is a necessary technology with respect to tailored fibre paths as it allows reproducible manufacture of non-conventional, i.e. curved, fibre orientations. The steering capability of AFP needs to be understood and improved further to enable manufacture of more complex geometries and tailoring of structures.

Another strong impact on productivity for AFP arises from the cut-clamp and restart capability where individual tows can be added or dropped during layup. ATL uses a serial

cutting operation, which strongly affects productivity for any part size. The cutting operation in ATL layup has to be revisited to improve ATL productivity. Similarly, a strong driver for AFP productivity is the downtime of the system due to cleaning and maintenance. Downtime is strongly affected by the feed system for the individual tows as they are delivered to the head. Two competing approaches are employed in this area. In the first approach material is stored directly on the head to minimize feed length, e.g. Electroimpact. This leads to a heavy head and additional cost for structures and grounding. The second approach is based on small, nimble layup heads that carry no material, which is fed into the head from the outside. This approach has to address issues regarding splicing, feeding and material storage, e.g. Ingersoll, MTorres or Coriolis. Both approaches for AFP layup have specific challenges as well as advantages. It is unlikely that there is a unique, but rather application dependent, optimal solution, and the process has to be studied in more detail to identify necessary trade-offs.

2.4 Conclusions

ATL and AFP have become mature manufacturing processes since their initial development. They are finding more wide-spread adoption in a number of industries due to potential reliability and economic improvements. ATL has been developed since the 1970's as an automated version of manual tape laying and offers high productivity and reliability for simple or low complexity components. It is in particular highly productive for large components and able to handle high areal weight materials with few modifications. Future developments in renewable energy, for example rotor blade manufacture, will likely rely on prepreg layup by ATL. Productivity can possibly be improved by addressing acceleration during layup, ply cutting and using multiple small rolls of prepreg tape, but overall the potential productivity gains are limited due to the robust nature and long history of ATL layup.

AFP enhances ATL layup by allowing direct layup of more complex components. In addition, scrap rates are reduced and productivity for aerospace components may be increased due to the unique cut-clamp-and restart capability. Since the 1980's AFP has become a relatively mature process, which also has greater potential for future improvements. Productivity improvements can be expected from improved programming, reduction of secondary operations, downtime and robot interaction. Currently, AFP seems more suitable for typical aerospace components and materials, and modifications are necessary to enable layup of wider and higher areal weight materials.

Both processes are currently not achieving their full potential due to a fundamental lack of understanding of materials processing, necessary material properties and virtual development tools. Improving materials and optimising simulation and development tools may enhance both processes further.

This literature review has given an overview of the historic development of ATL and AFP. Significant past development steps were presented for both processes. The current process characteristics were then discussed. It is clear that the main focus in the past has been on systems, system capability and novel materials. This has left a large gap regarding an understanding of the processing characteristics for thermoset layup. Neither the material, nor the layup process has been studied in detail, with the exception of Sarazin and Springer's [76] early work. Their work however simply extends a model which was derived for thermoplastic materials to thermoset layup and predicts the occurrence of delamination due to residual stresses after layup. This has never been mentioned elsewhere and can be considered a very limited case.

As previously mentioned the two prime aims of this work are to improve manufacturing rates by providing a better understanding of the layup systems, and to improve

the mechanical performance of components made by automated layup rates. Mechanical performance can be detrimentally affected by a number of defects, e.g. fibre misalignment, fibre waviness or voidage. Vacuum void removal during autoclave processing and reduction of voids by applying pressure are the most common methods for managing voidage in composite laminates. It is clear however that any void management during curing is tied to the laminate voidage prior to curing, i.e. laminates with high voidage prior to cure tend to have higher voidage after cure than laminates with low voidage prior to curing. The aim of this work is thus twofold, to mitigate void entrapment during layup by providing a detailed understanding of the interaction between layup system and prepreg material and secondly, to demonstrate that improved control during layup will improve the reliability of the entire manufacturing process.

3 Layup technology assessment

3.1 Introduction

Automated Tape Laying and Automated Fibre Placement productivity is influenced by both the system capability and component geometry. To compare both processes on an identical basis their productivity is assessed here for a simple flat part, using only the machine capability values. In the second part of this chapter individual productivity drivers are then identified, and lastly a direct comparison is presented. From the literature review it can be concluded that there is a significant uncertainty regarding the interaction between the layup system, uncured prepreg, and processing conditions. Thus, the third part of this chapter will aim to establish an understanding of the impact of processing conditions on laminate quality and layup reliability.

3.2 Productivity benchmarking

3.2.1 Benchmarking procedure

For benchmarking purposes a simple flat part with an aspect ratio of 2 is assumed, which is kept constant for all calculations, unless stated otherwise. The nominal length of the part is 16m and the width is 8m and the ply orientations are aligned with the part sides, i.e. 0° is oriented along the part length and 90° is oriented along the part width as shown in Figure 16. Furthermore, a quasi-isotropic layup of 8 plies with a $(0, 45, 90, 135)_s$ layup was used.

The baseline material was M21-IMA-268-12K [102], with an areal weight of 412g/m², and with a nominal cured ply thickness of t = 0.26mm. This results in a final part weight

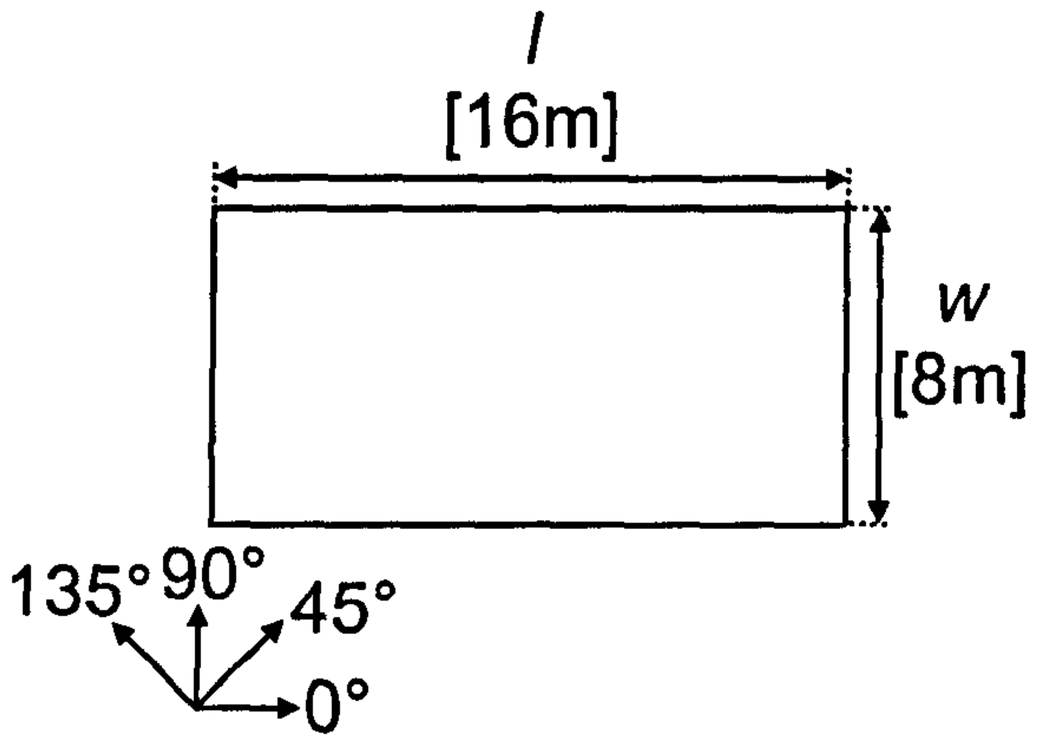

Figure 16: Baseline component including ply orientations.

approximately 423kg, which is comparable to the estimated weight of a composite wing-skin for an A350XWB [103], although a wing skin typically has a larger aspect ratio, around 1:5, and exhibits a far more complex layup, ramps and landings for stringer and rib integration and tapered plies. As such, the results presented herein are not applicable to estimate production times for such a component. However, the above benchmarking procedure is identical to the approach taken by Grimshaw [30] for calculating material waste rates for ATL, with respect to aspect ratio and part size, which allows a direct comparison to his results.

Parameters such as maximum speed and acceleration for process evaluation were taken from [103] and down-selected. To compare ATL and AFP systems on an equal basis, both systems had to be from the same supplier and MTorres was identified as supplier for both their layup systems are in use at Airbus (for example for the A400M wing skins in Filton, England, and the vertical tail plain for all aircraft families in Stade, Germany). Machine data for the MTorres systems used in the benchmarking procedure are shown in Table 2. Note that the presented results are only valid for the MTorres systems and may be different for other systems, though some general observations are likely.

Several observations can be made about the machine characteristics of both systems:

- The maximum in-plane speeds are identical for both systems.

Table 2: Benchmark performance characteristics of MTorres ATL and AFP layup systems.

Parameter		Unit	ATL Value	AFP Value
Acceleration	X-Axis	ms^{-2}	0.5	2
	Y-Axis	ms^{-2}	0.5	2
Maximum Speed	X-Axis	ms^{-1}	1	1
	Y-Axis	ms^{-1}	1	1
Time for cutting a ply		s	6	0
Time ply start with laying shoe		s	5	0
Time for material change		s	300	300
Time for subsequent bobbin		s	0	15
Minimal course length		mm	100	50
Material width		mm	302.4	6.35
Number of tapes		-	1	32

- Accelerations are different and higher for AFP.
- Secondary operations that may lead to a constant time penalty in ATL do not occur during AFP layup.
- ATL delivers more material with each pass, 302.4mm for ATL compared to 203.2mm (6.35mm tow width and 32 tows in parallel) for AFP

Further system performance characteristics, e.g. head rotation speed and acceleration are relevant for cylindrical parts, but they are not relevant for the flat part studied here. A specific procedure within Airbus is the finish of each ply course during ATL layup. After a ply course has been laid, the layup head normally returns to a position outside the part and lays a sequence with the minimal course length. This operation consequently depends on the processing variables and size of the part. The reason for this operation step is unclear.

The time for scrap removal is calculated as a function of speed, acceleration and part size and is another variable in the calculations as opposed to a fixed value, e.g. for turning the head. Scrap time is studied as a variable to show the sensitivity of productivity calculations to

this parameter. To calculate the time taken for each ply course, the time t_{acc}, and distance for speed up s_{acc} are first calculated by

$$t_{acc} = \frac{v_{target}}{a} \tag{3-1}$$

$$s_{acc} = \frac{a}{2} \cdot t_{acc}^2 \tag{3-2}$$

with v_{target}, is the speed being accelerated to, and a the acceleration. The above calculations are derived from simple kinematic physics and assume that the head accelerates from a standstill and decelerates to full stop at the start and end of a ply course respectively. For baseline ATL layup, the time for acceleration is t_{acc} = 2s and the distance for acceleration is s_{acc} = 1m. For baseline AFP, t_{acc} = 0.5s and s_{acc} = 0.25m. The layup distance at full speed is then calculated by subtracting the acceleration length from the total length

$$s_{layup} = s - 2 \cdot s_{acc} \tag{3-3}$$

The total time for acceleration and deceleration is calculated by multiplying the time to acceleration by two, and by adding the time for layup at speed, the layup time for each ply course can be calculated from

$$t_{course} = (2 \cdot t_{acc}) + \left(\frac{s_{layup}}{v_{target}} \right) \tag{3-4}$$

The time for a single 0° ply course for ATL is t_{course} = 18s and for AFP t_{course} = 16.5s. To calculate the layup time per sequence, the number of plies n is calculated, rounded, and multiplied with the time per ply course t_{course}. This simple approach is suitable for both 0° and 90° plies, a complete ply of 0° courses consists of 27 plies for ATL using 300m wide tape and 40 plies for AFP with 32 tows, each 6.35mm wide.

For ±45° plies the number of plies and their length varies according to the ply position in the layup. As the plies move closer to the edge they become shorter, but at the same time the shortest deposited ply has to be longer than or equal to the possible minimal course length. This extra material is referred to as lead-in, lead-out or crenulation. To calculate the layup of ±45° plies the sequence is examined from the centre of the part as datum. The layup is then calculated incrementally by calculating each course from the part middle to the outside and this procedure is illustrated by Figure 17. Depending on the ply position the ply length is calculated according to

$$l_{ply} = \begin{cases} l_{full}, & \text{if } l_i > 0 \\ l_{corner}, & \text{if } l_i < 0 \end{cases} \tag{3-5}$$

with l_{ply} the length to be calculated, l_{full} a full course length, l_{corner} the corner course length, and l_i the current course position along the length. The full course length is then simply calculated from

$$l_{full} = \frac{w_{part}}{sin(\alpha)} + 2 \cdot w_{ply} \cdot sin(\alpha) \tag{3-6}$$

with w_{part} the part width, α the ply angle, and w_{ply} the ply width. The first part of equation 3-6 gives the length along the tool, the second part adds the lead-in/ lead-out outside of the component. A full course length for ATL layup is 11.62m long, while the same course for AFP is 11.32m long. This difference is due to the material width only. To calculate subsequent full ply length the ply position counter is updated by solving

$$l_i = \frac{l_{part}}{2} - \frac{w_{part}}{2} - \frac{w_{ply}}{sin(\alpha)} \tag{3-7}$$

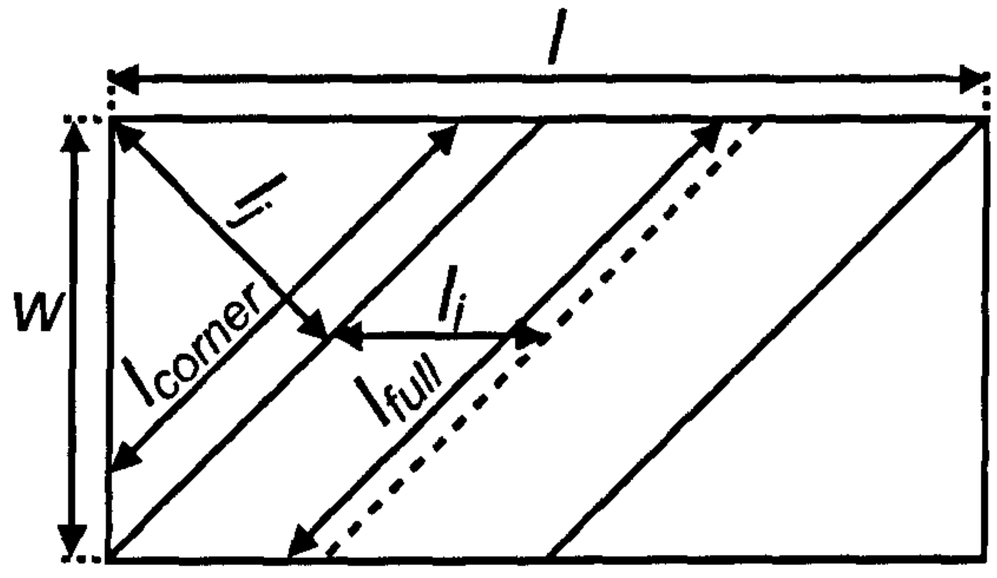

Figure 17: Illustration of the parameters for ±45° ply layup.

To obtain the length of all plies in the corner region, the coordinate system is transformed from tool coordinates to a ply coordinate system. If $l_i < 0$ (see equation 3-5 previously) the current ply number is calculated by a new counter l_j

$$l_j = w_{part} \cdot sin(\alpha) - j \cdot w_{ply} \cdot n \tag{3-8}$$

with j being a new counter for the corner section. The ply length for $l_j > 0$ is then calculated by

$$l_{corner} = \left(w_{part} - j \cdot w_{ply} \cdot n \frac{1}{sin(\alpha)} \right) \frac{1}{sin(\alpha)} + 2 \cdot w_{ply} \tag{3-9}$$

while for $l_j < 0$, $l_{corner} = 0$. Inserting equation 3-8 into 3-9 simplifies to

$$l_{corner} = \frac{l_j}{sin^2(\alpha)} + 2 \cdot w_{ply} \tag{3-10}$$

with l_{corner} the length of the ply to be laid down, and n the number of plies in each course (i.e 1 for ATL and up to 32 for AFP). The first part of the equation calculates the remaining corner width and this is multiplied with the layup angle to give the ply length. Lastly, the lead-in and lead-out are added. Note that the added length depends on material width only, i.e. for AFP layup each tow is stopped individually and the added length is therefore not a

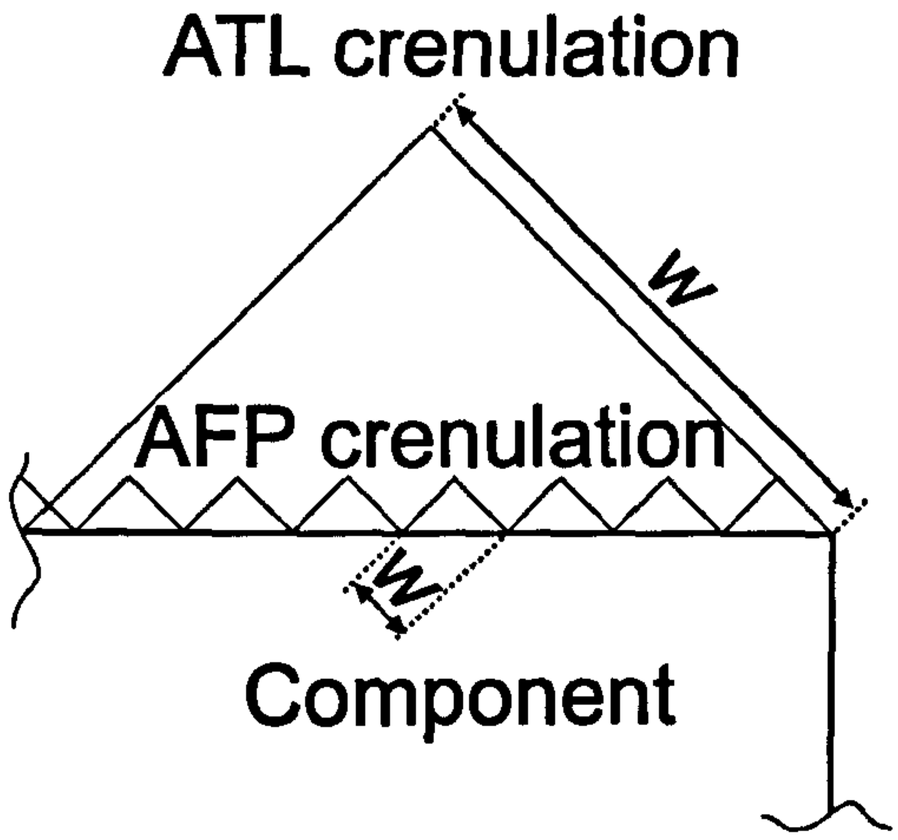

Figure 18: Illustration of the crenulation found at the end of a ply course for either ATL or AFP.

function of *n*, see Figure 18. For calculating the total ±45° layup time, the calculated time is multiplied by 2 since the aforementioned calculations only cover one half of the part.

The time for layup can now be calculated in the same way as previously for 0° and 90° plies and the time for starting and stopping the ply using a laying shoe and for cutting the ply is then added. The impact of cutting time on the overall productivity of ATL is analysed later. Time for removing scrap during ATL layup is added by adding a minimal course length laid up outside the component, which is in accordance with Airbus's layup procedure for MTorres machines. For AFP layup only the time for starting the course is added, as the time for deceleration is included in the layup time.

The time taken for secondary operations, such as time for roll change in ATL layup, or creel changes in AFP layup, is added to the total time. An overview of the timings to layup a single ply per orientation for both processes is given in Table 3. Even though the amount of material per ply per orientation is almost identical the layup times are different between 0°, 90° and ±45°. This difference is mostly found to be due to unproductive travel. The total time for

Table 3: Layup time for a complete ply for ATL and AFP for different ply orientations.

Ply orientation	ATL layup time in [s]	AFP layup time in [s]
0°	3785	1720
90°	6581	2133
45°	7157	2128
135°	7157	2128
Totals	24680	8109

all four plies is almost three times larger for ATL than for AFP. A large proportion of this time is recovered during refilling of the material supply, which can be significantly more time consuming during AFP layup than ATL. Timings for a complete component as given in Figure 16, are t_{comp} = 29098s for ATL layup and t_{comp} = 24455s for AFP layup, including material changes. The total time per part was then divided by the part weight to give the productivity. As an example, ATL layup will deliver 441kg in the time stated above, translating into a productivity of p = 54.4kg/h and 4.5% scrap. AFP delivered 427.5kg translating into a productivity of p = 62.4kg/h and 1.3% scrap.

3.2.2 ATL benchmarking

The calculated productivity for ATL layup using the baseline settings in Table 2 is p = 54.4kg/h. Since absolute values are not of interest for this calculation, but rather productivity drivers, the remaining results are normalised with respect to this baseline productivity, unless otherwise stated, only selected variables are changed to assess their impact on productivity whilst keeping all other values identical to the baseline.

The ATL process delivers a certain amount of material over an area as a function of time and it should therefore be expected that materials with a higher areal weight lead to a higher productivity. Figure 19 shows the productivity of three different prepreg grades as a function of speed. The prepreg areal weights used are typical for aerospace applications as

taken from [102]. Whilst this demonstrates the importance of the prepreg areal weight, it also demonstrates how misleading a solely weight-based process assessment can be as all three prepreg weights represent the same amount of part area. The layup system needs to travel the same distance to deliver the material over the geometry, only less material is delivered with each pass and the number of plies increase. An area-based assessment of the process can be considered part independent, however, as weight-based assessments of the productivity are far more common the data will be presented in this way.

ATL layup scales with layup speed, and higher speeds lead to higher productivity. However, it is interesting to note in Figure 19 that the relationship between speed and productivity is reaching a plateau at speeds higher than the baseline speed of $v = 1\text{m/s}$. Initially, small increases lead to significant productivity increases. Indeed, increases beyond the baseline have a negligible impact, for example a further increase by $\Delta v = 0.167\text{m/s}$, or 17% increase in speed, only yields 3% productivity increase. This is due to several factors that are normally not speed dependent, including acceleration and secondary operations. To harness the benefits of higher maximum speeds acceleration needs to increase accordingly, otherwise higher speeds may simply not be realised during layup. Furthermore, productivity for ATL is constrained by secondary operations, i.e. time for scrap removal, cutting the plies, and starting the course with a laying shoe. The ratio between layup time to secondary operations is initially high, more time is spent on the layup phase, but as speed increases the layup time will decrease while the time spent on secondary operations may remain constant, resulting in a decreasing benefit from increasing speed. Productivity as a function of prepreg areal weight is shown in Figure 20. It shows that ATL productivity scales linearly with increasing prepreg areal weight. When using high areal weight prepreg, the productivity of ATL layup can exceed 150kg/h.

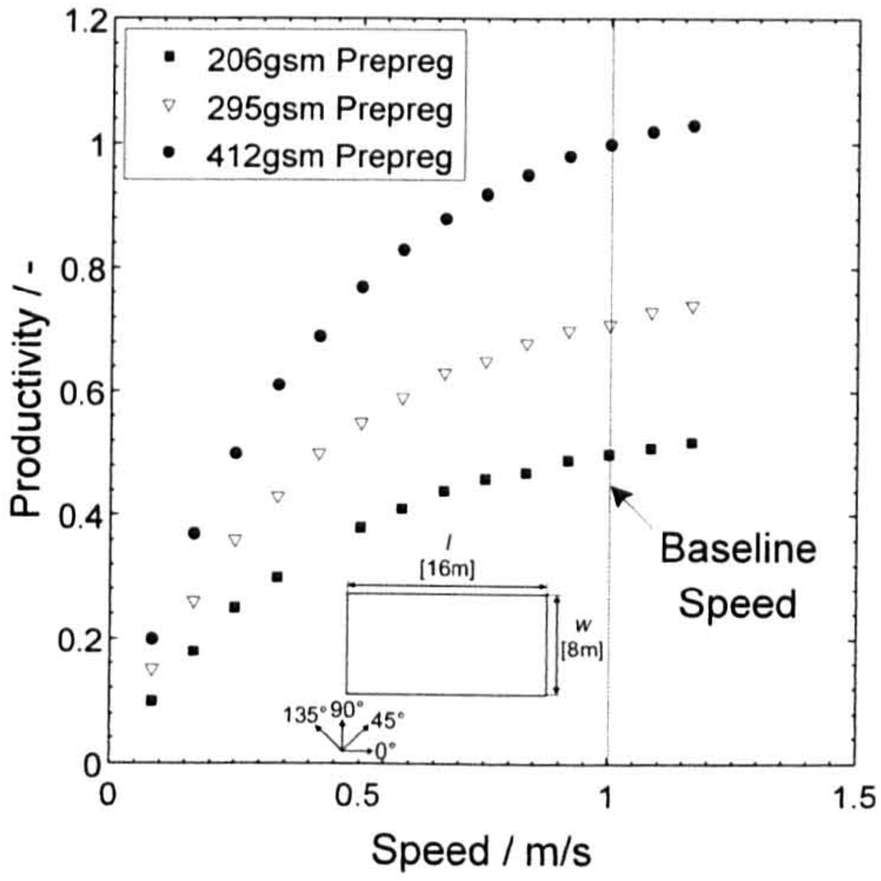

Figure 19: Normalised ATL productivity for three different prepreg area weight and different speeds.

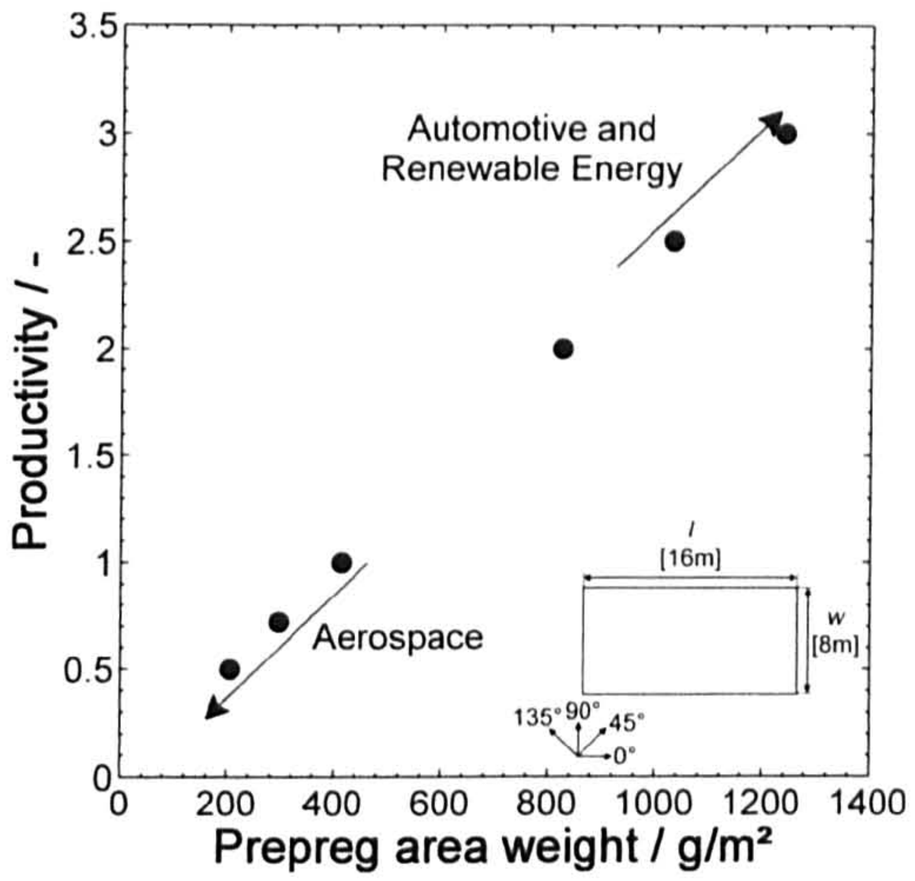

Figure 20: Normalised ATL productivity as a function of prepreg area weight. Typical applications are indicated.

Typical ATL systems have an acceleration of $a = 0.5$ ms^{-2}, but Figure 21 shows the productivity of ATL layup for various part sizes and at four different accelerations. As noted previously, for small part sizes or layup speeds acceleration does have an impact on productivity. Productivity as a function of part size is reaching a plateau due to the impact of secondary operations on the total layup time, which increases with increasing part size, such as the time for returning to a course start. A further breakdown of productivity as a function of part size is shown in Figure 22.

It can be seen that doubling acceleration to $a = 1$ ms^{-2} yields ~10% productivity increase, with smaller parts particularly benefitting. In general, increasing accelerations above the current baseline tends to yield only negligible productivity gains and may not be economical to pursue. To understand the sensitivity of the calculations, productivity was plotted against the time for cutting a ply at the end of a ply course, see Figure 23. Cutting time is a secondary operation that is independent of acceleration or speed, and thus greater penalises productivity,

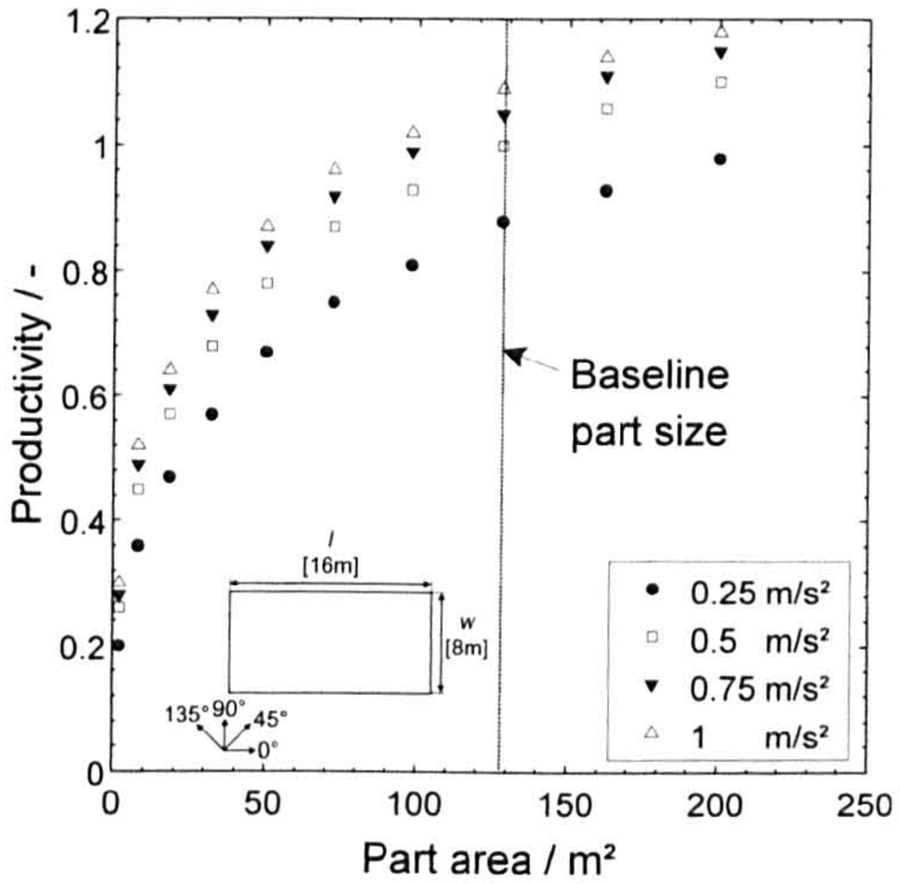

Figure 21: Normalised ATL productivity as for four different accelerations and different part sizes.

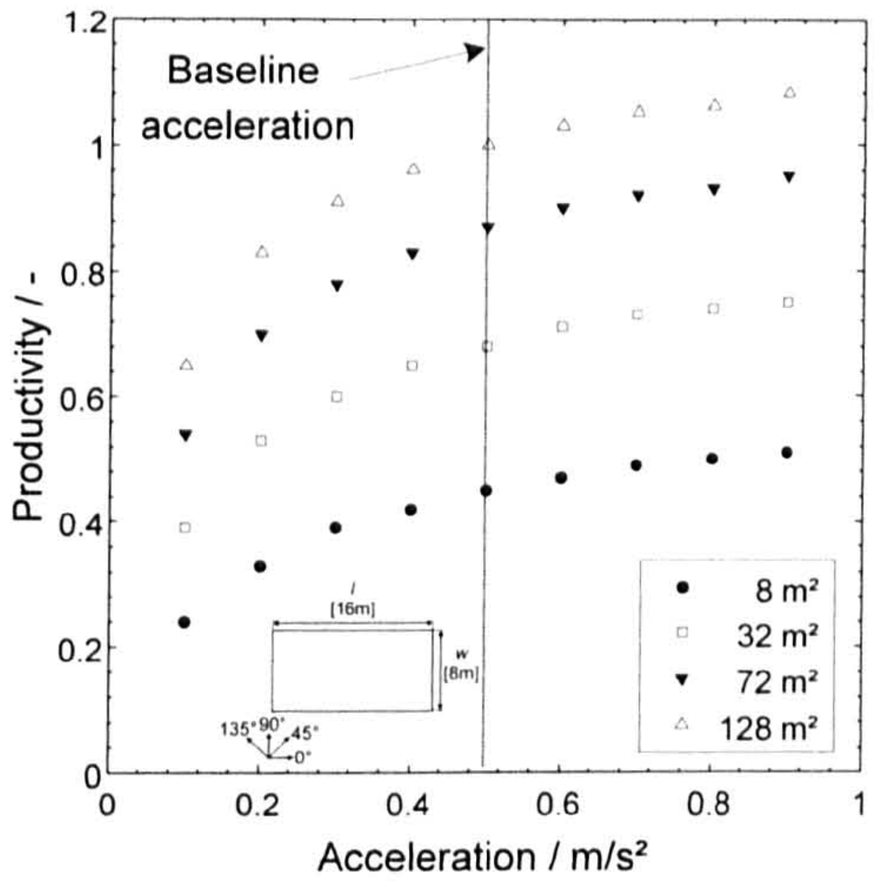

Figure 22: Normalised ATL productivity for four different part sizes and different accelerations.

as the time for layup decreases. To remove scrap the head returns to a position outside the part, lays a sequence of prepreg having minimal course length and returns to the start of the next ply. Productivity as a function of scrap time is presented in Figure 24 and the time for this procedure can be longer than the time for the actual part layup. Additionally, productivity for this particular parameter is not tied to the machine configuration, but simply to the operation of it and by reducing the time for scrap removal, productivity can be increased by up to 100%.

Most productivity drivers cannot be controlled during manufacture. They are either tied to the machine configuration, for example speed or acceleration, or they are controlled by the design, for example prepreg areal weight or part size. The results discussed so far show that changes to the machine layout may result in small improvements to productivity but may also not be economical. Controlling the time for secondary operations is therefore the simplest way to improve ATL productivity without affecting part design or machine layout.

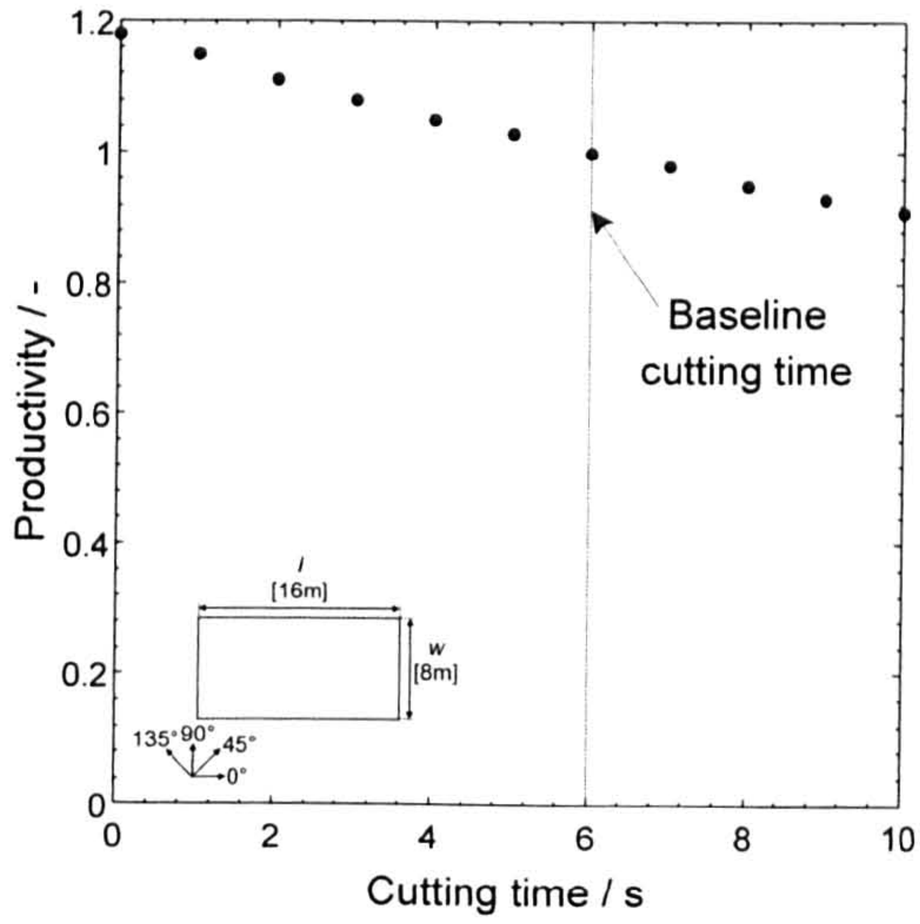

Figure 23: Normalised ATL productivity as function of cutting time.

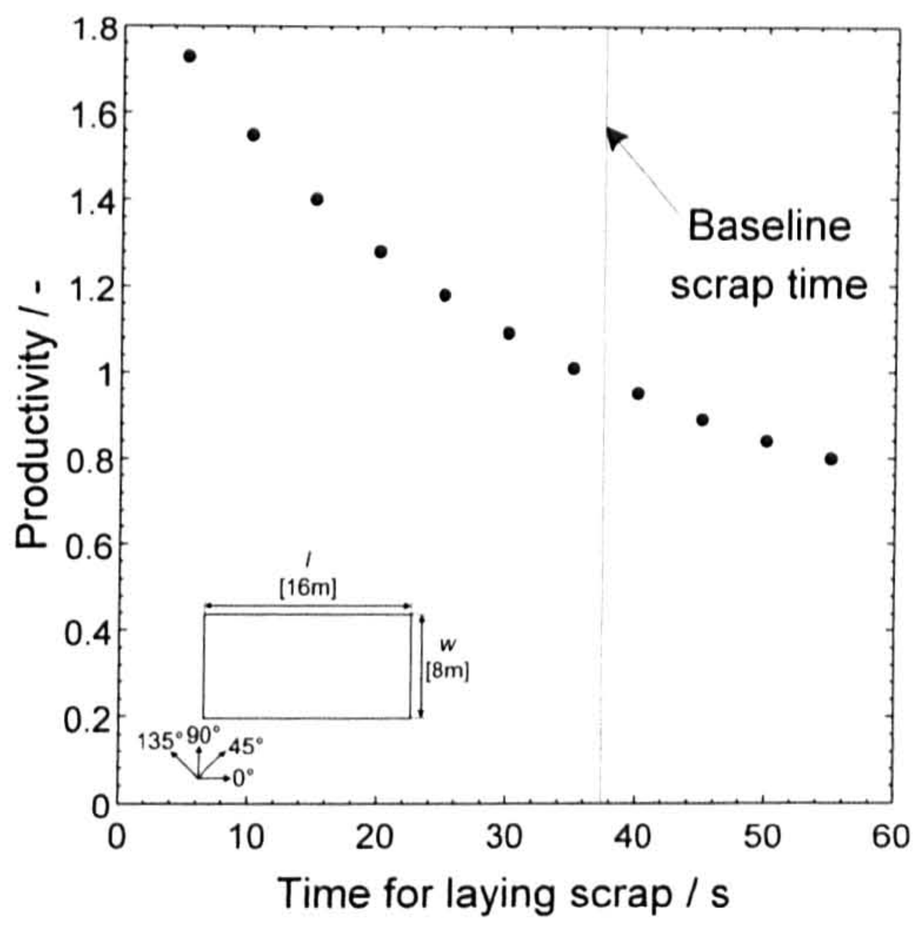

Figure 24: Normalised ATL productivity as function of the time for laying scrap.

3.2.3 AFP benchmarking

The calculated productivity for AFP layup using the baseline settings in Table 2 is p = 62.4 kg/h. The productivity for AFP as a function of speed for three prepregs with different areal weights is shown in Figure 25. AFP has a higher acceleration than ATL and lower time for secondary operations. In the case of AFP, secondary operations have the same effect as previously for ATL, although here the dominant secondary operation is material change and refilling of material. It is therefore not surprising that AFP does not reach a plateau as early as ATL for the same speed. Reducing secondary operations time, by either reducing the direct time for material change or reducing the number of material changes by having more material on a creel leads to a plateau at higher speeds.

To address the point of more material changes in more detail, a productivity analysis for some material change times per bobbin were conducted and are shown in Figure 26. AFP bobbins typically carry less material and material refilling takes longer due to the number of

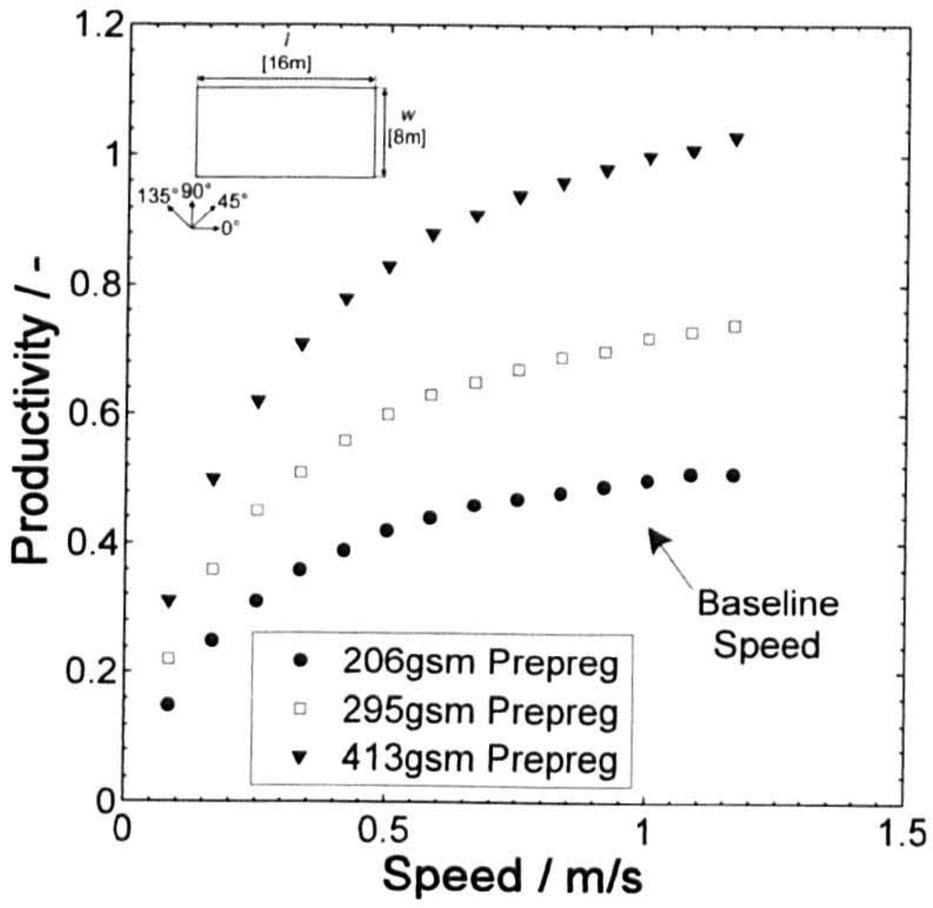

Figure 25: Normalised AFP productivity for three different prepreg area weights and different speeds.

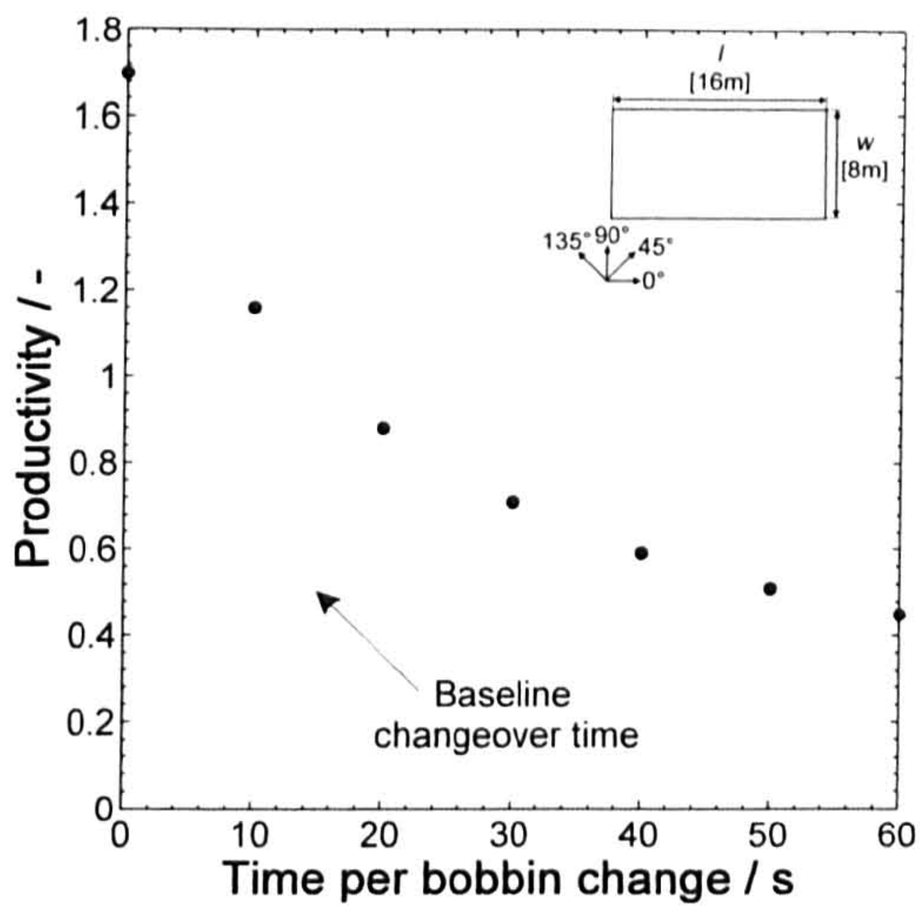

Figure 26: Normalised AFP productivity as a function of material change time.

bobbins that need to be changed. This feature currently presents the largest productivity penalty to AFP operation. As the changeover time per bobbin increases from t = 0s to 60s, productivity decreases exponentially. This feature can therefore be considered to be the primary area of interest for achieving improvements in AFP layup rates. In addition, slit tape bobbins tend to vary significantly in weight or amount of material in linear metres, which may result in repeated changes of only a few bobbins and can thus result in even higher total times required for material changes. This is shown in Figure 27 where the Productivity of AFP layup is plotted as a function of material on each bobbin. For direct comparison between ATL and AFP it was assumed that the amount of material in linear meters would be identical for both systems, corresponding to approximately 240 linear meters, however as pointed out by Evans [69], a typical AFP spool caries 460 linear meters of material, (wrongly converted there to 460km!) which would result in increase in AFP productivity of approximately 40%, due to a reduction in time for material refilling.

Potential benefits from using more or wider tapes are shown in Figure 28 and Figure 29. The productivity of AFP scales almost linearly with tape count and width.

Unfortunately this area is rarely controlled by manufacturing requirements and the number of tows and their width during layup is constrained by steering requirements when

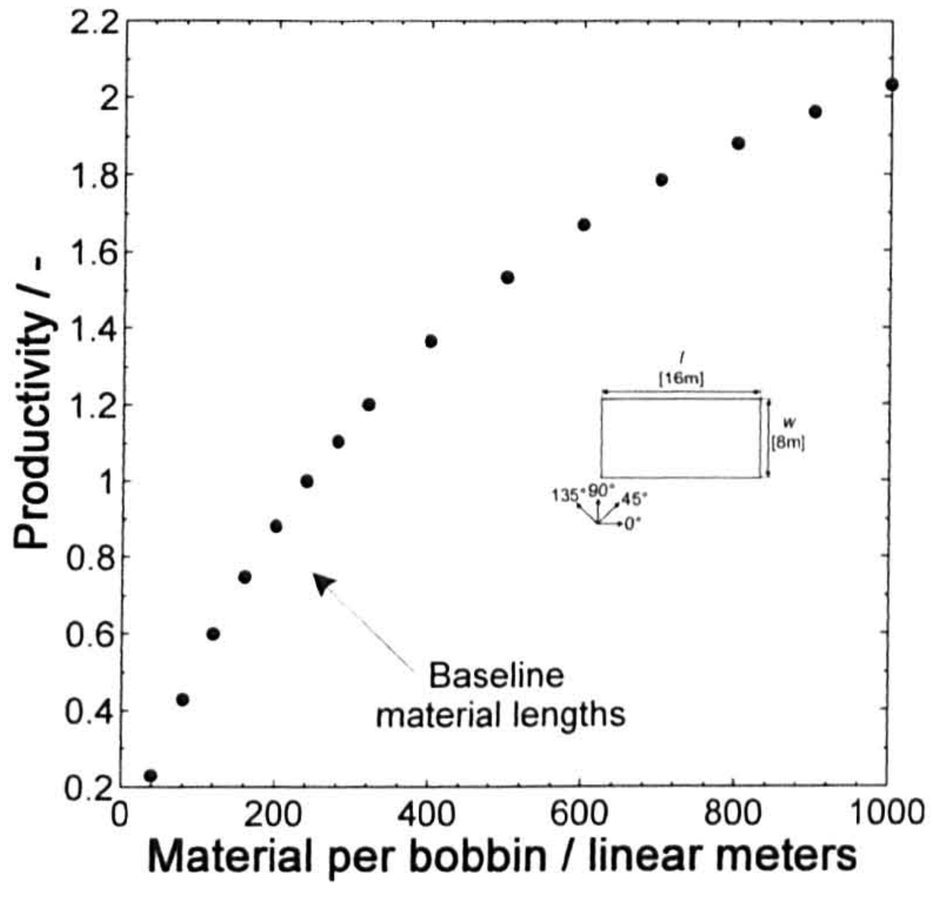

Figure 27: Productivity as a function of material on each bobbin.

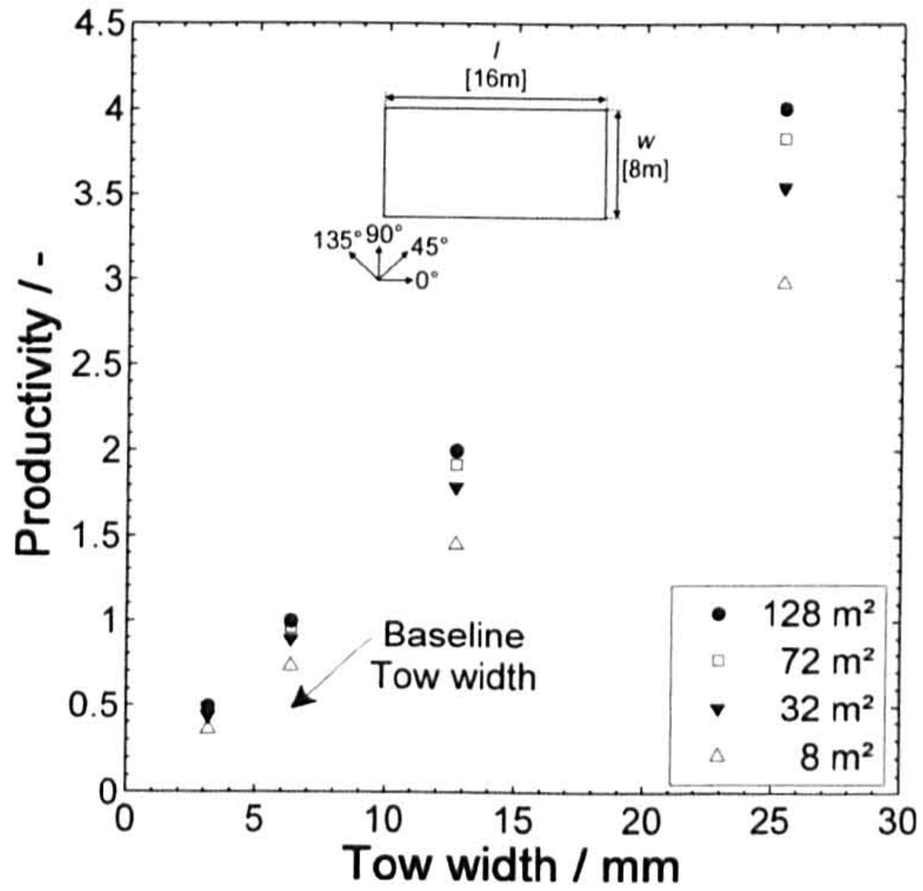

Figure 28: Normalised AFP productivity for four different part sizes and four tow widths.

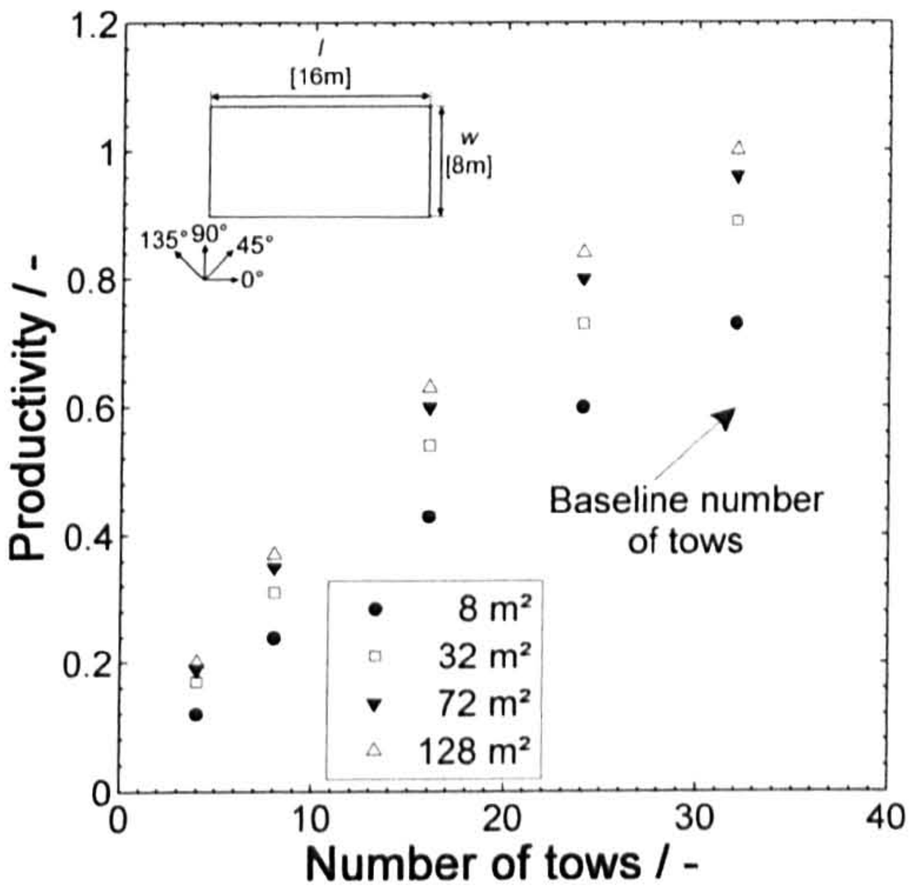

Figure 29: Normalised AFP productivity for four different part sizes and different tow counts.

laying over complex geometries. Tow width and material width should always be as high as possible. It may therefore be desirable to consider changes in the design of a component to allow higher productivity. It is interesting to note in Figure 28 and Figure 29 that for smaller parts AFP productivity is significantly higher than that of ATL.

With increasing part size this advantage, however, is mitigated and for baseline settings the difference reduces to only 14% in favour of AFP. For smaller part sizes AFP productivity benefits from higher acceleration and the lack of time consuming secondary operations, while ATL benefits from larger material width.

As demonstrated short-term improvements to AFP layup for existing components can be achieved by addressing the time for material changeover, for example by rapid change systems, pre-loaded change modules, and interchangeable layup heads. AFP can already be considered more productive for most applications than ATL but as the previous results show, even the potential for further productivity increases is greater for AFP than for ATL.

3.2.4 Discussion

Assessments for the capability of an automated layup system can often not be compared as different geometries are studied. Therefore, the layup model results presented are novel in the respect that they compare AFP and ATL productivity for the same simple part. The part geometry was adapted from [30] and can be argued to favour ATL through its size and simple shape. It is therefore surprising that the results indicate a higher productivity for AFP for all studied layup scenarios. Figure 30 shows a comparison of ATL and AFP productivity as a function of part size. Whilst AFP is generally more productive than ATL, this advantage is particularly clear with decreasing part sizes. ATL benefits from higher material width and high layup speeds for large parts, while AFP is constrained by the time for material

changes. ATL productivity is increasing further as the part size increases while AFP sees only negligible productivity gains. For parts larger than A = 288m², ATL is similar to AFP productivity, for larger parts ATL is thus more productive, although these part sizes can be considered uncommon. AFP is more suited for complex layups where the length per course is limited by pad-ups and ramps, which require the layup system to slow down. Figure 31 compares the processes productivity as a function of layup speed. Both processes scale similarly and productivity approaches a plateu at higher speeds, in excess of v = 1 m/s.

The presented model may allow the explanation of past developments efforts for both ATL and AFP and may also help identify future trends (in section 3.2.5). The data shows a desirable increase in productivity with increasing layup speed for ATL and with the number of tows in AFP. Both have previously, in the 1980's for ATL and the 1990's for AFP, been prime areas for improving the productivity of the respective layup process. Currently, both processes achieve maximum linear speeds of v = 1ms^{-1}.

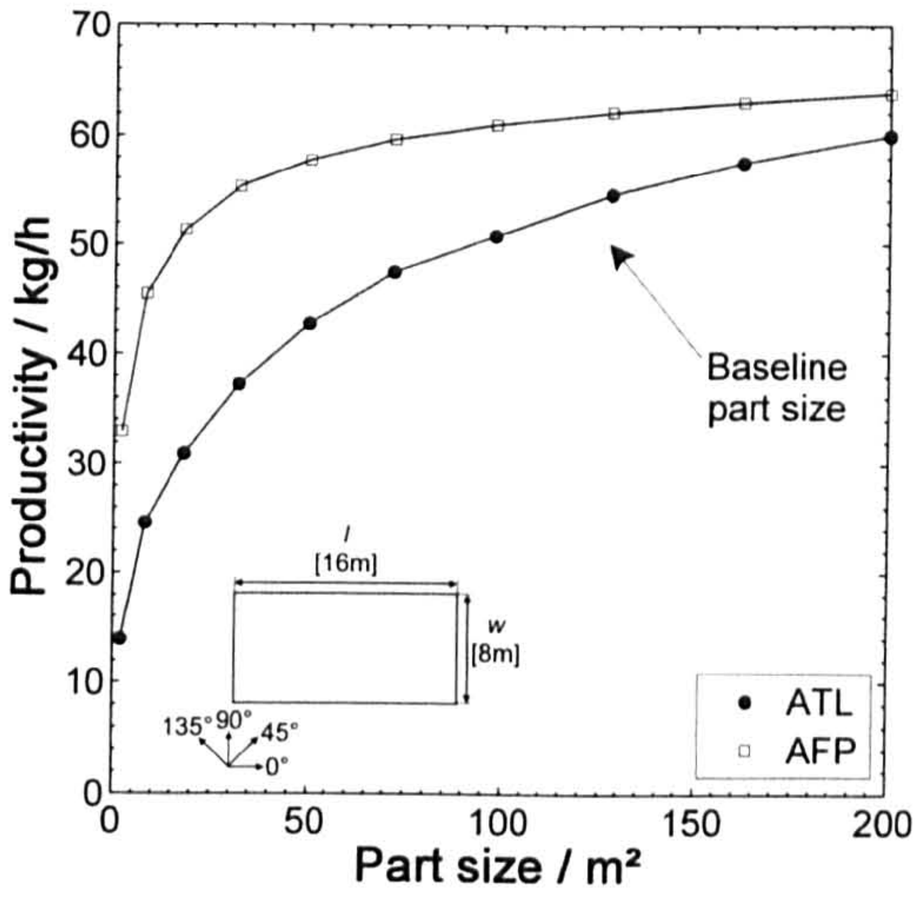

Figure 30: Comparison of ATL and AFP productivity for different part sizes.

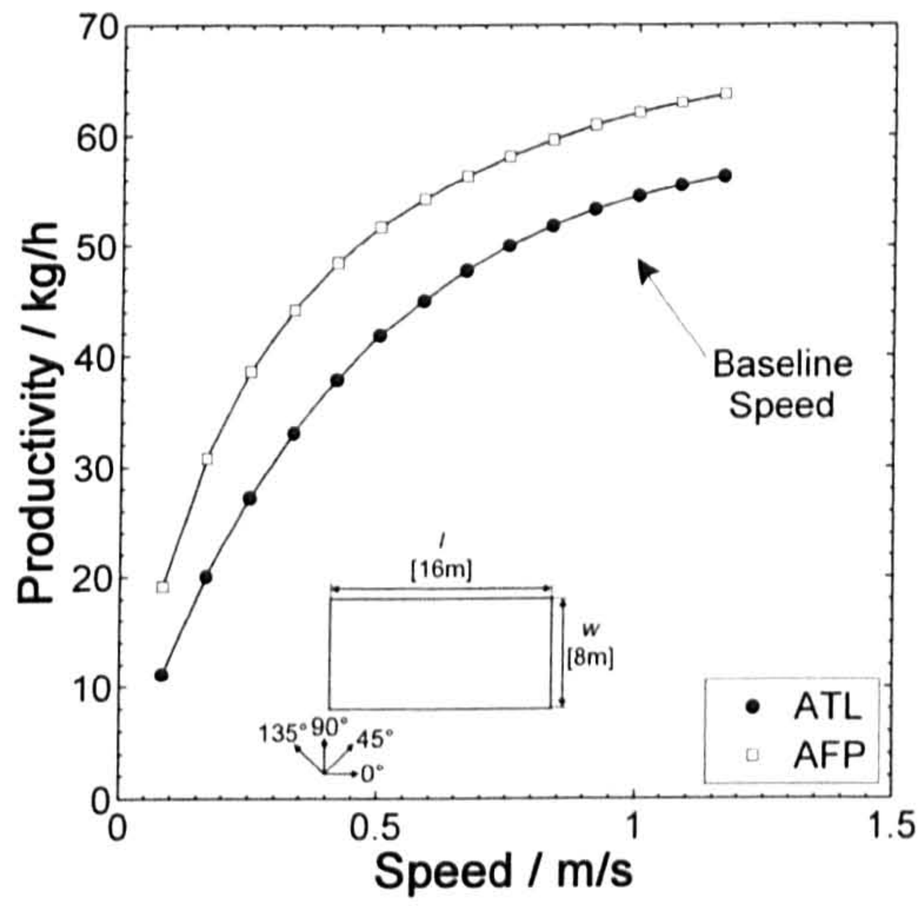

Figure 31: Comparison of ATL and AFP productivity for different layup speeds.

ATL has been capable of delivering tape at this speed since 1980 and our data shows that further gains in speed yield limited gains in productivity, which may explain why published development in this area has halted. AFP has been shown to scale strongly with scheduled downtime, such as material changes, and unscheduled downtime for example due to layup errors. Interchangeable heads are in development to allow faster material changes, while layup errors are minimised by online quality inspection.

The data presented predicts a far greater productivity potential for both ATL and AFP than typically quoted in the literature, with the most recent source for ATL and AFP lay-down rates being Airbus's assessment of the Boeing 787 program [10]. Estimated lay-down productivity is quoted at 100lbs/hr (45.36kg/h) and this is well within the estimates from this model. This can therefore be interpreted as an independent validation of the results. Current, un-optimised lay-down rates are estimated to be around 19lbs/hr (8.62kg/h), 20% of the above initial estimate.

To translate machine capability into component-centred productivity estimates, the typical course length has to be reconsidered. An aerospace component is optimised for low weight and integration with the subsystems attached to it. Laminates thicknesses vary locally, depending on the local load situation during application. Furthermore, structural integration, such as landings for rib-feet in a wing-skin, constrains the course length during lay-down. Morey [104] quotes a typical course length of $l = 2$m during automated layup. Calculations for the productivity of a simple flat component with a smaller size are thus given in Table 4 for the baseline performance data. A possible un-optimised ATL layup productivity of 29 kg/h is estimated, while Airbus target ATL productivity is 30 kg/h. For AFP a large difference between the expected and actual lay-down rates is found, 8.62 kg/h [10] compared to 41.34kg/h predicted. This may be explained by unreliable material layup and significant

Table 4: Overview of calculated productivity for two example components with reduced course length.

Process	Part size	
	1x1m	2x2m
AFP	20.02 kg/h	41.34 kg/h
ATL	11.69 kg/h	29.16 kg/h

productivity reductions due to part complexity, e.g. ramps, valleys and pad-ups, but does require further investigation.

3.2.5 Optimisation of Layup Rates

There are several ways of improving the layup rates for both ATL and AFP and these can include faster acceleration, higher maximum speeds, in-process inspection, and faster material changes. Generally though, these approaches can require significant capital investment and may not be applicable to legacy systems, since higher acceleration cannot be achieved by simple modifications of the drive. The most desirable way of improving layup rates then is by improving the operation of existing equipment. For ATL this is highlighted by the ratio between layup-time to secondary travel due to scrap removal. This unproductive travel, while necessary for layup, has to be minimised.

Scrap is typically laid at a specific position outside the part, prior to laying the next ply. The time for scrap removal is a function of part size and processing parameters. To reduce the length of travel the part could be subdivided into segments with their own scrap position, instead of a fixed scrap removal position this travels with the ply location. Furthermore, layup should not proceed from ply to ply, but segment to segment. This could imply that different segments of the part are at different stages in the layup.

The "classical" approach to laminating a structure is illustrated in Figure 32 and each ply is finished completely before the next ply is started. This also means that the layup system

has to perform unproductive travel along the entire sample length or width but by dividing the part into segments, which are finished separately, this unproductive travel can be reduced and the ratio of productive to unproductive time increased. This approach is illustrated in Figure 33 where the segments are separated along the layup direction for each ply. Ply courses with orientations along the short side of the part are then finished per segment, as the order numbers to the left in Figure 33 indicate. As an example the part is divided into two segments, but any number of segments down to the number of plies per ply course is feasible.

Using baseline machine data from Table 2, the productivity of the "classical' approach in Figure 32 is p = 54.6kg/h, and as aspect ratio is increased this productivity decreases.

For a typical ATL production part with a large aspect ratio, 1:5 or bigger, productivity would decrease to p = 41.5kg/h, a 24% reduction. Using this novel segmented approach productivity is estimated to be around p = 48.6g/h, corresponding to an only 11% productivity reduction while leaving the actual component and ply design unaffected.

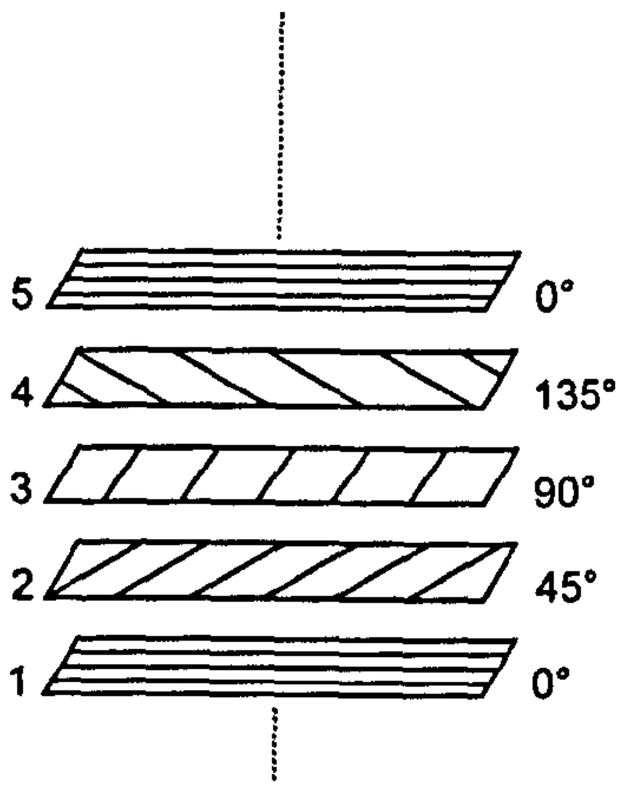

Figure 32: Classical laminating approach. Each ply is finished completely before the next ply is started.

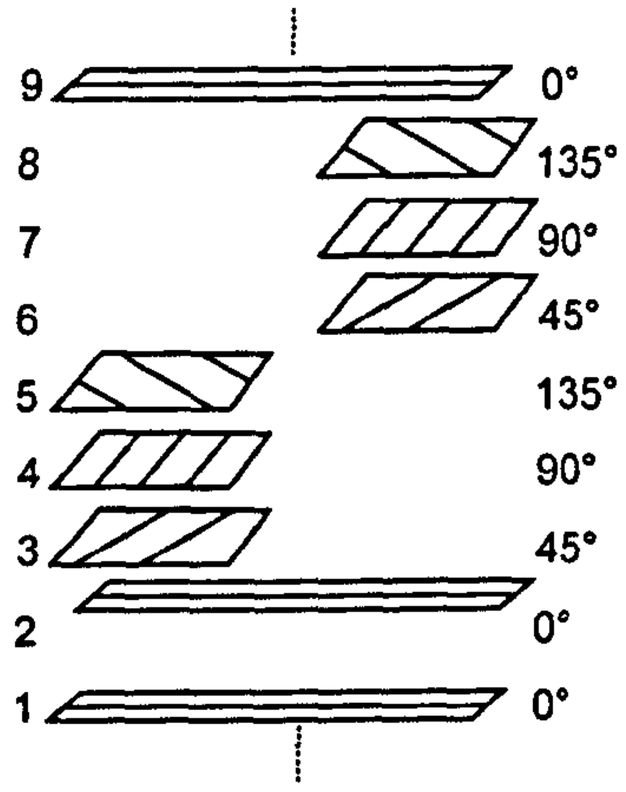

Figure 33: Optimised layup approach for large aspect ratios. Segments are finished having plies at different degrees of completion.

Whilst this approach addresses productivity drawback in ATL operations, it can be applied to AFP. Using small robotic layup systems with external material storage reduces the size of the layup system on the part to an extent where multiple layup heads could potentially operate on one part. Multiple head layup has previously only been addressed for layup into or onto cylindrical moulds [105, 106] and it is believed that this concept will greatly simplify multiple head interaction on flat or contoured parts. To allow effective utilisation of the layup heads, the part will have to be divided into segments, which are finished by each robot individually. Using multiple robots will thus not only increase the total productivity per part but the productivity for each robot as well.

Lastly, it is important to note that this work has addressed raw productivity alone. Slit tape, typically used in AFP is significantly more expensive than wide tape of the same quality. The recurring cost per part is thus higher for AFP than ATL. Though a higher productivity for AFP layup than ATL was predicted, this does not imply that the final part will be any cheaper if made by AFP due to the higher material cost.

3.3 Process control benchmarking

3.3.1 Introduction

Material inconsistency, such as dry fibres or lack of tack, leads to unreliable layup and/or downtime during automated layup. Quality inspection, if not suitably automated also reduces productivity in a similar way to downtime. In section 3.2.4 it was shown that a large proportion of productivity reduction cannot be explained by layup strategies, but these may be linked to the quality issues. This section addresses the issue of process control during layup for void reduction in more detail through using industrial scale layup systems to produce

composite laminates. The impact of processing conditions on those laminate's quality was studied in detail.

3.3.2 Experimental procedure

When planning the layup experiments, a particular challenge to overcome was the various sources of scatter in the response signal for the quality measure, i.e. void content. The main source of scatter was the prepreg itself but other sources of scatter could be changes in ambient conditions such as temperature or humidity or the outlife of the prepreg, which means that the layup properties change as a function of the material age. As such, an experimental approach using designed experiments was chosen. Designed experiments are able to reduce the number of necessary experiments and minimise the impact of random scatter on experimental results by employing statistics and prior assumptions for the expected results [107], for example normality of the results. The two main approaches used were full factorial designs (FFD), and central composite designs (CCD). FFD's allow the fitting of a linear regression model to the data. The model may contain the process variables or interactions between them, but depending on the nature of the system it can sometimes be assumed that the response of the individual variables is nonlinear. This is in particular true if the system operates close to its optimum where significant curvature can be expected. In this experiment case, the FFD can be augmented with centre runs to obtain an estimate for the nonlinearity, or a nonlinear model can be fitted. CCD's are basic nonlinear models that include linear effects and interaction effects as well as squared effects for process variables. A regression can be obtained for both models using a Gaussian least squares approach. The test matrix for the experimental setup used is shown in coded design units in Table 5. The units in Table 5 correspond to physical variables of the process via transfer functions. The significance of the entire model, as well as individual regression coefficients, was tested with

Table 5: Test matrix for designed experiments in coded design units.

Experimental Design	Test number	Consolidation Pressure	Heater Temperature	Ply Tension	Linear Speed
FFD+CCD	1	-1	-1	-1	-1
FFD+CCD	2	1	-1	-1	-1
FFD+CCD	3	-1	1	-1	-1
FFD+CCD	4	1	1	-1	-1
FFD+CCD	5	-1	-1	1	-1
FFD+CCD	6	1	-1	1	-1
FFD+CCD	7	-1	1	1	-1
FFD+CCD	8	1	1	1	-1
FFD+CCD	9	-1	-1	-1	1
FFD+CCD	10	1	-1	-1	1
FFD+CCD	11	-1	1	-1	1
FFD+CCD	12	1	1	-1	1
FFD+CCD	13	-1	-1	1	1
FFD+CCD	14	1	-1	1	1
FFD+CCD	15	-1	1	1	1
FFD+CCD	16	1	1	1	1
FFD+CCD	17	0	0	0	0
FFD+CCD	18	0	0	0	0
FFD+CCD	19	0	0	0	0
CCD	20	-2	0	0	0
CCD	21	2	0	0	0
CCD	22	0	-2	0	0
CCD	23	0	2	0	0
CCD	24	0	0	-2	0
CCD	25	0	0	2	0
CCD	26	0	0	0	-2
CCD	27	0	0	0	2

various methods of hypothesis testing. For the main model, an *F*-test was used with a 95% confidence level.

To test the significance of the individual regression coefficients t-testing was employed [108]. Specimens were manufactured from M21/35%/268/T800 prepreg [102]. Sample sets were obtained from an MTorres gantry ATL system at Airbus and an MTorres column ATL system at GKN. For the Airbus experiments 27 trials were conducted, allowing the fitting of the CCD model to the data to obtain a simple nonlinear regression. For the GKN experiments 19 trials

were conducted, allowing the fitting of the FFD model to the data. The machines and prepreg used were nominally the same although the prepreg was supplied with differing ply backing. For the trials at GKN prepreg was supplied with a white, rough, paper backing while the material for the trials at Airbus was supplied on brown, laminated and smooth, paper backing. The machines also operated at different line pressures and speeds. The maximum system pressure as read on the gauge on the layup head for the trials at GKN was $p = 5$ bar while it was $p = 8$ bar at Airbus. It was assumed that the force exerted by the head onto the laminate scaled with the system pressure. The maximum speed for the GKN machine was also slightly lower v = 50000mm/min compared to v = 60000mm/min at Airbus. Temperature and tension control were identical. Lastly, both trials were performed in a randomised order to minimise the effect of changes in the ambient conditions or other unknown sources of scatter as mentioned previously.

Once manufactured, samples were prepared for microscopy by polishing. Details will be given in Chapter 5. Imaging software [109] was used to analyse the developed micrographs and obtain the void results. The samples were analysed for their void content in three different locations of the sample cross-section. The reported void content is therefore the average of six measurements. The void content was chosen as a quality measure here, because vacuum void removal is commonly omitted in automated layup, which may result in higher voidage for the uncured laminate, and potentially the final part.

3.3.3 Experimental results

Table 6 shows the results from the trials with Airbus and a CCD is fitted to the data. For the CCD model all 27 responses are used with the test settings corresponding to the normalised test conditions, given in Table 5. Further, a statistical analysis of the CCD model is

Table 6: Test matrix for the trials at Airbus with machine settings and void fractions.

Test number	Consolidation Pressure [bar]	Heater Set Temperature [°C]	Ply Tension [%]	Roller Speed [mm/min]	***Uncured void content [%]***
1	4.4	55	55	35000	**26.7**
2	6.8	55	55	35000	**24.6**
3	4.4	85	55	35000	**18.9**
4	6.8	85	55	35000	**22.8**
5	4.4	55	85	35000	**22.3**
6	6.8	55	85	35000	**30.9**
7	4.4	85	85	35000	**12.6**
8	6.8	85	85	35000	**14.0**
9	4.4	55	55	45000	**16.5**
10	6.8	55	55	45000	**30.2**
11	4.4	85	55	45000	**26.0**
12	6.8	85	55	45000	**15.1**
13	4.4	55	85	45000	**21.9**
14	6.8	55	85	45000	**17.4**
15	4.4	85	85	45000	**23.7**
16	6.8	85	85	45000	**17.9**
17	5.6	70	70	40000	**16.2**
18	5.6	70	70	40000	**22.9**
19	5.6	70	70	40000	**23.1**
20	3.2	70	70	40000	**50.4**
21	8	70	70	40000	**34.1**
22	5.6	40	70	40000	**16.8**
23	5.6	100	70	40000	**16.5**
24	5.6	70	40	40000	**13.5**
25	5.6	70	100	40000	**18.1**
26	5.6	70	70	30000	**13.0**
27	5.6	70	70	50000	**18.4**

given in Table 7. For diagnostic purposes the residuals were plotted as a function of the run order in Figure 34 which allows for the identification of any bias to the data related to test time, for example due to aging of the tested material. This graph exhibits no trend for the residuals, and consequently no bias was expected as a function of the run order. Figure 35 shows the residuals of the CCD model as a function of the predicted responses and indicates whether data with an extreme response value, high voidage, may lead to skewed data. The residuals of

the predicted responses scatter randomly around zero and it was therefore concluded that the model was valid. To further improve the statistical significance the model was optimised by omitting insignificant regressors until a minimum of the root mean square error (RMSE) was achieved, as seen in Table 7.

Table 7: Statistical analysis for the un-optimised and optimised quadratic model for the uncured void content results from Airbus.

	CCD		CCD optimised	
R^2	0.76		0.74	
F_0	2.68		6.23	
p-value	0.05		0.001	
Model variable	**Regressor β**	**t-Value**	**Regressor β**	**t-Value**
Pressure	-1.19	-0.99	-1.19	-1.16
Temperature	-1.67	-1.40	-1.67	-1.64
Tension	-0.46	-0.38	-	-
Speed	0.27	0.23	-	-
Pressure/Temperature	-1.69	-1.16	-1.69	-1.35
Pressure/ Tension	-0.33	-0.23	-	-
Pressure/ Speed	-1.21	-0.83	-	-
Temperature/ Tension	-0.57	-0.39	-	-
Temperature/ Speed	2.07	1.41	2.07	1.65
Tension/ Speed	0.39	0.27	-	-
Pressure^2	5.17	4.08	5.17	4.77
Temperature^2	-1.23	-0.97	-1.20	-1.14
Tension^2	-1.43	-1.13	-1.43	-1.32
Speed^2	-1.48	-1.16	-1.48	-1.36

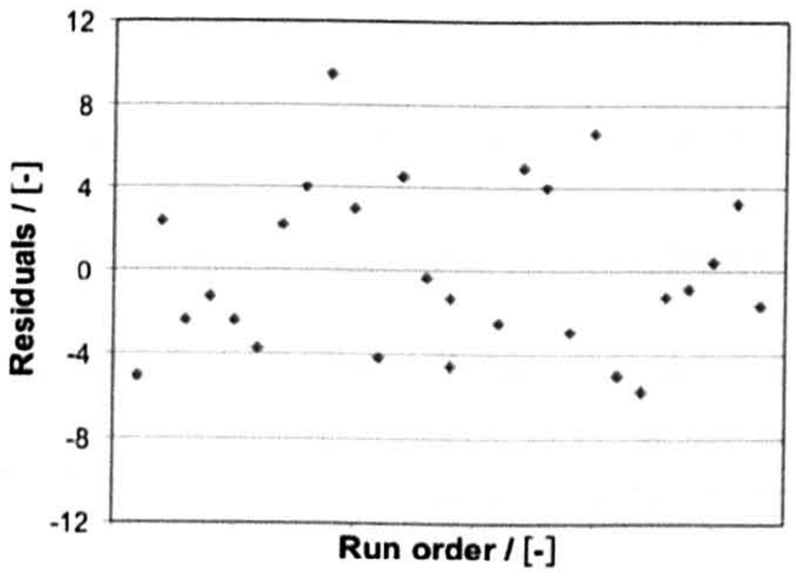

Figure 34: Residuals for the CCD model as a function of run order.

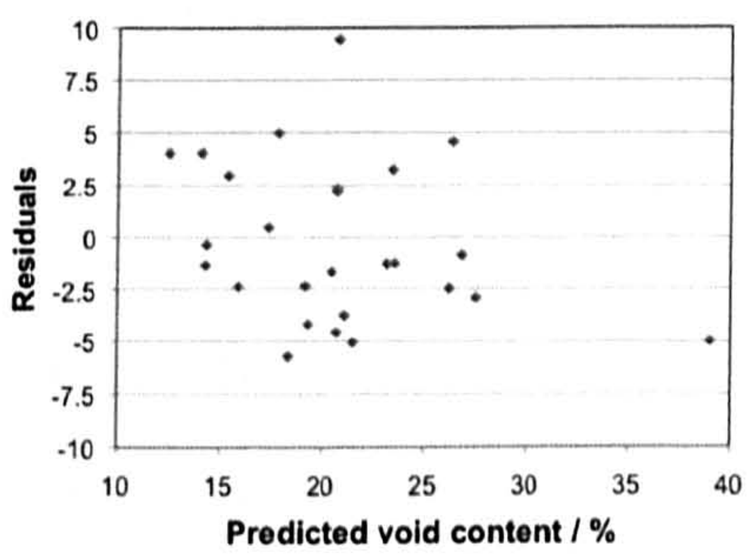

Figure 35: Residuals as a function of the predicted response for the CCD model.

A graphical representation for optimising the CCD model is shown in Figure 38 and omitting insignificant regressors, close to the straight line increases the model significance. The optimised model has a higher F_0 statistic than the un-optimised model by using less regressors. In both models it is evident, that a pressure-squared effect is dominant for the model. Extreme pressure values lead to high void content. This is illustrated by the response surfaces for the full CCD model in Figure 36, Figure 37 and Figure 39 to Figure 42. For the trials at GKN, 19 test laminates were manufactured and analysed for their void content as described previously. The trials at GKN differ from those at Airbus in the number of samples that were generated as well as the processing conditions that were employed as mentioned previously. The results of the trials are shown in Table 8. Since only 19 tests were conducted, the data was fitted with a linear Full-Factorial model with three centre runs. From the tests at Airbus it can be seen that the non-linearity is significant for ATL layup. However, the tests at GKN were conducted first, this information was not available when the trials at GKN were prepared. The available data from the trials at GKN were analysed and the model was optimisation but remained insignificant and could not be used to gain any insight into the impact of the process variables on the uncured void content. The method for void measurement was identical to the one employed for the laminates obtained from Airbus, where it yielded good results. Further details on these results are given in [110, 111]. A possible explanation for the problems with the GKN results was lower system pressure on the layup machine and the prepreg material that was employed. Other explanations can potentially be found in the modelling approach that was employed, due to the hitherto known strong non-linearity of the layup process. This would imply that a CCD model might in future better capture the curvature in the response.

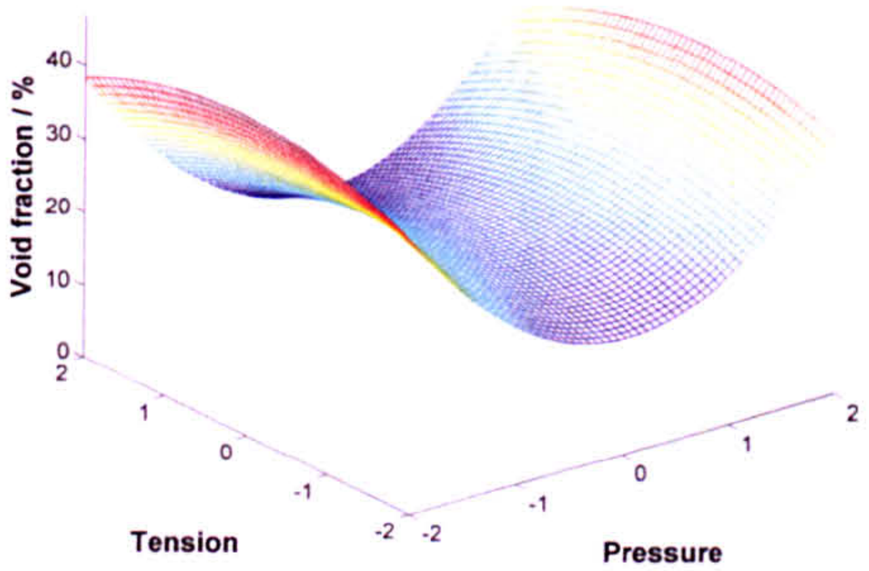

Figure 36: Uncured void content as a function of pressure and tension.

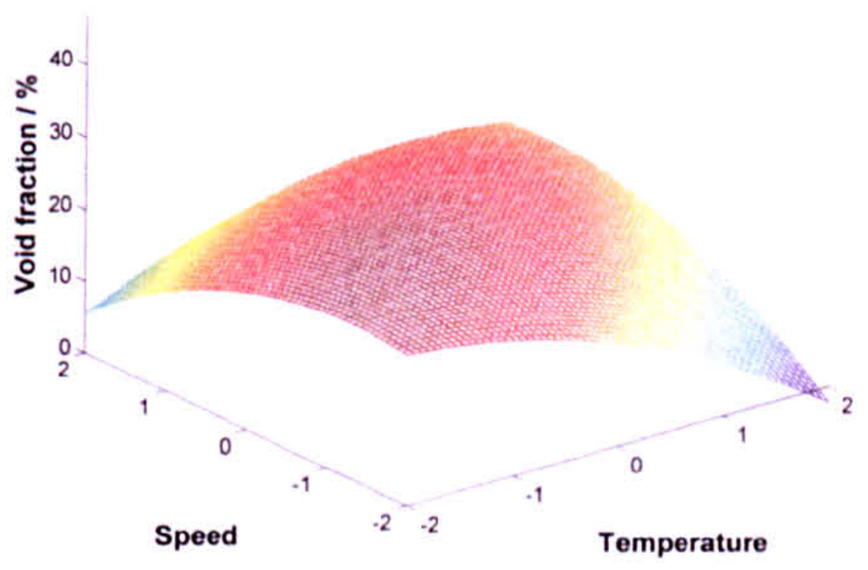

Figure 37: Uncured void content as a function of temperature and speed.

Table 8: Test matrix for the trials at GKN Isle of Wight with machine settings and void fractions.

Test number	Consolidation Pressure [bar]	Heater Temperature [°C]	Ply Tension [%]	Roller Speed [mm/min]	***Uncured void content [%]***
1	2.75	55	55	35000	**16.8**
2	4.25	55	55	35000	**8.3**
3	2.75	85	55	35000	**16.1**
4	4.25	85	55	35000	**17.7**
5	2.75	55	85	35000	**10.1**
6	4.25	55	85	35000	**11.1**
7	2.75	85	85	35000	**10.1**
8	4.25	85	85	35000	**14.0**
9	2.75	55	55	45000	**10.5**
10	4.25	55	55	45000	**14.0**
11	2.75	85	55	45000	**23.0**
12	4.25	85	55	45000	**5.4**
13	2.75	55	85	45000	**12.0**
14	4.25	55	85	45000	**11.0**
15	2.75	85	85	45000	**4.6**
16	4.25	85	85	45000	**17.5**
17	3.5	70	70	40000	**20.2**
18	3.5	70	70	40000	**25.8**
19	3.5	70	70	40000	**34.1**

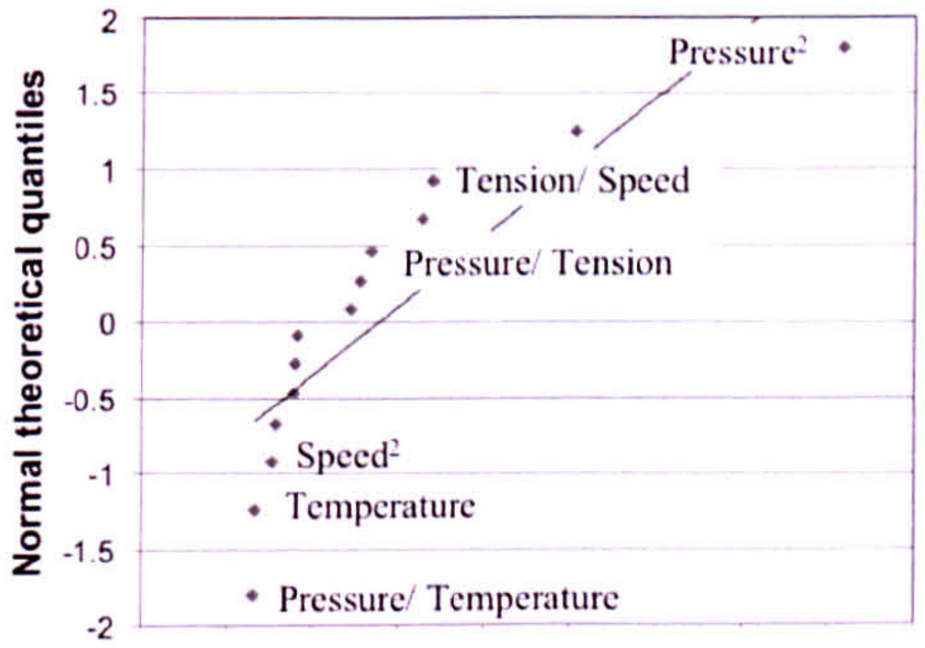

Figure 38: Normal distribution plotted over ranked regressors β from the CCD model.

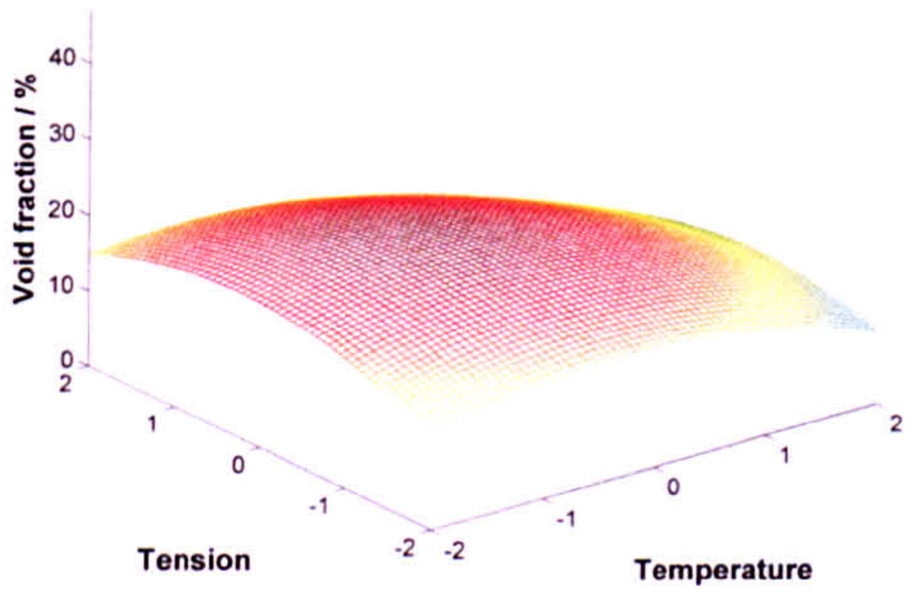

Figure 39: Uncured void content as a function of temperature and tension.

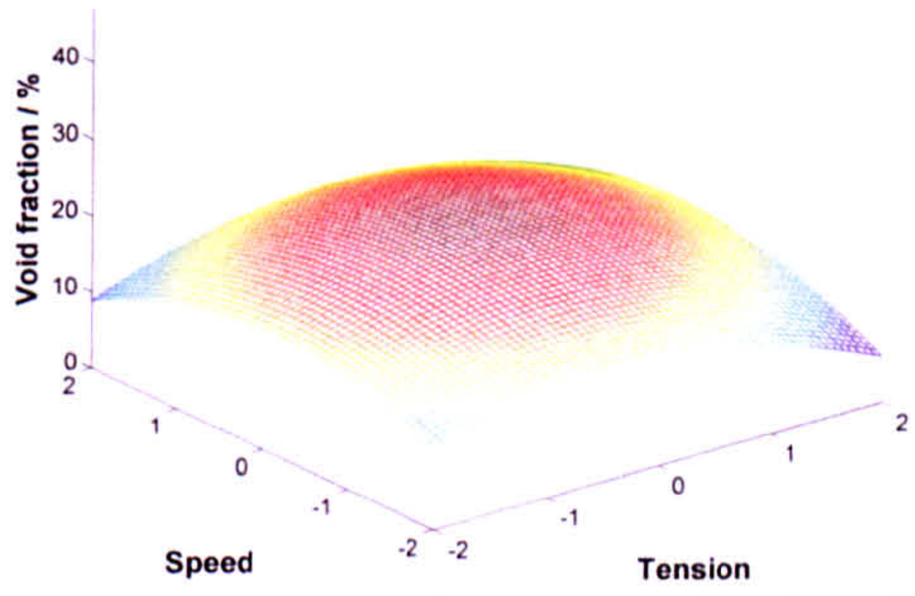

Figure 40: Uncured void content as a function of tension and speed.

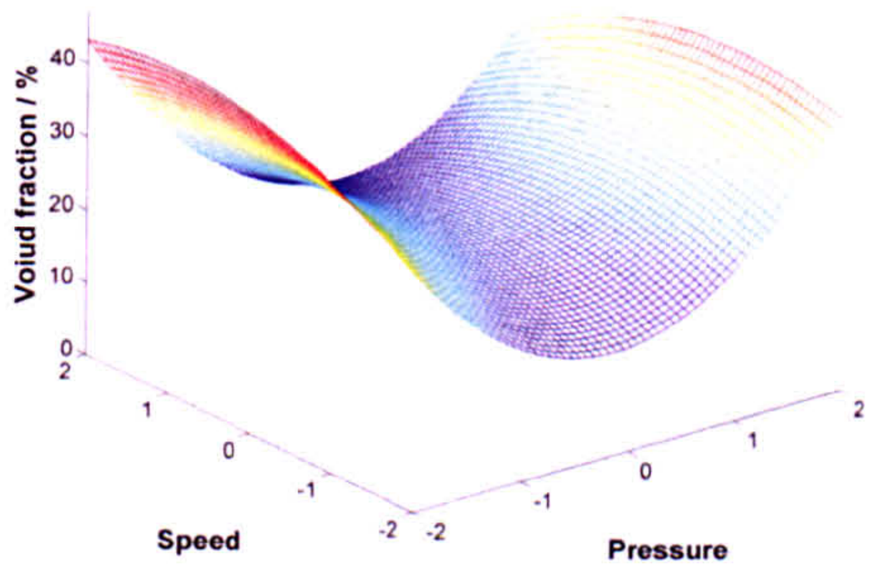

Figure 41: Uncured void content as a function of pressure and speed.

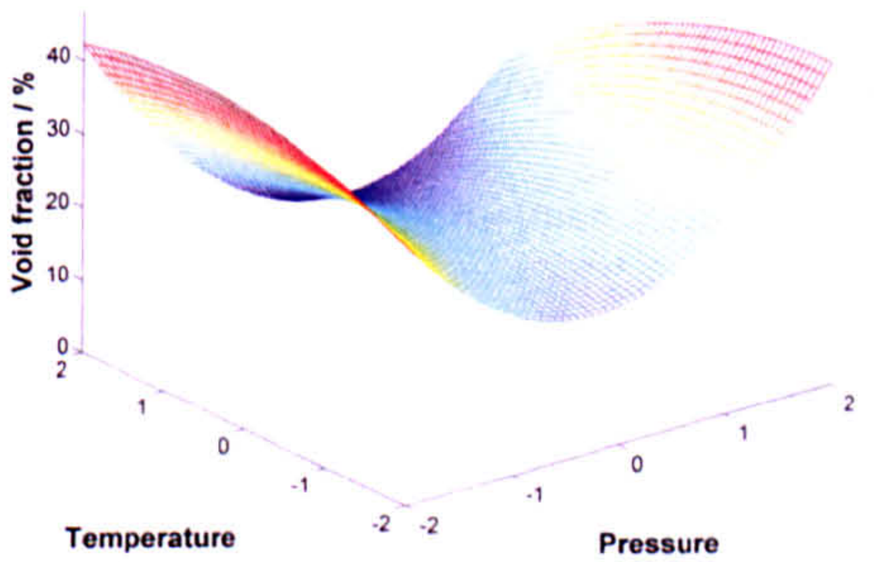

Figure 42: Uncured void content as a function of pressure and temperature.

3.4 Conclusions

An assessment of the productivity of automated layup processes has been given. ATL productivity was found to scale strongly as a function of part size, speed and secondary operations, i.e. scrap removal. AFP productivity scales as a function of the number of tows, their width and the time for material change. The results potentially challenge current conventions as they predict higher productivity for AFP layup than ATL [112]. Typically, manufacturing can only address secondary operations for ATL layup and the time for material change in AFP layup to improve productivity. Some recommendations were made to optimise layup rates for ATL and AFP, in particular by focusing on secondary operations and reduction of unproductive travel.

By improving secondary operations, ATL layup rates can potentially be improved by 20-30%, through addressing current scrap strategies and the time for cutting and starting plies. Higher accelerations may yield further improvements for small parts but further increases in linear speed are not beneficial for most part sizes. An exception would be wind-turbine manufacture, where the blades can now be more than 50m long [113]. For these long parts higher speeds may yield productivity improvements. For typical aerospace components, however, current speeds are sufficient. Lastly, multi-roll ATL could be an interesting option for improved layup rates if the increase in scrap rate does not result in an uneconomical process.

AFP layup rates can be improved in a number of ways and the potential benefits are higher as well, compared to the moderate increase in productivity achievable by optimising ATL layup. By laying more or wider tows, a linear increase in productivity is possible. Furthermore, addressing downtime can almost double AFP productivity. The two main areas for improvement are better material consistency, leading to less unscheduled downtime, and faster material changes, e.g. by automated splicing or rapid head changes.

Layup trials were conducted on two MTorres ATL systems to understand the layup process and in particular the process control. Layup quality was measured by quantifying the void content in uncured laminates. The results indicated that some improvements in layup quality can be achieved by using appropriate processing conditions, but the results were inconsistent, indicating a very low degree of process control and a high degree of material and process variability. Given the material quality, the manufacturing systems employed, and the procedures for sample analysis, the manufacturing models were very poor. This can only mean that most of the sources of variability are not within operator control, either because the machine is not controlled accurately enough or the prepreg variability is too high. The low impact of temperature control during layup was surprising as it was expected that temperature control would be critical for high tack. Figure 43 shows a plot of the layup point (nippoint) temperature over the setpoint temperature of the heater on an ATL head during layup. The x-

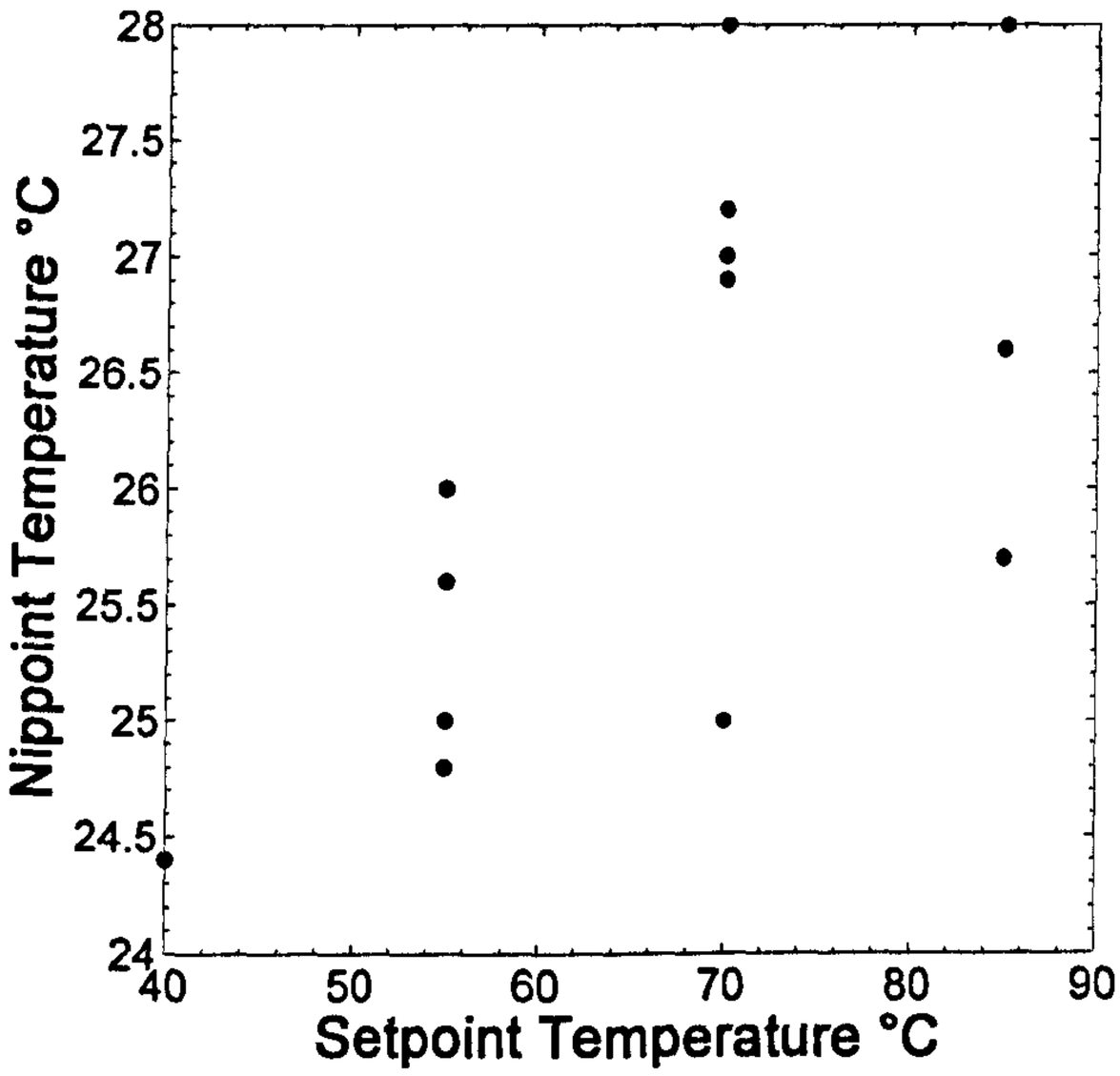

Figure 43: Temperature of prepreg during layup. The nippoint temperature is plotted over the control setpoint.

axis indicates the set temperature in the program; the y-axis indicates the measured tape temperature at the layup point as measured by a handheld laser pyrometer. The data indicates that higher temperatures on the heater lead to higher temperatures at the nippoint, although the heating is also vastly inefficient and poorly controlled. The following sections will therefore aim to address productivity issues during automated layup as quality issues. These quality issues can have three principal sources; material quality, the quality or level of control of the layup system, and the choice of correct processing conditions.

4 Development of a research-based layup system

4.1 Introduction

To improve layup processes it is desirable to test layup conditions, by modelling and experiment that are currently not achievable with existing equipment. Most automated layup systems are controlled using internal motor settings only, i.e. the machine is controlled in percentages of the total system capability. The latter is generally unknown to the user and while this does not pose problems in terms of program repeatability it militates against a scientific understanding and interchangeability of materials and processing conditions between different layup systems. A research-based layup system (R&D system) would instead have to take input in scientifically meaningful units and also provide feedback during operation with meaningful numbers. Section 3.2 has shown an experimental study of the influence of processing conditions on the final laminate quality. While this provides an insight into the layup process a lack of control and user feedback was found. Any subsequently developed process model will thus be hard to verify.

To address the desire for testing with higher accuracy and in a broad range of layup conditions, a bespoke layup research system was developed emulating the current layup process. A detailed description of the development and operation of this layup system will be given in the following section.

4.1.1 Preliminary design considerations

To emulate the existing automated layup process the forces and temperature changes experienced by the material during layup need to be replicated. A consolidation force is exerted

normal to the laminate while a layup head follows a predefined path at a set speed. The prepreg is supplied on a drum with single ply backing separating the plies from each other. The drum is fixed on a wheel mounted onto a drive, which can be located on the head or outside. The drive for the prepreg creel can be operated separately from the main head to adjust the tension on the material during layup. Material may be laid down under tension to improve the ply straightness and reduce gaps between plies, while layup over curved surfaces may require little or no tension on the tape to deliver the material successfully. If the material is mounted outside the head it needs to be fed to the head using appropriate guide systems while keeping the ply tension controlled.

During layup, a separate spindle takes up the ply backing. If the ply backing adheres strongly to the prepreg it needs to be removed under tension from the prepreg. For this purpose the backing spindle is driven to obtain a defined torque on the spindle, independent of the current lay-down speed. Certain material forms, e.g. slit tape for AFP layup, may be supplied without any backing. Instead the material is wound onto a bobbin in a helical pattern and is kept in storage, which may be cooled. This enables the plies to separate during layup at known and low force while preventing resin to stick to parts of the layup system.

Lastly, the tape is heated to increase tack and reduce ply stiffness. The material can either be heated directly on the head, prior to layup, or through the substrate in front of the head. A layup system replicating the current automated layup process would have to emulate these process characteristics, which are summarised as follows:

- Provide a user interface with input and output in scientifically meaningful numbers
- Deliver the material at controlled speeds of up to $v = 1\text{m/s}$, preferably higher.

- Exert an equivalent line load normal to the laminate of at least F_{nom} = 1000N over 300mm wide tape. This translates into a line load F_{nom} = 3.33N/mm. Higher loads should be achievable.
- Provide controlled tension or no tension on the backing paper.
- Deliver the prepreg material with controlled tension.
- Heat the tape continuously to at least T = 40°C. This corresponds to ΔT = 20°C with an accuracy of ±1°C. Higher temperatures are desirable.

4.1.2 Concept development

Most layup systems employ a movable head laying material onto a fixed tool or rotating mandrel. These layup systems are very flexible in terms of part geometries and ply orientations and they are therefore the standard configuration for most production environments. In most cases the material needs to be stored on the head, or in proximity to the head, which adds significant weight and leads to additional requirements for subsequent structures and grounding. Additionally, the added weight has a detrimental impact on machine dynamics.

By mounting the horizontal tool onto a linear drive, which is mounted onto another linear drive perpendicular to the former the same kinematics as for the moving head system can be achieved, i.e. a high flexibility regarding ply orientations. Additional technology on the fixed head, i.e. travel along the z-axis enables layup over more complex geometries and compaction control. Most fixed head layup systems are, however, limited to flat components. To simplify development of a layup system it was decided to develop a design that would integrate into a servo-hydraulic test-machine for accurate load control while also removing the need for another z-axis with additional control requirements. The test machine would have to

possess a large base to provide sufficient support to the additional structures, i.e. linear drives, while also allowing simple integration of said structures using existing mounting points.

An Instron Satec DX600 servo-hydraulic test machine with separate compressor was found to have a sufficiently sized base with integration points for a layup system. The machine consists of a compression section at the bottom, and a tension section between the middle and the top, see Figure 44. Integration points exist on the compression and tension side facilitating the integration of additional hardware.

Two initial concepts were thus evaluated for integration into the machine using either a moving tool or a moving head. A picture of the moving head concept is shown in Figure 45, while a picture of the moving tool concept in shown in Figure 46. Advantages of the moving head concept are a reduction of overall system length as well as a simplified tooling design. Furthermore, the linear drive is sufficiently stiff to deliver the desired compaction force over the entire length without bending excessively. Disadvantages of this concept include a difficult integration of all components into a small head, restrictions regarding the amount of material that can be stored and difficult wiring for additional motors and heating mounted onto the moving head.

Advantages of the moving tool concept include a simplified head development, which is spatially fixed, increased space for material storage and the possibility to utilize a smaller linear drive in conjunction with guide rails to optimize system stiffness and dynamics. Potential disadvantages are the higher overall length of the system and the potential for excessive bending of the tool during testing. An overview of the advantages and disadvantages of both design concepts, including a score based assessment, is given in Table 9. The two systems are evaluated with respect to current industrial ATL systems, which are used as a baseline. Baseline performance is denoted with an 'O', improvements are evaluated with '+' and '++', and

Figure 44: Picture of the Instron Satec 600DX showing the compression and tension section

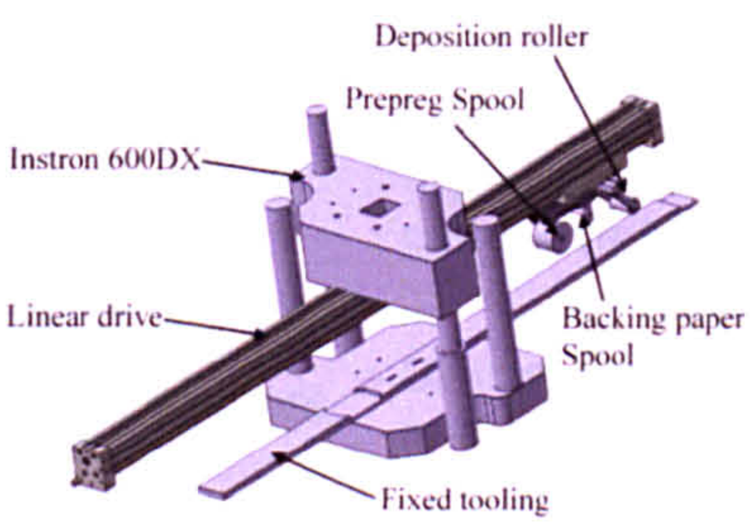

Figure 45: Drawing of a moving head concept in the compression section of the Instron 600DX.

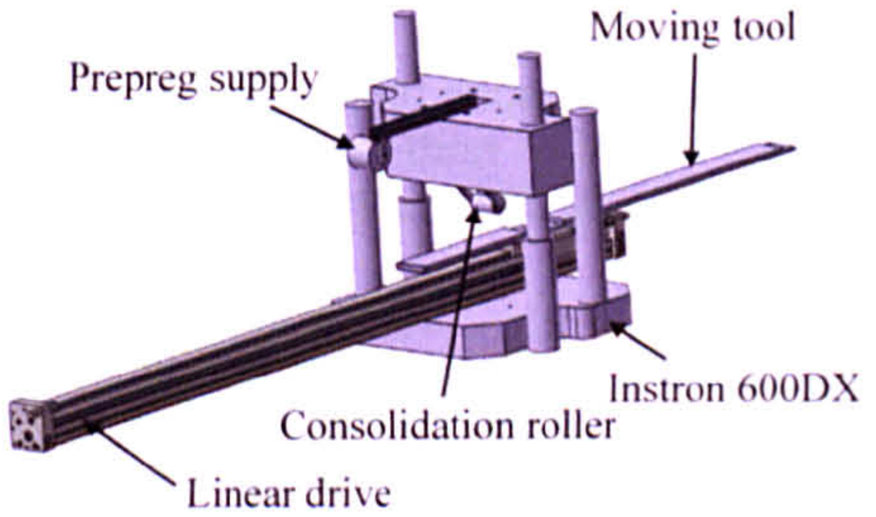

Figure 46: Drawing of a moving tool concept in the compression section of the Instron 600DX.

degradation with '-' and '--'. Overall, both concepts offer significant improvements over existing industrial layup equipment due to their specific and simplified design. The biggest drawback for both systems is the difficult manufacture of arbitrary ply orientations and the need to include a secondary axis to allow tow steering. Absolute improvements over existing systems are provided by improved means for rapid heating, high and accurately controlled loading of the tape under a consolidation roller and high dynamics due to low mass. Comparing the two design concepts against each other, it is apparent that the moving tool concept is simpler and likely to be cheaper than the moving head concept. The major drawback

Table 9: Overview of the advantages and disadvantages between the two main design concepts for an automated layup research system.

	Moving head		**Moving tool**	
Item	Comment	Score	Comment	Score
Load control	On Instron 600DX	++	On Instron 600DX	++
Temperature control	Infrared heater, size restrictions and advanced control required, short heating time	O	Infrared heater, limited size restrictions and simplified control, longer heating times	+
System acceleration	Limited by weight of the head and torque of the motor	O	Tool likely lighter than complete head, consequently higher acceleration	+
System speed	System speed governed by working envelope and acceleration, likely higher than current 1m/s baseline	++	System speed governed by working envelope and acceleration, likely higher than current 1m/s baseline	++
Head development	Difficult, moving head, many components	-	Simple, fixed head facilitates integration	+
Head Mass	High, detrimental impact on acceleration	-	Not relevant for dynamics	O
Head stiffness	High, due to linear drive	+	High due to Instron Integration	+
Tool stiffness	Fixed tool, not relevant	O	Bending expected, may exceed constraints	-
Tool mass	Not relevant	O	Intermediate, may have impact on acceleration	-
Wiring	Difficult, needs cables moving with the head	O	Simple, cables are fixed	+
Ply orientations	Arbitrary ply orientations by rotating tool section	O	Arbitrary ply orientations by rotating tool section	O
Tow steering	Not possible, requires another axis	-	Not possible, requires another axis	-
Cost	Significantly cheaper than existing systems	+	Potentially cheaper than moving head system	++

of this design is the lack of stiffness of the tool during compression loading which can lead to excessive bending. By simply using a thicker tool or different material the weight may increase to such an extent that the maximum acceleration may be affected detrimentally. This point needs to be addressed carefully in the following detailed design study.

4.2 Detailed mechanical system design

The previous section found a moving tool concept to be the best solution for the requirements stated in section 4.1.1 for a research layup system. The Instron DX600 test machine is a high load test machine with a $F = 600$kN test range. In the loading range around $F = 1$kN it is therefore inaccurate. A smaller load cell with a $F = 27$kN range was therefore set up with the controller to provide accurate load control during consolidation testing. This load-cell is integrated into the compression section of the Instron test machine and has the consolidation roller attached to it. A picture of the detailed design is shown in Figure 47, the assembled machine can be seen in Figure 48 and Figure 49. The main system consists of a tool attached to a linear drive. This x-axis is mounted into the compression section of the linear drive together with the consolidation roller and load-cell, which is not shown. A ply backing spindle is located behind the consolidation roller to continuously take up the backing material. Prepreg is delivered from the top, the lower side of the tension section, from a driven spindle and delivered past a heating zone. A ring that compresses the paper core fixes the prepreg on the delivery creel. The design of the creel is aimed at reducing mass and inertia by using an angled spoke design. The heating zone consists of a medium wavelength infrared heater. During layup the prepreg is clamped onto the tool with a bracket. To enable layup of different ply angles the tool is designed with a hexagonal pocket. Aluminium or glass plugs can be placed

in the pocket to define the test section. By rotating the plug, different ply angles can be manufactured. For the raw prepreg supply, slit ATL tape was identified as the most reliable and cost effective option. The raw material is supplied on a 290 mm paper core with approximately 240m linear material lengths. This typically translates into an outer diameter of $d \approx 600$mm for the raw material. The material is 75mm wide.

To accurately move the tool, it is mounted onto the sled of a linear drive. For the detailed design study a Bosch/Rexroth MLR 10-110 linear drive was selected. The total length of the tooling is $l = 1.5$m. The test section is located in the middle of the tool and is 160mm wide. As a first concept, the load, exerted normal to the tool, is borne by the sled alone. Tool and sled are assembled in the middle of the tool length-wise. The rough length of the sled is

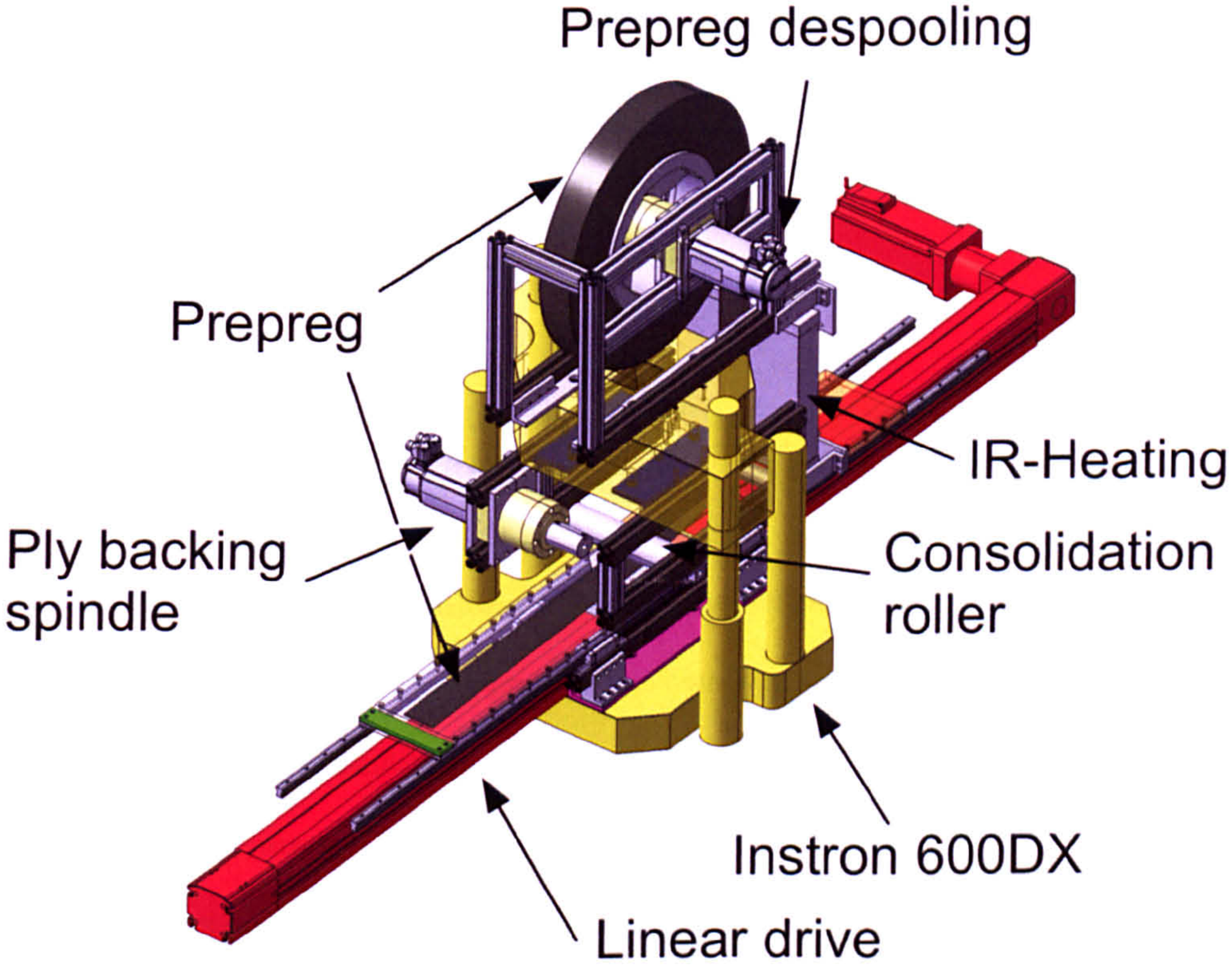

Figure 47: Digital model of an automated prepreg layup system for material research.

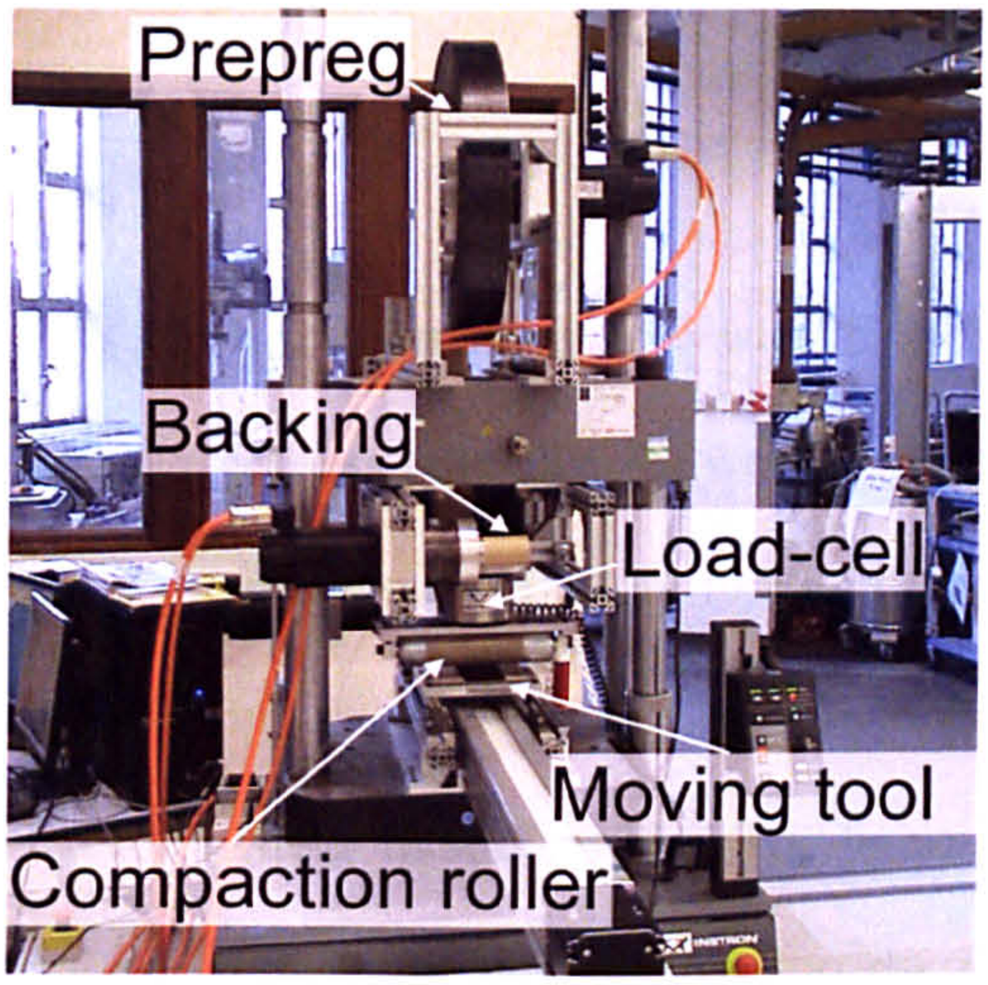

Figure 48: Picture of the assembled layup machine.

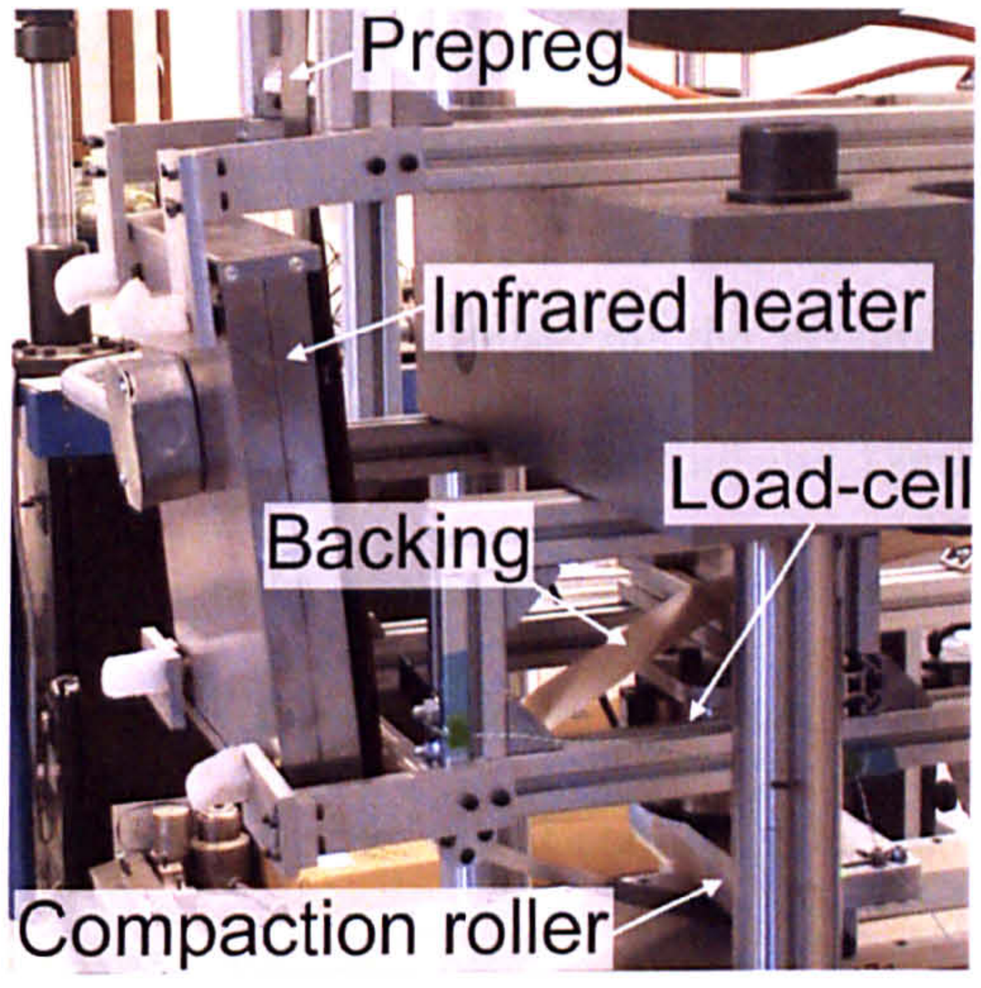

Figure 49: Close up of the heating and prepreg delivery.

expected to be around 300mm, which gives an unsupported length of L = 600mm in both directions. For a material width of 75mm a maximum load of F = 500N was defined which is equivalent to F = 2kN for 300mm wide prepreg. The bending moment at the end of the tool is M = 300Nm. For a given deflection constraint the required material thickness can be calculated from the Euler-Bernoulli beam equations to be [114]

$$w(x) = \frac{Fx^2(3L - x)}{6EI} + \frac{qx^2(6L^2 - 4x + x^2)}{24EI} \tag{4-1}$$

The first part of the right-hand side gives the deflection due to a load F, while the second part is the deflection of the beam under its own weight. Here we would like to limit the deflection at x = L and calculate the corresponding required material thickness and tooling mass, subject to constraints. The tooling mass should not exceed m = 10kg to avoid a detrimental impact on acceleration. For x = L equation (4-1) simplifies to

$$w(x) = \frac{8FL^3 + 3qL^4}{24EI} \tag{4-2}$$

For an aluminium tool with E = 75,000 MPa and ρ = 2700kg/m³ the maximum material thickness regarding the weight constraint is 25mm for a 100mm wide tool and 12mm for a 200mm wide tool. For the 100mm wide tool the maximum displacement at the tool end is w_{100} = 0.1mm and for the 200mm wide tool w_{200} = 0.2mm. The total bending moment is M_{100} = 324Nm for both tool widths. The linear drive specified for the initial concept tolerates a bending moment of M_l = 305Nm on the sled, which is exceeded by the expected bending moment stated above. A novel design supporting the outside of the tool with guide rails and a small linear drive (as opposed to specifying a larger linear drive) was found to be a cost effective solution for this application. Guide rails support the loads normal to the tool, while the acceleration would be provided by the linear drive as shown in Figure 47.

The moved mass of the drive is m_d = 3.3kg, the tool mass is m_t = 10kg and the total weight of the guide rails is m_g = 9.6kg. Total moved mass is thus m_t = 22.9kg. Additionally, the load normal to the tool will result in a force opposing the acceleration and movement of the drive due to some friction between the compaction roller and prepreg material. The effect of this load is unclear and cannot be approximated. For an ideally free rolling compaction roller it will be zero. For a flexible compaction roller it is expected to be significantly higher due to the energy dissipated during deformation of the roller. The design was thus limited to stiff, metallic roller for the initial tests to reduce the load resisting the movement of the tool.

The MLR 10-110 linear drive was specified with a reduction gearbox of i = 5, resulting in a maximum torque on the drive for acceleration of the sled and tool of M_t = 16Nm. The specified motor for the linear drive is an MSK061C-300. To achieve maximum torque it is limited to n = 2500rpm. With the lead constant of the linear drive of 57.92mm/rev this gives a

theoretical maximum speed of v = 2.4m/s. The inertia of the entire system is approximated from

$$J_s = \frac{1}{4} m_L D^2 , \tag{4-3}$$

with a drive wheel diameter of 140mm this gives J_s = 0.1122 kgm². The approximate angular acceleration of the drive is

$$a = \frac{M_d}{K_s \cdot J_s} , \tag{4-4}$$

with K_s being a safety factor of 2. The acceleration thus is α = 71rads^{-2}, or with the lead constant of the linear drive a = 26ms^{-2}. Any friction between the prepreg and roller will result in a reduction of the effective acceleration, as the total torque provided by the motor has to overcome the inertia of the system and the loads opposing the movement. Given a theoretical maximum speed of v = 2.4m/s the required acceleration can be calculated using the tooling dimensions. The total length for acceleration is l_a = 670mm, or approximately 600mm. The necessary acceleration can be calculated from

$$a = \frac{v^2}{2s} , \tag{4-5}$$

with s being 600mm. The required acceleration to reach the maximum speed over the given distance is a = 4.8ms^{-2}, around 20% of the theoretical system acceleration. The selected solution using an MLR 10-110 linear drive with an MSK 061C-300 can thus be considered adequate to meet the performance and loading requirements of the x-axis.

The delivery head components are integrated into the upper part of the compression section and the lower part of the tension section of the test machine. The prepreg is delivered

from the top into the gap between the tool and the roller and backing paper is removed prior to delivery. To deliver the material it is mounted on a creel attached to a motor. Similarly, the backing has to be taken up continuously under tension using a spindle with an attached motor. To simplify the system, identical motors were chosen for both winding applications. For this application two MSK050C-450 motors were selected. The maximum torque of the motor is M_{max} = 15Nm and the maximum speed is n = 6000 min^{-1}. To ensure that the system operates correctly under all test conditions the two spindles need to be able to accelerate at least as fast as the linear drive unit. At the same time, both spindles should be capable of achieving the same maximum speed during testing. If the material on the creel is at its minimum rotary speeds required to match the linear drive speeds are at their maximum. Prepreg is supplied on a core with d_{ID} = 290mm inner diameter and 12.5mm core thickness to give d_{OD} = 315mm. The initial design of the backing spindle is d_{OD} = 50mm. The surface speed of the rotating body can be calculated from

$$\omega = \frac{v}{\pi \cdot d}, \tag{4-6}$$

with ω being the angular speed in revolutions per second and d the outer diameter of the rotating body. The maximum speed of the linear drive is v_{linear} = 2.4m/s, for this speed the angular speed of the prepreg creel is $\omega_{prepreg}$ = 2.37 rps and of the backing creel $\omega_{backing}$ = 15.28 rps. To achieve the desired acceleration, both drives are fitted with a gearbox with a 12:1 transmission ratio, i.e. n_{Output} = 500 min^{-1} or ω_{Output} = 8.33 rps. The required angular speed on the backing creel is greater than the maximum angular speed of the gearbox. The entire system is thus limited due to the maximum angular speed on the backing creel. The output angular speed translates into a maximum linear speed of the tool of v = 1.3 m/s. To achieve higher speeds, i.e. the maximum linear speed of the system, the backing creel diameter would have to

increase from 50mm to $d_{creel} > 92$mm. Additional consideration needs to be devoted to torque control. The tolerance on the torque control is $\Delta M = 0.1$Nm. For a set tension on the tape the amount of torque on the drive decreases with increasing diameter, i.e. the relative impact of the absolute torque tolerance decreases. This means that the spindle for taking up the ply backing should be as narrow as possible to maximize accurate force control. For the initial testing the diameter was kept at 50mm.

Due to the high torque that can be transferred between the gearbox and the spindle, the gearbox shaft is modified with a keyway to reduce dead movement and improve torque transfer. The inertia of gearbox is $J = 2.56\text{x}10^{-4}$ kgm^2 and of the motor $J = 3.30\text{x}10^{-4}$ kgm^2. The mass of the backing creel is $m_{backing} = 0.34$kg and the inertia is approximated to be $J_{backing} = 1.26\text{x}10^{-4}$ kgm^2 from the digital model. The mass of the prepreg creel is $m_{prepreg} = 6.50$kg and the inertia approximated to be $J_{prepreg} = 0.101$kgm^2. With these values the maximum angular acceleration calculated from equation (1-4) on the backing creel is $\alpha_{backing} = 197498$rads^{-2} and for the prepreg creel $\alpha_{prepreg} = 885.95$rads^{-2} or $n = 140$ s^{-2}, i.e. both drives accelerate at least 5.5 times faster than the linear drive. The two motors and gearboxes thus meet the performance requirements for the design. The overall system speed is reduced from $v = 2.4$m/s to 1.3 m/s due to the diameter and gear ratio of the backing spindle.

To heat the material continuously a medium wavelength infrared heater is specified. The material is heated over a length of $l = 0.3$m. The required heating power can be calculated from

$$P = \frac{m \cdot c \cdot \Delta T}{t \cdot \epsilon}, \qquad (4\text{-}7)$$

with c being the specific heat capacity and ε the emissivity of prepreg. The typical mass flow m/t at maximum speed can be calculated to be 0.08kg/s, the emissivity of prepreg is 0.8 [41], the specific heat capacity c = 930 $Jkg^{-1}K^{-1}$ [41] and ΔT = 15K. For these values the required heating power is P = 1380W. This heating power needs to be concentrated on the tape area. A Watlow Raymax 1330 infrared heater was identified as a cost effective solution for the heating requirements. The heater has a heated area of 322.6x305mm and a heating output of 3060W, i.e. the approximate heating power concentrated on the tape is P = 765W. The maximum allowable speed for continuous heating of ΔT = 15K is v = 1.3m/s, see Table 10. It is believed that the actual heating power will be higher than calculated here due to convection heating and irradiation heating from the sides, however this needs to be established experimentally.

Depending on the desired operation, high heating rates as well as high layup rates with limited heating can be achieved. The temperature in the heating area is measured with a thermocouple at the end of the heating area. This is only a point reading and the relationship between heater temperature and prepreg temperature at the nip-point needs to be established.

To simplify temperature control the distance between the upper point of the heating zone and the nip-point are matched to the tooling length before the test section, i.e. the lead in

Table 10: Overview of the maximum temperature rise on the tape as a function of layup speed.

Speed [m/s]	Heating time [s]	Mass flow [kg/s]	Maximum temperature rise ΔT [K]
0.17	1.93	0.0055	117.3
0.33	0.97	0.0110	58.7
0.50	0.64	0.0166	39.1
0.67	0.48	0.0221	29.3
0.83	0.39	0.0276	23.5
1.00	0.32	0.0331	19.6
1.17	0.28	0.0387	16.8
1.33	0.24	0.0442	14.7
1.50	0.21	0.0497	13.0
1.67	0.19	0.0552	11.7

of the tooling is 670mm and the distance between the upper end of the heating zone and the nip-point is the same. This means that the tape in the test zone can be delivered at a temperature that can be achieved for continuous heating for a given speed and temperature setting. This should mitigate issues regarding over-heating after tape stop and time for heating-up of the infrared lamps.

4.3 Electrical systems

The electrical system consists of control and power supply for the three motors and control and power supply for the heater element. These are integrated into a single cabinet to utilize the same switches, relays and safety controls, see Figure 50. The actual enclosure is 600x600mm wide and high and 350mm deep. The main motor controller units are a single Bosch/Rexroth Indradrive HCS02 with an advanced control unit as master and two Indradrive HCS01 slaves with multi-ethernet connectivity. The slaves need to be spaced apart by 10mm due to cooling requirements. The communication protocol between master and slaves is SercosIII. This is a real-time capable protocol for advanced control. External communications with a personal computer running the control software are either running on serial connection or Multi Ethernet. An overview of the wiring of the mains connections is shown in Figure 51. Each motor controller is connected to a line filter which is connected to an outside main connection with U = 415V and I = 18A. The control voltage for the three motor controllers is U = 24V DC, which is provided by a laptop power supply at the top right of the cabinet. Resistor brakes are integrated into the controller units, which results in a high amount of heat

dissipated in the cabinet. To force cool the entire cabinet and all components inside a fan with an airflow rate of V/t = 1860 m^3/h was installed. Heater control is assembled on the left side of the cabinet. A single-phase transformer provides U = 24V AC for the heater control. The controller is connected to a solid-state relay that switches the single-phase power supply to the controller. A PID controller at the outside of the cabinet operates the heater.

Currently, temperature control is associated with a significant lag between start and finish of heat-up and this needs to be addressed in the future. To ensure that the desired temperature is achieved during sample layup, a thermal camera is used to monitor the compaction zone under the roller. To ensure safe operation all systems are turned on and off with a central switch- connector connected to the cabinet door. If the door is released, i.e. opened during operation all three-phase and single-phase power to the cabinet is disconnected. Additionally, if the door is closed and the main unit is connected to a single-phase power

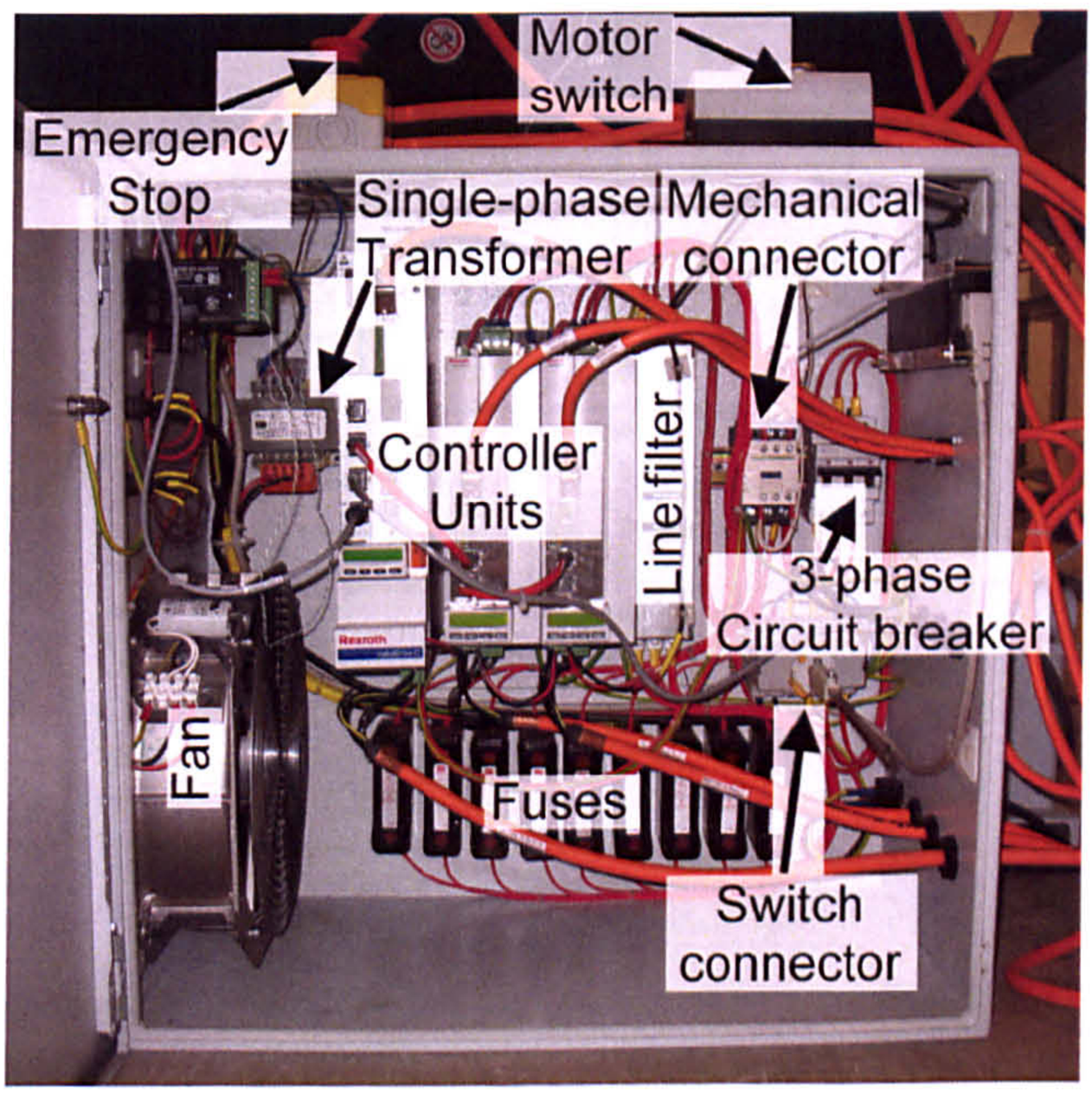

Figure 50: Control cabinet with key units highlighted.

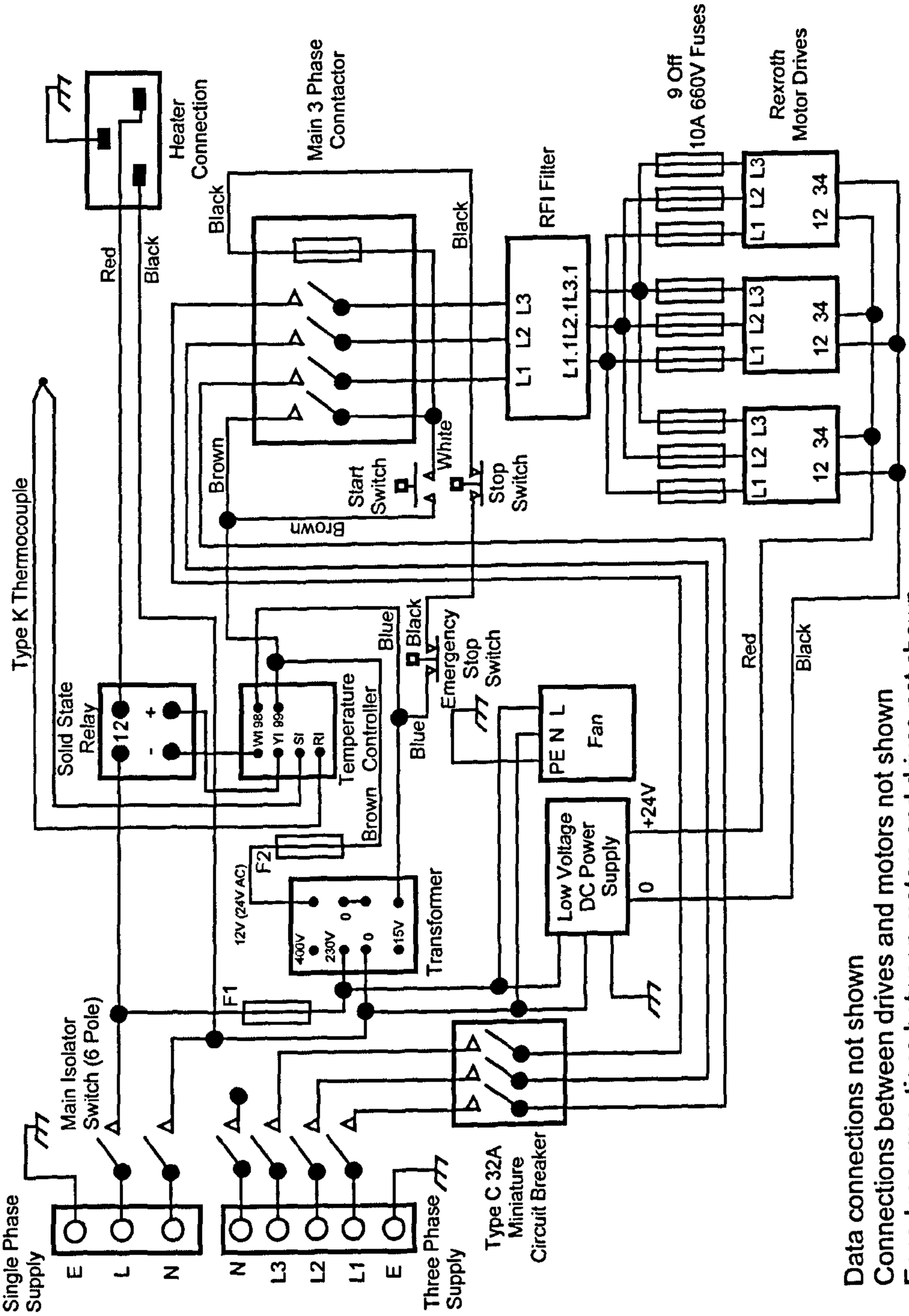

Figure 51: Wiring diagram of the control cabinet. Signal connections are excluded.

supply the fan will automatically run, irrespective of the remaining components, to ensure that the components do not overheat.

A start/stop switch for the motors and an emergency stop are located outside the main cabinet. Both disconnect the motor power supply using a three-phase contactor. The motor controllers can additionally be connected to the three-phase contactor for safety purposes, but this option was not used here. If the software should fail during a test it is therefore advisable to promptly disconnect the motor controllers by pushing the emergency stop.

4.4 Control software

The control software is executed on a programmable logic controller (PLC) in the motor control master. The PLC supports all IEC61131 programming languages, i.e. structured text, instruction list, ladder diagram and function block diagram. The advantage of this approach is that all programming languages are interchangeable, i.e. the main program can be any of the above types and may contain sub-programs in any of the programming languages. Additionally, the program has support for internal visualization on the PC. The machine can be operated entirely from this user-interface making it accessible to users without prior knowledge of the actual hardware and software.

The main program is written in structured text and function blocks. The input and output variables are linked to the visualization interface. Since all motion is linked to the movement of the linear drive this is reflected in the software. The linear drive operates in positioning mode, i.e. a target position, target speed and acceleration and deceleration profile are prescribed, the motor controller then ensures the correct operation of the motor subject to the motion profile. The linear drive has two operating modes, one for the layup test and a

second one for return to start. To run a test, the target position and speed are defined in the user interface. The test is then executed if the linear drive is at the start position. This also sets the prepreg delivery and backing creel into motion to continuously deliver material and rewind ply backing. All these motions are defined as positive motion. To return to the start at the end of a test, a button is available which returns the tool to the start position. This also operates the prepreg delivery and backing spindle, which now rotate in negative direction to rewind material and backing.

Material from the top is delivered in a synchronized motion, i.e. the mass flow of material from the top to the tool and under the compaction roller are held constant. The linear speed and acceleration of the tool are calculated into an angular speed and rotation using the prepreg delivery geometry and material data. The material data need to be provided by the user prior to start by entering them into the user interface. The core diameter, material height and ply height (including backing) needs to be entered. The system updates the total prepreg diameter as the function of the number of revolutions, i.e. as material is delivered the diameter decreases and angular speed and acceleration increase to match the speed of the tool.

Ply backing is rewound under controlled tension. Additionally, the ply spindle has to match the speed of the linear drive, i.e. the required torque is changing as a function of the test speed and the motion profile of the linear drive. The tension that is applied is defined as the force normal to ply and backing at the point of separation. This load is limited to a range between 0-10N. The angle between ply and backing at the separation point is $\alpha = 60°$. The normal force can thus be calculated into a tape tension, which needs to be applied onto the tape by the backing spindle. This is defined as over-torque. This torque can then again be calculated using the prepreg creel geometry. The ply backing is thin, but the typical revolutions on the backing creel are high, i.e. the backing creel diameter may change significantly during

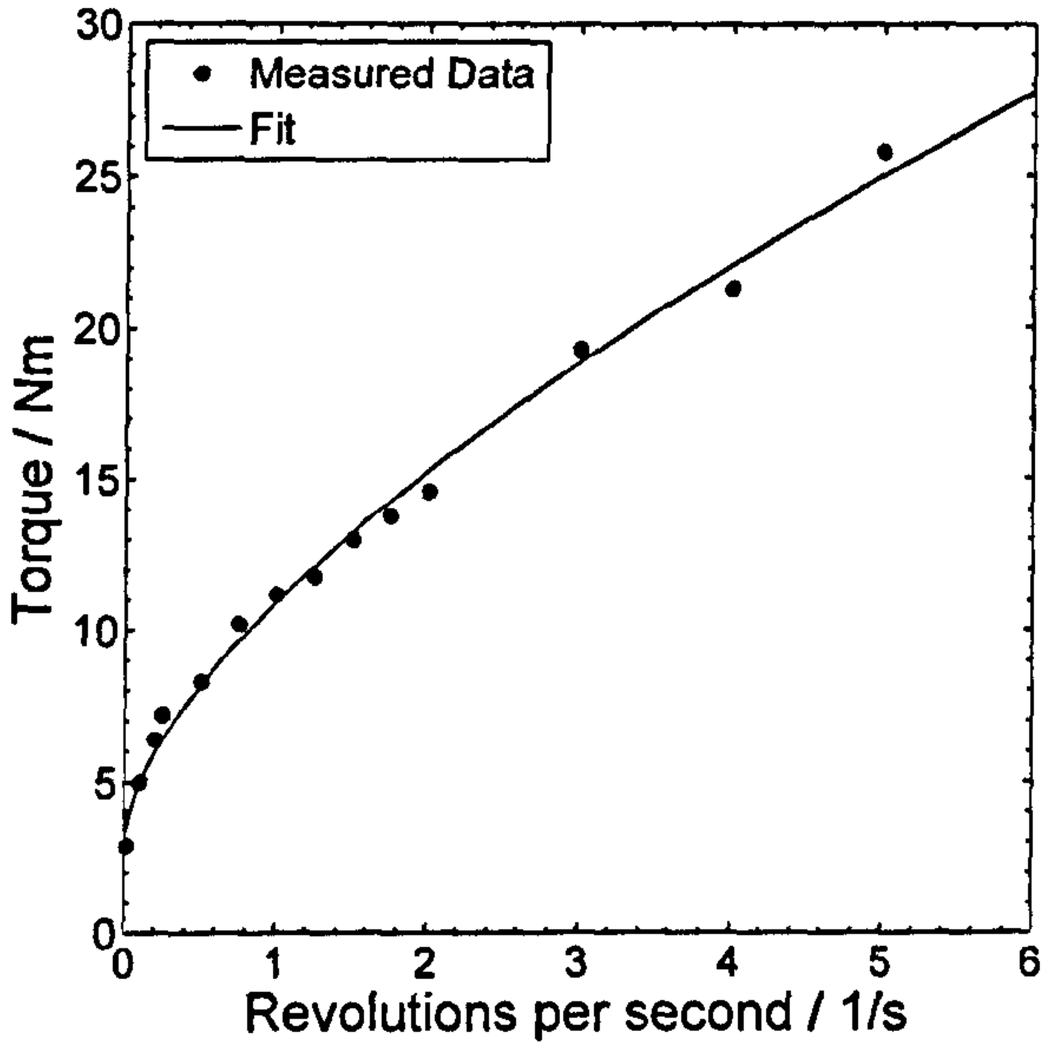

Figure 52: Torque applied to the backing creel as a function of the number of revolutions.

testing. The backing creel diameter is thus updated as a function of the number of revolutions; in this case the diameter increases. The total torque on the backing creel is the sum of the set torque for a certain speed and the over-torque. To measure the torque as a function of the backing creel speed, a digital oscilloscope was connected to the motor. The torque as function of speed was recorded for $t = 8192ms$. The measured data were then averaged. Figure 52 shows the recorded torque as a function of the spindle speed. An exponential function of the form

$$M_{speed} = (a \cdot \omega^b) + \omega_0 , \tag{4-8}$$

was fitted to the measured data. The total torque is thus the sum of the torque required to match the tooling movement and the over-torque defined in the user interface for the separation tension.

4.5 Discussion

To verify the correct function of the machine commissioning trials were conducted, were particular attention was given to the heating and compaction loading. The load over the test section was recorded for several different layup speeds and loads, see Figure 53 and Figure 54. Load control was within ±10% of the nominal load, but tended to yield spikes at higher loads, which were attributed to vibration in the system. The load cell was thus modified to be stiffer, which reduced the spikes and yielded improved accuracy at increasing layup loads.

To calibrate and verify the heating control a thermal camera was used, as shown in Figure 55 and Figure 56. Initially, the temperature uniformity was checked and the heater temperature was correlated to the tape temperature. In a second step, the heater temperature was calibrated against temperature readings from a laser pyrometer of the prepreg tape in front of the nip-point. The corresponding temperature drop was then used to calibrate the additional

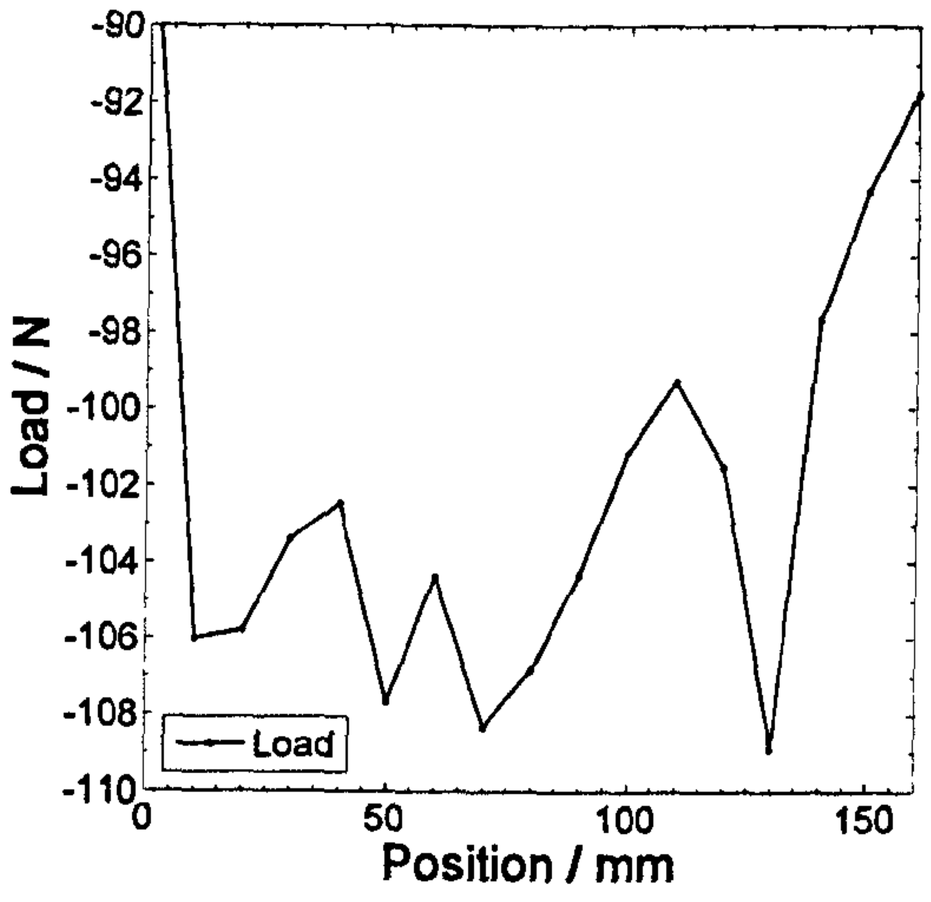

Figure 53: Load control during layup over the test section at a layup speed of 0.1m/s with a nominal load of 100N.

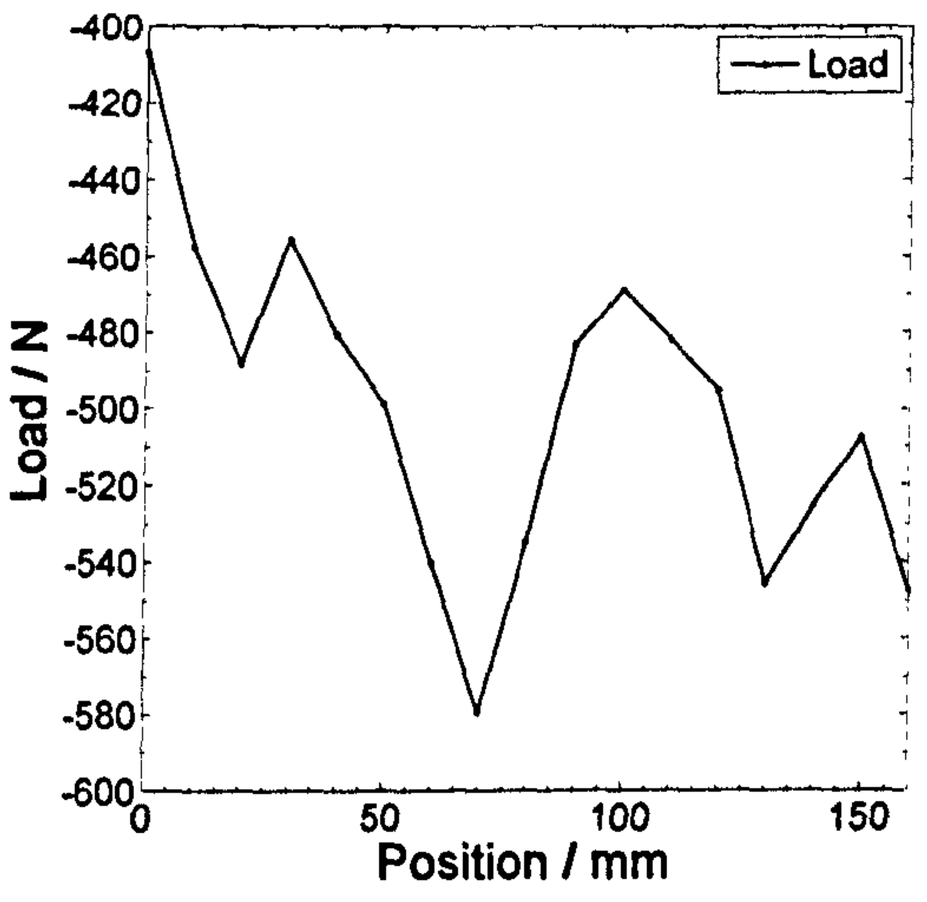

Figure 54: Load control during layup over the test section at a layup speed of 0.1m/s with a nominal load of 500N.

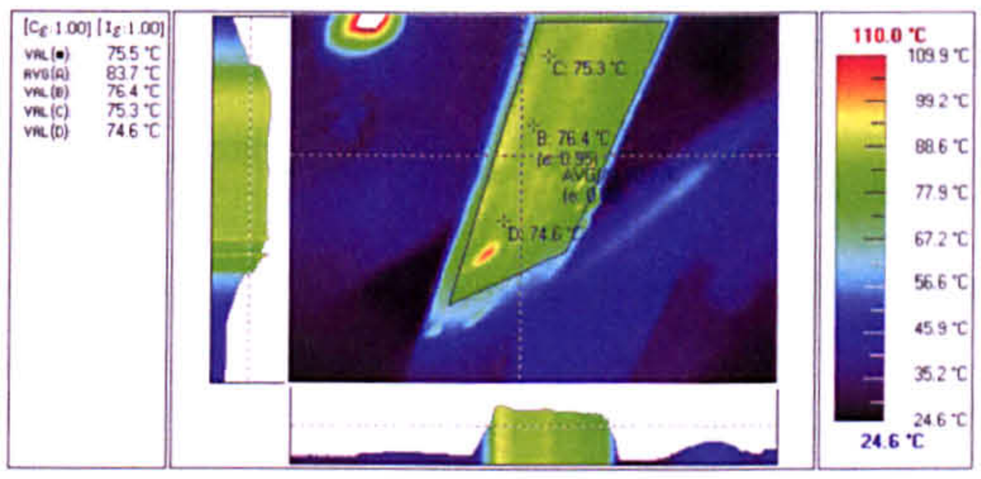

Figure 55: Thermal image of the prepreg in front of the heater at 17.5% heater power output.

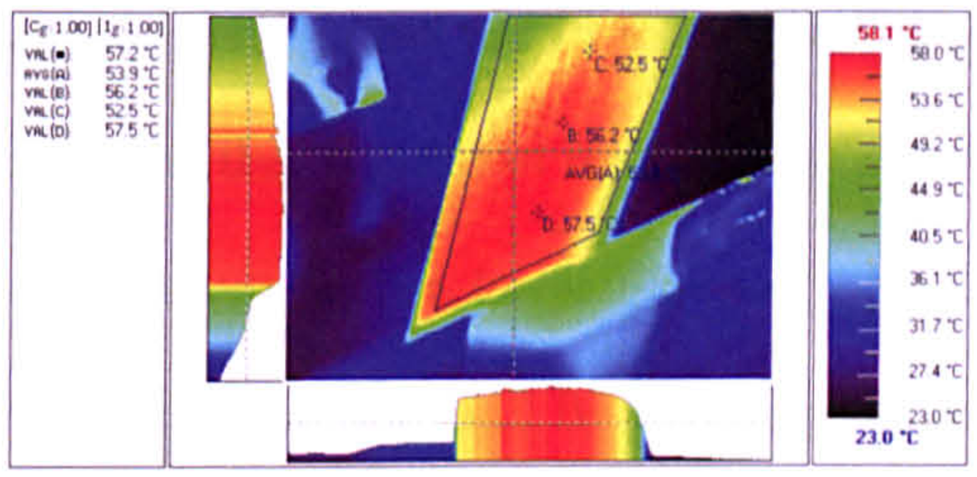

Figure 56: Thermal image of the heater after first calibration with a nominal heating output to 60°C.

heating from the infrared heater. A detailed discussion of the temperature control and further extensions towards a learning and self-calibrating system are given by Eales [115]. Typically, layup of the first ply will be at a slightly lower temperature compared to the subsequent plies. This is due to the control approach, which uses the first ply as a calibration reference. The system then automatically recalibrates and delivers all subsequent plies within a tolerance of ±1°C.

The development of the automated layup system has highlighted several trade-offs that need to be made for automated layup of thermoset tape. The overall speed of the layup system is governed by the heating requirements and the torque control on the ply backing creel. As demonstrated in section 3.1 further increases in speed are unlikely to be beneficial for typical aerospace components and as shown here can be difficult to achieve. The omission of backing tape during AFP layup removes this constraint on maximum layup speed. ATL layup rates are additionally limited by heating requirements, even for high power density infrared heating. AFP heads tend to be smaller than comparable ATL heads, which reduces the heatable material length, thus imposing an additional constraint on maximum layup rates. Heating systems with higher power density, i.e. laser or induction heating, are needed to sufficiently heat the material at high speed and over short heated length.

To improve the existing layup equipment the backing creel has to rotate faster while having highly accurate tape tension control. By increasing the diameter of the backing creel the tape tension tolerance will undesirably increase. A gearbox with a lower gear ratio, i.e. 1:5 instead of 1:12 or even lower, seems to be the best option for this case. By changing the gear ratio the torque on the backing creel decreases and the rotary speed increases. This leads to higher overall speed and more accurately controlled tape tension.

The same observation can be made for the prepreg creel. During layup the material should be delivered with controlled tension. The accuracy of the tension control increases with decreasing material diameter. This is most important for AFP layup over concave surfaces, where bridging occurs if the tape tension is too high. Slit tape is normally supplied on 3" core bobbins for AFP systems, which facilitates accurate tension control. However, the amount of material on each bobbin is small compared to ATL tape, leading to more frequent material refilling. As shown in section 3.1 material changes significantly decrease productivity. A trade-off is therefore necessary which has to balance accurate layup and productivity. Improved control would allow more material per bobbin, leading to higher productivity, or by reducing accuracy requirements existing systems could carry more material, again leading to higher productivity.

Currently, only 20% of the potential acceleration of the linear drive is used during layup. By increasing the acceleration the tool can be shortened, leading to lower material waste during layup, shorter tool length and lower system weight. If the tool can be shortened sufficiently, the outer supports could be removed, allowing a much simpler layup system design and a narrower and shorter tool, which is supported by the linear drive only.

5 Prepreg characterisation

5.1 Introduction

Variability of composite parts is an important issue in composite manufacturing. While it is possible to be well controlled in laboratory environments, variability in large-scale manufacture of complex series production parts still causes problems in terms of robust manufacture. A robust manufacturing process produces parts of known and high quality reproducibly whilst also achieving high productivity. The quality of a final part is governed by many features of the initial prepreg, but specifically the uniformity and the amount of defects that are introduced throughout manufacture. As a general rule it is easier, faster, and therefore cheaper to avoid creating defects in a certain operation instead of managing or reworking them in a subsequent operation. A good example is the use of vacuum void removal during manual layup - while variability and voids could theoretically be mitigated or removed during autoclave cure, removal during layup will improve the overall laminate quality [8]. The most common known defects in cured flat parts are fibre misalignment, porosity and fibre waviness [2]. It has long been recognised that the variability of the prepreg has an important effect on these defects, and in this study we are concerned with porosity and prepreg properties that may be linked to excessive voidage in the final part only.

Every prepreg exhibits a certain amount of voidage that stems from initial manufacture. This voidage is normally spherical and found in the centre of the plies [116]. The important difference between this intra-ply voidage and interply voidage concerns its shape and distribution. Interply voidage can be removed, to some extent, by vacuum void removal. Intra-ply voidage is normally not connected and can therefore not be controlled by applying a

vacuum. Intra-ply voids can only change size depending on the exact curing conditions, as diffusion through the thickness is fairly limited due to the low through thickness air-permeability of a prepreg [99, 117] and the main void evacuation path has been shown to be the interply zone [99, 118].

Volatiles from the prepregging process or absorbed water during layup can also lead to voidage during cure. Volatiles will undergo a phase-change from liquid to gaseous during autoclave processing and will form large voids in the laminate. Although being an important source of voidage this is not discussed here.

During manual layup plies are debulked regularly to remove voidage between the plies. This minimises the amount of entrapped air and improves the laminates quality prior to curing. For Automated Tape Laying (ATL) debulking is often omitted to achieve continuous processing. A controlled force is applied onto the laminate with a flexible roller to achieve the consolidation. No publications concerning the correct choice of pressure are available and it can be argued that this method may result in more entrapped air between the plies than if vacuum debulking is applied.

A high variability in resin content may also affect the layup detrimentally and lead to void development during cure or even shape distortion [119]. To explain a possible correlation between distortion and resin content variability, Buczek, Backman and Darfler [120] studied the resin content variability in a roll of as delivered, uncured prepreg. The authors observed a resin distribution across the width of a roll of prepreg with prepreg areal weight being highest in the middle of the ply, and decreasing to the outside. This variability was explained by a similar distribution for the fibre content, with resin variability having a smaller impact. Further, Potter et al. [121, 122] studied the prepreg areal weight and waviness in the context of geometrical distortions. A large variability for both the fibre waviness as well as the prepreg

area weight was found. They concluded that any attempt to understand processing of prepreg will have to include an assessment of the variability of uncured prepreg. Eom et al. [123] have also shown that the residual stresses in a laminate undergoing cure can exceed the instantaneous strength of the resin. As a consequence, the material will either flow or break away from the stress concentration and voidage and cracks may develop. To suppress void development during cure, the consolidation pressure has to be borne mostly by the resin to reduce void development and growth. Locally resin starved prepregs will thus be more prone to developing voids than prepregs with more uniform resin content [124].

Entrapped air during layup needs to be removed during the first ramp-up of a cure cycle when the resin is still liquid and has not fully set. Campbell et al. [125] argue that prepregs with preferred orientations, for example fibre markings on the surface, aid void removal because they provide channels for the air to escape during vacuum void removal. Thorfinnson and Biermann [126, 127] used prepregs with various degrees of impregnation to illustrate this effect. Voidage varied for laminates made from prepregs with different degrees of impregnation, which describes how fibre and resin are arranged relative to each other. Lee and Springer [128], and Mantell and Springer [74, 75], have developed models based on a unit cell approach to predict the amount of voidage between thermoplastic prepreg plies throughout manufacture. The prepreg surface is represented by a simplified sequence of rectangular blocks and these blocks are then consolidated during layup or cure. The instantaneous block height and shape allows for the prediction of the amount of voidage throughout manufacture. Yang and Pitchumani [129] have measured the surface roughness of thermoplastic tape to describe the interface during bond development and have proposed a concept that extends the previous rectangular block surface models. The surface roughness of a prepreg is therefore an important parameter for both the amount of entrapped air as well as its removal. Even though it is

accepted that surface roughness can be important for the voidage in a composite, this has not been extensively studied. Understanding both resin distribution and surface roughness may be critical to gaining a sound understanding of the voidage and tack of a material and how it changes with processing [130].

In this chapter the properties of uncured prepreg relevant to automated processing are identified. The voidage in the uncured tape is measured by light-microscopy and digital image analysis to establish the prepreg tape quality and a lower bound for the voidage in an uncured laminate. The spatial distribution and variability of the resin content is measured to understand its impact on tack and thus reliable layup. The prepreg surface roughness is characterised to understand the effect on void evacuation and entrapment. Lastly, the uncured tape thickness and variability is measured by digital image analysis to support the development of an automated layup machine and mechanical testing.

Currently, most of these properties, as well as their variability are unknown. Furthermore, their importance for automated manufacture is unclear. The work presented in this chapter has been conducted on two different prepregs and is reported elsewhere [131], for brevity only the data for the M21 prepreg material of primary interest are included here.

5.2 Material

All samples described in subsequent chapter were extracted from a roll of M21/IMA-ATL prepreg [102, 132], either 300mm, 75mm (Automated layup specimens) or 8 x 6.35mm wide (AFP specimens). They were either laid up automatically, or cut using an automated ply cutter and subsequently processed by manual layup. M21 resin is a toughened, modern, epoxy resin; the fibres are intermediate modulus fibres. The prepreg is curable in an autoclave at $T =$

180°C. For M21 the degree of impregnation is expected to be different from prepreg for manual layup. Furthermore, the prepreg has special backing-paper applied to only one side to facilitate handling during automated layup.

5.3 Experimental procedure

5.3.1 Voidage

A strip from the entire cross section of the prepreg was removed, approximately 300mm wide and 20mm long. The strip was then cut into 15 samples each, approximately 20mm wide and 20mm long. To remove volatiles and advance the degree of cure, samples were held in an oven at 70°C for 1h. After this treatment the samples are likely to be vitrified, however, they are not fully cured as the samples are stiff and non-tacky, but retain some flexibilty. The temperature and time were found through several studies to allow high quality sample preparation while limiting resin flow that would change the internal structure of the specimens. Each sample was mounted in Prime20LV [133], a room temperature curing, clear epoxy resin, and left to cure for $t = 24$h. The ply backing was left on the sample to improve the mounting by keeping the plies straight.

Samples were then prepared for void analysis by microscopy as follows. They are ground on an automated polisher using increasingly fine silicon carbide paper. Between every change of grinding paper the samples are cleaned in an ultrasonic bath to remove debris from previous grinding. After grinding, specimens were polished using a 6μm diamond suspension. Finally, the specimens were cleaned for microscopy using a fine cloth. The voidage of the uncured prepreg specimens was measured by light microscopy. While acid digestion is a more common method [134] we prefer light microscopy due to the absence of hazardous chemicals,

the ability to study the morphology of voids and the ability to retain the specimens. A Jenavert light microscope with Carl Zeiss objectives and a Pixera pro 150ES CCD camera was used to obtain digital micrographs. The micrographs were analysed for their void content on the surface by digital image analysis with Image J [135] software. The reported void data were therefore void area fractions. Analysis was done in two steps. First, the actual sample area was distinguished from the rest of the picture and secondly the void area was calculated. The sample area was analysed by separating the picture into background and sample area and then applying a threshold to the two areas. The pixels in the sample area were then counted; this analysis is illustrated in Figure 57 and Figure 58. To calculate the void fraction the voids were highlighted using a grey-level threshold and the area in pixels was counted. This procedure is shown in Figure 59 and Figure 60. The void fraction was calculated by dividing the void area by the sample area. Assuming that all voids in the ply are circular we calculated an average void diameter by dividing the void area by the number of voids for each picture.

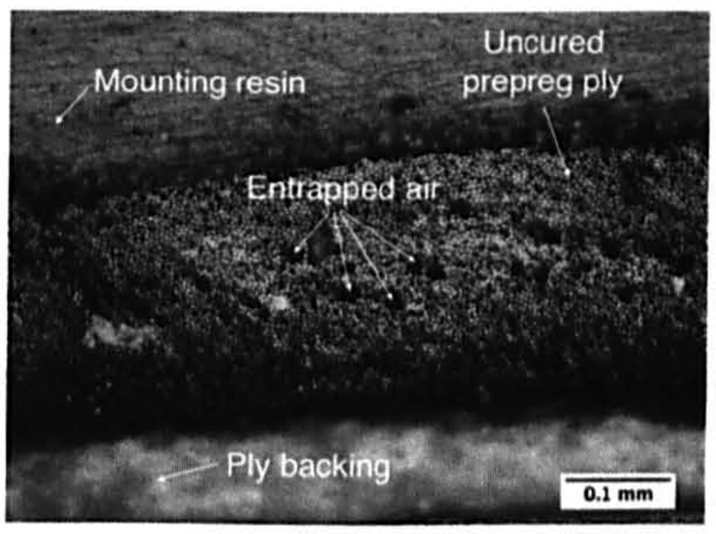

Figure 57: Original micrograph in greyscale with labelled areas of interest.

Figure 58: Sample area coloured black after digital image analysis. Note that voids are counted towards the total sample area.

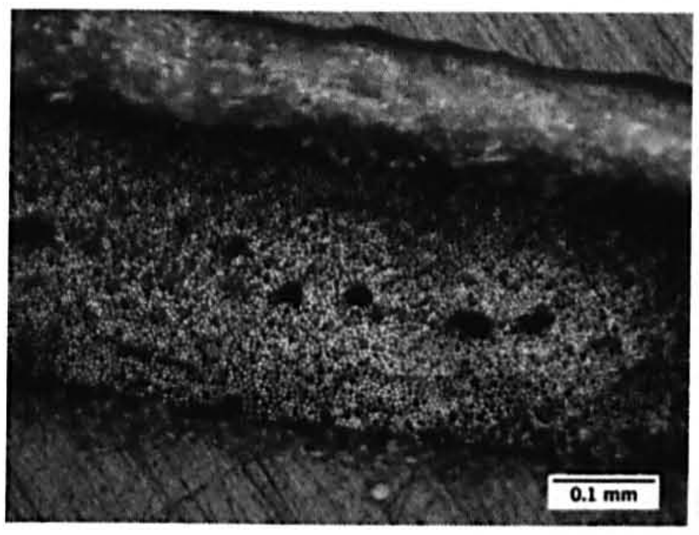

Figure 59: Original micrograph in greyscale.

Figure 60: Void area after counting. The outlined area is counted towards the void area.

5.3.2 Resin content

The resin content was measured over an area of 300 x 300mm. The sample area was cut into smaller specimens, 20 x 20 mm in size. We chose a small sample size to record more readings of the resin content along the width and length of the prepreg. The resin content of the prepreg was tested by resin burn-off. This method is normally used for glass-fibre and uncommon for carbon fibre due to potential oxidation loss of the fibre at high temperature [136]. Advantages of this method are the omission of aggressive solvents and potentially dangerous test arrangements as well as the potential to test samples faster. A muffle furnace was used to remove the resin. From the literature it was expected that temperatures above T = 400°C would degrade the fibre. Common test methods for glass-fibre, however, suggest to incinerate the resin at temperatures of T = 565°C [136]. We therefore conducted as series of measurements at temperatures between of $400 \leq T\ [°C] \leq 500$ and different test times to identify the optimal test conditions. First, the furnace was pre-heated to the test temperature. The samples were then placed in small ceramic crucibles. The crucible weight with and without sample prior to testing was recorded. Upon reaching the target test temperature the crucibles were placed in the furnace. After incineration, the crucibles were moved directly into a

desiccator to avoid moisture adsorption during cool down. The mass loss is calculated from the weight of the crucible and sample after incineration. The result is plotted in Figure 61. An increasing mass loss with increasing test times and temperatures was observed.

Burning the resin for t = 6h at T = 475°C and T = 500°C showed no further increase in the measured mass loss. To confirm this result, samples obtained at these test temperatures were investigated by Scanning Electron Microscopy (SEM) to verify the integrity and cleanliness of the carbon fibre. After burning the resin for t = 2h at T = 475°C residual resin remained on the fibre, see Figure 62. Increasing the test temperature and time to T = 500°C and t = 4h resulted in an almost clean fibre with some sizing left on the fibres, see Figure 63.

Oxidation of the surface is associated with a pitting of the fibre; this cannot be observed on the SEM pictures. All resin content samples were consequently tested at T = 500°C and t = 6h in a randomized order. To analyse the data they are reported as normalized results with respect to the nominal resin content by weight. For M21 this is reported by the manufacturer to be 35% by weight [102].

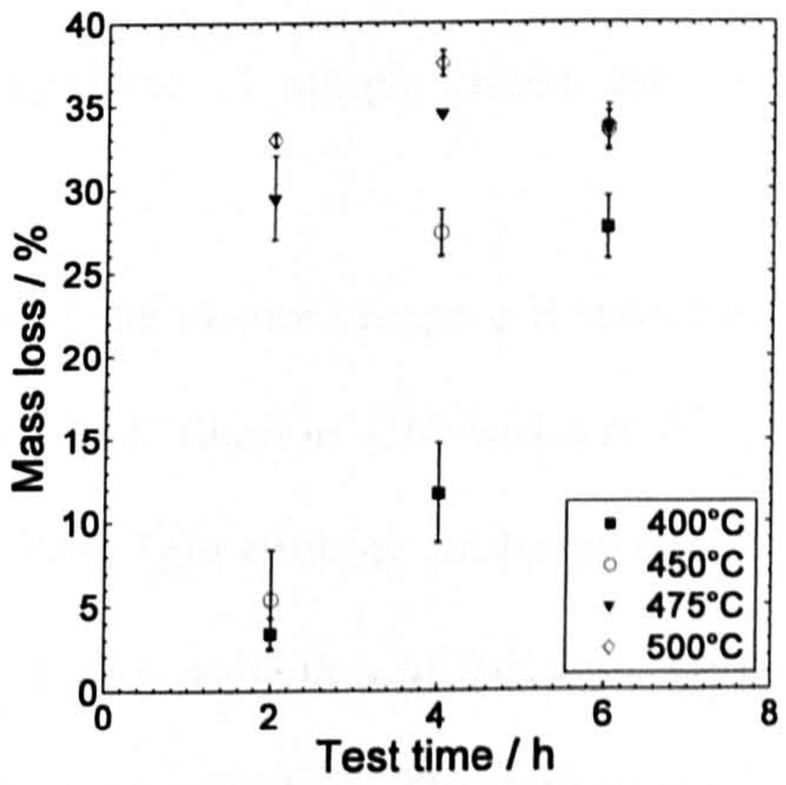

Figure 61: Average mass loss and standard deviation of M21 resin at different temperatures and exposure times.

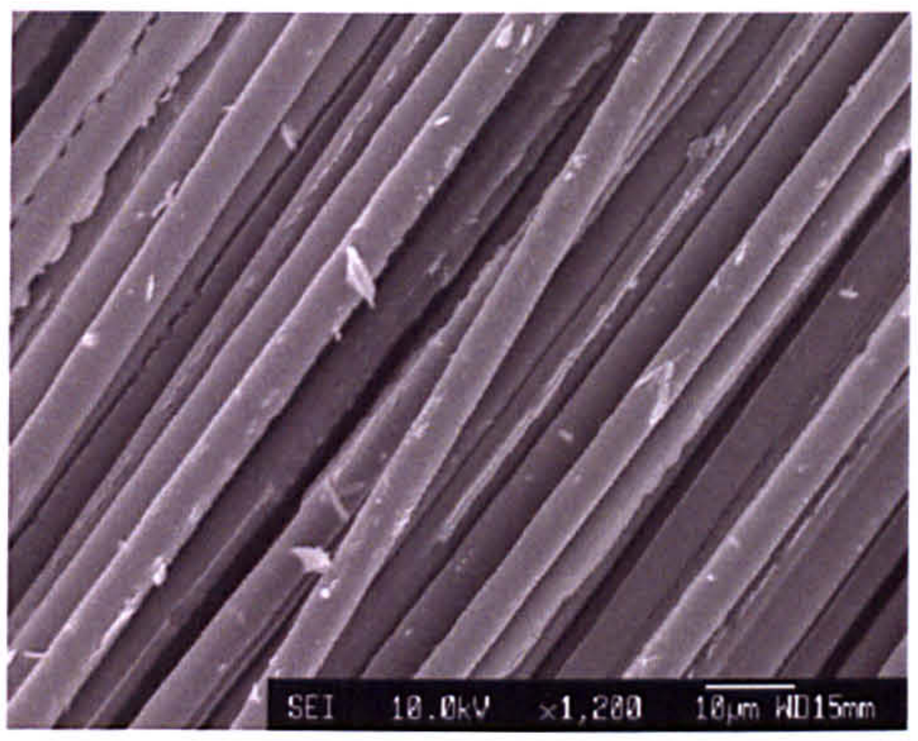

Figure 62: SEM micrograph of M21 prepreg after t = 2h treatment at T = 475°C. Residual resin covers the carbon fibre in some areas.

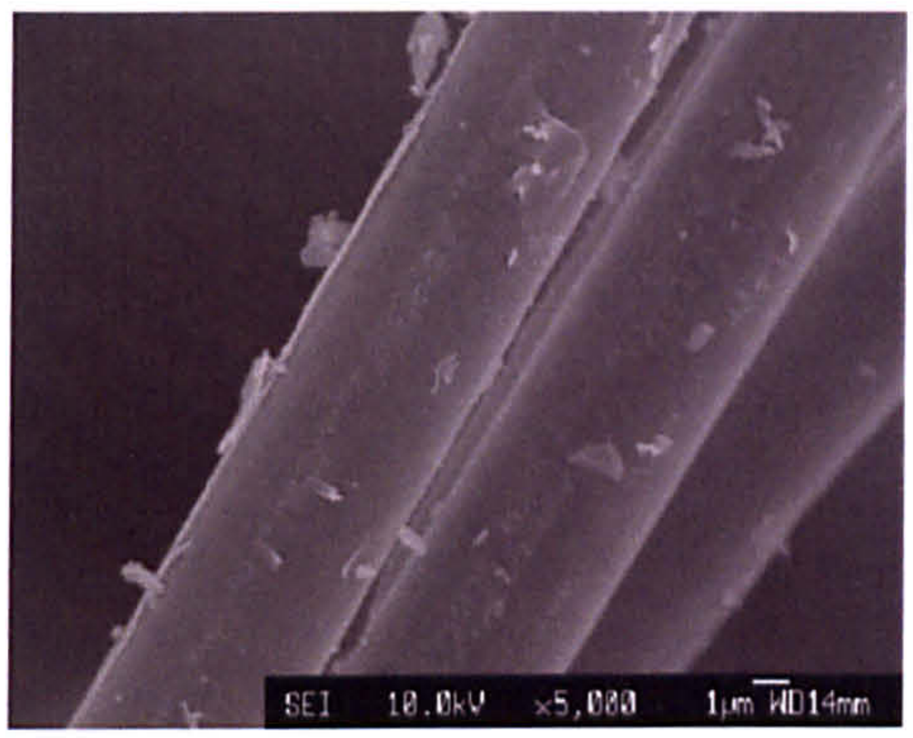

Figure 63: SEM micrograph of M21 prepreg after t = 4h treatment at T = 500°C. The carbon fibre is free of resin and showing no signs of surface attack due to oxidisation.

5.3.3 Surface characterization

Prepreg samples for evaluation of the surface properties were 40 x 40mm in size. Six samples were extracted from random locations within a roll of prepreg. Three samples are applied on the aluminium plates with the ply-backing side facing up and three samples with their ply-backing side facing down. A sample placed onto an aluminium plate is shown in Figure 64.

The surface profile of the uncured prepreg is measured using a Proscan 2000 system (Scantron Industrial Products Ltd. Taunton, UK) with a S5/03 probe. The system consists of a movable base plate and a fixed light-emitting probe mounted on the top. The probe has a measuring range of 300µm with a resolution of 0.01µm. To measure the surface profile the aluminium plate is placed on a movable base. The light source is then adjusted to measure the surface height. Here we measured the profile over an area of 35 x 35mm where the fibre was

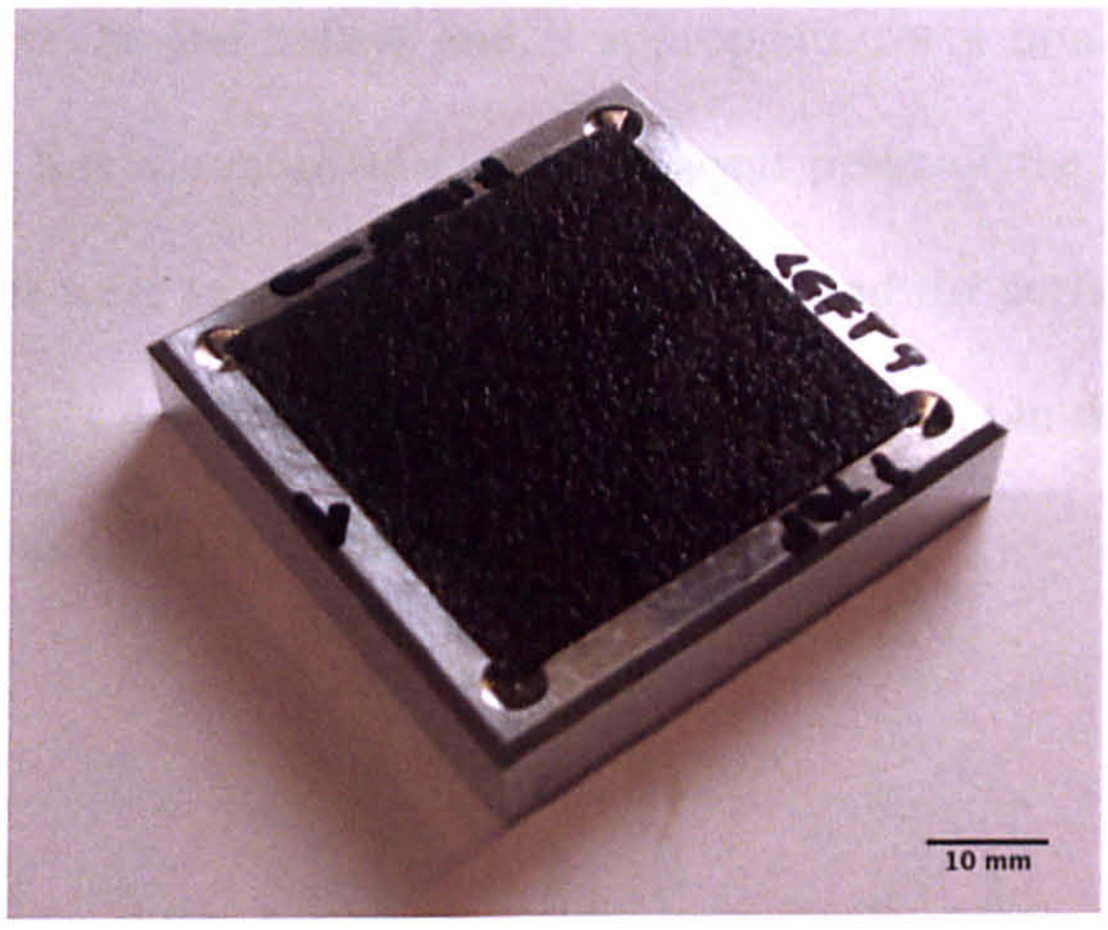

Figure 64: Picture of a prepreg sample for roughness measurements mounted onto a sample holder.

oriented along the x-axis. The x-direction and y-direction were divided into 200 increments each, which gives a spatial resolution of 0.175mm. Each measurement is the average of two readings, which was identified as the best compromise between accuracy and speed of measurement. In some circumstances the roughness measurement system will fail to obtain an accurate reading or any reading at all for a point on the surface. These spikes and gaps in the surface were removed by interpolation during post-processing. To obtain the roughness profile of the prepreg only, the warpage and shape of the prepreg and sample holder were additionally filtered with a surface filter.

The resulting data represents the surface roughness of the prepreg surface. They were extracted as averages for the entire sample surface. To obtain the roughness data, software was used to separate a 3D-roughness profile into segments, calculate the roughness parameters for each segment and then take the average of all segments. The roughness height was calculated according to ISO R_z and the roughness length was calculated according to ISO S [137]. ISO R_z is defined as the difference in height between the five highest peaks and the five lowest valleys along the assessment length of the profile, i.e in each segment, see Figure 65. This parameter is

sensitive to localized peaks and valleys and is appropriate for a non-uniform material like uncured prerpeg. ISO S is the mean spacing of adjacent peaks of the roughness profile, see Figure 66. The samples were stored at room temperature and the surface was examined as a function of outlife over 21 days (504h) to identify potential changes in the surface that can e.g. be used to explain changes in tack levels.

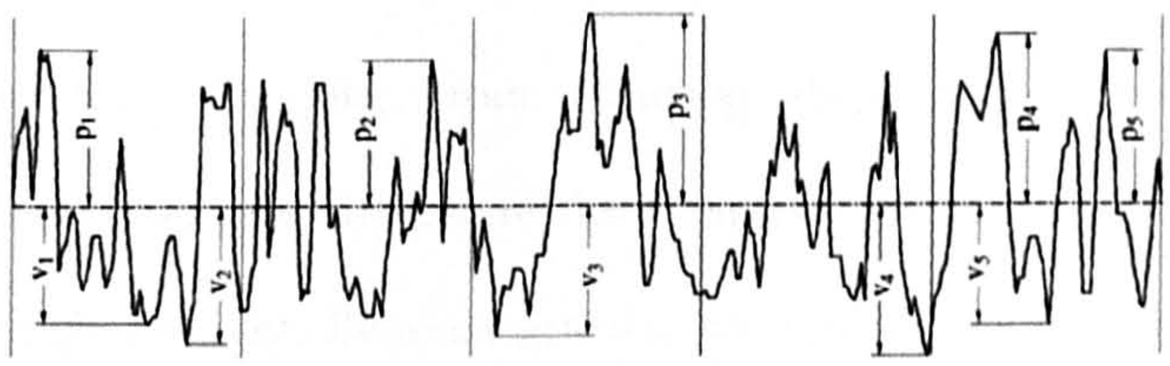

Figure 65: Example of a roughness profile from [137] with the measured valleys and peaks that contribute to Rz indicated.

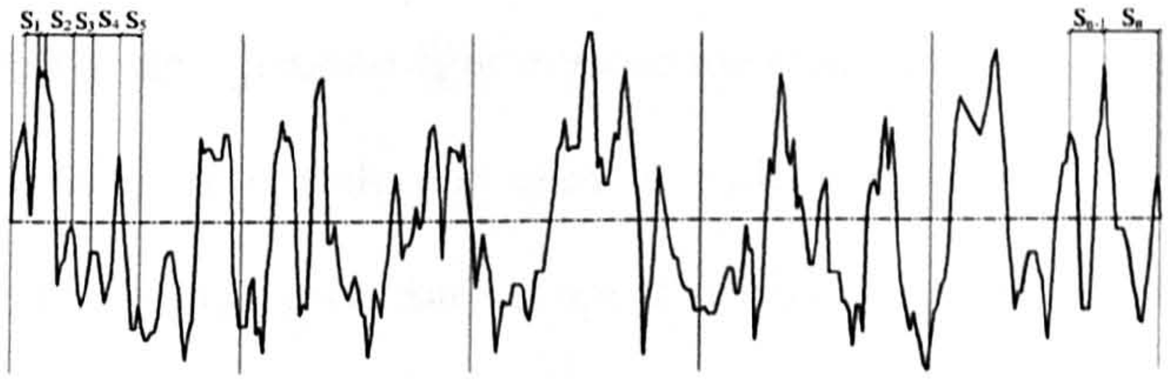

Figure 66: Example of a roughness profile from [137] indicating the measurements for Iso S.

5.3.4 Ply thickness

The thickness of raw prepreg is required for many applications, e.g. in mechanical testing the thickness is required to calculate effective stresses in the sample. Normally the thickness is measured using micrometer or a flat plate that is brought into contact with either a single ply or a stack of plies. The advantage of these methods is the relative ease of obtaining results. Disadvantages include point-to-point variation in the measurements and the fact that the prepreg is likely to be compacted during the measurement resulting in an erroneous

reading. The ply thickness was thus measured by microscopy. Samples were obtained from a strip approximately 300mm wide and 20mm long. Ply backing was left on the sample to facilitate handling. This strip was cut down into 15 specimens, 20 x 20mm each. The specimens were then kept in an oven at $T = 65°C$ for an hour to remove volatiles. After cool down the specimens were mounted in clear, room temperature curing, epoxy resin. Special attention was required to keep the plies straight. They were left to cure at room temperature for $t = 72h$. The advantage of room temperature cure is a reduction of cure shrinkage; this reduces the sample movement and prevents the plies from changing shape thus simplifying subsequent examination with a microscope. After cure the samples were polished with silicon-carbide paper with increasingly fine grit. Between grit-size changes the samples were cleaned in an ultrasonic bath. Finally, they were polished with a cloth and 3µm diamond solution.

The entire sample cross-section was examined using digital microscopy. Images of the sample were obtained using a Jenavert light microscope with Carl Zeiss objectives and a Pixera pro 150ES CCD camera. A reticule was used to scale the images. The micrographs were analysed in ImageJ [135] using a predefined script. The necessary steps for analysing the sample area are shown in Figure 67 to Figure 72. Figure 67 shows the original sample. The mounting resins, the sample, ply backing and entrapped air are highlighted for orientation. In a first step the quality of the picture is improved and a Canny-Deriche filter to pick out edges is used to highlight the sample area, as shown in Figure 68. To improve the identification a further background removal filter, developed by ETH Zürich for ImageJ, is applied as shown in Figure 69. A simple grey-level threshold is then applied to pick out the sample area, see Figure 70 and Figure 71. After having obtained a picture containing only black and white pixels, the

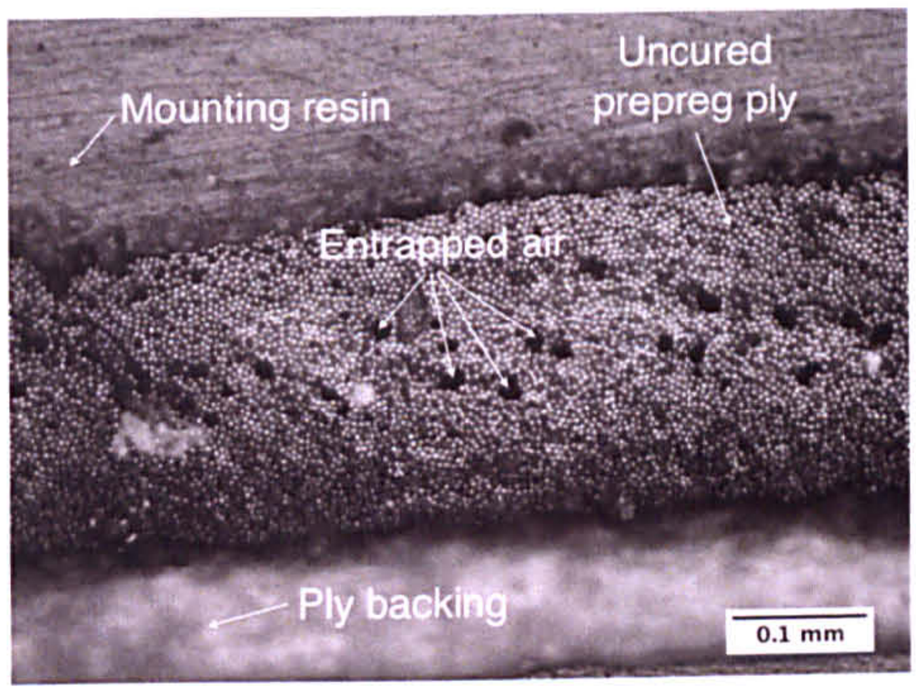

Figure 67: Original micrograph in black&white. Areas of interest have been labelled.

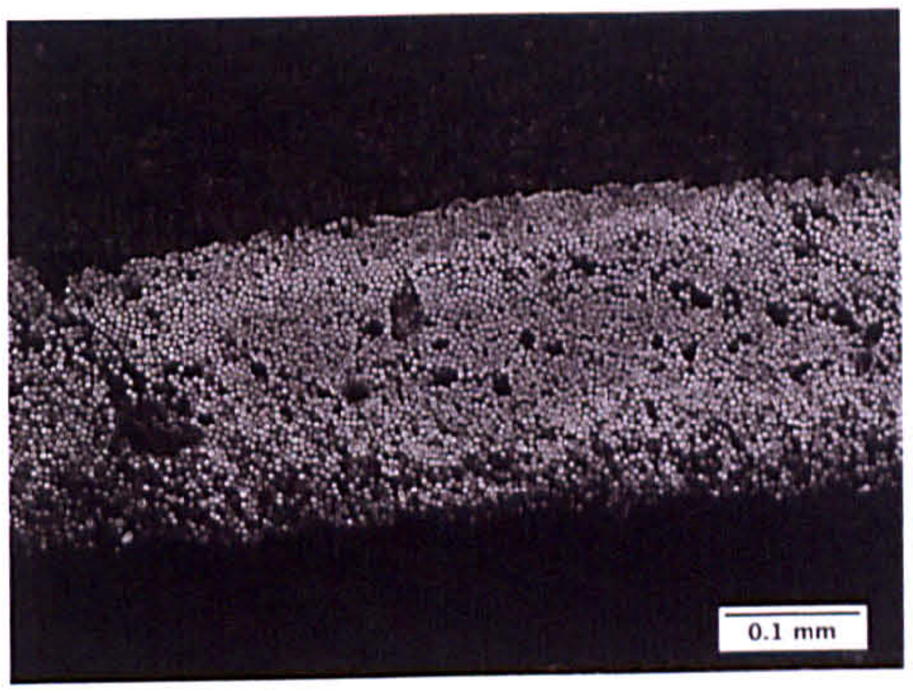

Figure 68: Micrograph after highlighting of edges.

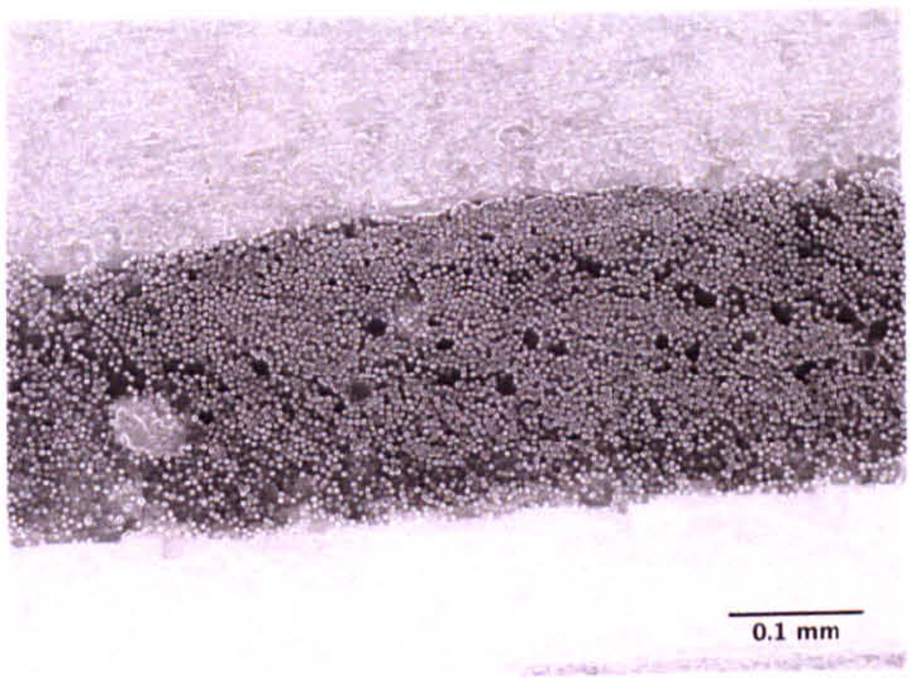

Figure 69: Additional removal of background pixels, shaded in light grey.

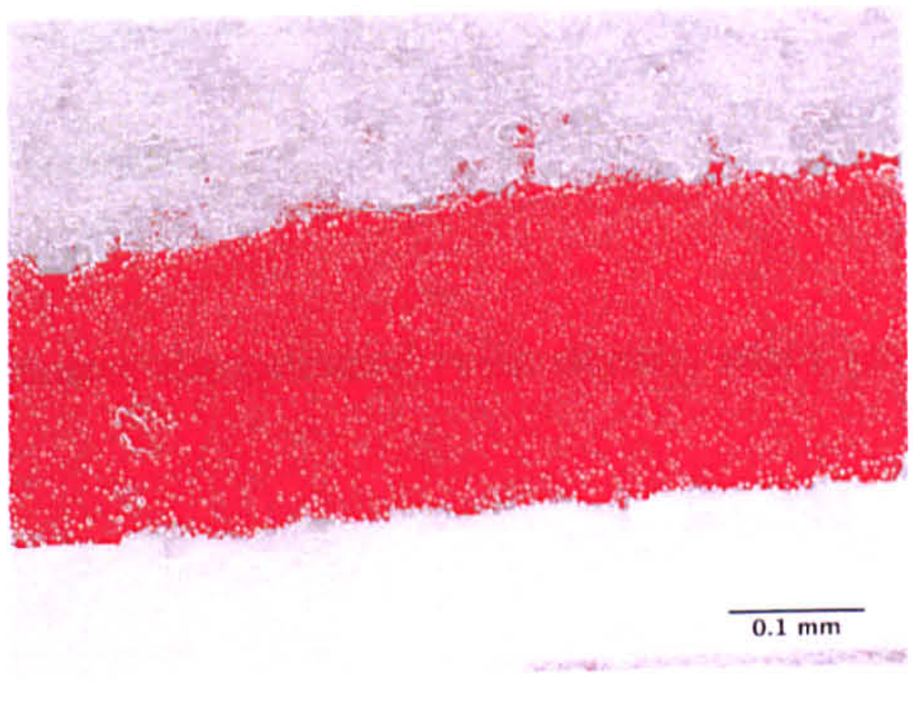

Figure 70: Picking out the sample area by threshold. Sample area highlighted in red.

Figure 71: Sample area marked in black

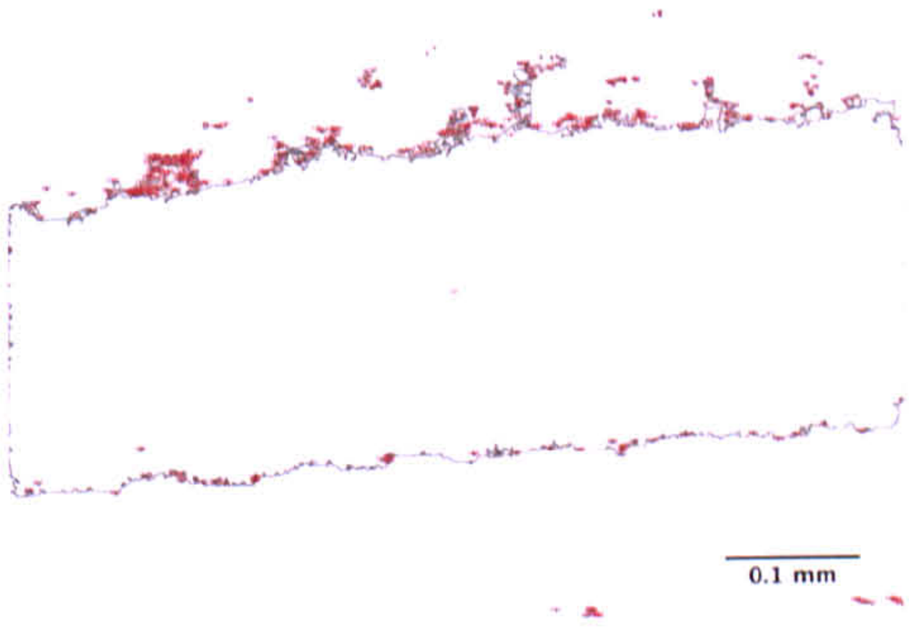

Figure 72: Sample area after counting. The outlined area is counted towards the sample area. The artefacts at the top are included but have limited bearing on the final result.

black pixels are counted towards the sample area as shown in Figure 72. The sample height is the average of 15 specimens.

To gain an understanding of the raw prepreg we may simply use available information from the manufacturers data sheet to calculate the nominal ply thickness before cure. The manufacturer's data are given in [102] and [132]. Typically, most modern resin systems have a very high viscosity throughout cure, to reduce bleeding of the resin. Furthermore, they give off very few volatiles, which reduces the prepreg mass. Thus, we may assume, that the prepreg area weight remains constant before and after cure, see Equation (5-1).

$$m_{cured} = m_{uncured} \tag{5-1}$$

Using simple rules of mixture we can calculate the uncured resin density prior to cure, with,

$$\rho_m = \frac{\rho_c - V_f \cdot \rho_f}{1 - V_f} \tag{5-2}$$

By accounting for the change in density due to cure shrinkage we arrive at the uncured resin density. Assuming a cure shrinkage of 2.5% the uncured resin density is calculated to be 1.24gcm^{-3}. For the uncured material the exact fibre and matrix fractions are unknown but can be calculated from the nominal fibre and prepreg areal weight. The weight fraction between matrix and resin is

$$\psi = \frac{m_f}{m_p}, \tag{5-3}$$

The uncured fibre volume fraction can then be calculated from,

$$\varphi = \frac{1}{1 + \frac{1-\psi}{\psi} \cdot \frac{\rho_f}{\rho_m}} \tag{5-4}$$

The uncured fibre volume fraction calculated from above is 56%. From this, the nominal uncured ply thickness can be calculated using the previously calculated values for the uncured fibre volume fraction and the matrix density with,

$$t_{uncured} = \frac{m_p}{(\varphi \cdot \rho_f + (1-\varphi) \cdot \rho_m)} \tag{5-5}$$

This results in a nominal uncured ply thickness of 0.269mm for the M21 prepreg, while the cured ply thickness is 0.262mm.

5.4 Results

5.4.1 Uncured prepreg void content

To deal with highly localized air bubbles typically found in uncured prepreg plies, a large number of micrographs were generated. Each specimen is represented by approximately 30 micrographs. The specimen void content and average void content for M21 are shown in Figure 73. The void content is highest on the outside and decreases towards the centre of the prepreg cross-section. The average void content over the entire cross-section is 5.1%. Results for the void size of M21 are plotted in Figure 74.

The void diameter changes randomly over the sample cross-section with limited scattering. Sample number 5, with a void content of 9.6% is a significant outlier. This sample only

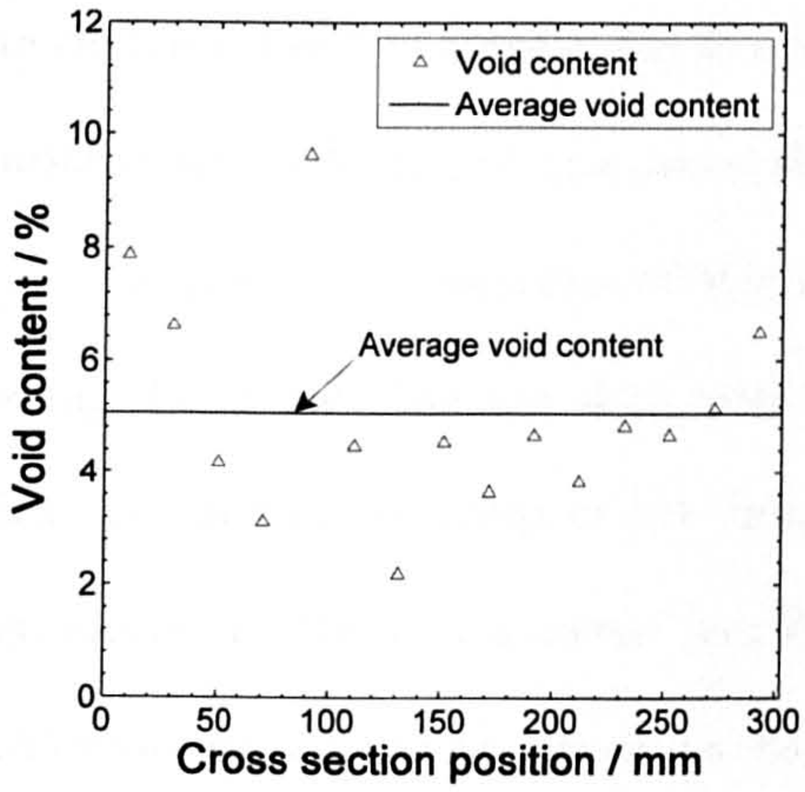

Figure 73: Void content of M21 prepreg as a function of cross section position.

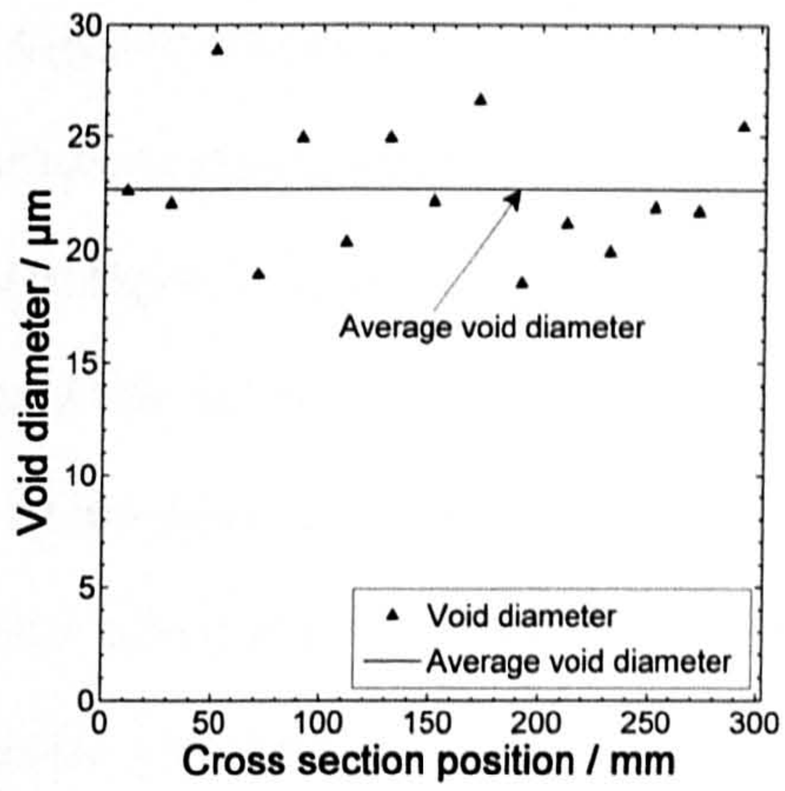

Figure 74: Calculated void size as a function of cross section position.

exhibited large elongated voids in the centre of the ply, yielding a higher void measurement. Overall, the result is a good indication that the analysis method is independent of void fraction and accurately captures the void size. The average void diameter over the entire prepreg cross-section is d = 22.6µm. Void size and void content are not correlated, again confirming the validity of the method for the range of void contents studied. These results are in excellent agreement with the results reported by Huang and Talreja [138] for epoxy resins, who found an average void diameter of d = 20µm for void contents between $5 \leq$ vf [%] < 6.

5.4.2 Resin content

For M21 the nominal resin content by weight is 35%. The measured average resin content from 225 individual specimens over an area of 300x300mm was V_r=35.0 ± 1.8% by weight. For M21, the mean corresponds to the known nominal resin content from [102], due to the normalization used to compensate for test effects. These test effects include change of

mean from one batch to another due to advancing degree of cure during outlife and changes in environmental conditions, i.e. changes in absorbed moisture prior to testing.

The normalized variability of M21 is plotted in Figure 75 along the width and in Figure 76 along the length. The raw data were interpolated for these plots to provide a smooth surface. The acceptance limits of 3% deviation from the mean are indicated as flat surfaces. Consequently all data points within specification were coloured grey. Data points below the specification are coloured in shades of blue and green, while data point above specification were coloured in red and yellow. The resin content profile of M21 measured along the width appears to be very similar to the voidage profile shown in Figure 73. This does not however imply that resin content variability is linked to internal voidage or vice versa. It seems that the ply-outside is compacted less during prepreg manufacture than the middle. Consequently less resin is squeezed out of the prepreg and the resin content as well as the voidage being high.

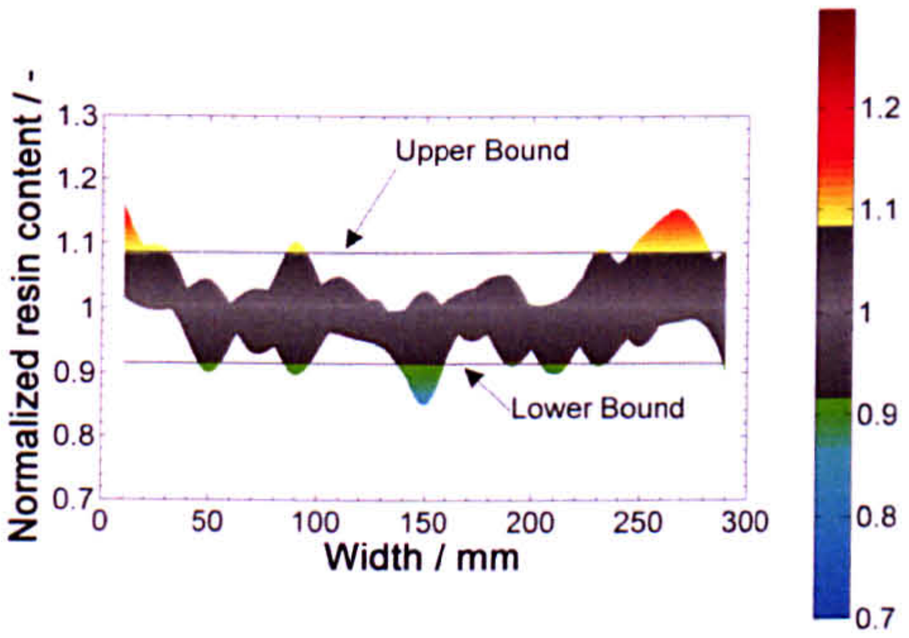

Figure 75: Resin content distribution of M21 prepreg along the width of a ply. The grey area is within the specification limits. Blue and green shaded areas are below and yellow and red areas above the acceptable resin content.

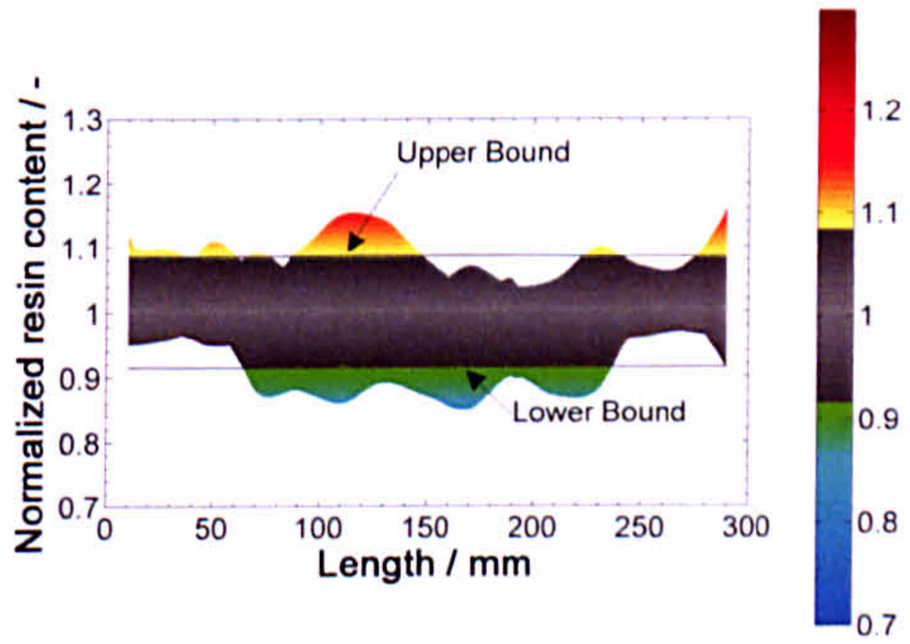

Figure 76: Resin content distribution of M21 prepreg along the length of a ply. The grey area is within the specification limits. Blue and green shaded areas are below and yellow and red areas above the acceptable resin content.

M21 prepreg is found to be within specification, i.e. both the mean and the standard deviation of the resin content by weight are within the acceptance limits. The existence of localized outliers has implications for handling and usage in automated manufacture in particular for process reliabilty. These outliers are partially due to the smaller sample size used for testing here compared to standard resin content tests.

5.4.3 Surface roughness

Results for the surface roughness were obtained as a function of outlife for backing- and non-backing sides of the prepreg. A representation of the Roughness R_z for M21 can be seen in Figure 77a for the backing side, and Figure 78a for the non-backing side. The height is colour-coded, peaks are red and valleys are blue. For both sides a characteristic pattern is observed which can be described as a series of peaks and valleys with respect to both x- and y-direction, i.e. the material has a fairly random roughness distribution but a preferred orientation transverse to the fibres. For comparison pictures of the surface of M21 were also generated using a light microscope. These can be seen in Figure 77b and Figure 78b. The fibres in the prepreg can clearly be distinguished from the resin on top that is melted onto the prepreg in a discontinuous form. The results for the peak surface roughness ISO Rz of M21 are shown in Figure 79 for the backing-side and in Figure 80 for the non-backing side, as a function of outlife. The averaged peak-to-peak distance ISO S of M21 is shown in Figure 81 for the backing side and in Figure 82 for the non-backing side, as a function of outlife. None of the graphs exhibit a clear trend with respect to outlife. It can be concluded that the resin does not

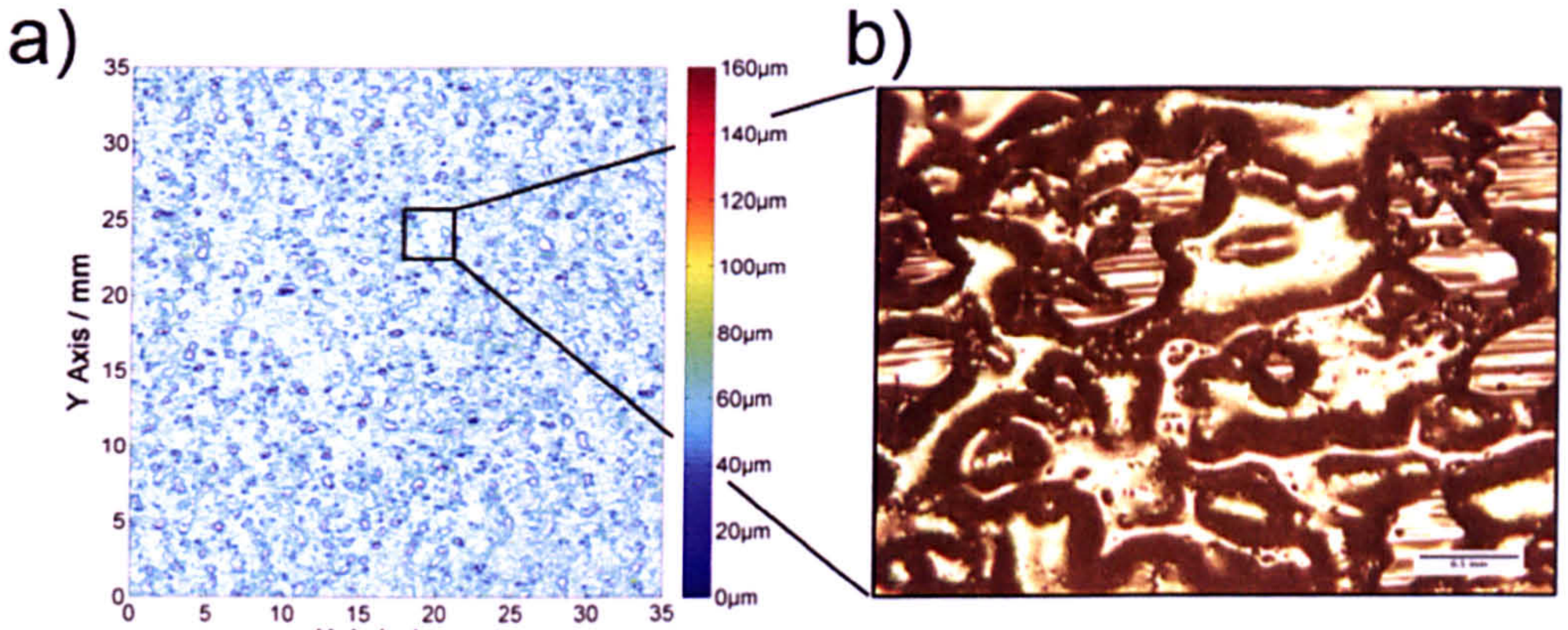

Figure 77 a) Contour plot of surface roughness for backing side of M21 prepreg and **b)** Micrograph of prepreg surface.

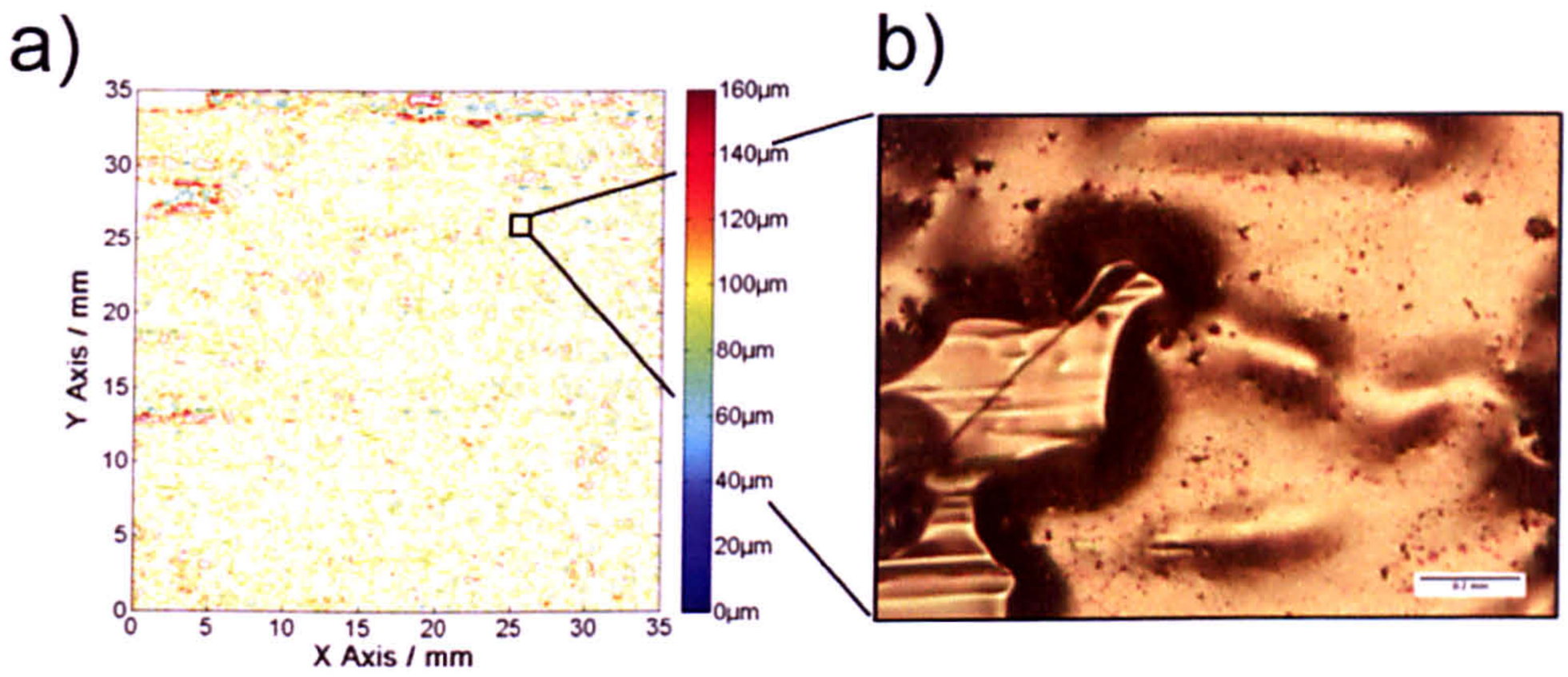

Figure 78 a) Contour plot of surface roughness for non-backing side of M21 prepreg and **b)** Micrograph of prepreg surface.

flow during aging at room temperature and the surface remains unaltered. The time-averaged values for the roughness of M21 for each side and direction are given in Table 11. Roughness values are not significantly different between backing and non-backing side for both materials. This result can be interpreted as a confirmation of the initial assumption that little or no flow will occur when the plies are brought in contact. If this were the case the application of the backing paper should have had a similar effect in reducing the roughness height and distance. M21 prepreg exhibits a preferred orientation transverse to the fibre.

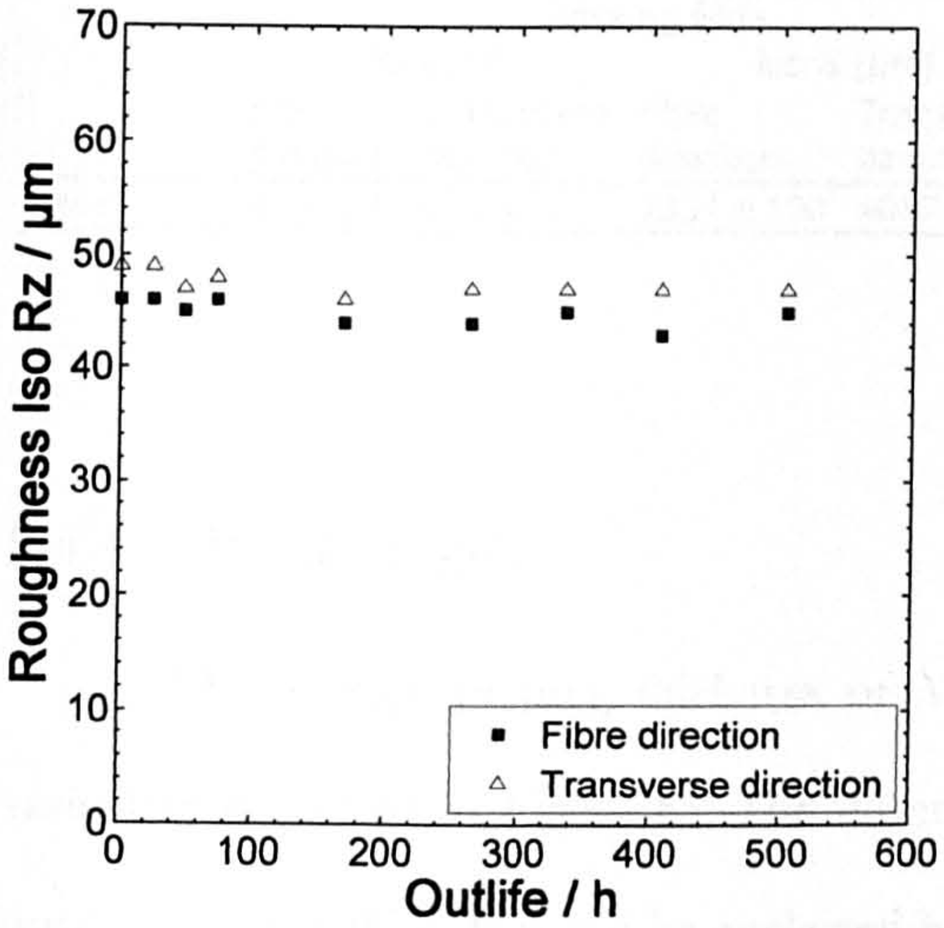

Figure 79: Peak surface roughness R_z for the backing side of M21 prepreg along the fibre- and transverse direction as a function of outlife

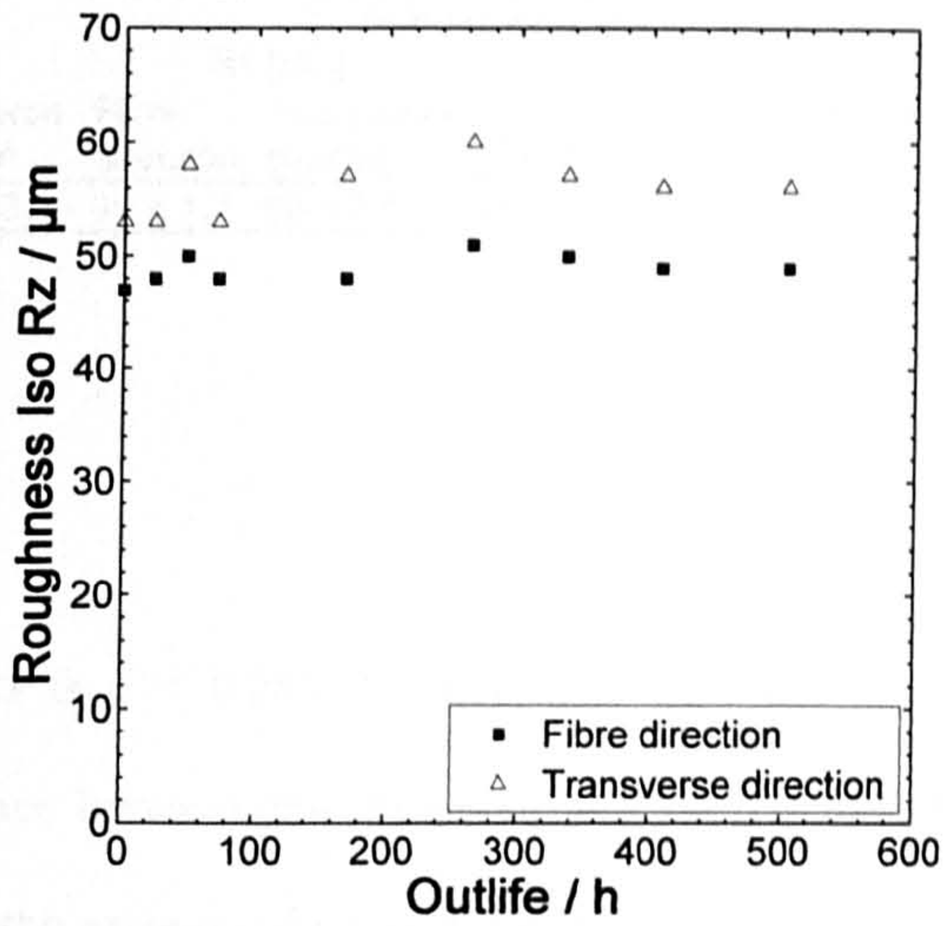

Figure 80: Peak surface roughness R_z for the non-backing side of M21 prepreg along the fibre- and transverse direction as a function of outlife

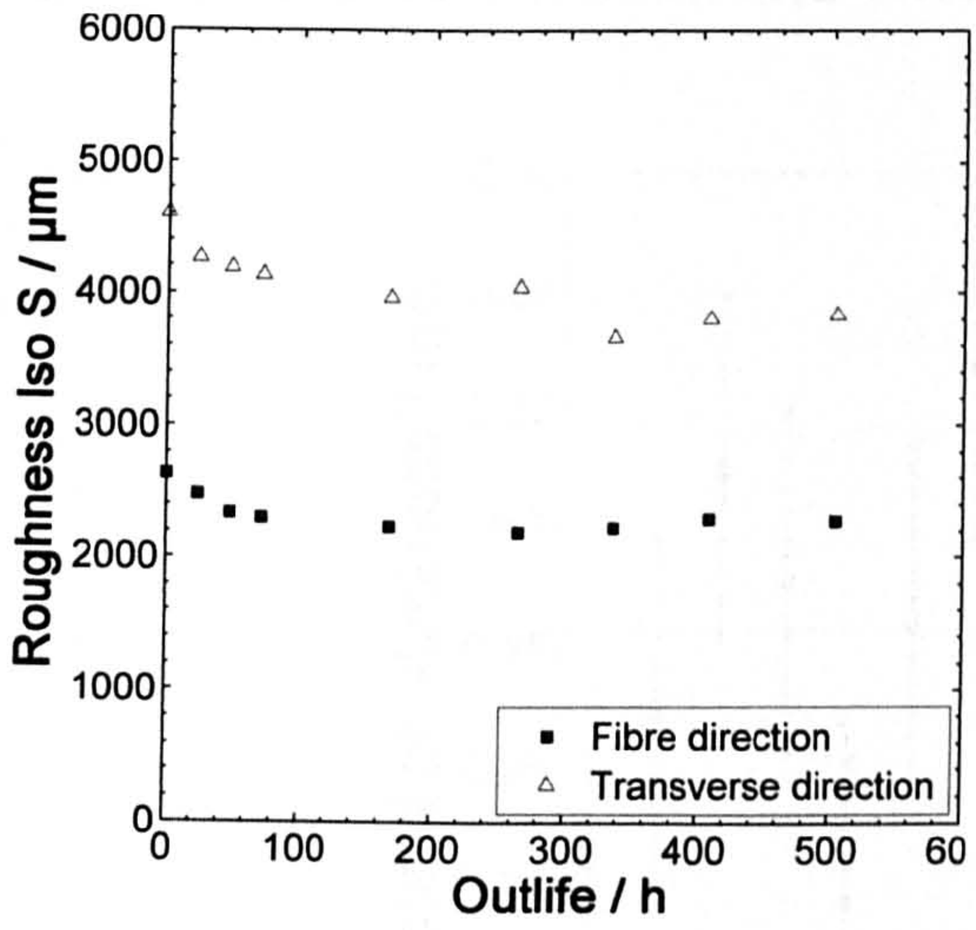

Figure 81: Roughness profile average peak distance S for the backing side of M21 prepreg along the fibre and transverse direction as a function of outlife.

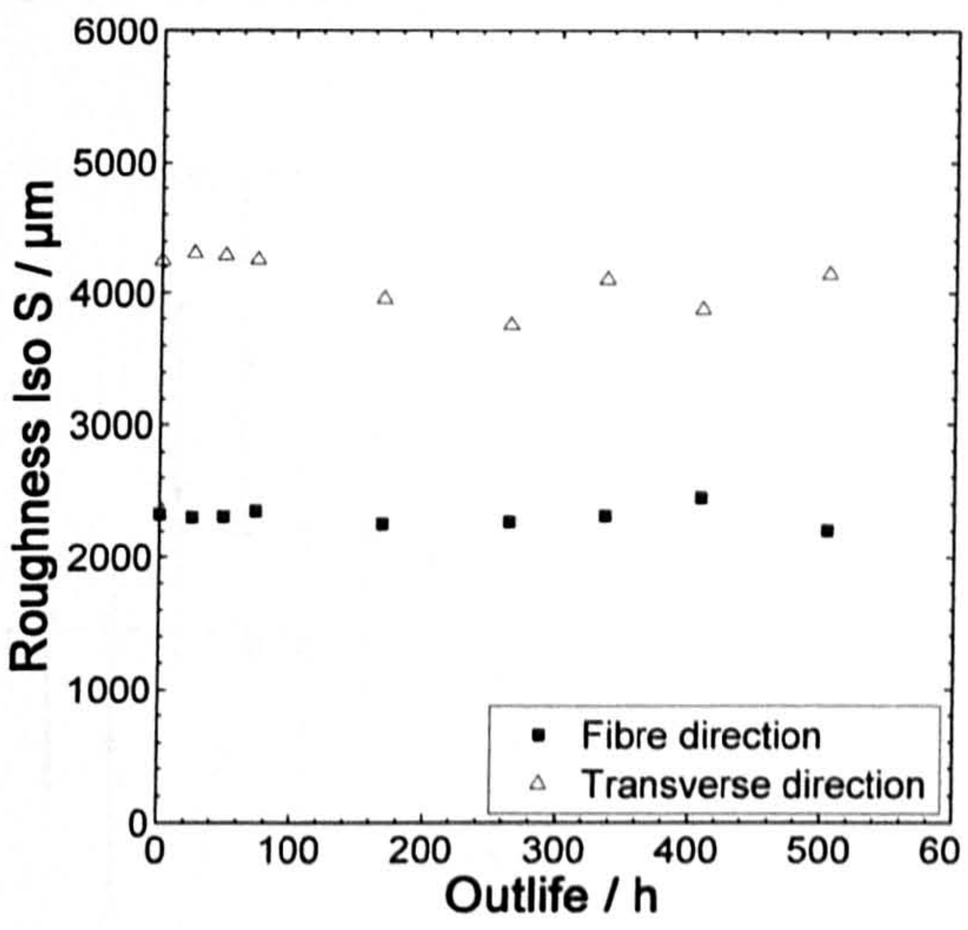

Figure 82: Roughness profile average peak distance S for the non-backing side of M21 prepreg along the fibre and transverse direction as a function of outlife.

Table 11: Results for the surface roughness analysis of uncured M21.

	Backing Side				Non-backing side			
	Rz [μm]		Iso S [μm]		Rz [μm]		Iso S [μm]	
	Fibre direction	Transverse direction	Fibre direction	Transverse direction	Fibre direction	Transverse direction	Fibre direction	Transverse direction
M21	45 ± 1.7	47 ± 4.1	2331 ± 190	4057 ± 374	49 ± 1.2	56 ± 7.6	2313 ± 230	4104 ± 524

5.4.4 Ply thickness

The average prepreg thickness of M21 is $t = 0.283 \pm 0.0285$mm with the local variability is plotted in Figure 83. The difference between the measured and the calculated result is 5% for M21. This can be explained by the amount of voids in the prepreg which has not been accounted for in the analytical calculation. The average void content for uncured M21 was found to be 5.1%. This could be interpreted as indication that the uncured ply thickness can indeed be calculated as demonstrated in section 5.3.4, if the change in volume due to

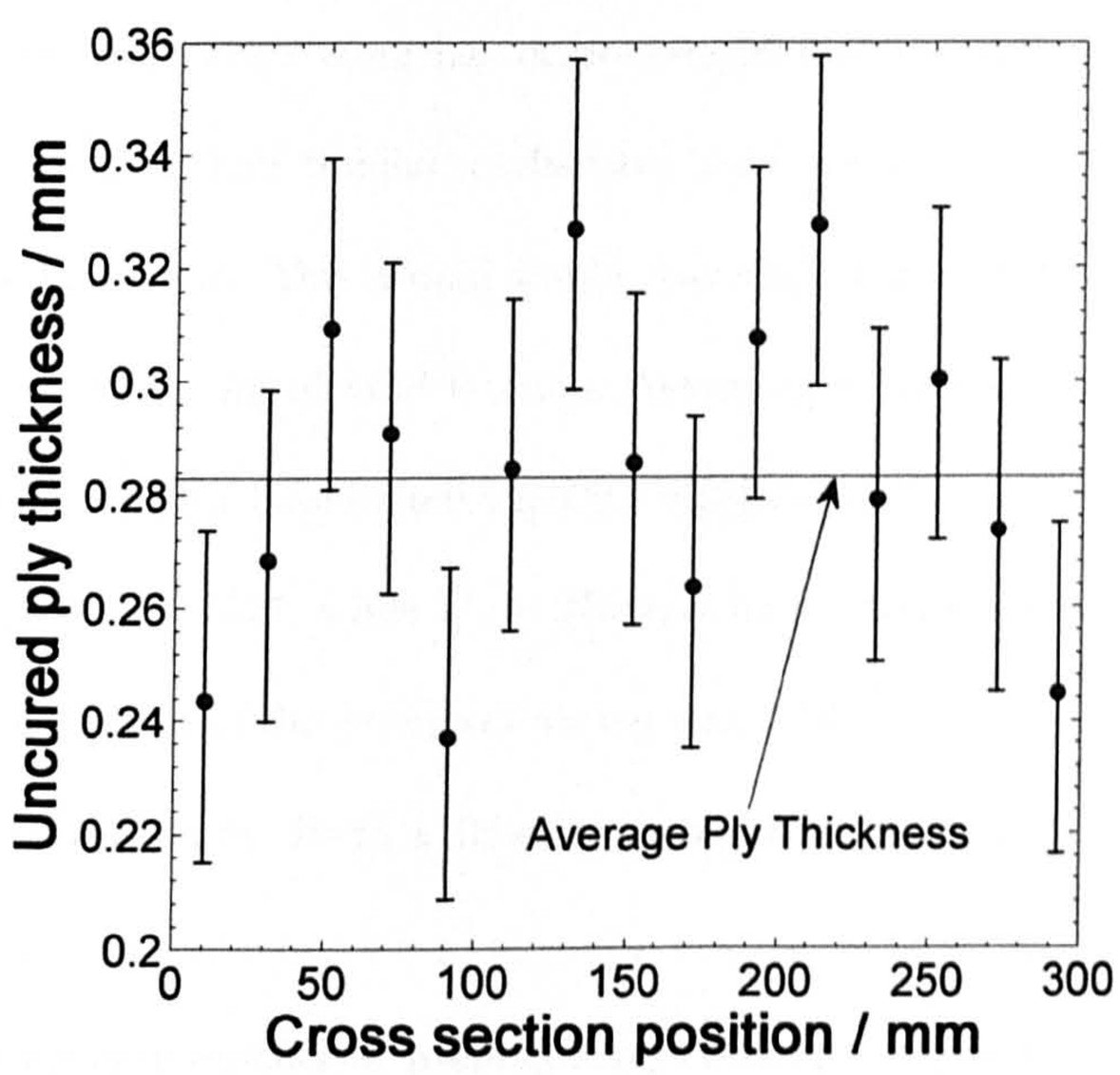

Figure 83: Uncured ply thickness of M21 as a function of cross section position.

voidage is taken into account.

The results for the uncured ply thickness do not show a trend similar to the void content. Additionally, it would be sensible to assume that areas with a higher void content exhibit higher uncured ply thicknesses. This cannot be observed for the specimens under investigation here. No correlation between the uncured ply thickness and the void content can be seen. The average ply thickness from this analysis is used in chapter 6 to calculate the nominal stresses in a ply during mechanical testing.

5.5 Discussion and conclusions

Void content and void sizes have previously been studied to understand the evolution of voids during cure and to optimize the cure cycle. Ledru et. al [139] use thermodynamic equilibrium conditions and a coupled diffusion model to calculate the evolution of voids throughout cure for M21. Their work has demonstrated that a standard cure cycle will only reduce the void diameter by half. Similar results have been obtained by Olivier et al. [140] for a different epoxy resin system. This would imply that the void area fraction could only be reduced to a quarter of the initial void fraction. Assuming perfect consolidation during cure and no diffusion of voids, the base material quality is high enough to obtain parts with a cured voidage of $V_v = 1.27\%$ for M21, while $V_v > 2\%$ may be found in radii and ply drops. While this is a gross simplification of the processes during cure it illustrates the importance of a high prepreg quality and uniformity. Even a flawless manufacture will not improve on the basic material quality.

Samples for measurements of prepreg resin content for specification and conformity purposes are larger (100x100mm) than the ones we used here. The materials studied are within

specification regarding the mean and the variability. Outliers are found randomly over the sample area, both above and below the variability limits. A characteristic variability can be observed along the width of a prepreg ply. The average resin content is higher on the outside and decreases towards the middle. This distribution is similar to the observed void distribution and may therefore be linked to prepreg manufacture. The amount of resin and its apparent concentration on the top and bottom of the prepreg allows for a controlled and high tack during layup. Narrow tape (6.35mm to 25.4mm width) for automated layup is normally produced by slitting an entire roll of prepreg tape into slices. The local variability of the resin content may affect the manufacturing process detrimentally due to dry fibre in the tows and irregular tack. Specification requirements should therefore be modified to reduce the observed variability in the material.

The assessment of the surface roughness is the first time such results have been reported for uncured prepreg. The surface of M21 is surprisingly rough with no preferred orientation of the roughness with respect to the fibre direction. This can be deemed as highly unsuitable for a robust high quality manufacture. The interply zone is likely to entrap voidage, which is highly localized and not connected. For small, laboratory scale parts this has little implications, as the air is likely to escape. For larger parts a significant amount of voidage between the plies can be expected, which needs to be mitigated against during cure. Such a part will exhibit void contents in excess of 2% which is generally considered unacceptable for aerospace components [8, 138].

6 Mechanical characterisation of uncured prepreg

6.1 Introduction

During manufacture by ATL or AFP, the layup system automatically places uncured prepreg tape or tows on a tool or previously laid up material. Common defective features that are associated with automated layup are bridging of geometric features, overlapping, and excessive gaps between tapes or tows. Higher porosity in the uncured part is also commonplace due to the regular omission of vacuum consolidation as void removal during layup may be ineffective for most large structures commonly made using automated layup [117, 118]. Most research work in the past was aimed at addressing issues during thermoplastic tape laying, see Ranganathan et.al. [141], Pitchumani et.al. [142] and Toso et.al. [143]. Also, Sarrazin and Springer [144] derived a process model for thermoset layup from existing thermoplastic models, but this area has in general received little attention.

The layup zone of an automated layup system consists of a flexible roller or stiff layup element that exerts a compression force onto a prepreg and a sequence of heaters to control the temperature [8]. The configuration of this layup zone is shown in Figure 84. Both ATL and AFP control the tension on the ply to some degree to enable layup into concave features and improve fibre straightness. Additionally, in ATL the ply-backing paper is automatically removed under a controlled tension. The uncured material is thus delivered into a gap between the flexible roller and tool at a set temperature and tension.

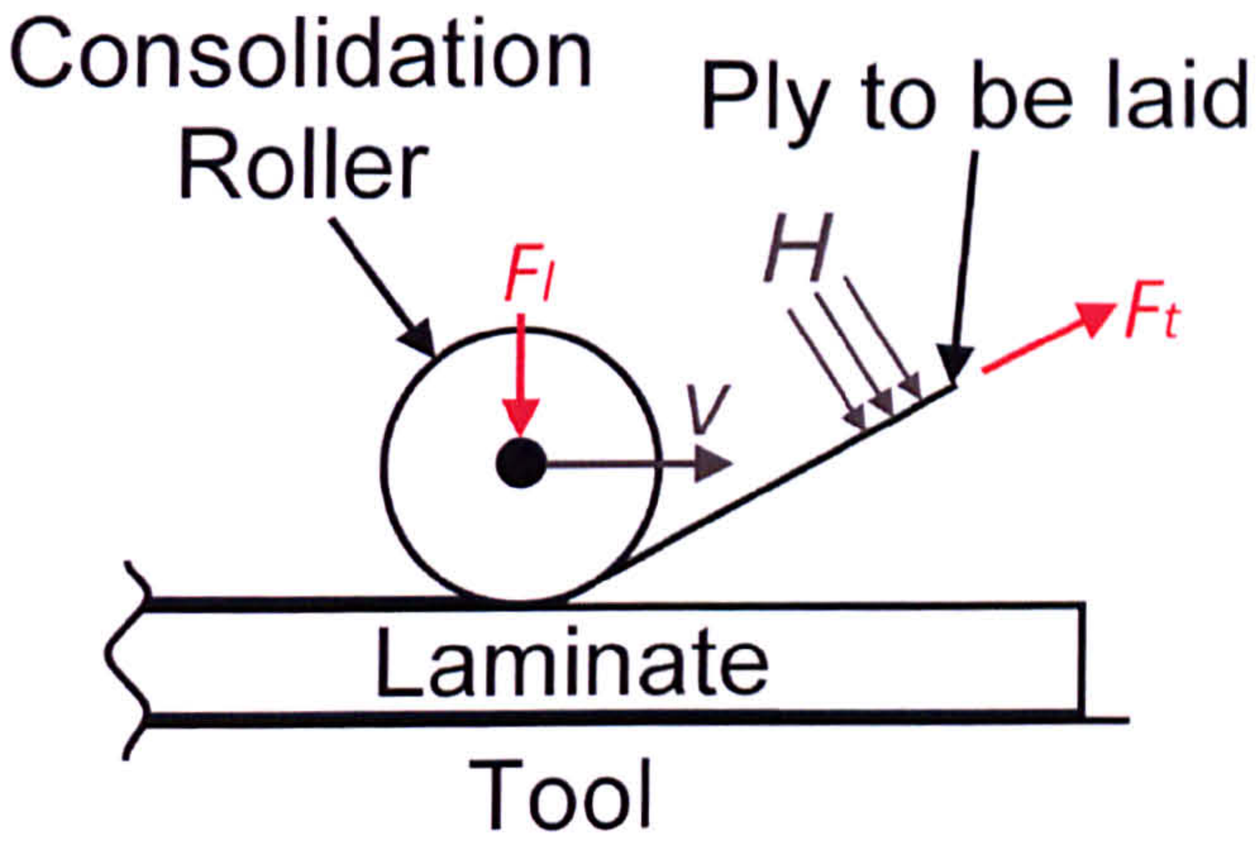

Figure 84: Initial undeformed configuration of an automated layup system.

A compaction load is then applied to the substrate, with common values of $F_l \leq 445$N (~100lbf) [145] for 75mm wide tape up to a maximum of $F_l = 1000$N for 300mm wide tape. The roller-sleeve that interacts with the material is commonly made of soft silicone rubber and typical diameters, R, vary between 15mm to 25mm. The soft silicone roller has been reported to deflect under the compaction force by up to $h = 5$mm [92]. The load deflection curve is thus nonlinear due to material behaviour of the silicone rubber and the geometry of the roller. The amount of deflection depends on the roller material, the prepreg material, temperature and applied load. The contact length between the roller and the prepreg can be approximated from,

$$l = 2\sqrt{2Rh - h^2}\,, \tag{6-1}$$

with l being the contact length, R the undeformed roller radius and h the deformed height, see Figure 85. For a roller with $R = 25$mm compacted by $h = 5$mm, the contact length l is approximated to be 30mm, and the above example assumes that the roller is fully deformed. The calculated contact length between roller sleeve and prepreg is therefore an upper limit.

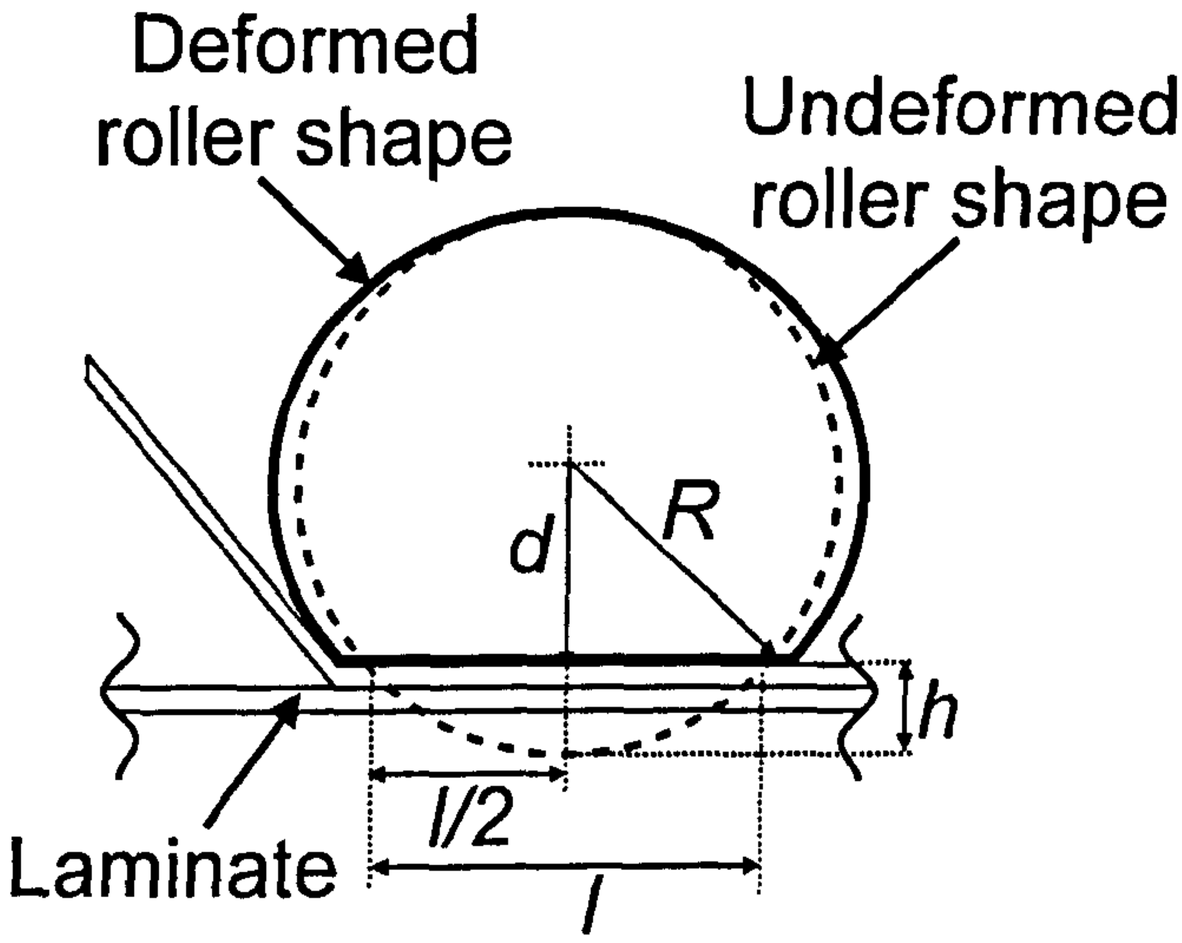

Figure 85: Deformed configuration of layup system and prepreg during automated layup.

Typical layup systems operate at speeds of $10 < v\ [\text{m/min}] \leq 60$, while some systems are capable of speeds up to 85m/min [118]. For the layup speeds given above, the total contact time can be calculated using,

$$t = l/v\,, \tag{6-2}$$

with t being the contact time, l the contact length and v the layup speed. For a contact length of $l = 30\text{mm}$ this will result in a contact time of $t = 0.18\text{s}$ at $v = 10\text{m/min}$ and $t = 0.03\text{s}$ at $v = 60\text{m/min}$. The total time for any load application is thus very small.

Lastly, the tape is typically heated to control tack and formability. Calawa and Nancarrow [41] reported that a layup temperature of $T = 35°\text{C}$ was ideal for most epoxy prepreg materials. A similar observation was made by Ahn et.al. [42], reporting that the tack of uncured prepreg reached a maximum at 20-25°C above the instantaneous glass transition temperature. This instantaneous glass transition temperature of uncured prepreg is a function of the resin formulation and degree of cure and is normally around room temperature for

automated layup grades. For most prepregs, layup thus occurs at temperatures between T = 20°C and T = 40°C to achieve high tack levels during layup. Consequently, for a 300mm wide tape and a speed of 10m/min a model for the automated layup process would have to accurately capture the material response over a temperature range of ΔT = 20°C and a load range of $0 < F_l$ [N] < 1000.

Prepreg undergoing cure is often treated with flow models, where the liquid resin flows through the fibre bed [146], or fibres and resin flow together due to a deviatoric stress [147]. Hubert and Poursartip have published an extensive review of the early literature in this area [147]. During cure, the viscosity advances with increasing degree of cure yielding changing material properties as a function of temperature and time. The earliest model by Loos and Springer [148] assumed simple shear flow while percolation flow models were developed by Davé [149] and Gutowski et al. [150] Thermoplastic forming is generally analysed using the shear flow approach, while percolation flow has been used extensively in the past to capture the consolidation behaviour of thermoset prepregs [151]. During percolation flow modelling the load is shared between the fibres and the resin and the resin flows due to an effective pressure on the laminate that is not born by the fibre bed. The fibre-bed compaction behaviour was studied by Gutowski et al. [152], Poursartip and Hubert [153] and Gu et al. [154]. Generally, the fibre-bed compaction behaviour is a non-linear stress-strain relationship as increasing compaction leads to a higher fibre volume fraction, which in turn leads to more loading of the fibre bed as opposed to the resin. It is assumed that the compaction behaviour is quasi-static, which is applicable for cure simulation, as the loading time is long. Gutowski and Dillon [151] have pointed out that consolidation models fail to accurately capture the material properties for short loading times.

Consequently, viscoleastic material models for uncured prepreg have been developed [155-161]. Schapery [162] proposed an approach for modelling viscoelastic or elastic viscoplastic material behaviour that can be extended to non-linear materials. This approach has been used successfully by Megnis and Varna [163, 164] to calculate the non-recoverable, permanent deformation, during consolidation of a prepreg. It was shown that a viscoleastic model was generated and the strains were separated into viscoelastic and viscoplastic strains. The error that is introduced from a simplified approach, e.g. assuming time-independent mechanical properties can be easily demonstrated by calculating the change of modulus with time in a relaxation experiment from a Prony series expansion of the form [165],

$$E(t) = E_e + \sum_{i=1}^{m} E_i e^{-(t/\rho_i)} \quad , \tag{6-3}$$

with E_e being the equilibrium modulus, E_i the relaxation modulus, ρ_i the relaxation time and m the number of Prony series coefficients. A simplified time-independent material model would be of a nonlinear elastic-plastic behaviour. This approach is commonly used to model forming of sheet metal but may be valid here due to the short forming times that need to be considered. The plastic material behaviour can be described as strain hardening of the material by a simple power law [166],

$$\sigma = A\epsilon^m + \sigma_0 \, , \tag{6-4}$$

with ε being the plastic strain, σ the instantaneous stress, σ_0 the yield stress, and A and m being the strain hardening coefficients.

Any attempt to model the behaviour of prepreg would have to identify whether the nonlinearity, the time-dependent behaviour, or both, need to be considered. If the error introduced by assuming time-independence of the elastic properties is small the material can be

modelled with an elastic/plastic model where the permanent deformation is nonlinear after reaching a yield stress/strain limit.

The purpose of this chapter is thus to evaluate experimental data from creep and compression experiments to obtain a viscoelastic and a elastic-plastic material description for uncured unidirectional prepreg. The two material models are then compared to identify an accurate and simple model for the through-thickness compression of uncured prepreg. The through-thickness tests show the validity of an elastic-plastic material model. The subsequent material characterisation is consequently carried out to obtain elastic material properties only, not taking into account time-dependant material behaviour.

6.2 Experimental procedure

6.2.1 Through thickness compression

The through-thickness compression or consolidation modulus is a relevant property for almost all prepreg applications, e.g. autoclave cure, press forming, debulking or automated layup. For small strains it is dominated by the matrix properties and is thus a time, temperature and load dependent value.

Samples for compression testing were prepared from M21/IMA-ATL prepreg. The laminates were 100mm long; 60mm wide and 8 plies thick. Samples were pressed under vacuum at room temperature for an hour prior to testing [153]. The test setup consists of two heated plates that are brought in contact with a stack of prepreg at a defined displacement between 0.1 and 0.5mm. The temperature range tested here is 20, 30 and 40°C. The heated plates were capable of controlling the test temperature within $\Delta T = \pm 1$°C. The loading time

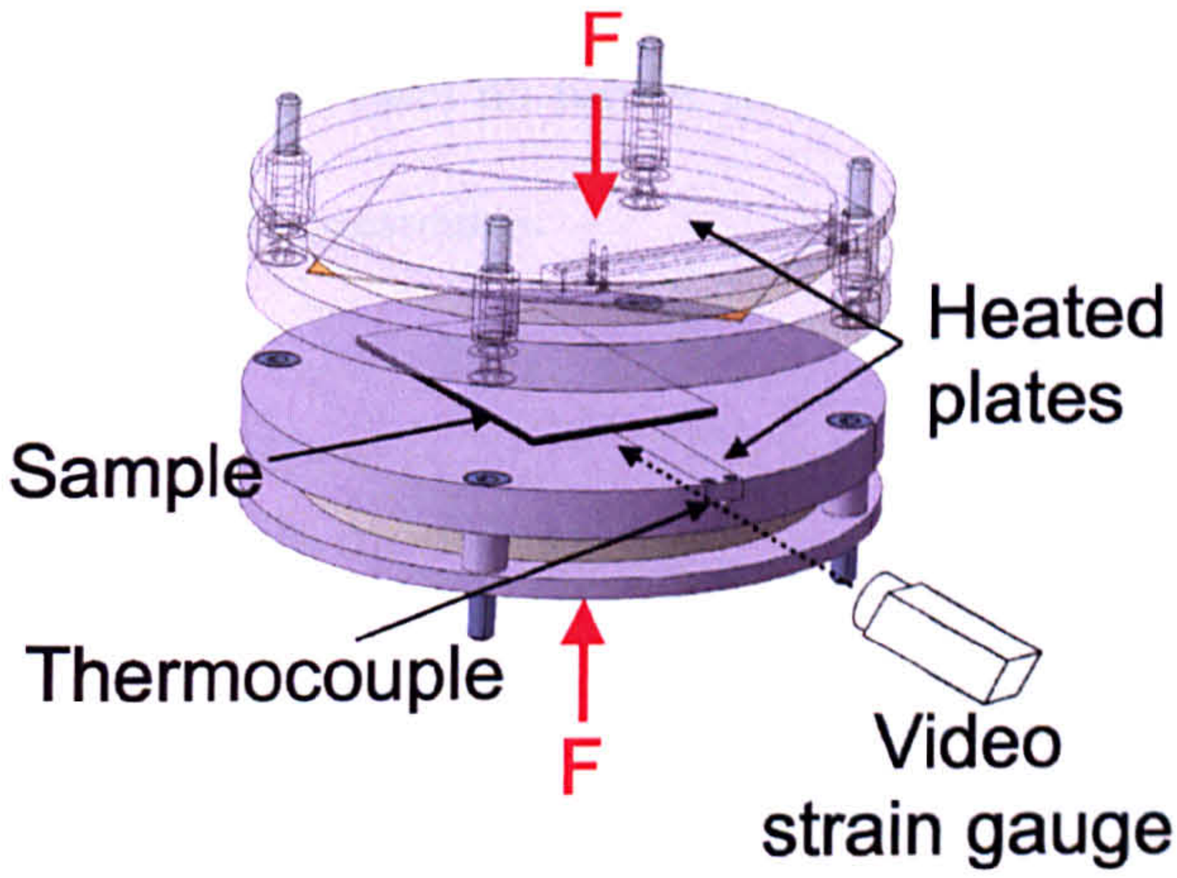

Figure 86: Scheme for the test setup for the transverse compression modulus.

was 60s in all cases. A schematic of the test setup is given in Figure 86. The plates were held in position for t = 60mins at 0.1mm to 0.3mm displacements and for t = 90mins at 0.4 mm and 0.5 mm displacements. The reduction of the load as a function of time is recorded and calculated into a relaxation curve. The transverse strains during the initial loading phase are recorded with a video strain gauge [167].

To measure the through-thickness stress-strain behaviour another set of samples with the same dimensions and layup were prepared. The sample dimensions before and after testing were recorded. The sample height was measured at six positions with a micrometer. The sample length and width were measured with a calliper. The sample width was recorded at both ends and the average was taken as sample width to compensate small shape changes after testing. A total of eight samples were tested under load control at T = 20°C, 30°C and 40°C each and in the range of loads between F = 0.2kN to F = 15kN. Samples were tested at a loading rate of 10kNmin^{-1}, which was the maximum that could be achieved with the test machine for the given test setup. The strain values were calculated after the experiment from the sample dimensions before and after testing and the pressure on the laminate was calculated

from the final sample dimensions. Samples were selectively measured again after t ~ 12h to verify any further relaxation. In all cases no further relaxation had occurred and it is believed that this is due to the lack of side constraints.

6.2.2 Fibre direction tensile modulus

Test methods and sample geometries were adapted from Langer [168]. The samples were single plies of M21/IMA-ATL prepreg cut with a ply cutter. The specimens were 520mm long and 75mm wide, see Figure 87. Composite endtabs were bonded to the ends using localized heating for 20min at 180°C. The endtabs were 60mm long and 75mm wide. The gauge length was thus 400mm. After endtabbing a spray paint speckle pattern was applied on the specimens to improve the accuracy of the video extensometer reading. The endtabs were then wrapped with emery cloth to improve the friction and avoid slippage when mounted in mechanical grips. An Instron servo-hydraulic test machine with 27kN load-cell was used for all tests. Samples were tested using controlled force at 100N/s until failure. Load control was found to yield more consistent results than displacement control, independent of the loading rate. This is likely due to a visco-elastic response of the sample to mechanical loading.

Strain was recorded using digital image correlation (DIC). A video extensometer with a telecentric lens was used. This lens reduces the sensitivity to out-of-plane displacement of the sample and reduces the scatter of the individual strain measurements. A total of nine markers were tracked on the speckle pattern, resulting in six strain readings. Two samples were tested up to a load of F = 2kN, approx σ = 100MPa. From these tests an initial pre-strain was calculated. This value was used to correct the total strain for the strength calculation for

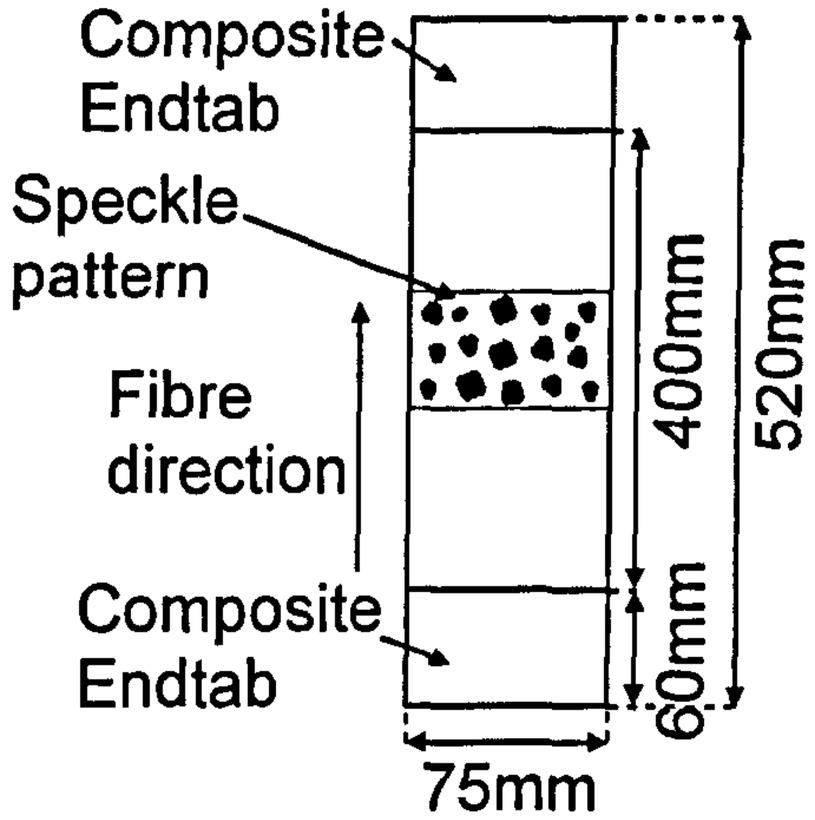

Figure 87: Geometry of an uncured single-ply prepreg specimen for tensile testing.

uncured prepreg. Another five samples were then tested to failure to calculate the tensile modulus, strength and strain to failure of uncured prepreg.

6.2.3 Shear modulus

Potter [169] has shown that uncured prepreg deforms under pure shear if the fibre direction is at an inclination of 15° to the test direction. The author used four ply thick laminates for testing that were vacuum debulked for an hour before testing. Similar sample dimensions and preparation methods are used here. The sample length was modified slightly to accommodate different grips. The samples are 50mm wide and 420mm long. The grips are 60mm long so the effective gauge length is 300mm. The samples are prepared with a speckle pattern to improve the accuracy of the strain measurement. Specimens were mounted directly into mechanical grips. The test setup is shown in Figure 88.

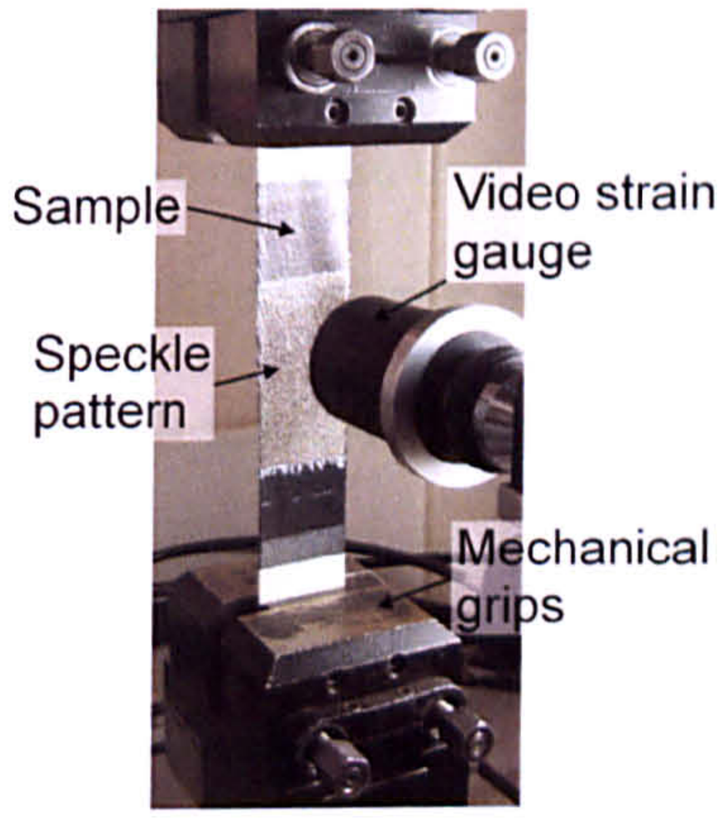

Figure 88: Test setup for shear testing of uncured prepreg specimens.

A 27kN load-cell was fitted to the test machine. Samples were tested using a controlled displacement rate of 1mm/min. The strain was recorded directly on the sample using a video extensometer. A total of five samples were tested to failure.

6.2.4 Poisson's ratio

The Poisson's ratio was tested in a simple tensile test. Initial tests were performed on specimens identical to the tensile test described previously. Strain was recorded using a video extensometer. Unfortunately, this did not yield any consistent results since the mechanical response was dominated by the individual tows. During loading these would push against each other and form bands running down the length of the specimens, see Figure 89. The lines indicate a negative Poisson's ratio, i.e. the tows expand in the transverse direction under longitudinal loading. The test was therefore modified by testing individual tows. These were extracted from the prepreg as follows. A tensile specimen, using the same geometry as described previously, was taken to failure in a load-controlled test. Failure occurs randomly in the sample width and the test is stopped immediately after the first tows fail. Some tows remain intact during this test and can thus be cut out from the failed specimen. These individual tows

were between 1.5 and 2mm wide, which is consistent with the approximate flat tow width of a 12K tow of 5µm diameter fibre. The tows were then prepared for another test using a second test machine with a 1kN load cell. Endtabs were prepared by casting the tows into room temperature curing epoxy resin at both ends, see Figure 90.

The final gauge length was approximately l = 80mm. A total of five samples were prepared. For testing the samples were preloaded to F = 30N to straighten them. The sample was then loaded up to 300N at 100N/min, while the longitudinal and transverse strains were recorded with a video extensometer.

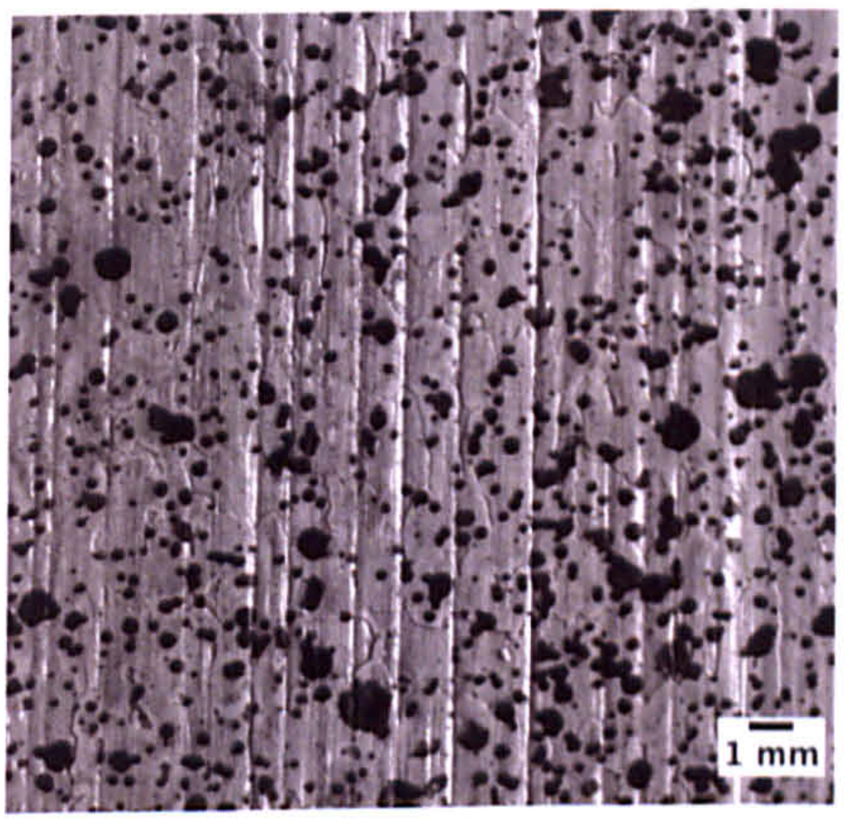

Figure 89: Lines forming in a prepreg during tensile loading.

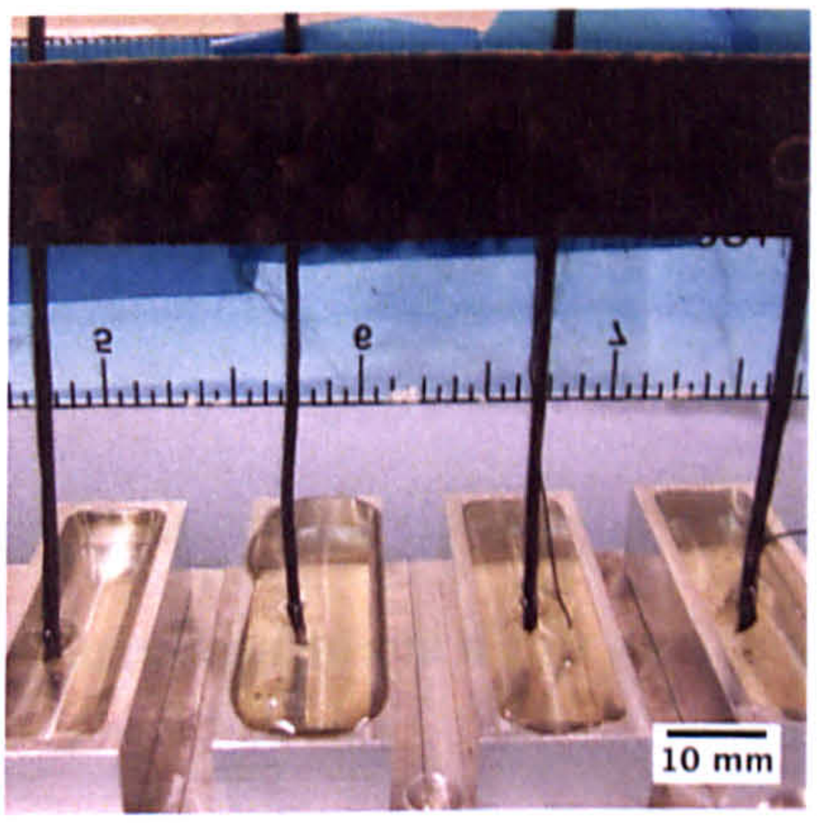

Figure 90: Individual tows cast into epoxy resin as endtab.

6.3 Experimental results

6.3.1 Through thickness compression

Material response in the transverse direction is governed by a time-dependent response from the matrix and the nonlinear behaviour of the fibre-bed during consolidation. Based on these results a suitable model for uncured prepreg during layup can be developed. To measure the final strains of the specimens, their dimensions were recorded before and after testing. The modulus was then calculated from the equivalent stress data and the final strain in the through-thickness direction. The modulus as a function of time is plotted for 20°C in Figure 91, for 30°C in Figure 92 and for 40°C in Figure 93.

Initial and relaxed moduli are a function of strain and temperature. The time-dependence of the compression modulus was estimated using a Prony series expansion given in Eq. (6-3) with m = 5. The fitted Prony series coefficients are summarized in Table 12 for 20°C, Table 13 for 30°C and Table 14 for 40°C. The fitted interpolation is plotted as a line on each data set in Figure 91, Figure 92 and Figure 93. The change in modulus is then calculated for a range of load application times, encompassing the load application times expected in automated layup, presented in Table 15. This change in stiffness can be interpreted as the error that is introduced by the assumption of time-independent material properties. For the typical timeframe of automated layup of $t < 0.1$s the maximum change in stiffness is 1.26%, which was observed at $T = 40$°C and 0.2mm displacement. This is inconsistent with the other test conditions, which yielded significantly smaller changes in mechanical properties. Generally, the error decreases with shorter contact duration and higher displacement. Currently, this singular

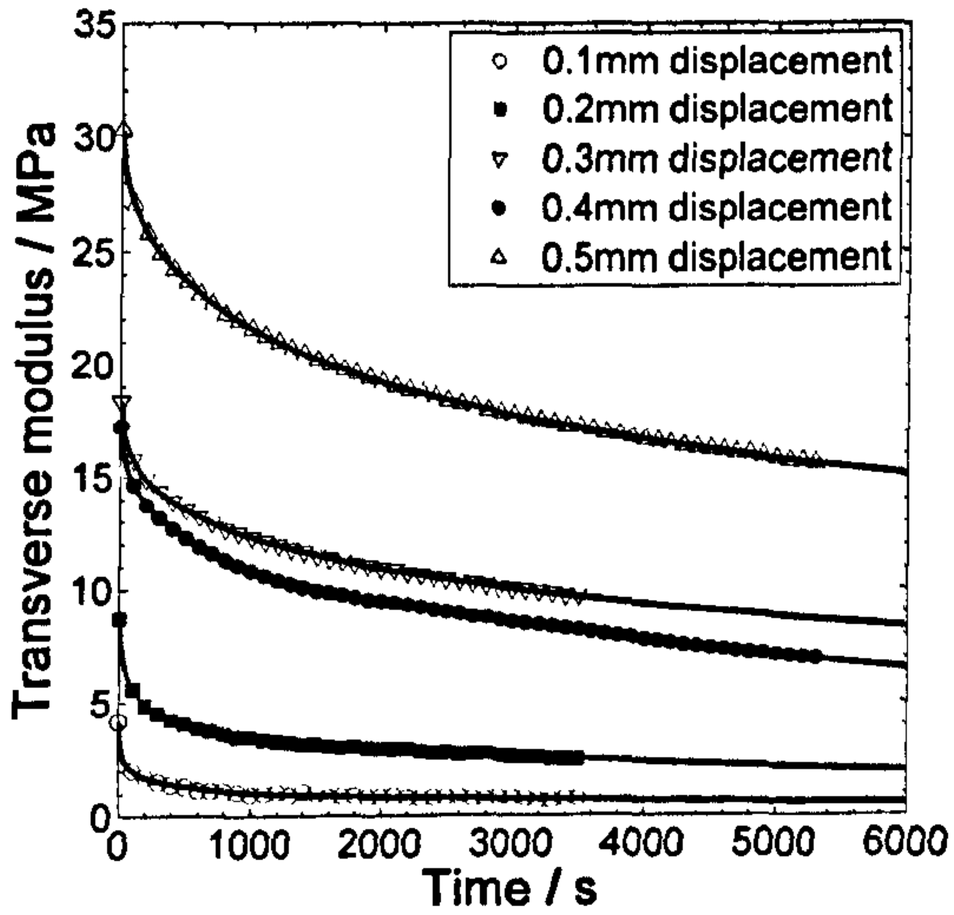

Figure 91: Relaxation curves for uncured prepreg at different displacement at 20°C. The fitted Prony-series is plotted as line.

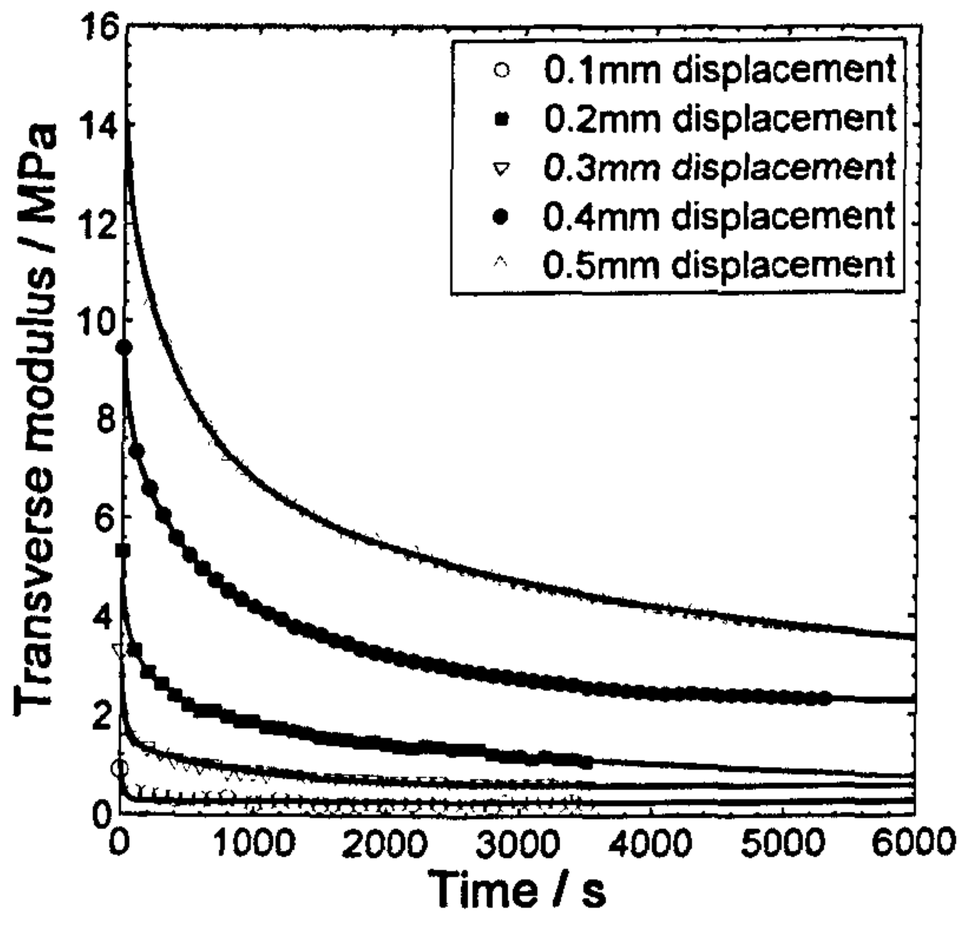

Figure 92: Relaxation curves for uncured prepreg at different displacements at 30°C. The fitted Prony-series is plotted as line.

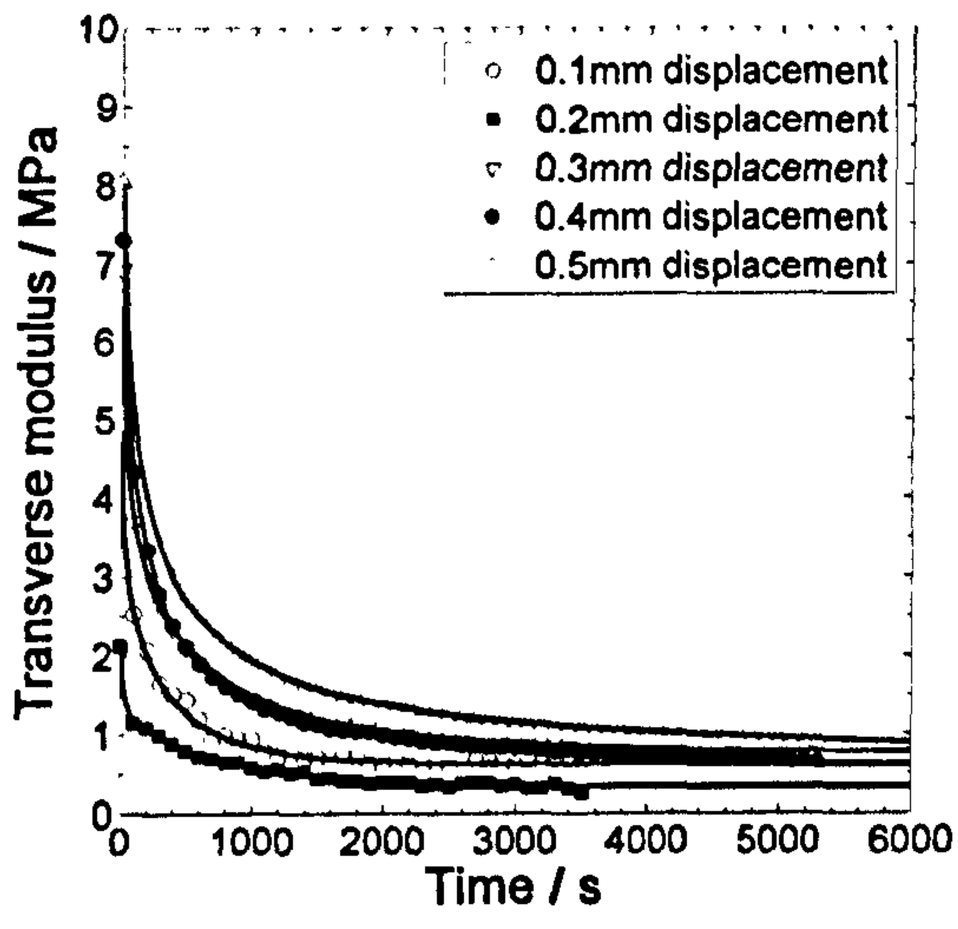

Figure 93: Relaxation curves for uncured prepreg at different displacements at 40°C. The fitted Prony-series is plotted as line.

outlier cannot be explained. By assuming time independent material properties a negligible error is introduced since typical contact time in automated layup are shorter than 0.18s. The stress-strain responses during through-thickness compression loading for three different

Table 12: Prony-series coefficients for M21 prepreg at 20°C for various displacements.

		20°C				
		Displacement [mm]				
Coefficient	Unit	0.1	0.2	0.3	0.4	0.5
E_e	MPa	0.00	0.60	0.00	0.00	2.05
E_1	MPa	0.38	1.49	1.94	0.42	3.07
p_1	S	2.27	78.52	263.83	5.49	371.95
E_2	MPa	0.85	1.10	0.59	11.29	16.69
p_2	S	10.70	15.84	8.96	10746.94	22986.90
E_3	MPa	0.98	2.10	3.27	4.09	0.90
p_3	S	10914.05	399.85	1354.78	490.41	13.00
E_4	MPa	0.86	2.99	11.25	0.01	5.99
p_4	S	65.94	7420.78	19545.07	0.10	1679.08
E_5	MPa	1.05	0.38	1.25	1.39	1.60
p_5	S	501.29	3.14	49.60	42.54	69.18

Table 13: Prony-series coefficients for M21 prepreg at 30°C for various displacements.

		30°C				
		Displacement [mm]				
Coefficient	Unit	0.1	0.2	0.3	0.4	0.5
E_e	MPa	0.27	0.00	0.58	2.21	2.62
E_1	MPa	0.00	0.86	0.94	3.60	5.17
p_1	S	26.15	20.17	58.73	1602.94	428.37
E_2	MPa	0.14	1.14	0.86	0.34	0.00
p_2	S	27.15	117.73	913.73	9.74	25.07
E_3	MPa	0.17	1.95	0.22	2.29	0.17
p_3	S	26.88	6259.92	8.35	299.46	27.32
E_4	MPa	0.21	0.28	0.22	0.05	4.77
p_4	S	26.56	2.92	8.34	1.53	3698.85
E_5	MPa	0.25	1.09	0.22	0.96	1.38
p_5	s	27.30	561.30	8.36	48.09	52.91

Table 14: Prony-series coefficients for M21 prepreg at 40°C for various displacements.

		40°C				
		Displacement [mm]				
Coefficient	Unit	0.1	0.2	0.3	0.4	0.5
E_e	MPa	0.27	0.00	0.58	2.21	2.62
E_1	MPa	0.00	0.86	0.94	3.60	5.17
p_1	S	26.15	20.17	58.73	1602.94	428.37
E_2	MPa	0.14	1.14	0.86	0.34	0.00
p_2	S	27.15	117.73	913.73	9.74	25.07
E_3	MPa	0.17	1.95	0.22	2.29	0.17
p_3	S	26.88	6259.92	8.35	299.46	27.32
E_4	MPa	0.21	0.28	0.22	0.05	4.77
p_4	S	26.56	2.92	8.34	1.53	3698.85
E_5	MPa	0.25	1.09	0.22	0.96	1.38
p_5	s	27.30	561.30	8.36	48.09	52.91

Table 15: Overview of percentage differences between initial and time dependent modulus at various temperatures, times and displacements.

	Temperature								
	20°C			30°C			40°C		
	Time								
Displacement	0.01s	0.1s	1s	0.01s	0.1s	1s	0.01s	0.1s	1s
0.1mm	0.06	0.62	5.47	0.03	0.27	2.69	0.03	0.33	3.04
0.2mm	0.02	0.25	2.27	0.03	0.28	2.54	0.13	1.26	8.21
0.3mm	0.01	0.06	0.54	0.03	0.31	2.99	0.03	0.27	2.52
0.4mm	0.01	0.11	0.72	0.01	0.10	0.92	0.01	0.15	1.43
0.5mm	0.00	0.03	0.34	0.00	0.03	0.32	0.01	0.10	0.95

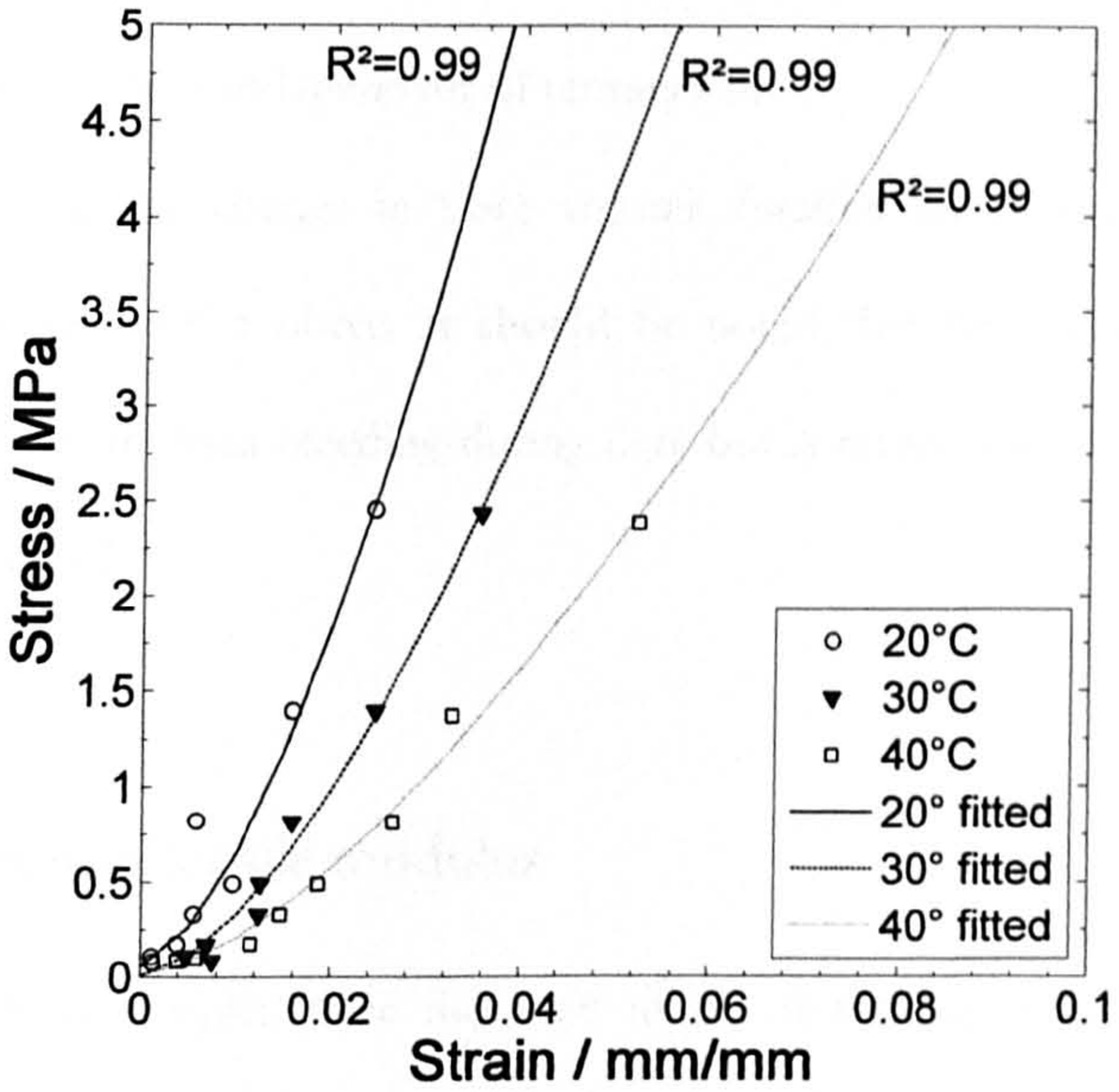

Figure 94: Stress-strain relationships for prepreg at three different temperatures.

Table 16: Fitted Parameters for the strain-hardening power law.

Temperature [°C]	Parameter	
20	A_{20} [MPa]	3502
	m_{20} [-]	1.912
	$\sigma_{0,20}$ [MPa]	0.06
30	A_{30} [MPa]	546.4
	m_{30} [-]	1.597
	$\sigma_{0,30}$ [MPa]	0.006
40	A_{40} [MPa]	659.6
	m_{40} [-]	1.81
	$\sigma_{0,40}$ [MPa]	0.006

temperatures are plotted in Figure 94. For all test ranges and temperatures a nonlinear stress-strain relationship was observed, similar to the results by Hubert and Poursartip [153]. For fibre-bed compaction the strain-hardening coefficient m is greater than 1.

The coefficients are given in Table 16, the resulting curves can be seen in Figure 94. The material is deformed elastically up to the yield limit σ_0, and as the material is compacted

further the plastic stress increases until at sufficiently high strain the stress/strain curve is almost linear and the slope is independent of temperature.

This is due to the change in fibre volume fraction with increasing strain and the increase in load borne by the fibres. It should be noted that this increase in fibre volume fraction is not identical to resin bleeding during cure but is rather due to the reduction of gaps and voids in the material.

6.3.2 Fibre direction tensile modulus

The two initial samples were mounted in the test setup and carefully aligned and tensioned without applying any preload. These results were then used to calculate the initial stiffness and compensate the strain for all following measurements using pre-loading. To calculate the stresses in the ply the sample thickness an average uncured ply thickness of t = 0.283mm was assumed, see section 5.3.4. A pre-stress of 100MPa is roughly equivalent to a preload of 2kN for the sample geometry tested.

Two samples were thus tested between 0 and 2kN load to calculate the initial strain and stiffness for the lead in part of the test. The results for the test are shown in Figure 95. The samples respond non-linearly up to 0.0015 mm/mm. A linear fit is then applied between 0.0015 mm/mm and the maximum strain at 2kN load. The slope of this linear fit is the modulus of the sample. The modulus is thus calculated as E_{11} = 56.4GPa for sample 1 and E_{11} = 56.4GPa for sample 2. The average modulus of E_{11} = 56.4GPa is used to calculate a strain of 0.00355 mm/mm at 2kN load. This initial fit will underestimate the stiffness of the material due to the non-linear lead in. Another set of five specimens was then tested to failure. Samples were initially pre-loaded to 2kN and held at preload for 60 seconds to adjust the video extensometer and start the measurement. Samples were then tested to failure at a rate of

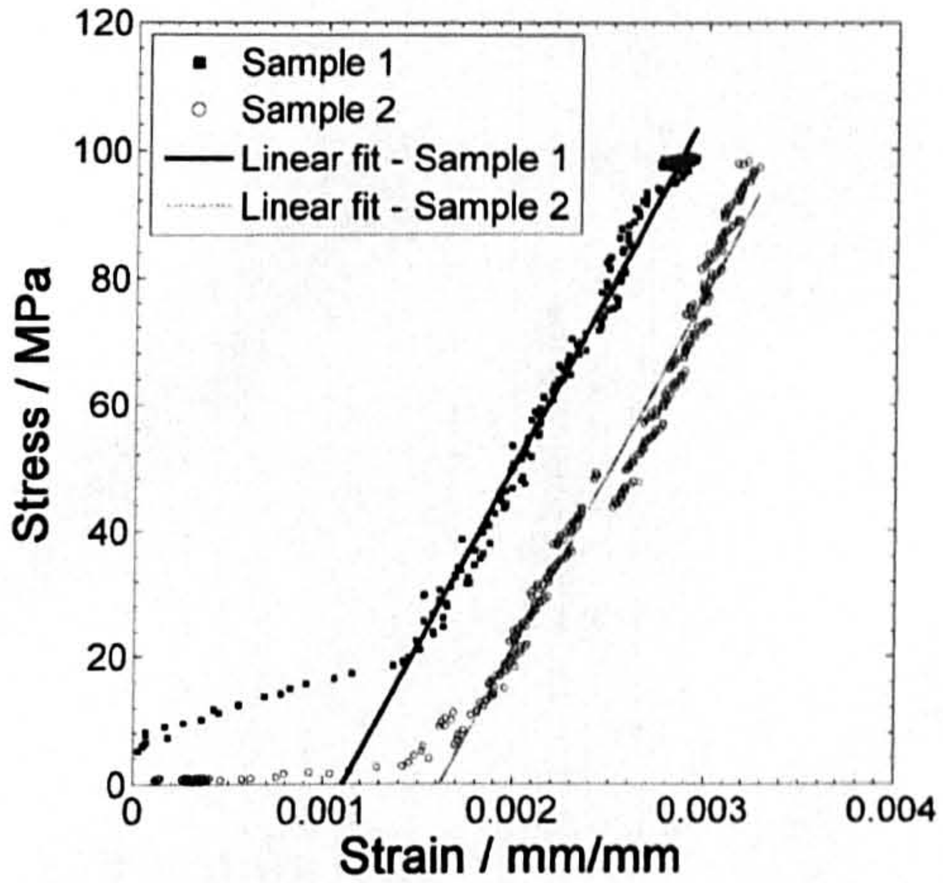

Figure 95: Stress-strain plot for small strain tensile testing with linear fits.

100N/s. A linear fit between 0.004 mm/mm and 0.007 mm/mm was used to calculate tensile modulus data. This range was selected to avoid any overlap between the first modulus fit and to exclude data close to the failure strain of the sample. All samples failed randomly in the gauge. In no case did the failure initiate at the sample edges or close to the end-tabs. This indicates a good sample preparation and fibre alignment. The results of the tensile test are shown in Figure 96 and the fitted moduli are shown in Figure 97. A summary is presented in Table 17. The average tensile strength is 648 ± 64 MPa and the average tensile modulus 83 ± 9 GPa. The calculated average strain to failure is 0.0077 mm/mm.

Table 17: Results for tensile testing of uncured composite specimens

Sample	Nominal cross section [mm]	Load at yield [kN]	Strength [MPa]	Tensile Modulus [GPa]
3	21.225	12.3	580	74
4	21.225	13.8	652	83
5	21.225	15.1	712	76
6	21.225	15.1	711	87
7	21.225	12.4	586	96

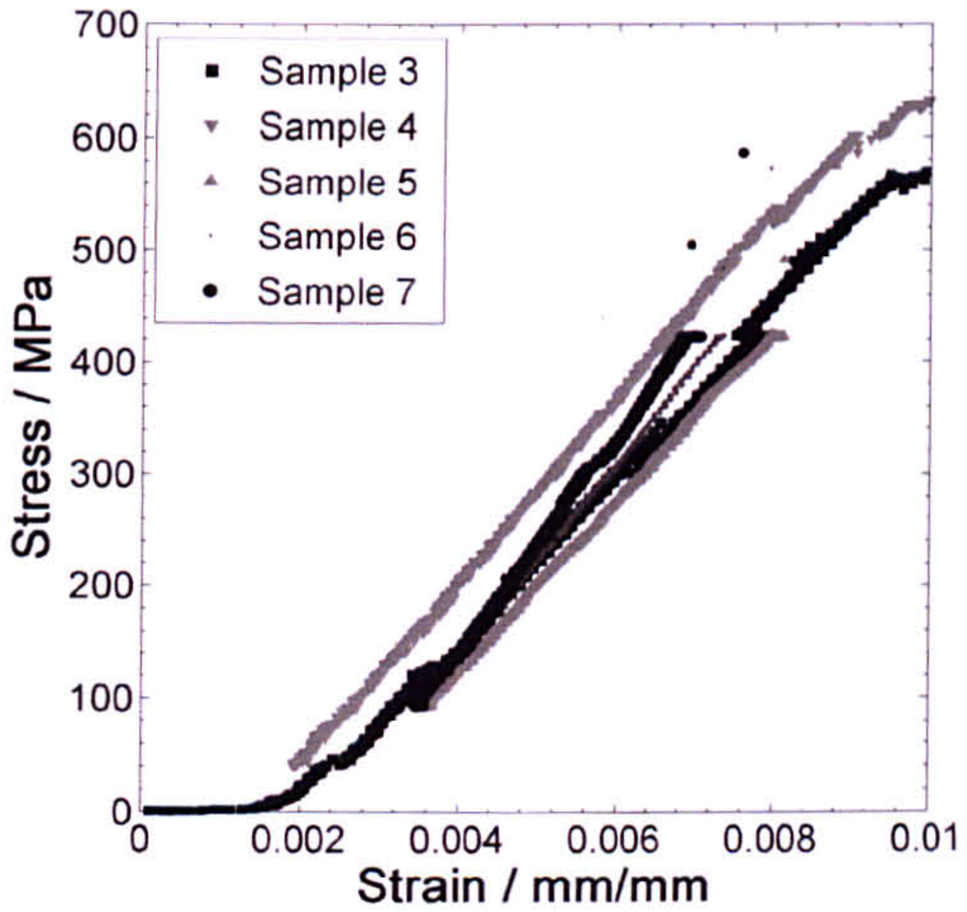

Figure 96: Stress-strain results for tensile specimens.

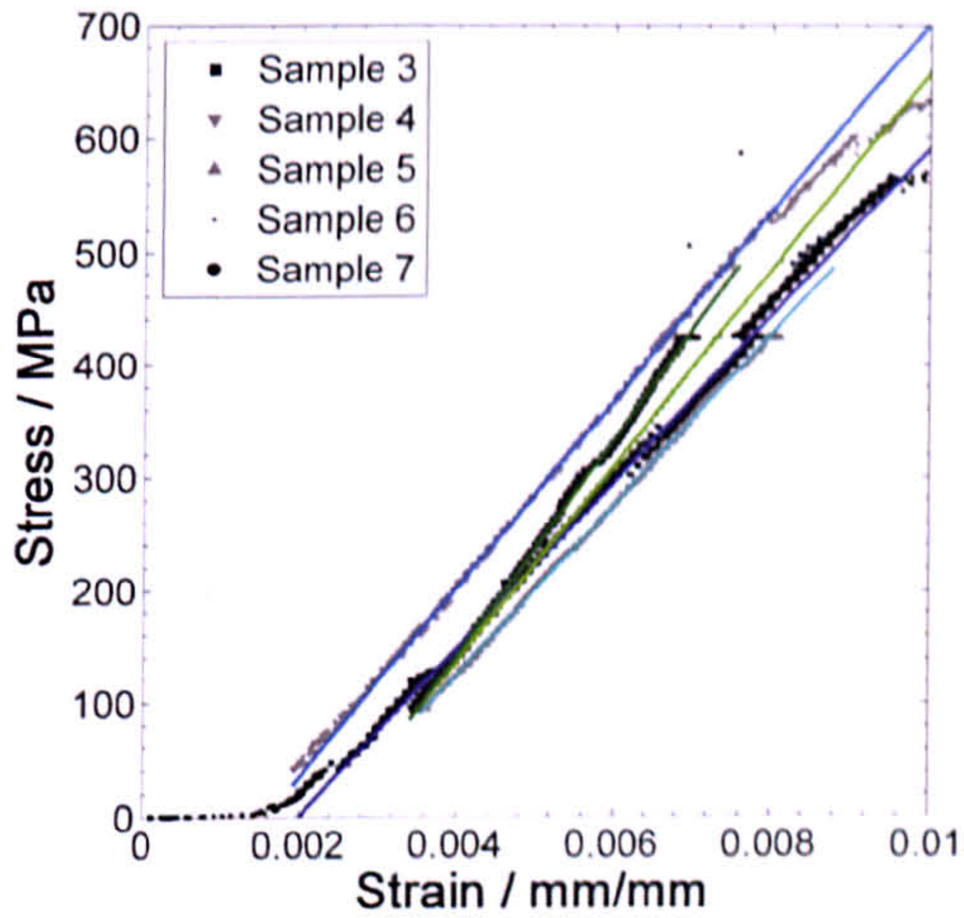

Figure 97: Stress-strain data for tensile testing of uncured prepreg. The fitted moduli are plotted as line.

6.3.3 Shear modulus

A total of five samples were tested for their shear modulus G_{12} using the controlled displacement approach. This can be interpreted as the elastic response of the material. During testing it became apparent that the strain strongly varied locally. This was attributed to the out-of-plane displacement of the specimen under shear and the subsequent rupture of the sample. The video gauge was thus set up to record strain values at the edges and in the middle of the sample using the widest possible spacing between the markers. The strain readings in the middle of the sample were strongly affected by the aforementioned out-of-plane displacement and were consequently omitted from the analysis. Only outside strain readings were recorded. Preload was not applied to the samples due to the low stiffness and strength of the specimens. The average strength from the tests is 6.33MPa. The modulus was calculated from a linear fit between 0.003ε and 0.01ε. The average modulus is 156MPa and the strain to failure 40580με.

An overview of the test results is shown in Table 18. The shear modulus is governed by the properties of the uncured resin and it therefore likely that the shear modulus measured here is dependent on the resin properties, which are degree of cure and temperature dependent.

Table 18: Results for shear tests on uncured prepreg

Sample	Nominal cross section [mm]	Load at yield [kN]	Strength [MPa]	Shear Modulus [MPa]
1	56.60	0.38	6.6	180
2	56.60	0.36	6.4	157
3	56.60	0.36	6.3	156
4	56.60	0.35	6.1	144
5	56.60	0.35	6.1	144

6.3.4 Poisson's ratio

The results for the Poisson's ratio measurements are plotted in Figure 98 as a function of time and in Figure 99 as a function of longitudinal strain. In both cases we see an initial lead in where the apparent Poisson's ratio changes substantially and in some cases oscillates between very high and very low values, before the measurement stabilises. In all cases a negative Poisson's ratio was observed, which was expected from previous ply experiments, see Table 19. The average Poisson's ratio from all measurements is ν_{12} = -2.1, however the scatter is large and this average is not significant. This is of course an unusual result and similar results have not been reported previously. Poisson's ratios have previously been reported for fully cured material or gelled prepreg undergoing cure. Cured carbon-fibre/epoxy has a Poisson's ratio ν_{12} between 0.29 [170] and 0.34 [171] while the resin is incompressible and isotropic and thus has a Poisson's ratio close to ν_{12} = 0.5 [172]. Typically it is assumed that the Poisson's ratio is bound by these limits. This is not the case as the results indicate. The apparent Poisson's ratio of an uncured material is a mechanism rather than a material property. This is

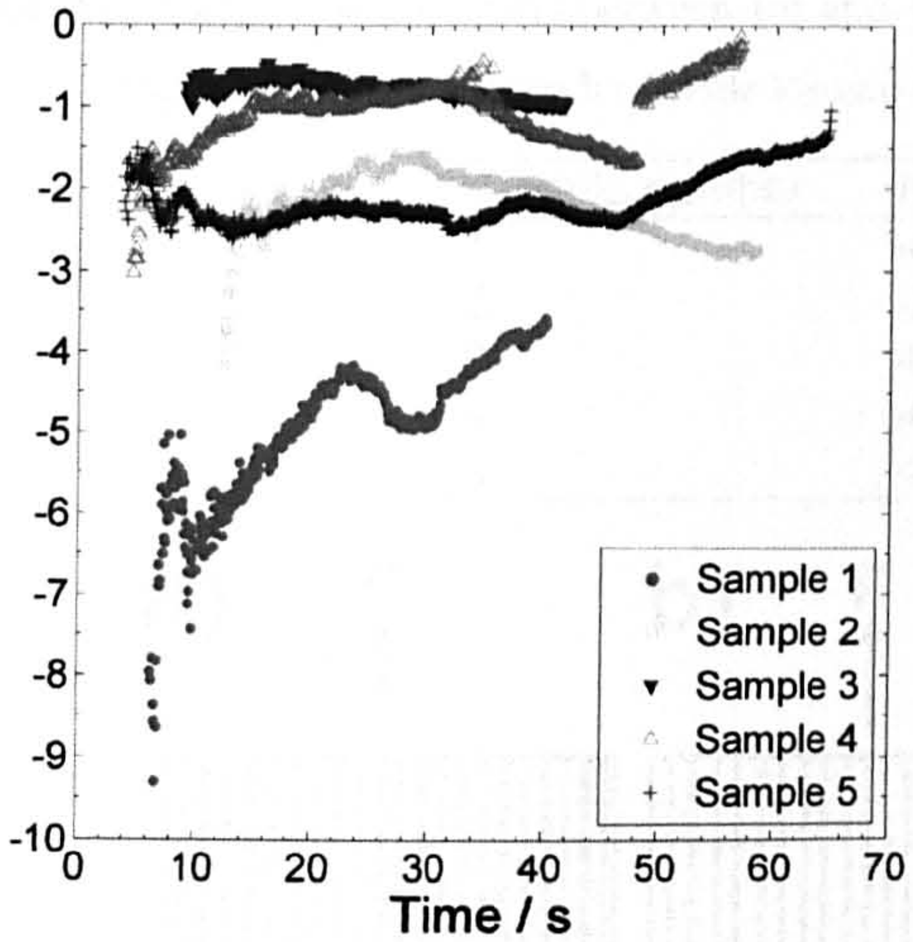

Figure 98: Measured Poisson's ratio as a function of time.

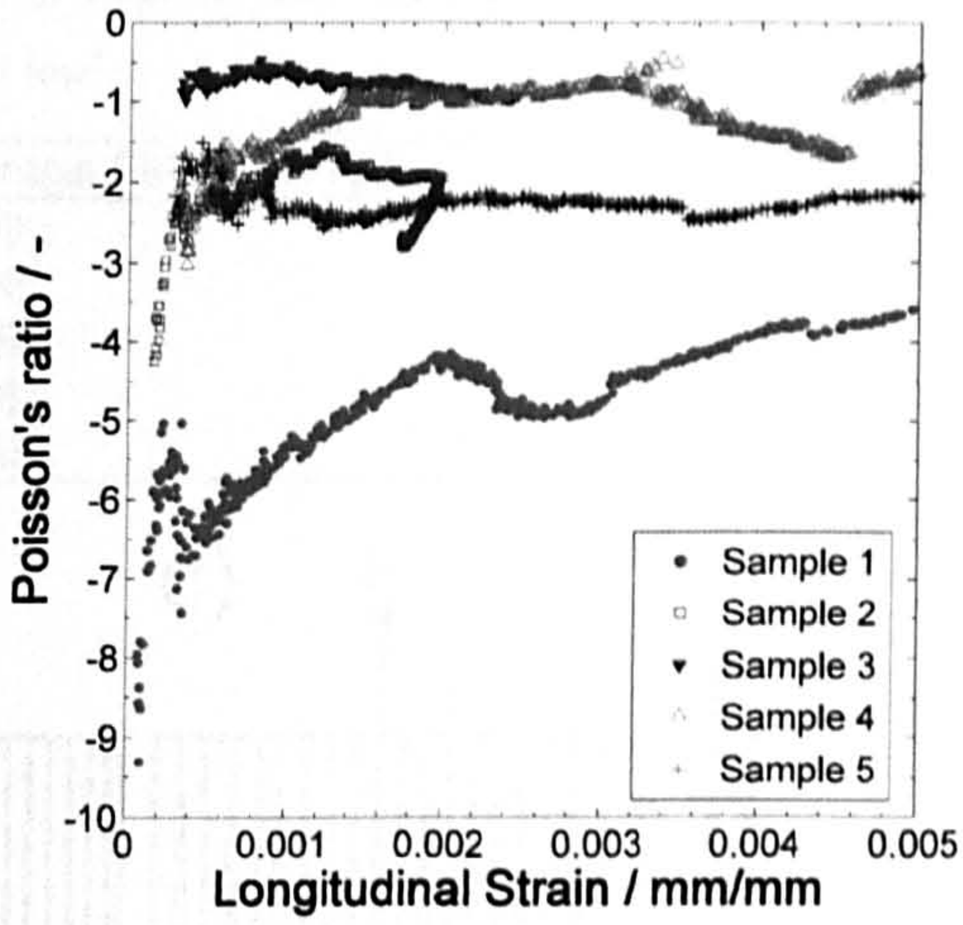

Figure 99: Measured Poisson's ratio as a function of longitudinal strain.

simply due to the fact that the uncured prepreg does not respond as a composite material to external loading but rather like an assembly of fibre and resin. While the difference seems subtle the implications are significant. The Poisson's ratio is governed by the tow architecture. The resin plays an insignificant role in this case because only very limited load transfer can occur between the very stiff fibres and the soft uncured resin. There are three different types of response for the uncured material, which can be linked in a manner in which the tows are brought into the prepreg. The first and most simple case is a Poisson's ratio of zero. In this case neither gaps nor lines will occur in the prepreg on a ply level, see Figure 100b. A Poisson's ratio of zero will likely be observed for flat tows that have a thickness roughly equivalent to the prepreg thickness. This would be the case for prepregs with a low fibre count per tow, e.g. below 12K. The two other cases are characterised either by lines or gaps in the material, depending on whether the tows are expanding, see Figure 100a, or contracting, see Figure 100c, when loaded in tension. The first case was observed here, while Langer [168] has reported a formation of gaps during tensile testing of uncured 8552/IM7 prepreg. It is clear

Table 19: Average Poisson's ratio between 15s and 40s test time. All values are negative, i.e. the material expands transversely under tensile longitudinal load.

Sample number	Average Poisson's ratio
1	-4.49
2	-2.16
3	-0.79
4	-0.98
5	-2.10

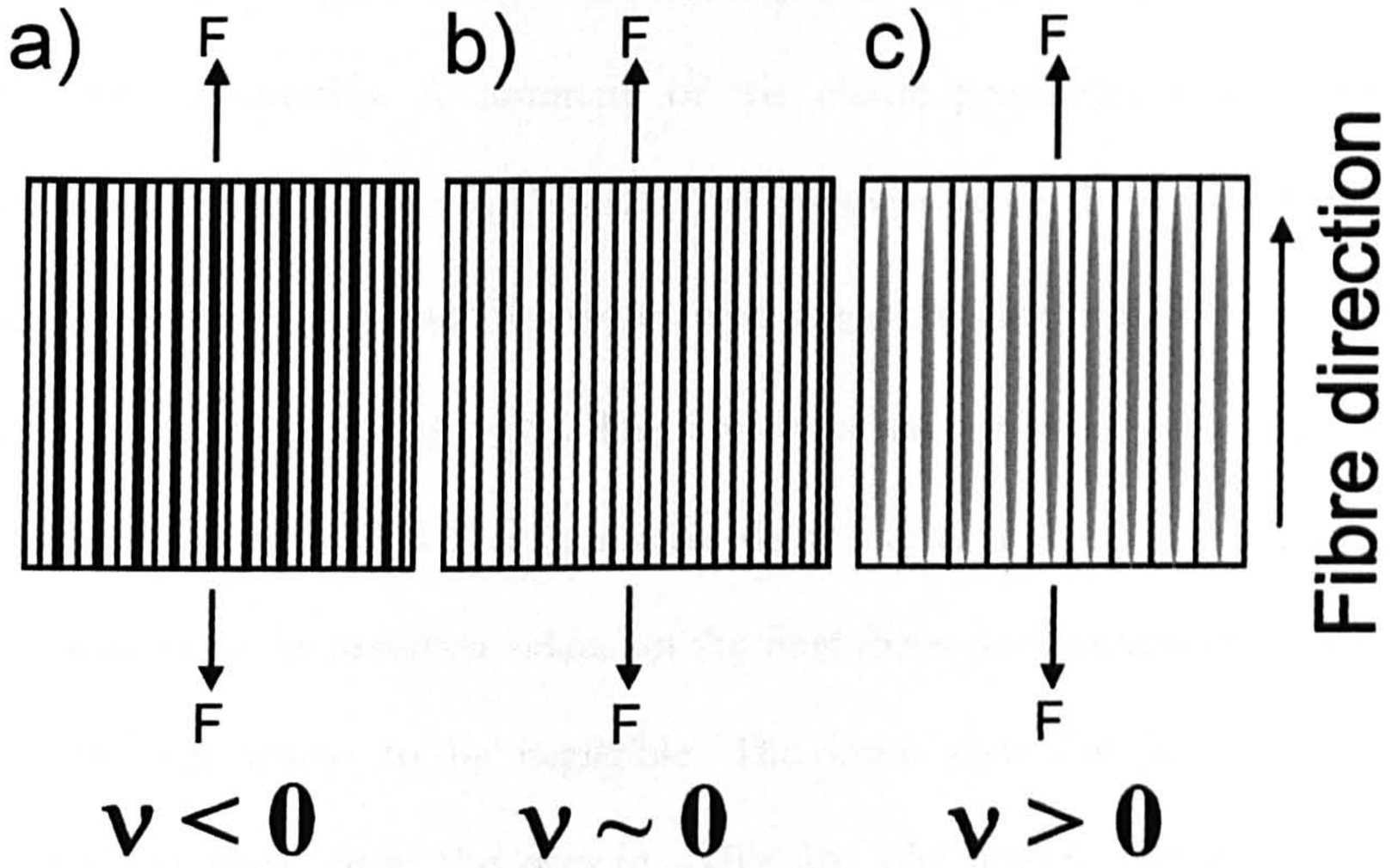

Figure 100: Illustration of the three different ply responses during tensile testing.

that a more detailed study is required to examine the validity of Poisson's ratios in modelling of uncured prepreg [173].

6.4 Numerical validation

A numerical model for the prepreg forming process was set up in the commercial finite element code ABAQUS [174]. The purpose of this model was to validate the accuracy of the previously reported elastic/plastic mechanical properties for ply forming simulations at temperatures up to $T = 40°C$. It was assumed that forming occurs at isothermal conditions and

three forming temperatures of T = 20°C, 30°C and 40°C were modelled by changing the mechanical properties. . The model sample was 60mm wide, 100mm long and 2.26mm thick. It was meshed with 240 three-dimensional continuum elements of the type C3D8 [174]. The material coordinate system and generated finite element mesh are shown in Figure 101.

Prepreg samples were modelled as a homogenous material with transversal orthotropic elastic and plastic properties. A summary of the elastic properties at the three different temperatures studied here is given in Table 20. The tensile modulus E_1, transverse modulus E_2,

E_3, shear modulus G_{12} and Poisson's ratio μ_{12} were determined experimentally. It as assumed that $G_{12} = G_{13}$ and $\mu_{12} = \mu_{13}$. The Poisson's ratio μ_{23} was taken from the rubbery prepreg results reported in [175]. The transverse shear modulus G_{23} was assumed to be $G_{23} = 2/3\ G_{13}$. The impact of the assumed values on the final through-thickness strain was calculated qualitatively and was found to be negligible. The input data for the plastic stress-strain behaviour were calculated from the data in Table 16. The model sample was 60mm wide, 100mm long and 2.26mm thick. It was meshed with 240 three-dimensional continuum elements of the type C3D8 [174]. The material coordinate system and generated finite element mesh are shown in Figure 101.

Table 20: Input data for the elastic properties of uncured prepreg for ABAQUS.

Temperature [°C]	E_1 [GPa]	E_2 [MPa]	E_3 [MPa]	μ_{12} [-]	μ_{13} [-]	μ_{23} [-]	G_{12} [MPa]	G_{13} [MPa]	G_{23} [MPa]
20	83	50.05	50.05	-1	-1	0.495	156	156	104
30	83	28.86	28.86	-1	-1	0.495	156	156	104
40	83	11.86	11.86	-1	-1	0.495	156	156	104

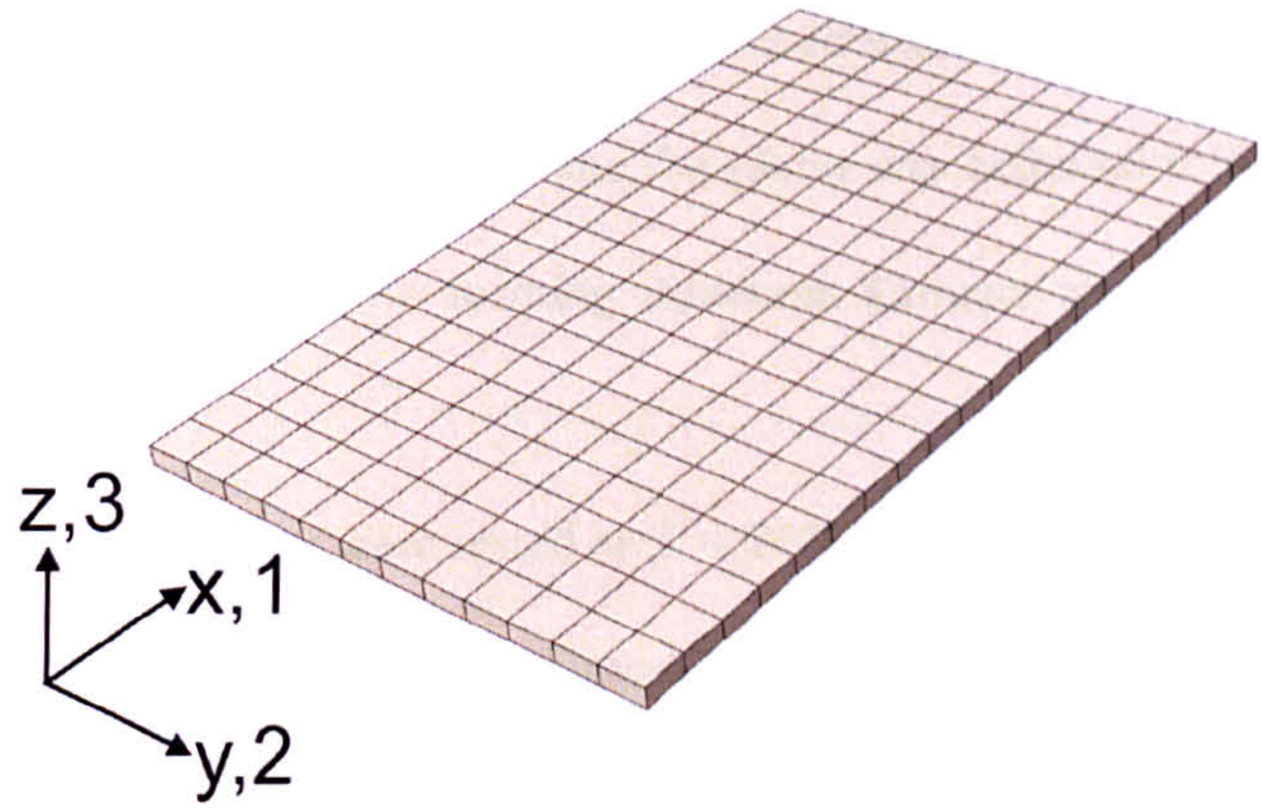

Figure 101: Material orientations and initial mesh.

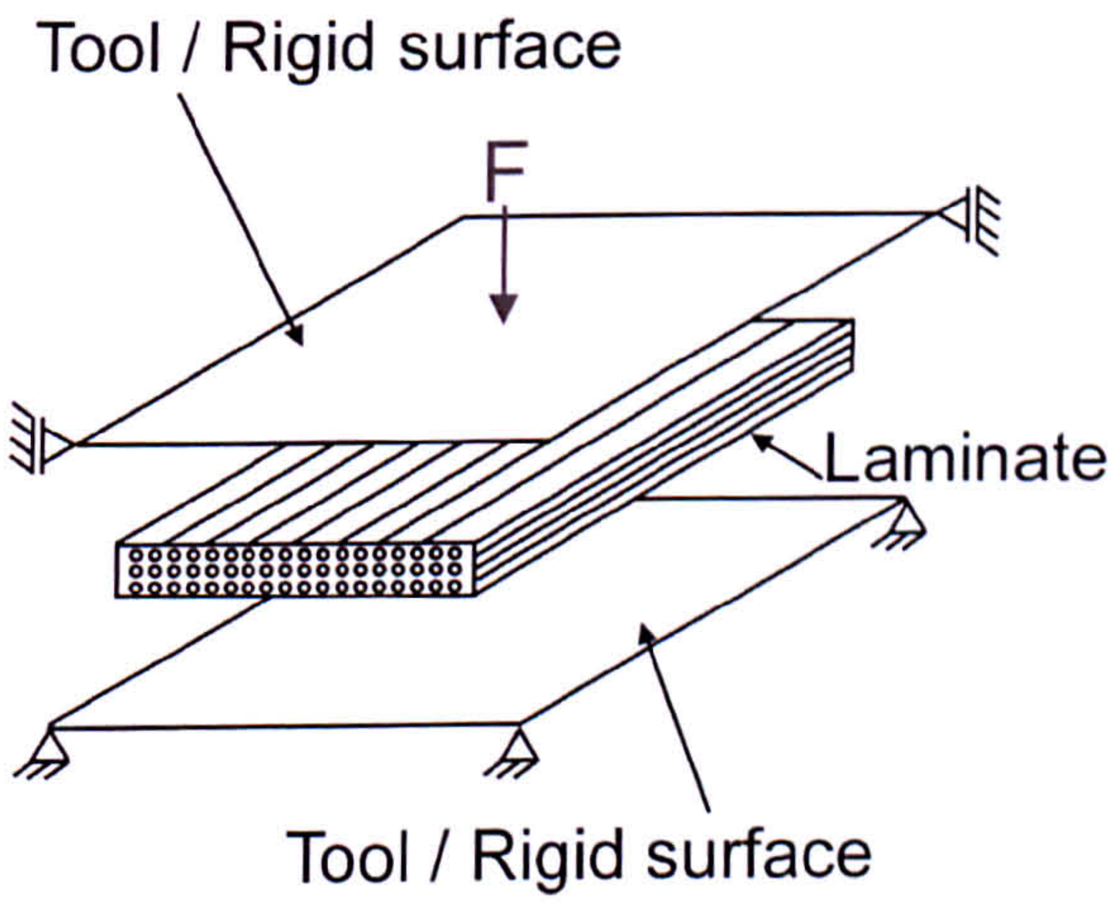

Figure 102: Model setup and boundary conditions. The lower surface is fixed and the upper surface can only translate along the z-axis.

The sample was placed between two perfectly rigid surfaces. The lower rigid surface was constrained to have no degrees of freedom. The upper rigid surface was constrained to have only a degree of freedom in the z-direction, normal to the sample surface. An overview of the boundary conditions is given in Figure 102.

Contact definitions between the rigid surfaces and the prepreg sample were used to model the interaction during forming. During testing the sample was wrapped in release film

and it was therefore assumed that negligible friction load was transferred between the surfaces and the plies. Furthermore, the stiffness of the flat plates was assumed to be much larger than the uncured prepreg stiffness in the forming direction. Contact was thus modelled as hard contact with no friction.

Three additional samples were tested at T = 20°C, 30°C and 40°C each, at a previously untested load of F = 6000N to validate the model. The load application rate was 10kNmin^{-1}. The samples were nominally 60mm wide, 100mm long and 2.26mm thick. The sample dimensions before and after loading were recorded and calculated into strains.

A comparison between the experimentally measured through-thickness strains and the numerically calculated through-thickness strains is given in Table 21. For T = 20°C the FE-model underpredicts the strain by 8.5% while it overpredicts the strain for T = 30°C and T = 40°C by 8.7% and 9.2% respectively.

Table 21: Comparison between experimental strains and predicted strains from the FE-model.

Temperature [°C]	Measured Strain [$\mu\varepsilon$]	FE Calculated Strain [$\mu\varepsilon$]	Difference [%]
20	14130	13026	-8.5
30	18115	19850	8.7
40	25274	27820	9.2

6.5 Discussion

The through-thickness compression modulus of uncured prepreg was studied as a time and temperature dependent property. A viscoelastic model was established for the time-dependence of the through-thickness compression modulus. In the range of conditions expected for automated layup it was found that the time dependence of the compression

modulus can be neglected and the material has a strong linear elastic, non-linear plastic behaviour with a small yield limit. A numerical model that showed good agreement between the experimental and numerically calculated results supports this approach. The tests were conducted in a range of very high resin viscosities, but further work will be necessary to evaluate whether and at what temperature this simplified approach is invalid, or whether it may be necessary to include time-dependent material behaviour by including strains due to creep [176].

While aiming to develop a simple model for uncured prepreg it has to be ensured that the approach taken captures the material response to loading correctly. The approach to relaxation experiments used here is untypical for most experiments where viscoelastic or viscoplastic properties are measured. Typically, the sample will be loaded quickly, over the course of a few seconds. Data are then recorded after a sufficient equilibrium time, which is reported to be between 5-10 times longer than the load application time. Here, the sample is loaded relatively slowly, but the modulus is recorded immediately. This approach was chosen in order to capture the stress-strain behaviour during loading which was limited by the speed and fidelity of the video strain gauge system.

Load applications times observed during automated layup are much shorter than those investigated here, while the loads can be higher. This will result in higher strain rates, which may lead to changes in the transverse modulus during layup. For a typical layup scenario the strain rate can be expected to be at least 0.34 1/s, (the strain was calculated from the measured and nominal ply thickness, see section 5.4.4, while the loading time was calculated from equation (6-2)) while the loading rate used here is approximately 0.01 1/s. The material is thus likely to be stiffer during layup loading than during the experiment, which may result is less permanent deformation during layup for the same pressure used in the experiment here. It is

therefore advisable to study the strain-rate dependent behaviour of uncured prepreg at various temperatures to ensure that automated layup is modelled accurately. This would introduce a simple and implicit time-dependence of the material properties, which may improve the accuracy of layup modelling further.

For process modelling it is desirable to identify the simplest model that captures the observed material behaviour accurately, within a given range of conditions. This simplifies material development and testing for manufacture. By describing the through-thickness compression response of prepreg using an elastic-plastic model, as opposed to a viscoelastic model, the material behaviour can be captured accurately within the context of automated layup.

Uncured prepreg is not a composite in the sense that the properties of the material can be derived from the properties of the individual constituents. The work reported herein has focused on establishing test methods and results for the properties of a prepreg with respect to automated layup. During automated layup the material is heated and a force is applied over a very short time to attach and consolidate the plies. The through-thickness compression modulus was thus studied as a time and temperature dependent property. A viscoelastic model was established for the time-dependence of the through-thickness compression modulus. In the range of conditions expected for automated layup it was found that the time dependence of the compression modulus can be neglected and the material has a strong linear elastic, non-linear plastic behaviour with no distinct yield point. All subsequent material properties are thus tested in the context of an elastic-plastic material behaviour.

The prepreg manufacturer reports a tensile modulus of 276GPa for the fibre alone [132]. The tensile strength of the fibre is 5450MPa and the strain to failure 1.8%, or 18,000με. The tensile modulus of M21 prepreg is reported to be 166GPa for a similar IM7GS fibre [102].

The measured values for uncured prepreg are significantly smaller for all properties, e.g. the tensile modulus is 50% smaller than in the cured prepreg. This difference can be explained by different volume fractions and small difference in the fibre alignment in the actual prepreg. This will result in loading of only a few tows while some tows may not carry any load. The apparent strength, modulus and strain to failure of the prepreg are lower than the fibre simply because the cross section carrying load is smaller than the entire sample width.

The observed results for the Poisson's ratio are inconsistent and exhibit a large amount of scatter. It is therefore reasonable to identify areas for improving the experimental procedure.

Twisting of the tow would show in the video strain data as a large transverse strain in relation to longitudinal strain. It would also lead to an apparent negative Poisson's ratio. The procedure of sample preparation and testing was aimed at minimizing any potential twisting of the tows. Initial twist in the tow due to prepregging however could not be minimized and may affect the results reported here. The manufacturer claims the tows are brought into the prepreg without any twist [132], which seems unlikely given the strongly negative Poisson's ratio's observed here. Because tows were extracted from a failed prepreg specimen it cannot be guaranteed that the tows were completely undamaged when tested for their Poisson's ratio. This is supported by the fact that three of five samples failed prematurely, while two samples did not fail. The exact effect of this pre-damage on the Poisson's ratio is unclear. Damaged fibres in the tow may lead to stress localisation and higher longitudinal strains. This would translate into a higher (smaller negative) Poisson's ratio.

The results obtained on a tow level need to be interpreted for the ply level. As observed previously, tows will push against each other and form lines in the ply. The ply Poisson's ratio is therefore higher, because the transverse tow expansion is blocked. The majority of the tows in the prepreg are blocked on each side by tows expanding towards them

whilst the respective tow expands as well. It can therefore be assumed that the Poisson's ratio of the prepreg on the ply level is around half of the tow level, i.e. $\nu_{12,ply} = 0.5\ \nu_{12,tow} \sim -1$.

The shear modulus was tested as a purely elastic function. The modulus was obtained by fitting a linear function against the stress-strain curve at small strains.

The strain modulus is matrix dominated in the same way as the transverse compression modulus. We have demonstrated that the latter can be approximated as nonlinear elastic-plastic property. It is reasonable to assume elastic-plastic behaviour for the shear modulus as well. Additionally, the property would be dependent on temperature in a similar manner as the transverse compression modulus. Previously, it has been argued here, that strain-rate testing of the transverse compression modulus might be required to improve the accuracy of the model. Similarly, by measuring the temperature and strain-rate dependence of the shear modulus further model improvements can be made.

7 Numerical modelling of the lay-up process

7.1 Introduction

Increasing amounts of unidirectional carbon fibre reinforced composite components are manufactured by automated layup. The pre-dominant material form for automated layup is currently thermoset prepreg. Thermoplastic composites, bio-composites and dry-fibre/liquid resin composites are unlikely to entirely replace thermoset prepreg for the next generation of aircraft due to a lack of high volume manufacturing processes and/or insufficient mechanical properties. This leads to a strong requirement regarding process and material development for large-scale manufacture of thermoset composites.

Main automated layup processes are Automated Tape Laying (ATL) and Automated Fibre Placement (AFP). Both processes are used extensively in exiting aircraft programs and can therefore be considered to be at a high technology readiness level [9]. However, current productivity requirements from aerospace and renewable energy manufacturers can not be met with either system [10]. This is due to unreliable processing, which results in significant quality inspection and rework time thus reducing overall productivity. To reduce the impact of quality control, methods are required that allow virtual optimization of the layup process with respect to rate and quality.

The goal of this work to provide a basic understanding of the interaction between layup system, tool and prepreg during layup and thus allow an enhancement of productivity and quality during automated manufacture. First, an overview of the past research into automated layup and thermoset material modelling is given. The quality critical interaction between material and layup system is then modelled using a two-step FE approach that

ultimately allows prediction of the uncured void content. The results from the model are then reported and some conclusions regarding a layup system having optimised quality and rate are presented.

7.1.1 Process modelling

Process models for automated layup have been developed mostly for thermoplastic layup. The early work by Springer and co-workers [74, 76] focused on identifying optimised processing conditions by studying the degree of bonding. Consistent heating above the melting point of the matrix was identified, as prerequisite for thermoplastic layup and an interaction between layup speed and temperature was found critical for layup quality. This observation has since been confirmed and extended by many other groups, in particular Gillespie Jr. and co-workers [77-80] and Akbulut and co-workers [177, 178]. Typical melting points of matrices for aerospace applications, e.g. PEEK and PEKK, are in the range from 300°C to 400°C [179]. This normally limits the speed of the entire process to the speed at which continuous heating can be achieved and hot gas torches and laser heating are therefore common [85]. Typical manufacturing rates for thermoplastic layup of simple components are around 2-5kg/h [180], while thermoset layup achieves rates of 8.6 kg/h or more [181] for complex components. It should however be noted that the overall production time for a thermoset layup may be larger due to a subsequent curing operation. The consolidation pressure during thermoplastic layup can be as high as $p = 3.6$MPa [182] while effective consolidation pressures during thermoset layup are unknown. Lastly, for thermoplastic layup the quality of the final laminate is governed by the incoming material quality [100], e.g. tape uniformity, surface topology and voids in the virgin prepreg [131]. It is instructive to assume that the same material properties govern high quality layup of thermoset prepreg. However, the impact of processing conditions during

thermoset layup, i.e. layup speed, temperature and pressure on laminate is unclear. For thermoset layup the manufacturing speed may be affected by temperature and consolidation pressure similar to thermoplastic layup [110, 111].

In this work, an FE-model for the thermoset layup process is introduced. In a first step the ply layup interaction is studied in detail as a function of layup speed, pressure and temperature. Three different temperatures, several different roller configurations, and a range of consolidation loads and speeds are investigated. In a second step the information from this macro-analysis of the layup process are transferred to a meso-scale ply model encompassing the roughness typically found in prepreg tape. This model is used to predict the amount of entrapped air during layup as a function of processing conditions. Optimised processing conditions for a specific material are then proposed and some general observations regarding the process/material interaction are made.

7.1.2 Layup system considerations

During automated layup a flexible roller or stiff layup element exerts a compression force onto a prepreg and a sequence of heaters control the temperature of the substrate or incoming tape [183]. The configuration of this layup zone is shown in Figure 103. Both ATL and AFP control the tension on the ply to some degree to enable layup into concave features and to improve fibre straightness. The uncured prepreg is thus delivered into a gap between the flexible roller and tool at a set temperature and tension. The roller-sleeve that interacts with the material is commonly made of flexible silicone rubber. Typical diameters are around 25mm. The layup element then applies a compaction load to the substrate, common values are

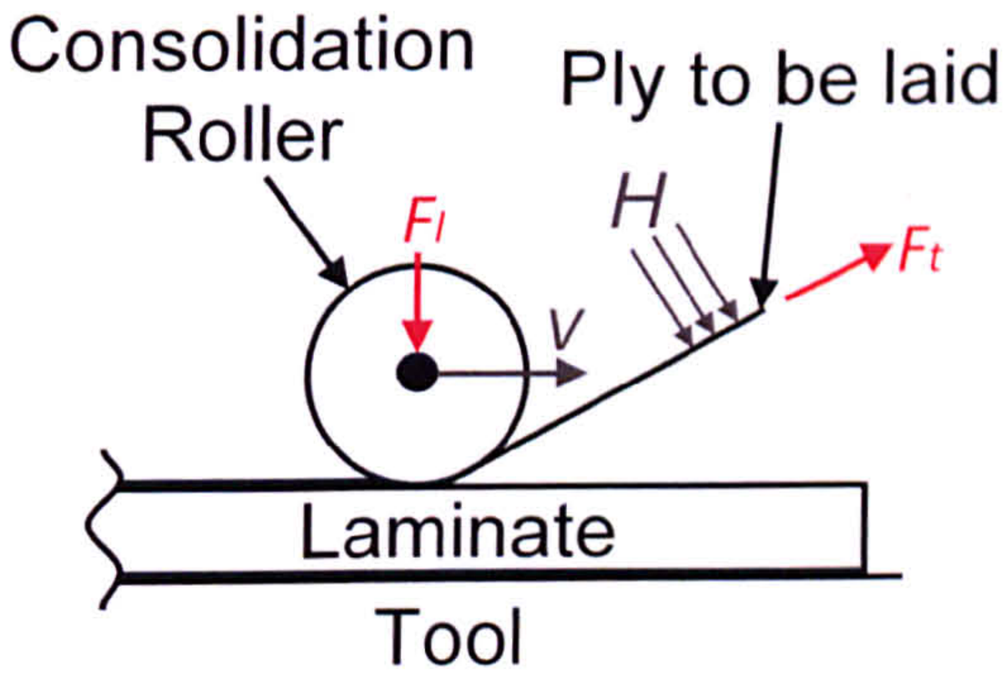

Figure 103: Illustration of the layup zone including thermal and mechanical loads.

around $F_l < 445$N [145] for 75mm wide tape, or a maximum of $F_l = 1000$N for 300mm wide tape. Most layup systems operate at speeds up to $v = 60$ m/min, while some systems are capable of speeds up to 85m/min [118]. Lastly, the tape is typically heated to control tack and formability, Calawa and Nancarrow have [41] reported a layup temperature of $T = 35°C$ as ideal for most epoxy prepreg materials and a similar observation was made by Ahn et.al. [42] who reported that the tack of uncured prepreg reached a maximum at 20-25°C above the instantaneous glass transition temperature. The best layup temperature may thus depend on the material system, but most layup systems will be able to achieve continuous heating of $\Delta T = 20$K using infrared heating, which translates into a layup temperature range of 20-40°C.

7.1.3 Material modelling

To model the automated layup process M21/IMA prepreg was used, which is a typical aerospace material system. The matrix is a toughened epoxy resin [102] combined with an intermediate modulus fibre [132]. Uncured prepreg is a visco-elastic/plastic material. For the very short contact times typically found in automated layup the time dependent material behaviour may be neglected in favour of an accurate description of the non-linear plastic

behaviour. This greatly simplifies the modelling of the uncured prepreg material behaviour to an elastic/plastic material description. The mechanical properties of uncured M21 prepreg used here have been reported in chapter 6.

7.2 Modelling of uncured prepreg layup

7.2.1 Ply-deposition model

The interaction between the ply, layup system and processing conditions was modelled in the commercial finite element code ABAQUS [174]. In all cases, the layup of a single ply of prepreg onto the mould or substrate was modelled, while the roller was either assumed to be perfectly rigid, or deformable.

Shirinzadeh et. al. [92] have published a load-deformation curve for a layup system under various consolidation loads. While the published data includes displacement of the robotic arm, it can be assumed that the majority of the deformation occurs in the flexible, rubber roller. The geometry of the roller was not published and the values were assumed for the model, the diameter d was assumed to be 50mm and the width w was 10mm.

Values for the deformable roller model were thus generated by identifying material properties for the roller that would allow matching the published load deformation curve. A comparison between the published and calculated load-deformation curve is shown in Figure 104 while the resulting mechanical properties are shown in Table 22.

Based on these data a model for the layup of a single ply was developed. A model using a rigid roller is shown in Figure 105. The ply was meshed with 848 linear continuum elements of the type C3D8R, which is an 8-node linear brick element with reduced integration

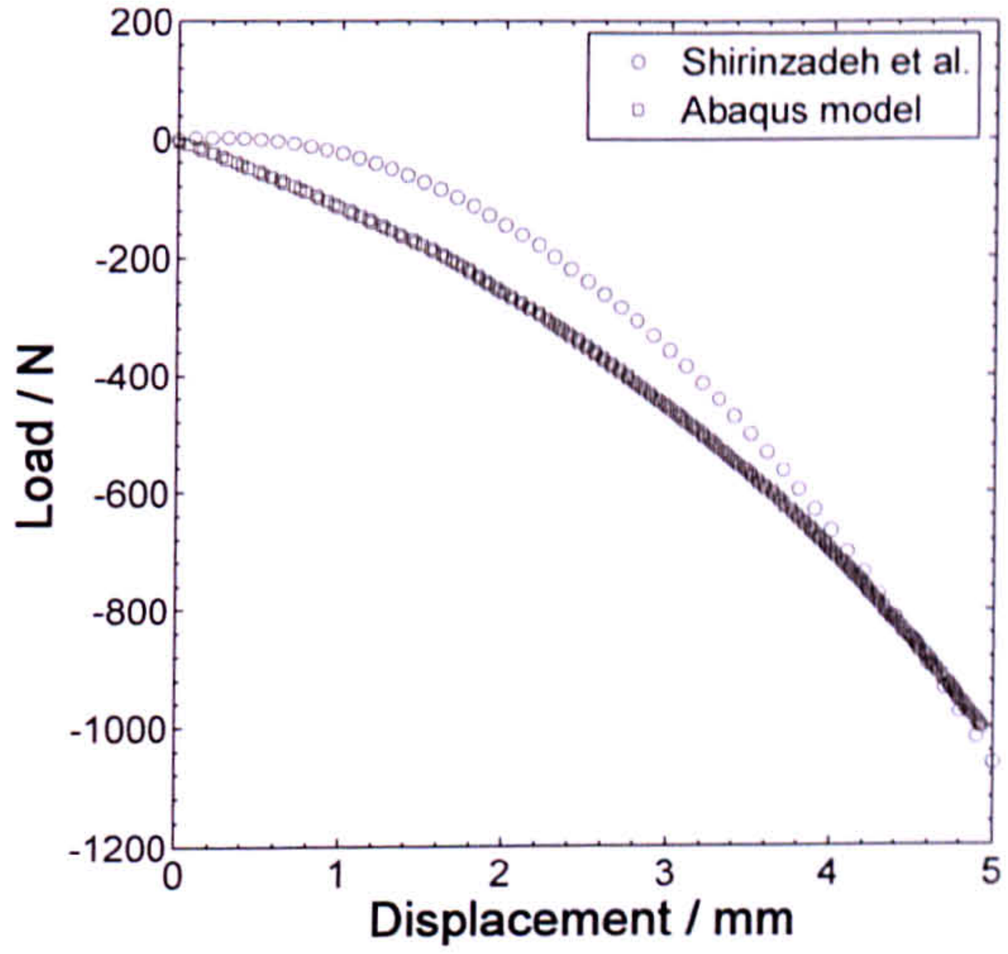

Figure 104: Comparison between the load-displacement curve of a layup roller published by Shirinzadeh et.al [92] and the roller used here.

Table 22: Mechanical properties of a flexible layup roller, derived from [92].

Material property	Unit	Value
Modulus E	[MPa]	0.75
Poisson's ratio μ	[-]	0.495
Density ρ	[kgm-3]	1250

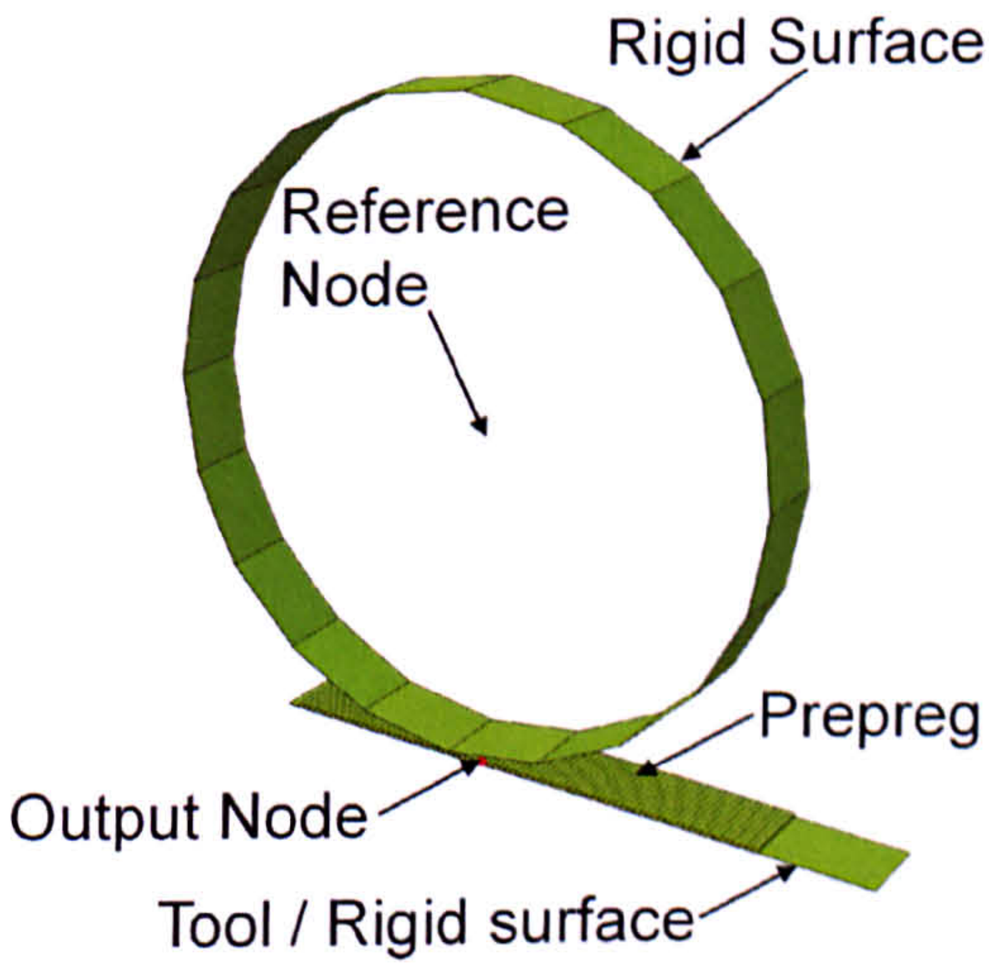

Figure 105: Initial configuration of the stiff roller model with single ply and tooling.

and hourglass control. Boundary conditions were applied to the side of the ply to prevent out-of-plane deformation and to yield a plane-strain loading condition. The tool was constrained to a reference node, which was fixed in space with all degrees of freedom. The motion of the rigid roller was constrained to a reference node in centre of the roller and the respective load, speed and angular velocity values were applied to this node. Contact definitions between the tool, the ply and the roller were used to simulate the ply forming during layup. It was assumed that negligible friction force is transferred between the roller and the plies. Furthermore, the stiffness of the tool is assumed to be much larger than the uncured prepreg stiffness in the forming direction. Contact was thus modelled as hard contact with no friction.

A deformable roller model is shown in Figure 106. The ply was meshed with 848 linear continuum elements and the roller was meshed with 800 linear continuum elements of the same type C3D8R, as used previously. Boundary conditions on the ply and tool were also identical to the previous model. The flexible part of the roller was constrained to the rigid inner surface. Load and speed boundary conditions were then applied to the reference node of the inner surface. Rotation of the roller was omitted to simplify the model. Contact was again modelled as hard contact with no friction.

Both models were set up as plain strain models using appropriate meshes as shown in Figure 105 and Figure 106. For the stiff roller and flexible roller model boundary conditions were applied to the sides of the ply to prevent out-of-plane displacement. Additionally, in the case of the flexible roller model the roller sides were constrained to exhibit no out-of-plane displacement. To model the layup process, the roller was brought in contact with the ply by applying the desired test force. After load application the roller was moved along the ply.

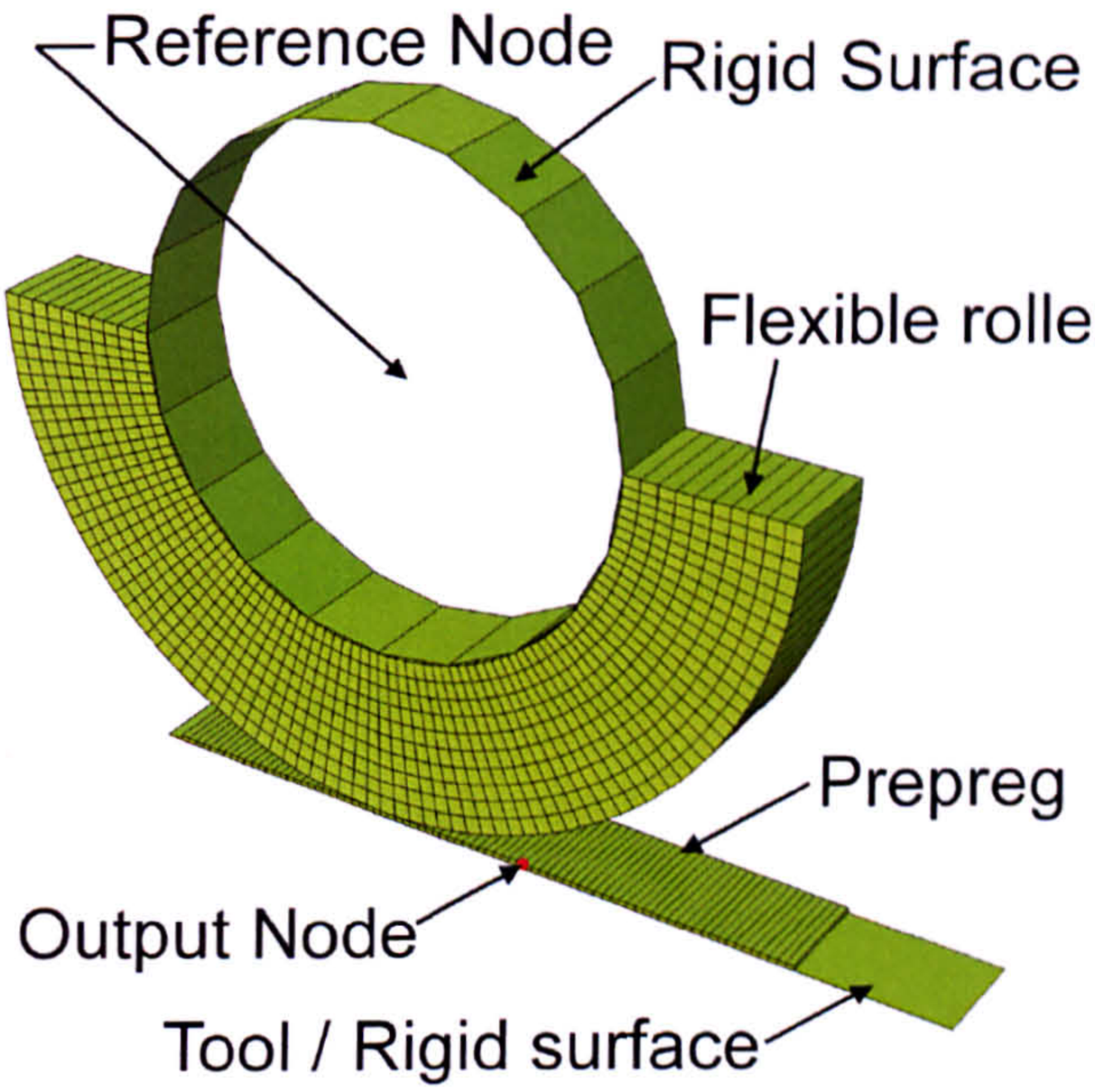

Figure 106: Initial configuration of the flexible roller model with single ply and tooling.

Table 23: Overview of the variables of the parametric study for the ply layup model.

Variable	Unit	Levels
Temperature	[°C]	20, 30, 40
Load	[N]	50, 100, 200, 300, 400, 500, 600, 750, 800, 1000
Speed	[mm/s]	83.3, 166.67, 333.33, 500, 666.67, 833.3, 1000
Roller Modulus	[Mpa]	0.75, 1.5, 3, 6, 12, 24, 48
Roller diameter	[mm]	30, 40, 50, 60, 70

A parametric study based on these two base models was used to understand the impact of various processing conditions and layup systems. Generally, the test temperature was defined and the layup speed and compaction force were then varied. In addition, roller stiffness and diameter were systematically varied to study the impact of the layup system and for this model the layup temperature was $T = 30°C$, the layup pressure was $F = 500N$ and the layup speed was $v = 1000m/s$. An overview of the variables of the parametric study is given in Table 23. Not all possible combinations of variables were tested. In total 251 unique models

were tested. In all cases the effective pressure on the laminate and the through-thickness strain as a function of time were extracted.

7.2.2 Mesoscale ply model

During manual layup plies are regularly vacuum-pressed to remove voids entrapped between the plies. Vacuum void removal is omitted during automated layup in favour of a continuous layup. To compact the prepreg it can be heated and laid down under pressure as discussed previously. The optimum level of heating and pressure depends on the amount of flow that is required to prevent void entrapment during layup. This has been previously studied for thermoplastic layup [74] and it was shown that the amount of entrapped voidage is a function of the initial tape roughness, the higher the roughness the more gaps are in the material. High quality layup should thus aim to reduce the amount of entrapped air in the final laminate by mitigating the effect of the initial roughness of the prepreg tape.

Recently, the roughness of two aerospace prepregs was measured using optical methods [131]. It was shown that both prepregs exhibited a characteristic roughness pattern. For the M21 prepreg considered here, the roughness was aligned transverse to the fibres and exhibited a closed cell pattern, see Figure 107. This is developed into a representative volume element (RVE) of the meso-scale prepreg roughness, illustrated in Figure 108. The roughness and ply geometry data are listed in Table 24.

A simple ply-forming model was then developed, where two plies were held between two rigid surfaces with another rigid surface between them. The pressure data from the previous ply-deposition model were used to load the RVE and obtain predictions for the reduction in surface roughness and predict the amount of air entrapped between the plies after

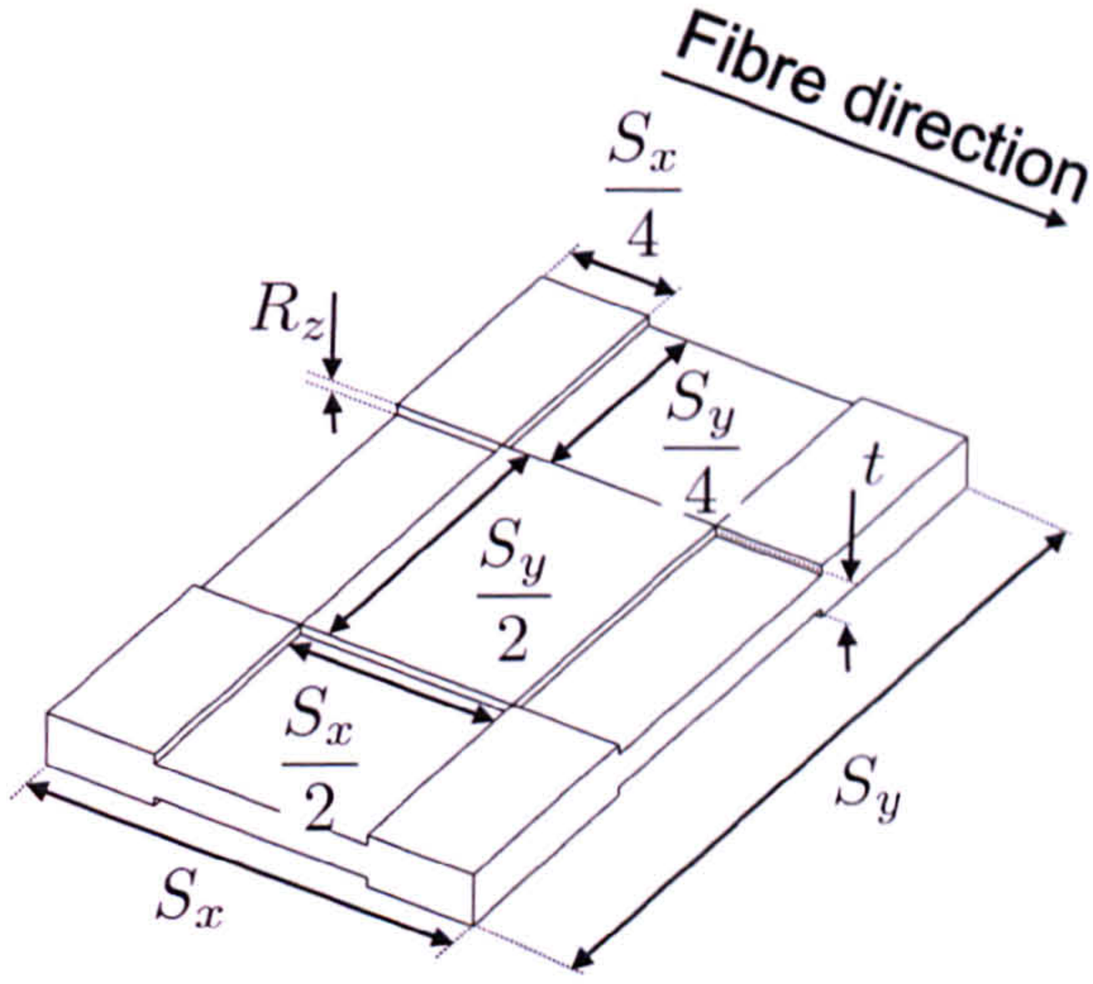

Figure 107: Representation of the surface roughness model of M21 prepreg.

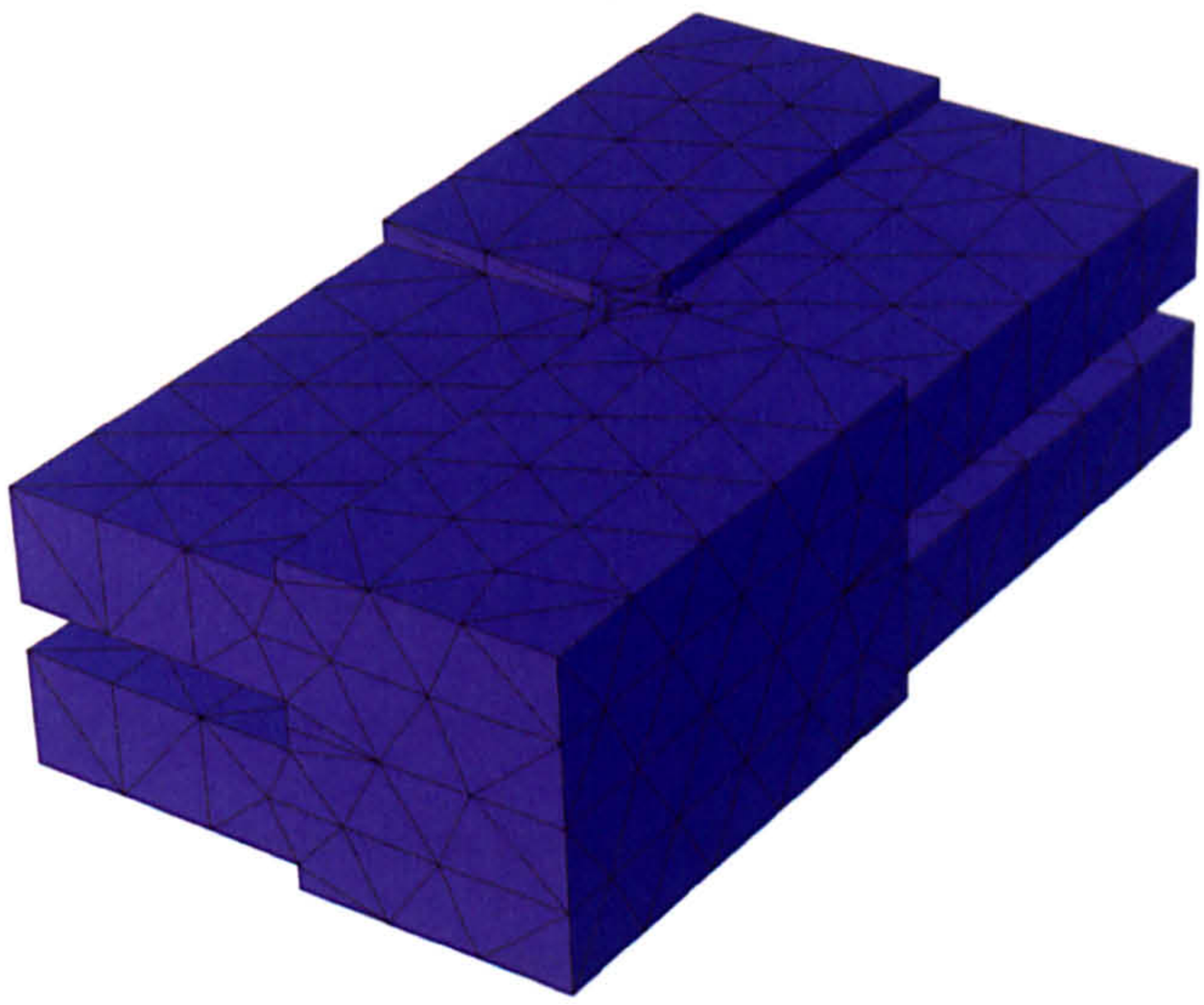

Figure 108: Mesoscale ply model implemented in ABAQUS. The picture shows a stack of two representative volume elements in the initial, undeformed, configuration.

Table 24: Geometry parameters for the meso-scale roughness RVE of M21 prepreg.

Variable	Unit	Value
t	[μm]	283
S_x	[μm]	2322
S_y	[μm]	4080.5
$R_{z,backing}$	[μm]	46
$R_{z,non\text{-}backing}$	[μm]	52.5

layup. The aim of this study is to provide bounds on allowable surface roughness for prepreg and to study optimal layup conditions.

7.3 Model results

7.3.1 Ply deposition model

The numerical results were analysed for the effective pressure on a certain point of the laminate as a function of time and the total contact time. A comparison between layup using a flexible and stiff roller can be seen in Figure 109. The peak pressure for a flexible roller is lower than for a stiff roller, conversely the contact time is significantly higher. The contact time for various loads and layup speeds at $T = 20°C$ is plotted in Figure 110 for a soft roller and a summary is provided in Table 25. Figure 111 shows the contact time for a stiff roller, with a summary in Table 26 for a stiff roller, with some data removed for brevity. In all cases the contact time is a function of the layup speed and increases with increasing load.

The increase in contact time due to a compaction load is higher for the flexible roller than for the stiff roller. For layup with a flexible roller contact time is governed by the roller deformation while it is governed by the laminate deformation for layup with a stiff roller. The maximum pressure during layup using a stiff roller is significantly higher than for a soft roller. Additionally, layup with a stiff roller scales strongly as a function of layup pressure and temperature. The results indicate that the amount of pressure on the laminate during layup can be enhanced by increasing the stiffness of the roller and by modifying the roller diameter. Contact time increases with increasing diameter and decreasing roller stiffness as shown in Figure 112. Figure 113 shows that the pressure on the laminate increases with increasing roller stiffness and decreasing roller diameter. This demonstrates the possibility to tailor the layup

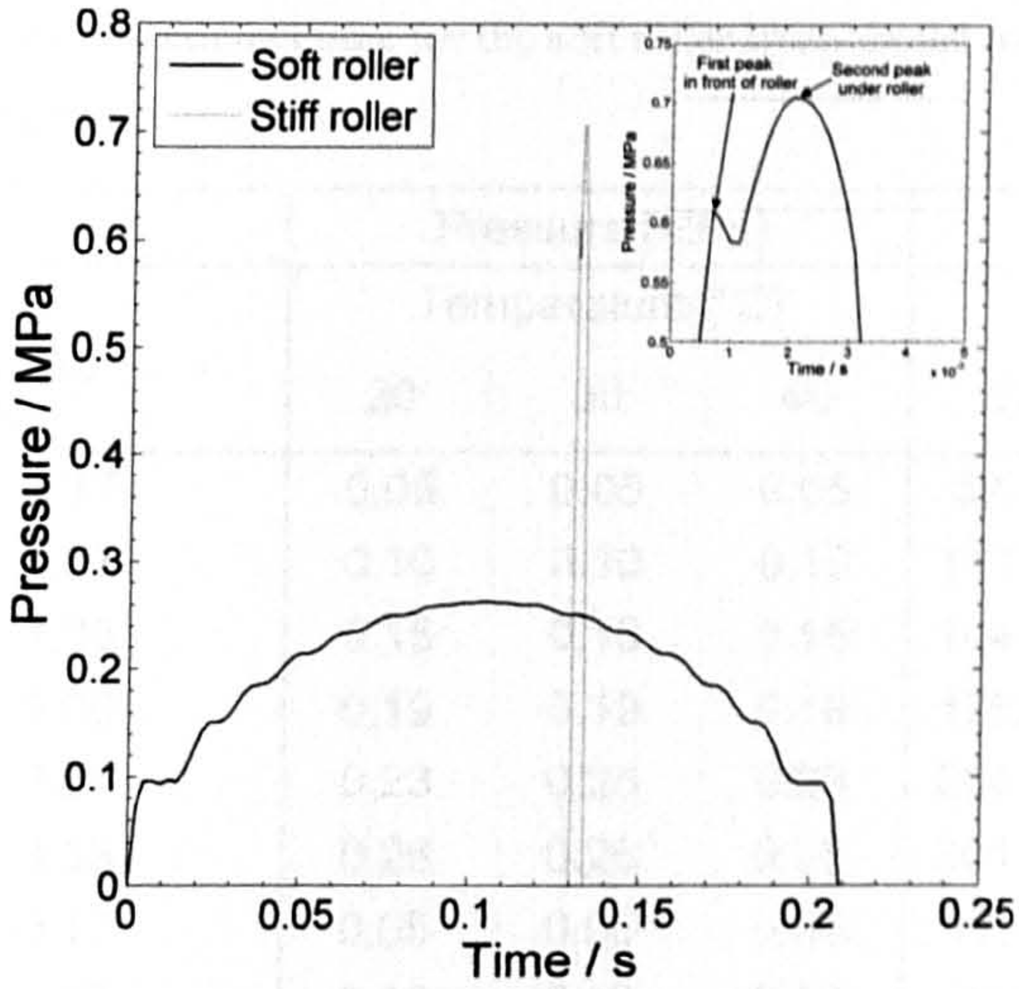

Figure 109: Comparison between pressure distributions for stiff and soft layup roller for identical processing conditions.

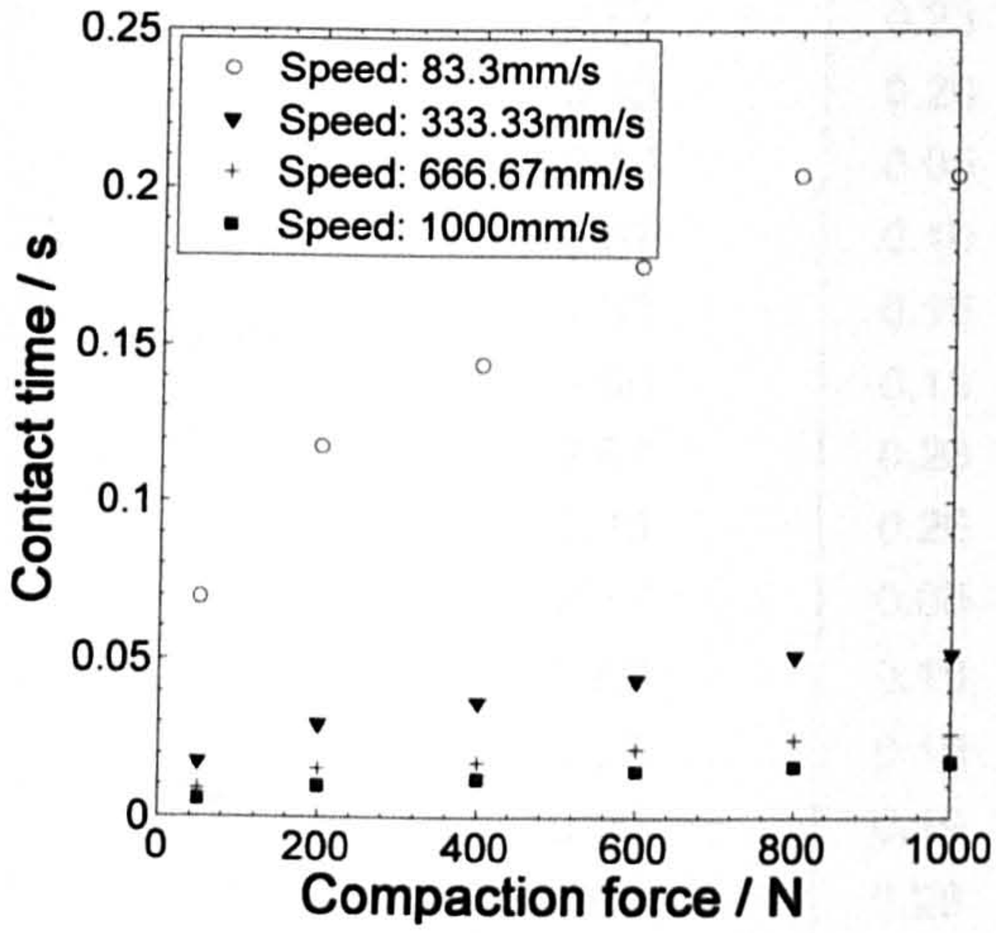

Figure 110: Contact time for a soft roller at a layup temperature of T = 20°C for various compaction forces and layup speeds.

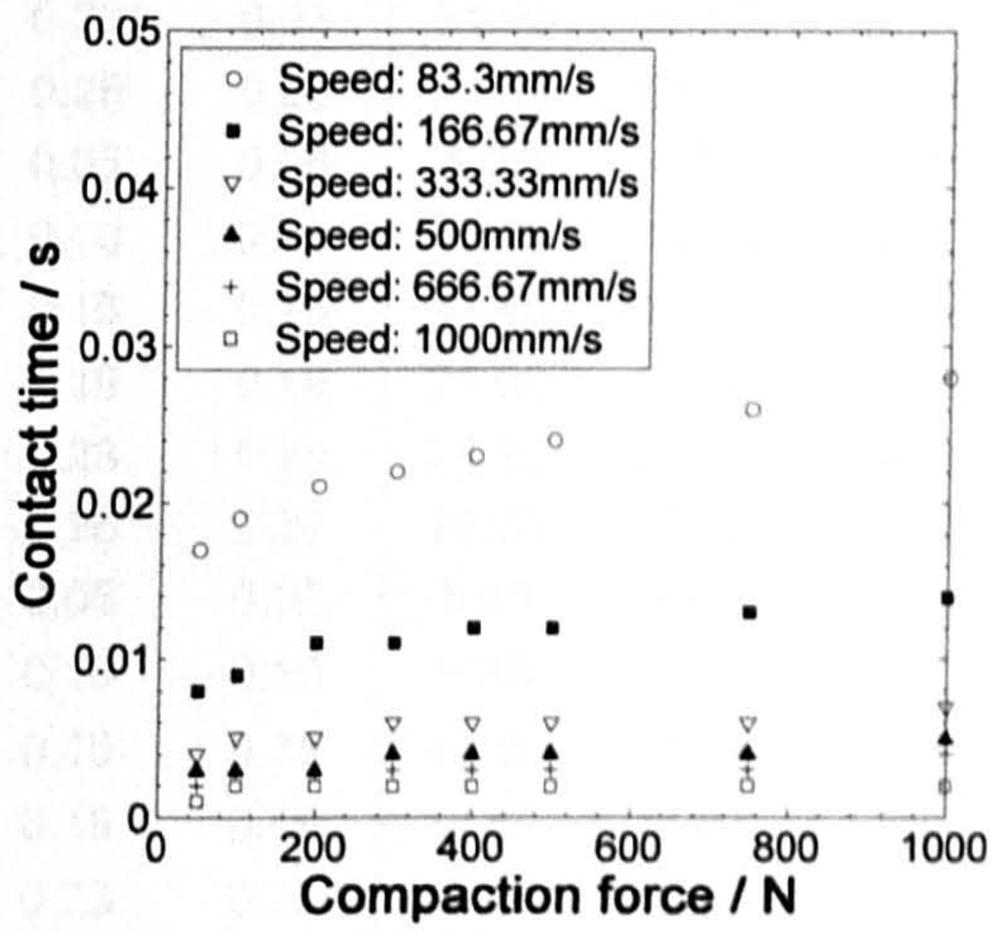

Figure 111: Contact time for a stiff roller at a layup temperature of T = 20°C for various compaction forces and layup speeds.

Table 25: Results for pressure and contact time for the soft roller layup model for various layup speeds, loads and temperatures.

		Pressure [MPa]			Contact time [*ms*]		
		Temperature [°C]			Temperature [°C]		
Speed [mm/s]	Line Load [N/mm]	20	30	40	20	30	40
83.3	0.17	0.05	0.05	0.05	69.60	69.60	65.10
	0.67	0.10	0.10	0.10	117.60	117.60	113.40
	1.33	0.15	0.15	0.15	144.00	146.40	140.70
	2.00	0.19	0.19	0.19	175.20	175.20	170.10
	2.67	0.23	0.23	0.23	204.00	204.00	195.30
	3.33	0.26	0.26	0.26	204.00	204.00	201.60
333.33	0.17	0.05	0.05	0.05	17.40	17.40	15.73
	0.67	0.10	0.10	0.10	29.40	29.40	28.37
	1.33	0.15	0.15	0.15	36.60	36.60	35.69
	2.00	0.19	0.19	0.19	43.80	43.81	43.07
	2.67	0.23	0.23	0.23	51.00	50.98	49.84
	3.33	0.26	0.26	0.26	51.61	51.53	50.88
666.67	0.17	0.05	0.05	0.05	8.70	8.66	7.95
	0.67	0.10	0.10	0.10	15.30	15.25	14.83
	1.33	0.15	0.15	0.15	17.40	17.43	16.96
	2.00	0.19	0.19	0.19	21.90	22.00	21.76
	2.67	0.23	0.23	0.23	24.91	24.90	24.64
	3.33	0.26	0.26	0.26	26.33	26.32	25.18
1000	0.17	0.05	0.05	0.05	5.60	5.65	5.49
	0.67	0.10	0.10	0.10	9.80	9.59	8.57
	1.33	0.15	0.15	0.15	12.00	12.17	11.89
	2.00	0.19	0.19	0.19	14.80	14.81	14.51
	2.67	0.23	0.23	0.23	16.60	16.74	15.56
	3.33	0.26	0.26	0.26	17.74	17.99	17.30

system and the layup conditions to achieve optimal layup conditions for a number of different materials. The following mesoscale ply modelling is aimed at indicating such optimal layup conditions and uncured material properties.

Table 26: Results for pressure and contact time for the stiff roller layup model for various layup speeds, loads and temperatures.

		Pressure [MPa]			Contact time [*ms*]		
		Temperature [°C]			Temperature [°C]		
Speed [mm/s]	Line Load [N/mm]	20	30	40	20	30	40
83.3	0.17	0.35	0.39	0.38	16.80	18.60	8.70
	0.67	1.50	1.42	0.74	21.00	22.80	14.71
	1.33	2.45	1.82	1.13	23.40	25.20	18.90
	1.67	2.68	1.99	1.35	24.00	26.40	20.70
	2.50	3.08	2.37	1.69	25.80	28.80	24.00
	3.33	3.37	2.81	2.05	28.20	31.20	26.71
333.33	0.17	0.35	0.39	0.38	4.20	4.65	2.10
	0.67	1.50	1.39	0.73	5.25	5.70	3.61
	1.33	2.45	1.84	1.13	5.85	6.30	4.80
	1.67	2.67	1.98	1.34	6.00	6.60	5.11
	2.50	3.09	2.37	1.70	6.45	7.20	5.97
	3.33	3.36	2.80	2.06	7.05	7.80	6.62
666.67	0.17	0.35	0.39	0.37	2.10	2.32	1.09
	0.67	1.50	1.41	0.73	2.63	2.85	1.83
	1.33	2.45	1.83	1.14	2.93	3.15	2.35
	1.67	2.67	1.97	1.35	3.15	3.30	2.51
	2.50	3.09	2.37	1.69	3.23	3.67	3.00
	3.33	3.48	2.79	2.04	3.53	3.90	3.28
1000	0.17	0.35	0.39	0.37	1.40	1.54	0.65
	0.67	1.50	1.40	0.73	1.75	1.90	1.17
	1.33	2.45	1.82	1.14	1.95	2.10	1.56
	1.67	2.67	1.98	1.32	2.00	2.20	1.65
	2.50	3.08	2.35	1.68	2.15	2.40	1.94
	3.33	3.48	2.78	2.03	2.35	2.59	2.23

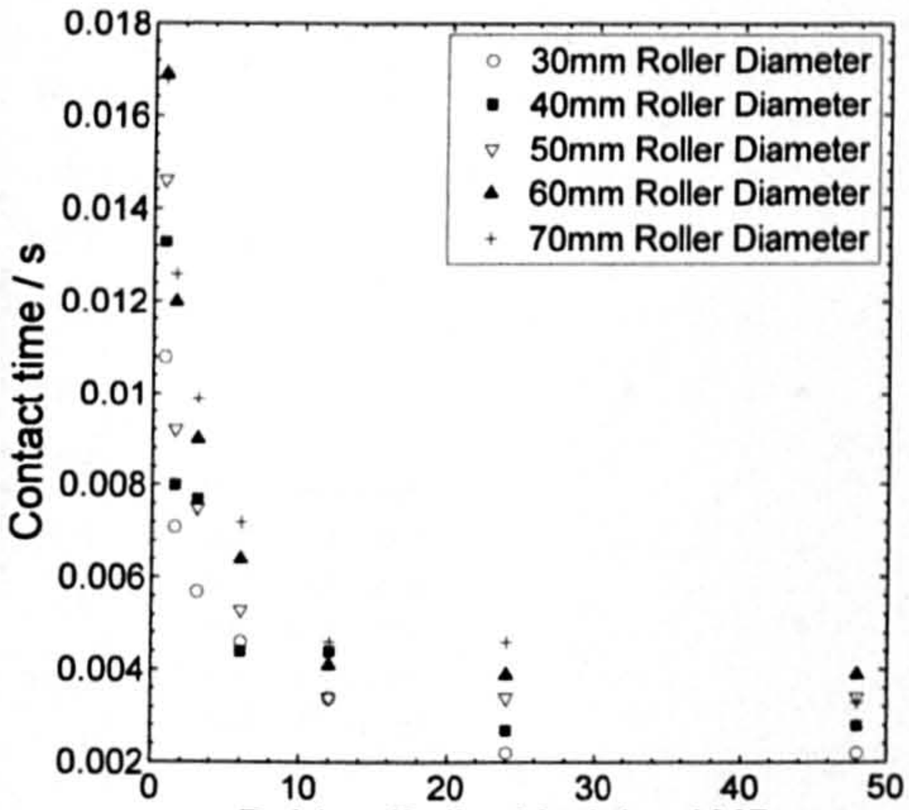

Figure 112: Contact time for a ply layup at T = 30°C, F = 1000N and v = 1000mm/s for various roller stiffness's and diameters.

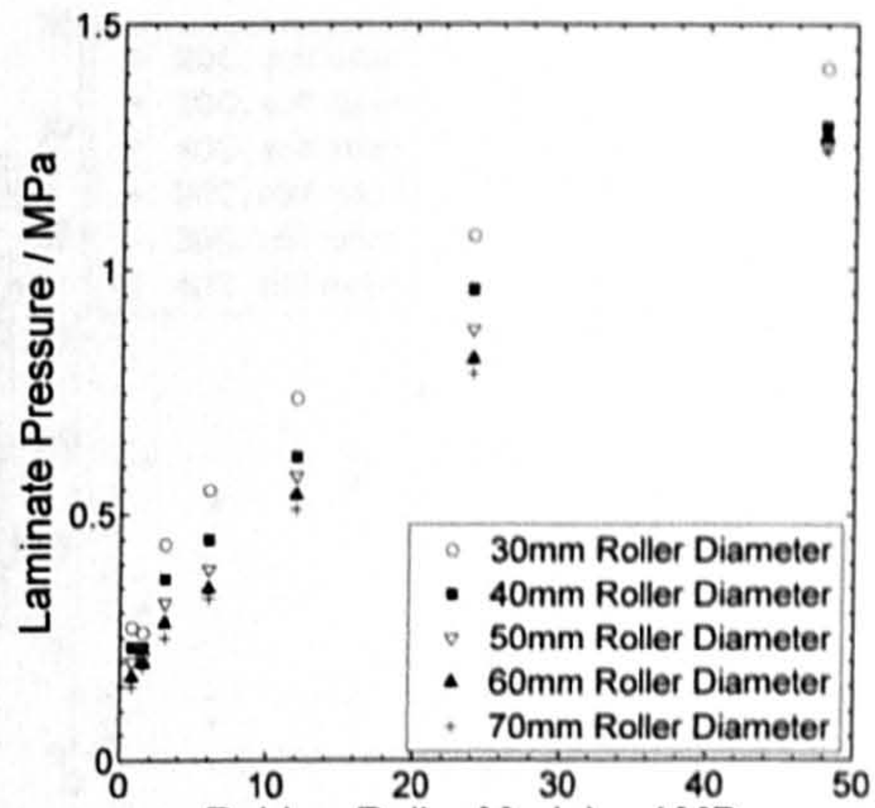

Figure 113: Laminate pressure for a ply layup at T = 30°C, F = 500N and v = 1000mm/s for various roller stiffness's and diameters.

7.3.2 Mesoscale ply model

During modelling of the impact of processing conditions on the layup interaction it was found that the ply forming behaviour was independent of the layup speed and controlled only by the layup pressure and temperature. By tailoring the layup system to the material, optimised material quality during layup may be achieved. This second study is aimed at identifying processing conditions and layup system parameters that allow robust processing of highly variable materials by modelling the deformation of the interphase to predict the amount of voidage in the material. Figure 114 shows the predicted interply voidage due to surface roughness as a function of layup conditions. The baseline interply voidage for two plies in contact is 14.8%. Generally, voidage decreases with increasing load and temperature. For the soft layup roller the maximum voidage reduction is 0.7% and 3.9% for a stiff roller, both at T = 40° and F = 3.33 N/mm. Similarly, Figure 115 shows the change of surface roughness as a function of layup conditions for several different layup conditions and soft and stiff roller

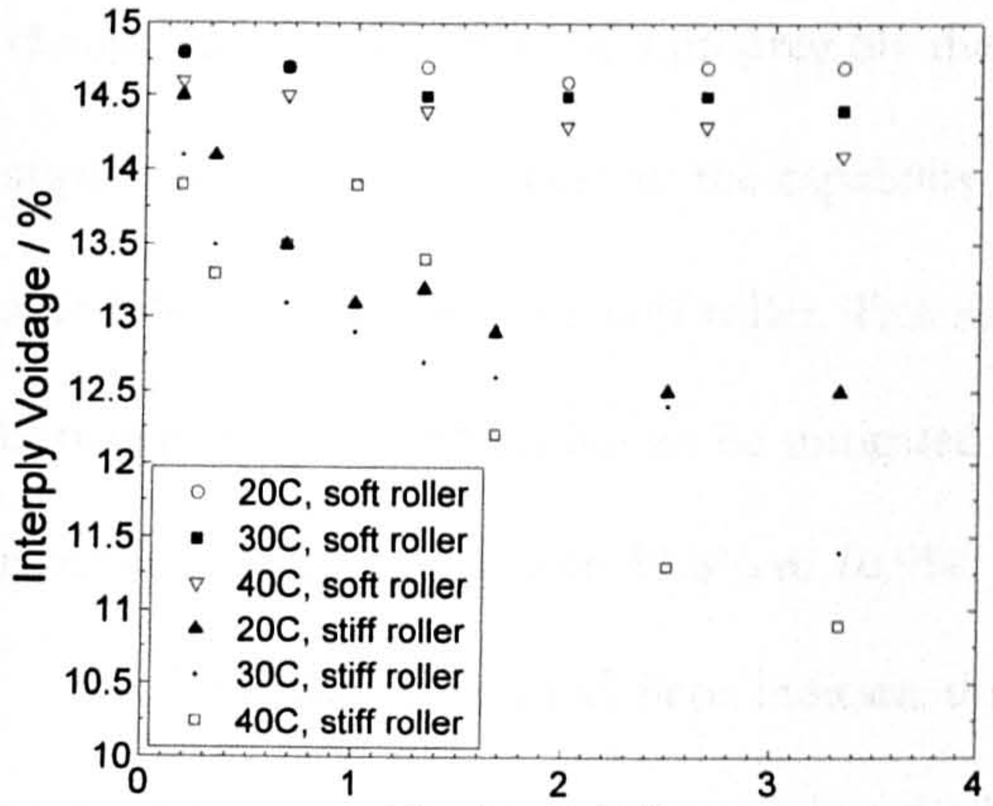

Figure 114: Predicted interply voidage as a function of laminate line load during layup and different layup temperatures and roller configurations.

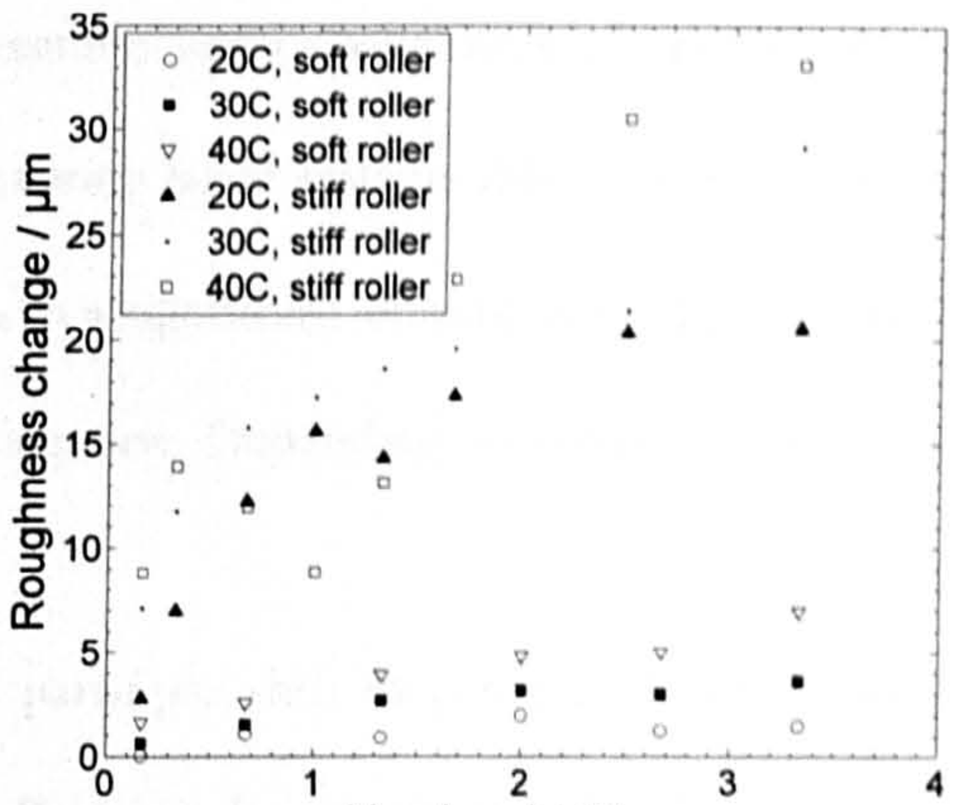

Figure 115: Predicted change in surface roughness as a function of layup load, temperature and roller element.

elements. Again, roughness decreases with increasing line load and layup temperature. The maximum roughness change at $T = 40°$ and $F = 3.33$ N/mm is $\Delta R_z = 7$ µm for a soft roller and $\Delta R_z = 33$ µm for a stiff roller.

7.4 Discussion and conclusions

The results presented herein show that layup quality is independent of layup speed and controlled by layup load, temperature, layup system and material quality alone. For the very soft rollers currently being used the layup load is distributed over a large surface and the roller deflects significantly. For a soft roller this results in a large contact time, while a stiff roller is in contact with a laminate for very short times. Conversely, the model results show that it may be beneficial to increase the pressure on the laminate by either increasing the layup elements stiffness or by increasing the layup load. Increasing the layup temperature effectively decreases the pressure on the laminate but allows for permanent material deformation. By modelling the

change in microstructure of a prepreg ply the maximum surface roughness of a prepreg can be approximated. With respect to the capability of existing layup systems this value is 7 μm for a soft roller and 33 μm for a stiff roller. This results in a significant amount of voidage remaining between the plies, which has to be mitigated during cure. Depending on layup conditions this interply voidage varies from 14.8% to 10.9%.

The data presented here indicate that a paradigm shift in automated layup may be necessary to improve layup processing further. Previous layup systems aimed at achieving around 0.1MPa pressure, while maximising contact time, as shown in Figure 109. However, if the effective pressure on the laminate is below the yield limit of the material no effective work will be done. At the same time, existing layup elements are vastly inefficient in translating the system pressure onto the laminate due to the large amount of deflection in the roller, yielding a large contact surface. It seems that existing layup systems, using very low modulus layup elements, have been designed to minimize the impact of layup system variability and to maximize the amount of energy transferred to the laminate. This approach neglects the material variability, which needs to be addressed for high quality layup. To effectively deform the material pressure needs to be sufficiently high. Lastly, to allow layup with high quality it may be beneficial to reduce the surface roughness of prepreg tapes to reduce the amount of entrapped air during layup.

A model for the interaction between prepreg material, layup system, and layup conditions was presented. It was shown that layup quality is independent of layup speed. It is rather a function of incoming material quality, layup system and layup conditions. Quality, as measured here by the amount of interply voidage, improves with increasing layup load, layup temperature and layup roller stiffness. Lastly, the model results present bounds on the amount of prepreg roughness that can be tolerated for high quality layup

8 Characterisation of laminates manufactured by optimised layup processing

8.1 Introduction

Chapter 7 introduced a model for the layup of thermoset prepreg, which may enable prediction of voidage after layup. The model predicts a reduction in voidage at the point of layup, for high temperatures and layup loads. The impact of voidage on mechanical properties has been extensively studied. Hancox [184, 185] studied the effect of voids and fibre waviness on the mechanical performance of composites and found a significant reduction of all matrix-dominated properties as a function of increasing void content and flaw length. Yoshida et al. [186] studied the effect of voids, determined by resin burn-off, on the ILSS of unidirectional carbon-fibre reinforced epoxy and carbon-fibre cloth reinforced polyester with voids artificially introduced into the laminates by employing a foaming agent. They reported that an increase in void fraction by ~1% results in a reduction of the ILSS by ~7.65%. Harper et al. [187] studied the effect of voids on the tensile moduli in the longitudinal and transverse direction as well as the shear modulus in-plane of AS4/3502 prepreg. Tensile properties were unaffected by voidage, but the transverse tensile modulus and the shear modulus declined linearly with increasing void content. Olivier et al. [140] investigated the effect of voids on the strength values of different carbon/epoxy systems and observed a reduction of matrix dominated properties. Finally, Wisnom et al. [188] studied the effect of voids on the ILSS of carbon epoxy laminates by introducing PTFE filaments into the laminate to simulate the effect of voids. Their findings predict an exponential reduction in the ILSS with an increase in void fraction by

1% yielding a reduction of 3.6%. While the detrimental impact of voids on the mechanical properties of composites is thus undisputed, uncertainties remain regarding the exact impact of voids on mechanical performance. Huang and Talreja [138] recently highlighted the importance of void size and position, which was not reported in all earlier works. Voids between the plies and larger voids are found to have a more detrimental effect than small distributed voids in the individual tows.

During layup it is most likely that large voids between the plies are introduced, however, this received little attention as the laminates were subsequently cured in an autoclave, which mitigated the voids. Evans, Vaniglia and Hopkins [60] compared the strength of laminates made from filament winding and fibre placement and reported an improvement in strength of 2% for the fibre placed part. Barth [63] compared the strength in Compression After Impact (CAI) for laminates made from IM7/8551-7A using manual layup and fibre placement, reporting no discernible difference for manual layup and automated layup. Measom and Sewell [62] studied the impact of automated fibre placement on mechanical performance for various mechanical properties of a laminate, and a 6% reduction in open-hole compression (OHC) between manual layup and AFP layup was observed. While these results were meant to demonstrate that automated layup was comparable to manual layup the results can equally be interpreted as an indication that autoclave curing mitigates defects, such as voids, during cure.

Recently, Blom et. al. [56] proposed a model for AFP layup to study the impact of gaps and tow drops on the material performance and predicted a reduction in mechanical performance of 5 - 30%, depending on tow drop area and fibre angles. This work, however, is contradicted by the findings of Croft et.al [96] who test the impact of various AFP layup defects such as tow drops and tow twist on the mechanical properties of composite laminates. The authors observed a variation of properties of 5% to 13%, which is significantly lower than

previous predictions. Overall, the impact of layup on mechanical performance is unclear and warrants further study. While most studies have investigated the impact of voidage and layup processing on the ILSS and OHC, no clear conclusions regarding the impact of layup on the mechanical properties can be drawn due to the number of conflicting results. The issue is also confounded due to the different materials employed, uncertainty from cure processing, and exact layup conditions.

To validate the model, laminates are manufactured from a range of layup conditions and subjected to mechanical testing and microstructural analysis. Samples were manufactured from a variety of layup methods and then cured in an oven and autoclave, to study whether the layup process and subsequent curing had significant impact on the mechanical performance of composite laminates.

8.2 Experimental procedure

8.2.1 Sample manufacture

Sample laminates are manufactured from M21/IMA prepreg [102, 132] using manual layup, a commercial AFP layup system from Coriolis Composites (Quéven, France) with a load of F_l = 10N/mm and a soft roller, and a research automated layup system (R&D system) of chapter 4. An overview over the layup conditions tested using the research layup system is given in Table 27, this results in 18 laminates with an 8-ply UD layup. Laminates manufactured using the research layup system were 75mm wide and 160mm long. The laminates were then cut up into different sections for mechanical testing and voidage analysis. Samples for microstructural analysis were left to cure at room temperature for several days prior to casting into epoxy resin.

Table 27: Overview of the test conditions evaluated for layup testing using the R&D machine.

Batch	Temperature [°C]	Speed [mm/min]	Line load [N/mm]
1	30	100, 500, 1000	6.7
2	20	100	2.7, 6.7, 13.3, 26.7, 53.3
3	30	100	2.7, 6.7, 13.3, 26.7, 53.3
4	40	100	2.7, 6.7, 13.3, 26.7, 53.3

They were then prepared for microscopy using the procedures detailed previously in chapter 5.

The remaining sections from manual layup and AFP layup using a commercial AFP system were cured in an autoclave and in an oven. During autoclave cure vacuum was applied up to 120°C, the autoclave pressure was 0.7MPa, the heating and cooling rate was 2°C/min, and the material was cured for 2h at 180°C. For the oven cure samples were cured at the same temperature and heating rate, with vacuum throughout the cure, but without any additional consolidation pressure. Overall, this resulted in two sample batches from two manufacturing routes yielding, four baseline data sets for the mechanical performance of laminates manufactured from these routes.

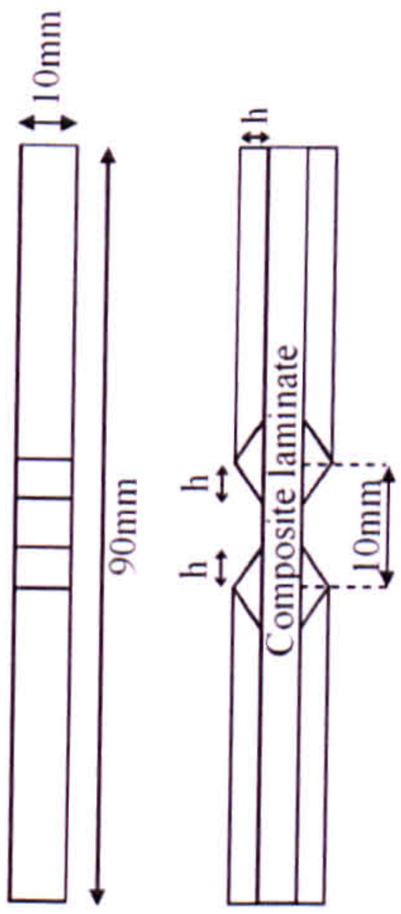

Figure 116: Specification of the compression samples for the Imperial College test rig [189].

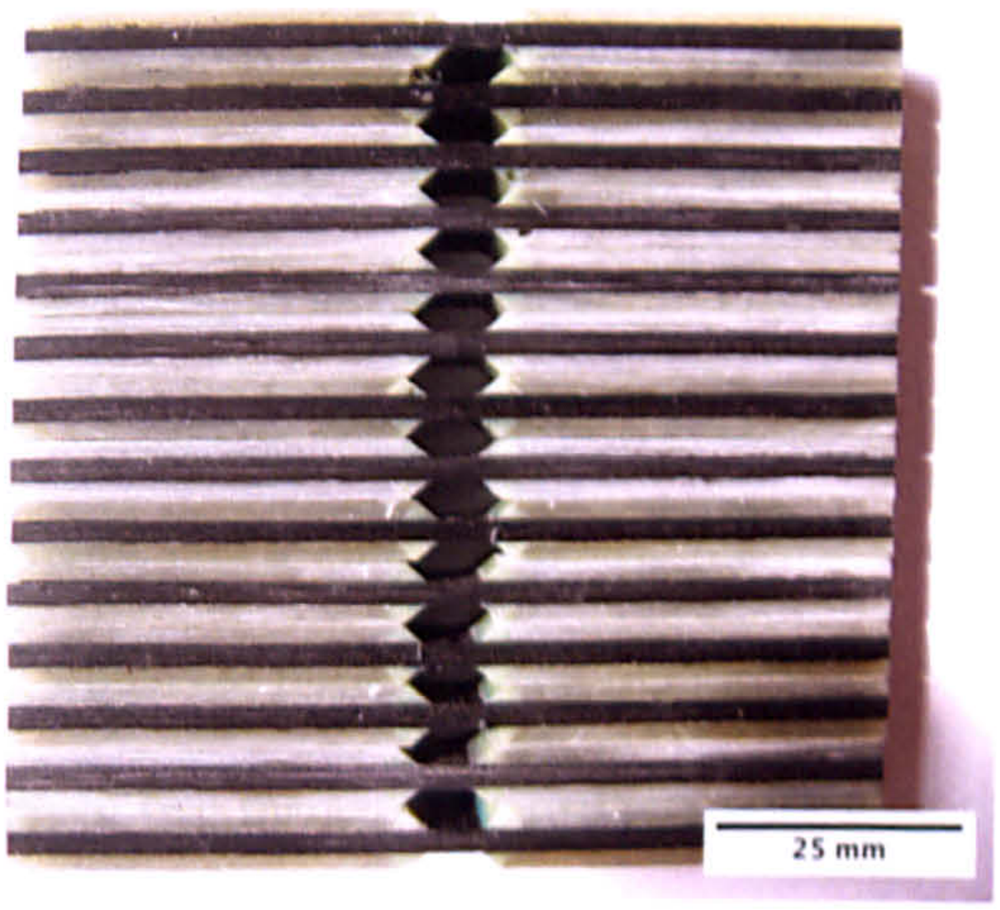

Figure 117: Close-up from the side on compression samples ready for testing. The glued chamfer can be seen.

The laminates from the R&D system for mechanical testing were oven cured only to minimise additional consolidation during cure, which might affect the mechanical testing results. The curing was identical to the procedure given previously for oven curing of the manual layup and commercial AFP layup oven baseline data.

All samples were prepared for compression testing using glass-fibre-reinforced-epoxy end-tabs. Laminates and end-tabs were grit blasted, cleaned with acetone, and then glued using Hexcel Redux 810. Additionally, a fillet of glue was formed between the chamfer and the gauge section, and entabs were then cured in an oven at 70°C for an hour. To finish the samples they were cut and ground to their exact dimensions, see Figure 116 and Figure 117.

8.2.2 Mechanical testing

Compression specimens were tested using a Zwick servo-hydraulic test system with a 100kN load-cell. Samples were tested at rate of 1mm/min to failure using a compression setup test introduced by Haberle and Matthews [189]. The samples were mounted into the upper half and secured with the screws, which press against a square cylindrical insert. The upper test section is then lined up with the lower half and lowered into the guide rails. The sample is secured in the lower section using another two screws. Digital image correlation (DIC), using a video extensometer by Imetrum [167], was used to capture the strain in the samples. The system uses a camera with a high resolution and frame rate to monitor the sample and virtual markers are generated on the sample via software, which are tracked during testing. Strain data are generated from the relative displacement between two markers. Six markers were used to generate four strain readings, which were then averaged.

Two failure types were found during testing, either in the gauge section in pure compression, or at the end-tabs. The latter are not reported here since this is not considered a valid failure. For manual layup, 18 samples were tested after oven cure and 9 after autoclave cure, for the commercial AFP layup 6 samples were tested after oven cure and another 6 samples were tested after autoclave cure. For the research layup system, 5 samples were tested for each laminate. The results were then averaged. Since the samples supported the weight of the upper test section of m = 15kg the load values needed to be corrected manually after testing.

8.3 Experimental results

The baseline pure compression strength of laminates manufactured from M21/IMA using manual layup and autoclave cure was 1458 ± 53 MPa. For laminates manufactured using manual layup and oven cure this reduced to 689 ± 107 MPa, corresponding to a 53% reduction in compressive strength. In addition, the variability of the results significantly increases from 3.6% to 15.5%. For commercial AFP layup a compressive strength of 1522 ± 94 MPa was measured for the autoclave-cured laminates, whilst laminates cured in an oven exhibited a compressive strength of 1066 ± 168 MPa.

A summary of the compression results for the laminates manufactured from the research layup system and the corresponding results is given in Table 28. From Table 28 it can be seen that the laminate strength results for the three different layup speeds does not differ significantly with speed. Specimen micrographs for uncured laminates, available in Figure 118 to Figure 120, yielded an increasing void content as a function of layup speed. However, the

Table 28: Overview of the strain to failure and compression strength of laminates manufactured by the research layup system and subsequent oven cure.

Batch Number	Sample Number	Temperature [°C]	Speed [mm/min]	Line load [N/mm]	Strength [MPa]	Voidage [%]
1	1	30	100	6.7	1088.8 ± 87.9	5.0
	2		500		1107.3 ± 70.7	5.3
	3		1000		1156.0 ± 57.1	6.5
2	1	20	100	2.7	1139.0 ± 49.0	6.5
	2			6.7	1186.4 ± 103.0	9.3
	3			13.3	1208.2 ± 78.0	5.6
	4			26.7	1052.6 ± 50.2	11.0
	5			53.3	903.9 ± 53.2	6.3
3	1	30	100	2.7	1006.3 ± 102.0	27.0
	2			6.7	1226.7 ± 124.7	14.4
	3			13.3	1054.5 ± 132.5	7.2
	4			26.7	1118.8 ± 79.2	6.4
	5			53.3	1189.0 ± 86.2	11.4
4	1	40	100	2.7	1455.7 ± 122.3	26.5
	2			6.7	1062.1 ± 148.0	14.5
	3			13.3	1182.5 ± 105.1	5.5
	4			26.7	1317.4 ± 127.2	12.4
	5			53.3	1463.4 ± 62.5	12.5

differences were small and the voidage results not consistent with the mechanical test results. This is likely due to changes in the sample during handling and preparation for microscopy.

The first speed results suggest that the model predictions from Chapter 7 with respect to the impact of layup speed, which would not affect layup quality, are accurate. Subsequent laminates were therefore manufactured at a layup speed of 100mm/min, which enabled accurate control over both temperature and layup load to study those separately. The temperature was held constant for each batch and the layup load was varied. From Table 28 it can be seen, that for each temperature there is no trend with respect to layup line load. This contradicts previous results from the layup model, which predicts a reduction in voidage as a function of layup load, as the compression strength is expected to increase with decreasing void content. However, consistent with the model, an improvement in compression strength as

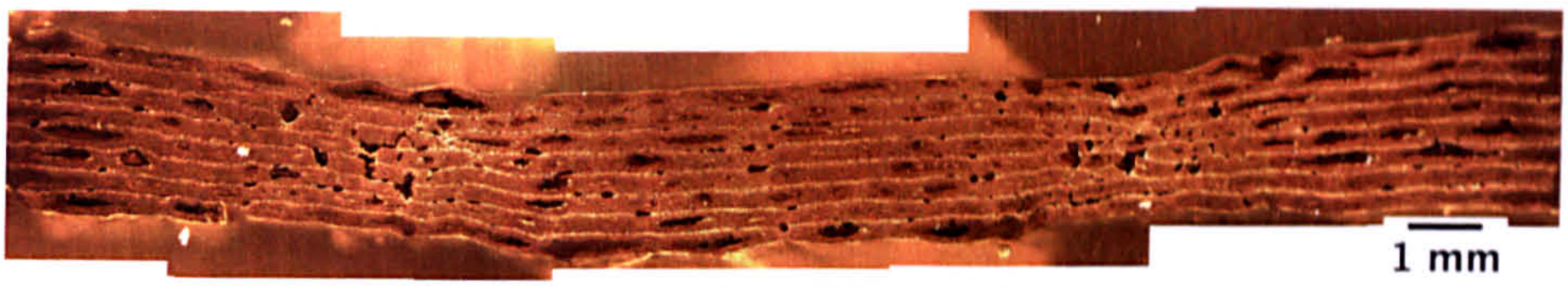

Figure 118: Micrograph of uncured laminate 1-1 with a void content of 5.0%.

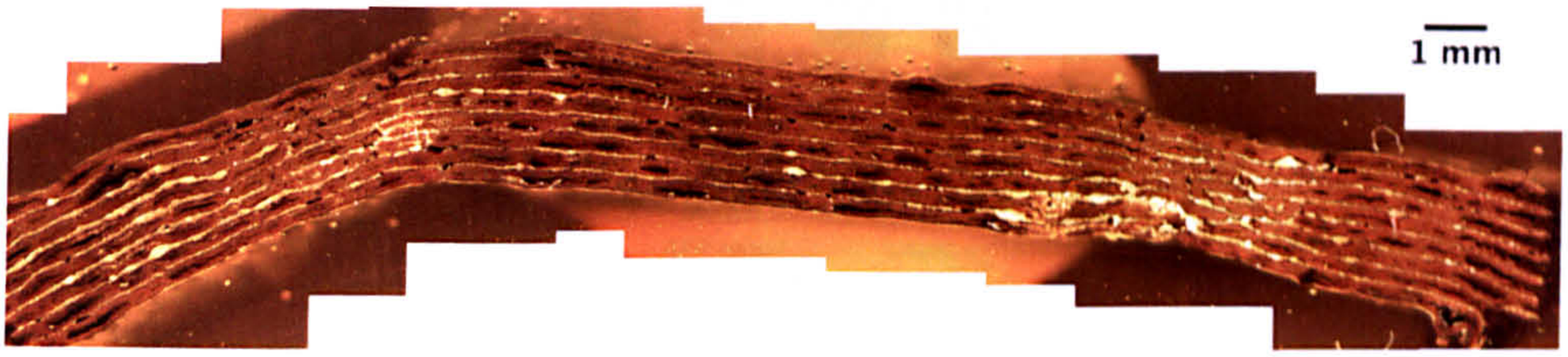

Figure 119: Micrograph of uncured laminate 1-2 with a void content of 5.3%.

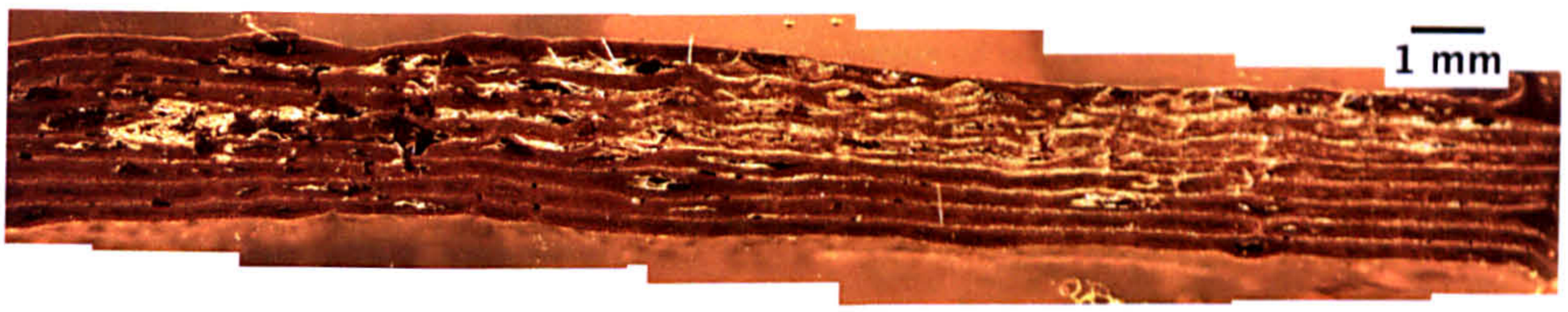

Figure 120: Micrograph of uncured laminate 1-3 with a void content of 6.5%.

a function of layup temperature can be observed, if all the results for each layup temperature are averaged, shown in Figure 121. Generally, automated layup improves on the mechanical performance of the laminates if the manual layup and AFP layup results for autoclave and oven cure are compared. This improvement is 4% for laminates manufactured by AFP layup and cured in an autoclave and 54% for laminates manufactured by AFP layup and cured in an oven. Compression strength results for oven cured laminates obtained from the research layup system for layup at 20°C and 30°C are similar to the previous AFP results, yielding an improvement of 59% and 62% respectively, compared to manual layup. There is, however, a significant further improvement upon heating the prepreg to 40°C prior to layup, yielding an improvement of 88%, 11% below the benchmark results for autoclave cure. The voidage results in Table 28 are varied and do not correlate with the mechanical test results, making their interpretation difficult.

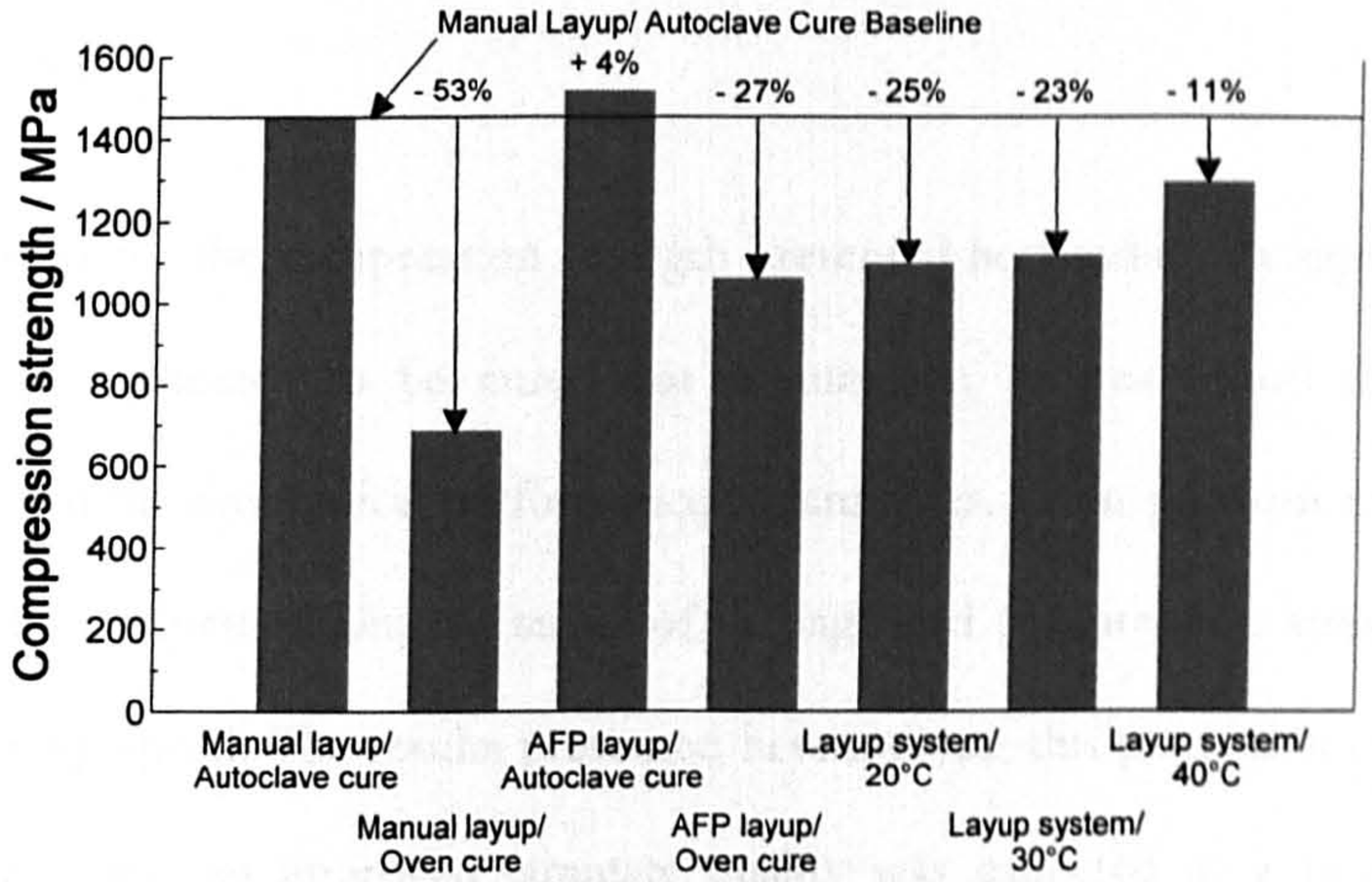

Figure 121: Comparison between compression strength results from different manufacturing and curing procedures. Automated layup generally yields improved laminate quality compared to manual layup. This effect increases with increasing layup temperature.

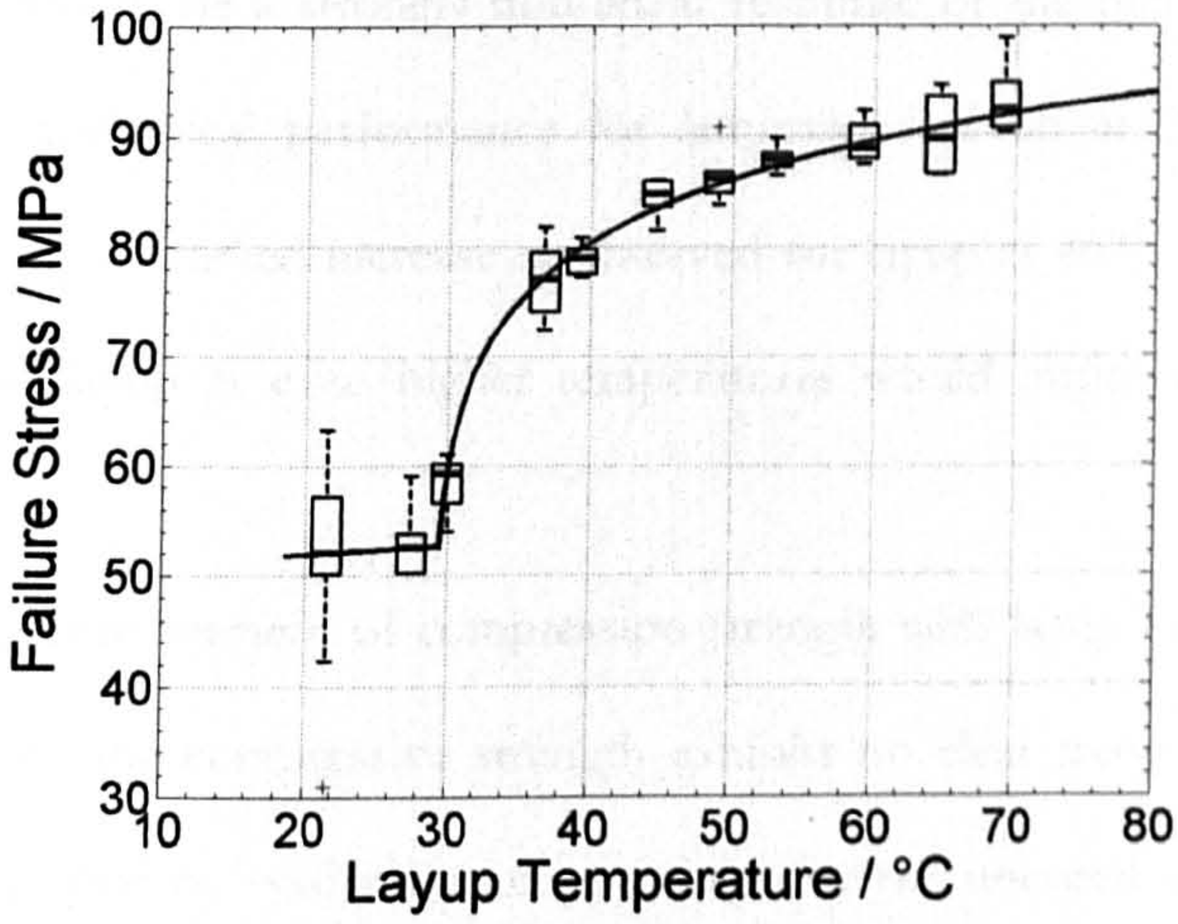

Figure 122: Interlaminar-shear strength of laminates manufactured using the research layup system and various layup temperatures during layup, from [115]. Laminates were cured in an oven only after layup.

8.4 Discussion

The results for the compression strength presented here indicate a significant possible improvement for laminates to be cured out-of-autoclave. It was found that automation generally improved the mechanical performance of laminates. From previous modelling it was expected that the laminate quality, in terms of voidage and compression strength, would be unaffected by layup speed. The results presented here indicate this prediction of the model to be valid. Furthermore, an improved laminate quality was expected as a function of layup temperature, due to the increase in flow during layup and an associated reduction of gaps in the material. The mechanical test results from oven-cured laminates indicate this to be correct, however, there seems to be a strongly non-linear response of the material to heating during layup. While the mechanical performance for laminates laid up at 20°C and 30°C is not significantly different, a marked increase is observed for layup at 40°C and possibly above. It can be argued that layup at even higher temperatures would improve the laminate quality further.

Further, an improvement of compression strength with layup load was expected from the model. However, the compressive strength exhibits no clear trend with respect to layup load, which is supported by void microscopy results for the uncured laminates. First, this is likely due to the high layup line loads tested. Secondly, the reported voidage results are too inconsistent to allow any conclusions, similar to the results for the layup benchmarking in chapter 3. First, it can be argued, that the assessment of sample voidage for such high voidage results may be inaccurate, because the voidage area result of the slice may not be representative of the laminate void volume. However, some tests comparing voidage results for such laminates when compared to results from micro-computerized tomography (μ-CT) have

indicated voidage area measurements on a single slice can generally be considered to be accurate within ±1% of the total void volume of a sample [190].

This implies that the sample has been modified during preparation for microscopy to such an extent that the microstructure has been altered. The exact source of this modification, however, is currently unclear, as every effort has been made to minimise material changes after layup and during preparation for microscopy. It must therefore be concluded that the entire method for microstructural analysis employed here may yield inaccurate results. A possible solution to this has been proposed by Ward [191] who suggested to laminate the material onto a glass plate. Pictures could then be obtained from the backside of such a plate, which would allow evaluation of the air entrapped between the ply and glass plate, Figure 123.

While this demonstrates a possible improvement of layup quality the results are neither extensive nor consistent, which leaves a gap in the current approach. To this end Eales [115] worked on the R&D layup system for his MEng thesis supervised by this author. He tested the impact of layup temperature on the ILSS of laminates cured in an oven. Laminates were manufactured using the research layup system from chapter 4. The layup speed was 100mm/min, the line load was 6.67N/mm, chosen to be at the high end to reduce load related variations, and the layup temperature was varied between 20 and 60°C. Samples were then cured in an oven and tested for their ILSS. An overview of the results is given in Figure 122. Initially, the ILSS is unaffected by the layup temperature up to 30°C. Upon further heating the ILSS increases as a function of layup temperature, approaching the autoclave ILSS baseline, which is reported to be between 90 to 105 MPa [102], depending on the fibre. The results reported for the ILSS are consistent with the compression strength results reported here. The

ILSS results are consistent with the model predictions and indicate that interply void

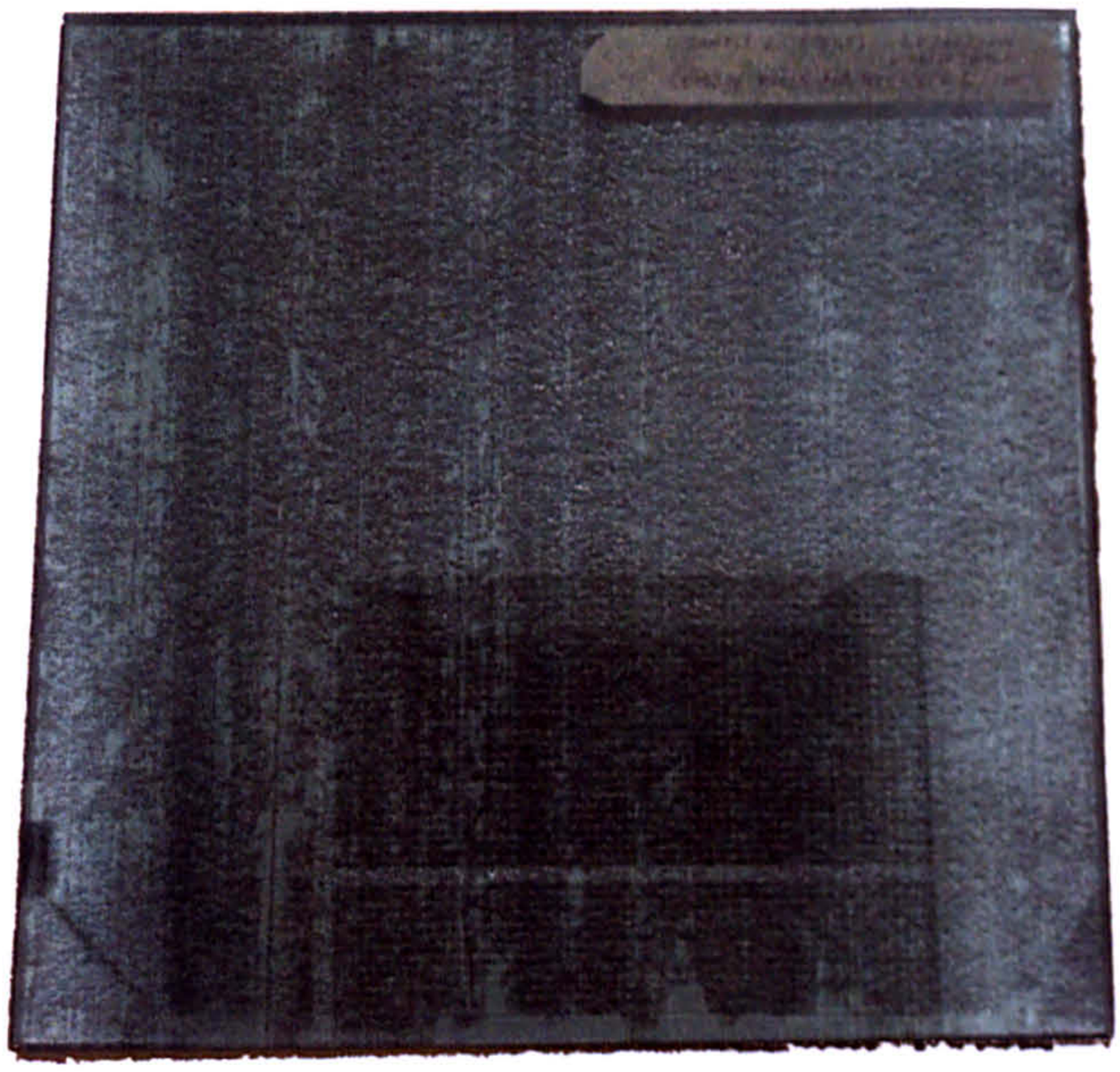

Figure 123: Picture of the backside of an ATL laminate deployed onto a glass plate, from [191]. Voidage can be identified by the light blue colour, which indicates no contact between the ply and the glass plate.

elimination occurred during layup between 40°C to 60°C, yielding very high quality laminates without additional autoclave pressure. Further FEA modelling and experimental work at higher temperatures would thus be warranted to verify the model and experimentally capture the voidage between the plies.

This chapter has demonstrated the impact of layup temperature on laminate quality. Heating during layup can enable layup close to cured ply thickness and with few defects. The mechanical properties of such laminates cured in an oven only reach or even surpass autoclave properties. While this was predicted by the model introduced in chapter 7, this chapter has been unsuccessful in confirming predictions regarding the impact of layup load. Further, the mechanical properties are only an indirect measurement of the laminate quality while direct measurements of the void content have been unsuccessful. Overall, this chapter provides strong evidence that an improved understanding of the interactions, which occur during layup,

may enable significant production time savings, energy and cost savings as well as improving product consistency.

9 Conclusions and future work

To reiterate, chapter 1 posed 6 questions regarding current automated layup processes for thermoset prepreg, these were:

- What is the current manufacturing capability of the processes and what are their limitations?
- What is the current degree of control during layup and how critical is it for successful layup? Furthermore, how can "successful layup" be defined consistently?
- What are desirable material properties for the prepreg used in automated layup, by comparison to prepreg for manual layup?
- Can the impact of the interaction between layup system, prepreg material, and mould, on final part properties be predicted by modelling?
- Is it possible to improve the stability of both processes by enhancing the degree of control?
- Can automated layup be enhanced to enable out-of-autoclave cure of high performance components?

Chapter 2 has provided a guideline for the AFP productivity of 8.6kg/h, values for ATL were expected to be approximately twice as much. To address automated layup capability, a model for the layup of an aerospace component, representative of a wing skin in size and weight, was used to study both layup processes. The model indicated theoretical productivity values of ~29.16 kg/h for ATL and ~41.34 kg/h for AFP. Both values considerably exceeded existing manufacturing capabilities as quoted above and require further clarification. The

calculations predict a higher productivity for AFP than ATL, due to the assumed width and number of tows, which can scale AFP productivity linearly. A large reduction of AFP layup productivity is expected to be due to downtime, and the model predicts that this can reduce productivity by up to 50% in the range studied. Improvements to this area are possible using optimised material qualities, see Chapter 5, and by using interchangeable heads or heavier bobbins to reduce the time for material refilling. For ATL layup, a combination of several factors is found to affect productivity, including acceleration, maximum speed, and material areal weight. Generally, unlike AFP there is no unique way of achieving significant ATL improvements.

Secondly, the current degree of layup control was questioned. In Chapter 3 a study was conducted to assess the control capability of existing processes. The outcome was that either existing process or materials or both are too variable for consistent manufacturing. This was illustrated by analysing the void content of uncured laminates manufactured on ATL layup machines. A correlation between void content and layup pressure, as well as layup temperature and speed was found. But the correlation with temperature was found to be surprisingly weak and a comparison between the set and actual laminate temperature showed that the heating method was ineffective and would thus not have a significant impact. Successful layup can be defined to be a combination of high productivity during layup, with no negative impact on layup system uptime, defect free layup and lastly laminates with minimal defects, i.e voidage, volume. So far, this work has established directly and indirectly that none of these requirements can be achieved with current materials and equipment.

Since both the material and layup system variability confound each other, as shown in chapter 3, strong models are difficult to develop. In addition, any test procedures would have to be conducted within the limitations of existing machines, such as speed, temperature or

pressure. Chapter 4 was therefore dedicated to the development of a research-based layup system, specifically intended to extend current layup systems capability, and be flexible and modular for simple reconfigurations. The developed layup system is currently capable of laying material at up to v = 1.3m/min, accurately control the backing tension - typically set to 10N, and accelerate linearly at a rate of 26m/s^2. Temperature control using an infrared heater allows continuous heating of ΔT = 15K, but in addition the machine can operate in a stationary mode where only the material that is later used for testing is heated, and this was demonstrated at temperatures of up to ΔT = 50K. Simple mechanical modifications and control software changes will enable this system to deliver material at a maximum speed of up to v = 2.4m/min, should this be necessary.

Since it was established that prepreg material quality was likely to be inadequate for successful automated layup, material properties relating to manufacture were studied. The void content, resin content, surface roughness and ply thickness of an aerospace-grade prepreg for autoclave cure were reported in Chapter 5. The materials exhibited an uncured void content of ~5%, with a distribution having lower values in the middle and higher void contents to the outside of a ply which may be linked to the initial prepreg manufacture. A similar observation was made for the resin content, found to vary significantly across the width of a prepreg, but being fairly stable lengthwise. However, uniform tack levels, high degrees of impregnation and little fuzziness due to dry fibres govern successful layup and reduce downtime. This was found to be a possible explanation for the low productivity of AFP layup, which was previously linked to unreliable layup. AFP material is obtained by slitting tape into very narrow slices, typically 3.2 or 6.4 mm wide. If the material properties due to an uneven distribution of resin vary, then this will affect layup as every tow could behave differently. The surface roughness was studied to understand the amount of voidage defects that might be entrapped between the

plies during layup. While it is instructive to assume that voids will be mitigated during cure through resin flow, it still has to be considered that they might only be mitigated, but not necessarily eliminated. This is demonstrated further in chapter 7. It can be concluded that the material roughness is an important parameter, and it should be considered during prepreg manufacture for automation. Lastly, the ply thickness was measured to link it to voidage and resin content and to allow subsequent mechanical testing. It was found that the ply thickness is not linked to voidage and resin content and as such the void content or the quality of layup are unlikely to be inferred from the thickness measurement of a laminate.

As has been discussed earlier, existing layup systems are too variable to accurately study the layup process and this was addressed by developing a research layup system. However, to study the impact of automated layup on a more fundamental level, models are required that link the layup process variables and the material response. Layup Models were therefore developed, that allowed to study the impact of the interaction between layup system, the prepreg material, and the mould, on final part properties. Initially, this required an understanding of the uncured prepreg material response to the mechanical and thermal loads during layup. To this end, uncured prepreg was compressively tested at three different temperatures and using two separate test setups, as discussed in chapter 6. First, it was observed that the relaxation for typical loads, times, and temperatures was very small, and thus the corresponding material viscoelastic strains were small. Also observed was, that the material behaves strongly nonlinear as a function of total strain, exhibiting a power law strain hardening behaviour upon reaching a yield limit. It was therefore concluded that the material could be modelled accurately using an instantaneous elastic-plastic material behaviour with power-law strain hardening. An FE model and additional experimentation showed this approximation to be correct.

This material model was employed in chapter 7 for the interaction between the layup system and the material. Two FE models were developed - a ply-level layup, and a meso-scale prepreg model. The first allowed for the prediction of the contact time and pressure-time distribution for different layup system configurations. Contact times during layup were found to vary between 0.2 - 0.0065s depending on prepreg material, layup speed, layup force and roller stiffness. However, for the same layup speed an inverse correlation between layup pressure and layup time was found. The pressure-time results obtained from the ply model were then used to calculate the ply deformation on a meso-scale, taking into account the material roughness results from Chapter 5, to predict the amount of entrapped air between the plies. The meso-scale model showed that roughness decreased as a function of layup temperature and pressure, i.e. the two were inter-exchangeable. However, higher layup temperatures had a stronger effect than higher layup pressures. Limits on the total ply roughness, the sum of the roughness depths on both sides, that can be controlled during layup were calculated and these were 7μm for existing layup elements, and 33μm for very stiff layup elements, and conditions that can be achieved with current layup systems. Lastly, it was found that the quality critical material deformation is governed by the effective laminate pressure and the mechanical properties of the uncured prepreg. The laminate quality and the reliability of the layup process should therefore be independent of layup speed, however, this has been observed in Chapter 3, not to be the case.

Finally, the stability of automated layup processes was increased by improving the degree of control and automated layup could be enhanced to enable the out-of-autoclave cure of high performance components. The layup system in Chapter 4 was used to manufacture laminates using layup conditions currently not achievable using existing equipment. Laminates manufactured with identical layup load and temperature but different layup speeds exhibited no

significant difference in voidage as well as compression strength and it was therefore concluded that the quality was independent of speed. Further tests at higher loads and temperatures indicate that quality control during layup can be enhanced to the point where it can be used to manufacture laminates with such high quality and adequate fibre volume contents, that they can be cured in oven cure only, without the need for autoclave curing.

To summarise, this work has provided the following conclusions and insights for the automation of prepreg layup:

- AFP can be more productive than ATL for automated layup of identical components.
- But process control can be very inconsistent making reliable layup difficult.
- A new research-based layup system was developed and successfully tested.
- Prepreg material can have high property variability, which may affect successful layup or the quality of the final product. Surface roughness can be important for prepreg used in automated layup.
- Prepreg material can be approximated as elastic-plastic material for process modelling of automated layup.
- Modelling shows that there are no process inherent limitations to layup speed, however, limitations arise from the degree of accurate control. Pressure and layup temperature are important parameters for quality control during layup with higher layup temperatures being favourable over further increases in pressure.
- The roller material and geometry can be optimised to improve layup quality and to meet conflicting requirements regarding layup quality and layup dexterity. Limits on the acceptable roughness for high quality layup are demonstrated.

- Lastly, laminates manufactured under layup conditions informed from the previous results and oven-cured demonstrate improved mechanical performance. Oven cured laminates can reach autoclave properties using correct layup conditions.

Further work in this area should focus on understanding the material behaviour further. Firstly, the work should be extended to cover more material systems, as understanding of uncured prepreg regarding its variability or mechanical behaviour is limited. To improve the mechanical model, a direct comparison between a viscoelastic model based purely on material stiffnesses compared to the elastic-plastic approach taken here should be made. Further, it might be necessary to separate the response of the fibre rich centre of the ply and the resin rich top and bottom side. This would yield a three-phase ply configuration where the top and bottom side are dominated by the resin properties, for example isotropic and strongly time and temperature dependant properties, while the ply centre would be an anisotropic, fibre rich area with only weak time and temperature dependence.

Measuring the material properties over a wide range of temperatures to create the material model is a time-consuming and difficult process. However, it is highly likely that the matrix dominated properties, scale with the viscosity of the prepreg. This opens up the opportunity to use an approach similar to a Williams-Landel-Ferry (WLF) [192] equation to model the mechanical properties as a function of temperature. This would only require a pre-existing viscosity model, which is more commonly available, and the measurement of the mechanical properties at a reference temperature.

Secondly, improved mechanical modelling should be complemented by a non-isothermal model for the layup process. This work demonstrated the importance of significant heating to achieve improved layup and material properties, and further work is therefore required to develop optimised heating methods, as well as study their impact on the material

and the layup process. To achieve this, the heat capacity and thermal conductivity of the uncured prepreg material must be measured. Alternative heating methods with a higher heating efficiency need to be identified. To heat the tape on the head prior to layup these methods are most likely to be irradiation processes, such as infrared, laser, and microwave heating. However, entirely different heating arrangement should be considered as well and these could include heated moulds or layup rollers and induction heating either of the tape on the head or the mould.

This work demonstrated an improvement in compression strength at elevated layup temperatures up to 40°C was possible, while additional tests of the ILSS at higher temperatures exhibited autoclave properties for oven cured laminates. These results, however, need to be confirmed for the compression strength of high-temperature layup laminates, as well as to verify the suggestion that oven cure can yield autoclave properties for appropriate layup conditions. The voidage results reported here were found to be too inconsistent to support the proposed model and further work needs to be aimed at identifying appropriate test methods to measure the voidage between the plies directly, such as laminating onto a glass-plate and subsequent image capture and analysis of said glass-plate.

The modelling approach taken here is valid in a limited range and temperature and test conditions and further work towards its generalisation is necessary, in particular with respect to temperature dependent behaviour, resin/fibre interaction and time-dependent material behaviour.

It can be concluded that automated prepreg laminating is not mature enough for reliable automated manufacture and may require significant further research and development to harness its potential. The interaction between layup system, material and layup conditions has been the focus of this work and it was shown that there is significant potential in

improving the productivity and quality of the layup process. This work has for the first time successfully investigated the potential improvements of the entire composite manufacturing system with respect to automation. The results provide a clear route map to the industrialisation of composites on a large scale. It is hoped that this work may provide some novel insights into the automated layup of thermoset prepreg as well as a building block for the future.

References

[1] McMullen P. Fiber resin composites for aircraft primary structures - A short history, 1936-1984. Composites. 1984;15(3):222-30.

[2] Potter KD. Understanding the origins of defects and variability in composite manufacture. ICCM-17 Edinburgh, UK, 27-31 July 2009 2009.

[3] Hexcel. Prepreg Technology; http://www.hexcel.com/Resources/DataSheets/Brochure-Data-Sheets/Prepreg_Technology.pdf, Accessed 27th November 2010.

[4] Campbell FC. Manufacturing processes for advanced composites. Oxford, UK: Elsevier Advanced Technology; 2004.

[5] Oldani T. Increasing Productivity in Fiber Placement Processes. SAE Aerospace Manufacturing and Automated Fastening Conference & Exhibition North Charleston, South Carolina, USA, 16-18 September 2008.

[6] Chitwood, Composite tape laying machine with pivoting presser member; 6th April 1971, Patent US, 4627886.

[7] Goldsworthy WB, Geodesic path length compensator for composite-tape placement method; 14th May 1974, Patent US 3,810,805.

[8] Anon. MIL-HDBK-17-3F-Composite materials handbook: Departement of Defense; 2002.

[9] Nolte, Kennedy BC, J. DJR. Technology readiness level calculator. NDIA Systems Engineering Conference San Diego, CA, 20th October 2003.

[10] Airbus SAS. Boeing 787 - Lessons learnt; http://www.slideshare.net/aergenium/b787-lessons-learnt-presentation, Accessed 6th September 2010.

[11] Buckley M. The effect of high-speed deposition of thermosetting tapes and fabric systems on residual stress levels in components. Bristol, UK: Airbus UK; 2008.

[12] Gutowski TG. Advanced composites manufacturing. New York: John Wiley & Sons, Inc.; 1997.

[13] Åström. Manufacturing of Polymer Composites. London, UK: Chapman& Hall; 1997.

[14] MTorres Diseños Industriales S. Torreslayup - Tape Layer Machine; http://www.mtorres.es/pdf/torreslayup.pdf, Accessed 29th June 2010.

[15] Goel A. Economics of composite material manufacturing equipment [BSc Thesis]. Cambridge, MA: Massachusetts Institute of Technology; 2000.

[16] Torres Martinez M, Tete enrubanneuse pour l'application de bande en materiau composite; 9 May 2001, Patent EP 1097 799 A1.

[17] Grimshaw MN, Machine for applying composite and presser assembly therefor; 8 November 1989, Patent EP 0371289-A1.

[18] Grimshaw MN, Hecht JR, Method and apparatus for laying composite material; 8 November 1994, Patent EP 0644040-A1.

[19] Grone RJ, Grimshaw MN, Composite tape laying machine with pivoting presser member; 30 May 1985, Patent US 4627886.

[20] Land IB. Design and manufacture of advanced composite aircraft structures using automated tow placement [Master Thesis]. Cambridge, MA, USA: Massachusetts Institute of Technology; 1996.

[21] Colton JS, Baxter J, Behlendorf J, Halim T, Harris B, Kiesler G, et al. The automation of the lay-up and consolidation of PEEK/Graphite fiber composites. 32nd International SAMPE Symposium Anaheim, California, USA, 6-9 April 1987.

[22] Lamontia MA, Gruber MB, Waibel BJ. Conformable Compaction System used in Automated Fiber Placement of Large Composite Aerospace Structures. Proceedings of the 23rd Sampe Conference

[23] Grant C. Automated processes for composite aircraft structure. Ind Robot. 2006;33(2):117-21.

[24] Huber J. Automated lamination of production advanced composite aircraft structures. SAE International Congress and Exposition Detroit, Michigan, USA, 23-27 February 1981.

[25] Stone KL. Automation in composite processing. 29th National SAMPE Symposium Reno, Nevada, USA, 3-5 April 1984.

[26] Eaton HL. Cost effective tape laying. 29th National SAMPE Symposium Reno, Nevada, USA, 3-5 April 1984.

[27] Saveriano JW. Automated contour tape laying of composite materials. 16th National SAMPE Technical Conference Albuquerque, New Mexico, USA, 9-11 October 1984.

[28] Krolewski S, Gutowsi T. Economic comparison of advanced composite fabrication technologies. 34th International SAMPE Symposium Covina, California, USA, 8-11 May 1989.

[29] Postier RA. Factory automation for composite structures manufacturing. Sampe Quart. 1985:45-8.

[30] Grimshaw MN. Automated Tape Laying; Accessed 25 December 2009.

[31] Krolweski S, Gutowski T. Effect of the automation of advanced composite fabrication processes on part cost. Sampe J. 1987;23(3):21-6.

[32] Foley MF. Techno-economic analysis of automated composite manufacturing techniques. 22nd International Sampe Technical Conference Boston, Massachusetts, USA, 6-8 November 1990.

[33] Meier RA. An advanced control system for composite material placement. 31st International SAMPE Symposium Covina, California, USA, 7-10 April 1986.

[34] Lewis HW, Romero JE, Composite tape placement apparatus with natural path generaton means; 29.9.1987, Patent US 4,696,707.

[35] Leemon V, Bullock DE, Roylance ME, Woods JA, Boyce JS, Player JC, Ultrasonic method for fabricating a thermosetting matrix fiber-reinforced composite structure and the prodcut thereof; 19 October 2000, Patent US 6432236-B1.

[36] Muric-Nesic J, Compston P, Noble N, Stachurski ZH. Effect of low frequency vibrations on void content in composite materials. Compos Part A-Appl S. 2009;40(4):548-51.

[37] Thomsen DT, Roylance ME. Ultrasonic tape lamination for net thickness composite processing. 45th International SAMPE Symposium Long Beach, California, USA, 21-25 May 2000.

[38] Benda BJ, Stump KH. A case study of contoured tape laying. American Helicopter Society 52nd Annual Forum Washington D.C., USA, 4-6 June 1996.

[39] Evans DO. Fiber placement. Cincinnati: Cininnati Machine; 1997.

[40] Grimshaw MN, Albers JS, Rust RJ, Method for laying cut composite tape on a mold having scrap removal; Patent US 5,114,519.

[41] Calawa R, Nancarrow J. Medium wave infrared heater for high-speed fiber placement. SAE Aerofast Los Angeles, California, USA, 17th September 2007.

[42] Ahn KJ, Peterson L, Seferis JC, Nowacki D, Zachmann HG. Prepreg aging in relation to tack. Journal Of Applied Polymer Science. 1992;45(3):399-406.

[43] Ahn KJ, Seferis JC, Pelton T, Wilhelm M. Deformation parameters influencing prepreg tack. Sampe Quarterly-Society For The Advancement Of Material And Process Engineering. 1992;23(2):54-64.

[44] Ahn KJ, Seferis JC, Pelton T, Wilhelm M. Analysis and characterization of prepreg tack. Polymer Composites. 1992;13(3):197-206.

[45] Crossley RJ, Schubel PJ, Warrior NA. The experimental characterisation and investigation of prepreg tack. Proceedings of ICCM-18 Edinburgh, 27-31 July 2009.

[46] Dubois O, Le Cam JB, Béakou A. Experimental analysis of prepreg tack. Exp Mech. 2009.

[47] Popp A, Klosterman D, Chartoff R. Correlation of prepreg tack with process performance in laminated object manufacture. 45th International SAMPE Symposium Long Beach, California, USA, 21-25 May 2000.

[48] Torres Martinez M, Head for application of carbon-fibre strips and application method; 21 February 2008, Patent WO 2008/020094 A1.

[49] Tillement PAH, Charra SRE, Composite lay-up head with a retractable device for separating a prepreg from its support tape; 27 November 2008, Patent WO 2008/142273 A2.

[50] Tillement PAH, Charra SRE, Device for separating and discharging trimmings cut in a pre-impregnated strip; 13 November 2008, Patent Wo 2008/135645 A1.

[51] Lopes CS, Gurdal Z, Camanho PP. Variable-stiffness composite panels: Buckling and first-ply failure improvements over straight-fibre laminates. Computers & Structures. 2008;86(9):897-907.

[52] Blom AW, Abdalla MM, Gurdal Z. Optimization of course locations in fiber-placed panels for general fiber angle distributions. Composites Science And Technology. 2009;70(4):564-70.

[53] Kau. Automated fabrication of grpahite-epoxy composites. 32nd International SAMPE Symposium Anaheim, California, USA, 6-9 April 1987.

[54] Izco L, Isturiz J, Motilva M. High speed tow placement system for complex surfaces with cut / clamp / & restart capabilites at 85m/min (3350IPM). SAE Aerospace manufacturing and automated fastening conference and exhibition Toulouse, France, September 2006 2006.

[55] DeVlieg R, Jeffries K, Vogeli P. High-speed fiber placement on large complex structures. SAE Aerofast Los Angeles, California, USA, 17th September 2007 2007.

[56] Blom AW, Lopes CS, Kromwijk PJ, Gurdal Z, Camanho PP. A Theoretical Model to Study the Influence of Tow-drop Areas on the Stiffness and Strength of Variable-stiffness Laminates. Journal of Composite Materials. 2009;43(000264086700002):403-25.

[57] Kisch RA, Vogeli P, Jeffries K, DeVlieg R, End effector and methods for contructing composite membranes; 4th December 2008, Patent US 2008/0295954 A1.

[58] Hamlyn A, Hardy Y, Fibre applicator head including systems for cutting individual fibres; 6th November 2008, Patent WO 2008/132299 A2.

[59] Torres Martinez M, Multi-application head for fibre strips; 10 September 2003, Patent EP 1342555 A1.

[60] Evans DO, Vaniglia MM, Hopkins PC. Fiber placement process study. 34th International SAMPE Symposium Covina, California, USA, 8-11 May 1989.

[61] Pasanen MJ, Martin JP, Langone RJ, Mondo JA. Advanced composite fiber placement: process to application. Schenectady, NY: Automated Dynamics Corporation; 1997.

[62] Measom R, Sewell K. Fiber placement low-cost production for complex composite structures. American Helicopter Society 52nd Annual Forum Washington D.C., USA, 4-6 June 1996 1996.

[63] Barth JR. Fabrication of complex composite structures using advanced fiber placement technology. 35th International SAMPE Symposium Anaheim, California, USA, 2-5 April 1990.

[64] Albus JS. Research issues in robotics. 16th National SAMPE Technical Conference Albuquerque, New Mexico, USA, 9-11 October 1984.

[65] Hamlyn A, Hardy Y, Fibre application machine with fibre supply flexible tubes; 28 February 2007, Patent WO 2008/122709-A1.

[66] Torres Martinez M, Tete pour l'application de bande de composite; 30 November 1994, Patent FR 2713213-A1.

[67] Grant CG. Fiber placement process utilization within the worldwide aerospace industry. 45th International SAMPE Symposium Long Beach, California, USA, 21-25 May 2000.

[68] Enders ML, Hopkins PC. Developments in the fiber placement process. 36th International SAMPE Symposium San Diego, California, USA, 15-18 April 1991.

[69] Evans DO. Design considerations for fiber placement. 38th International SAMPE Symposium Anaheim, California, USA, 10-13 May 1993.

[70] Vaidya UK, Chawla KK. Processing of fibre reinforced thermoplastic composites. Int Mater Rev. 2008;53(4):185-218.

[71] Bourban P, Bernet N, Zanetto J, Manson J. Material phenomena controlling rapid processing of thermoplastic composites. Compos Part A-Appl S. 2001;32(8):1045-57.

[72] Hulcher AB. Processing and testing of thermoplastic composite cylindrical shells fabricated by automated fiber placement. 47th International SAMPE Symposium Long Beach, California, USA, 12-16 May 2002.

[73] Lamontia MA, Gruber MB. Limitations on mechanical properties in thermoplastic laminates fabricated by two processes: Automated Thermoplastic Tape Placement And Filament Winding. 26th SAMPE Europe Conference Paris, 5-7 April 2005.

[74] Mantell SC, Springer GS. Manufacturing process models for thermoplastic composites. J Compos Mater. 1992;26(16):2348-77.

[75] Mantell SC, Wang QL, Springer GS. Processing thermoplastic composites in a press and by tape laying - experimental results. J Compos Mater. 1992;26(16):2378-401.

[76] Sarazin H, Springer GS. Thermochemical and mechanical aspects of composite tape laying. J Compos Mater. 1995;29:1908-43.

[77] Tierney J, Gillespie J. Modeling of heat transfer and void dynamics for the thermoplastic composite tow-placement process. J Compos Mater. 2003;37(19):1745-68.

[78] Pitchumani R, Ranganathan S, Don R, Gillespie J, Lamontia M. Analysis of transport phenomena governing interfacial bonding and void dynamics during thermoplastic tow-placement. Int J Heat Mass Tran. 1996;39(9):1883-97.

[79] Pitchumani R, Gillespie J, Lamontia M. Design and optimization of a thermoplastic tow-placement process with in-situ consolidation. J Compos Mater. 1997;31(3):244-75.

[80] Ranganathan S, Advani SG, Lamontia MA. A nonisothermal process model for consolidation and void reduction during in-situ tow placement of thermoplastic composites. J Compos Mater. 1995;29(8):1040-62.

[81] Hassan N, Song X, Thompson JE, Loos AC, Batra RC. A three-dimensional heat transfer model of the fiber placement composite manufacturing process. 48th International SAMPE Symposium Long Beach, California, USA, 11-15 May 2003 2003.

[82] Goodmann DL, Weidman DJ, Bryne CA, Bykanov AN, Pond TW, McMahon WM, et al. Automated tape placement with in-situ electron beam cure: a viable process. 46th International SAMPE Symposium Long Beach, California, USA, 6-10 May 2001.

[83] Burgess JW, Wilenski MS, Belvin HL, Cano RJ, Johnston NJ. Development of a cure-on-the-fly automated tape placement machine for electron curable prepregs. 46th International SAMPE Symposium Long Beach, California, USA, 6-10 May 2001.

[84] Rosselli F, Santare M, Guceri S. Effects of processing on laser assisted thermoplastic tape consolidation. Compos Part A-Appl S. 1997;28(12):1023-33.

[85] Pistor C, Yardimci M, Guceri S. On-line consolidation of thermoplastic composites using laser scanning. Compos Part A-Appl S. 1999;30(10):1149-57.

[86] Rudolf R, Mitschang P, Neitzel M. Induction heating of continuous carbon-fibre-reinforced thermoplastics. Compos Part A-Appl S. 2000;31(11):1191-202.

[87] Grant C, Martin J. Automated processing technology for composites: Current status and vision for the future. 48th International SAMPE Symposium Long Beach, California, USA, 11-15 May 2003.

[88] Oldani T, Jarvi D, Forming a composite structure by filament placement on a tool surface of a tablet; 27th October 2005, Patent US 2005/0236735 A1.

[89] Torres Martinez M, Faserstreifenverbinder fuer Bandwickler; 2nd October 2008, Patent DE 10 2008 010 424 A1.

[90] Hamlyn A, Hardy Y, Fibre application machine with tool changing system; 11th December 2008, Patent WO 2008/149004 A1.

[91] Debout P, Chanal H, Duc E. Tool path smoothing of a redundant machine: Application to Automated Fiber Placement. Computer-Aided Design. 2011;43(2):122-32.

[92] Shirinzadeh B, Alici G, Foong CW, Cassidy G. Fabrication process of open surfaces by robotic fibre placement. Robotics And Computer-Integrated Manufacturing. 2004;20(1):17-28.

[93] Shirinzadeh B, Cassidy G, Oetomo D, Alici G, Ang MH. Trajectory generation for open-contoured structures in robotic fibre placement. Robotics And Computer-Integrated Manufacturing. 2007;23(4):380-94.

[94] Wiehn MP, Hale RD. Low cost robotic fabrication methods for tow placement. 47th International SAMPE Symposium Long Beach, California, USA, 12-16 May 2002.

[95] Moon RS, Johnson CC, Hale RD. Nondestrcutive evaluation and mechancial testing of steered fiber composites. 47th International SAMPE Symposium Long Beach, California, USA, 12-16 May 2002.

[96] Croft K, Lessard L, Pasini D, Hojjati M, Chen J, Yousefpour A. Experimental study of the effect of automated fiber placement induced defects on performance of composite laminates. 2011.

[97] Bannister M. Challenges for composites into the next millennium - a reinforcement perspective. Compos Pt A-Appl Sci Manuf. 2001;32(7):901-10.

[98] Grone RJ, Schnell LR, Vearil L, Composite tape laying machine and method; 5 December 1983, Patent US 4557783.

[99] Arafath ARA, Fernlund G, Poursartip A. Gas transport in prepregs: model and permeability experiments. Proceedings of ICCM-18 Edinburgh, 27-31st July 2009.

[100] Lamontia MA, Gruber MB, Tierney JJ, Gillespie Jr. JW, Jensen BJ, Cano RJ. In situ thermoplastic ATP needs flat tapes and tows with few voids. 30th International SAMPE Europe Conference Paris, France, 23-25 March 2009.

[101] Schledjewski R, Latrille M. Processing of unidirectional fiber reinforced tapes - fundamentals on the way to a process simulation tool (ProSimFRT). Compos Sci Tech 2003;63:2111-8.

[102] Hexcel. Hexply M21 - Product Data; http://www.hexcel.com/Products/Downloads/Prepreg_Data_Sheets/, Accessed 12th March 2008.

[103] Belfourd D, Effenberger M, Winter D. HIVOL WP 2.3 - Optimised Manufacturing Processes. Airbus S.A.S; 2008.

[104] Morey B. Automating composites fabrication. Manufacturing Engineering. 2008;140(4).

[105] Braun R, Composite fuselage machine and method of automated composite lay up; 25th July, Patent US, 7,080,441.

[106] Johnson BA, S. SS, Multiple head automated composite laminating machine for the fabrication of large barrel section components; 24th February, Patent US, 10/646,509.

[107] Myers RH, Montgomery DC, AndersonCook CM. Response Surface Methodology: Process and Product Optimization Using Designed Experiments. 3rd ed: Wiley-Blackwell; 2009.

[108] Myers RH, Montgomery DC, Anderson-Cook CM. Response Surface Methodology. Hoboken, Canada: Wiley; 2009.

[109] Rasband WS. ImageJ, http://rsb.info.nih.gov/ij/. Bethesda, Maryland, USA: U. S. National Institutes of Health; 1997-2008.

[110] Lukaszewicz DH-JA, Weaver PM, Potter K. An empirical model for the automated deposition of thermoset composite. ACS - 24th Technical Conference Newark, Delaware, USA, 14-17 September 2009.

[111] Lukaszewicz DH-JA, Weaver PM, Potter K. The impact of processing conditions on the final part quality in automated tape deposition technologies. Sampe Seico Paris, France, 23-25 March 2009.

[112] Lukaszewicz DH-JA, Weaver PM, Potter K. An automated ply collation system for material and process development. SAMPE Seico Paris, France, 12th-14th April 2010.

[113] Veers PS, Ashwill TD, Sutherland HJ, Laird DL, Lobitz DW, Griffin DA, et al. Trends in the design, manufacture and evaluation of wind turbine blades. Wind Energy. 2003;6(3):245-59.

[114] Timoshenko P, Gere JM. Mechanics of materials. New York: McGraw Hill; 1997.

[115] Eales J. personal communication. Bristol2011.

[116] Purslow D. On the optical assessment of the void content in composite materials. Composites. 1984;15(3):207-10.

[117] Tavares SS, Michaud V, Månson JAE. Through thickness air permeability of prepregs during cure. Composites Part A: Applied Science and Manufacturing. 2009;40(10):1587-96.

[118] Shim S, Seferis J. Thermal and air permeation properties of a carbon fiber toughened epoxy based prepreg system. J Appl Polym Sci. 1997;65(1):5-16.

[119] Radford DW. Volume Fraction Gradient Induced Warpage in Curved Composite Plates. Compos Eng. 1995;5(7):923-34.

[120] Buczeck MB, Backman D, Darfler S. The effect of variation in prepreg attributes on cured ply thickness. 45th International SAMPE Symposium Long Beach, California, USA, 21-25 May 2000.

[121] Potter K, Khan B, Wisnom M, Bell T, Stevens J. Variability, fibre waviness and misalignment in the determination of the properties of composite materials and structures. Compos Pt A-Appl Sci Manuf. 2008;39(9):1343-54.

[122] Potter K, Langer C, Hodgkiss B, Lamb S. Sources of variability in uncured aerospace grade unidirectional carbon fibre epoxy preimpregnate. Compos Part A-Appl S. 2007;38(3):905-16.

[123] Eom Y, Boogh L, Michaud V, Sunderland P, Manson JA. Stress-initiated void formation during cure of a three-dimensionally constrained thermoset resin. Polym Eng Sci. 2001;41(3):492-503.

[124] Halpin JC, Kardos JL, Dudukovic MP. Processing science - an approach for prepreg composite systems. Pure Appl Chem. 1983;55(5):893-906.

[125] Campbell FC, Mallow AR, Browning CE. Porosity in carbon-fiber composites - an overview of causes. J Adv Mater. 1995;26(4):18-33.

[126] Thorfinnson B, Biermann TF. Production of void free composite parts without debulking. Proceedings of 31st international SAMPE symposium and exhibition Las Vegas, April 1986.

[127] Thorfinnson B, Biermann TF. Degree of impregnation of prepregs - effects on porosity. Proceedings of 32nd international SAMPE symposium and exhibition Anaheim, April 1987.

[128] Lee WI, Springer GS. A model of the manufacturing process of thermoplastic matrix composites. J Compos Mater. 1987;21(11):1017-55.

[129] Yang F, Pitchumani R. A fractal Cantor set based description of interlaminar contact evolution during thermoplastic composites processing. Journal of Materials Science. 2001;36:4661-71.

[130] Dubois O, Le Cam JB, Beakou A. Experimental analysis of prepreg tack; Accessed

[131] Lukaszewicz DH-JA, Potter KD. The internal structure and conformation of prepreg with respect to reliable automated processing. Compos Pt A-Appl Sci Manuf. 2011;42:283-92.

[132] Hexcel. Hextow IM2A - Product Data; http://www.hexcel.com/Products/Downloads/Carbon+Fiber+Data+Sheets.htm?ds=Continuous, Accessed 1st December 2009.

[133] Gurit. Prime 20LV - Product data; http://www.gurit.com/downloads.asp?section=000100010037&sectionTitle=DataSheets+%26+Brochures&letter=P&page=4, Accessed 10th September 2010.

[134] ASTM. D2734 - 94 - Standard test methods for void content of reinforced plastics. ASTM International; 2003.

[135] Rasband WS. Image J. US National Institutes of Health, Bethesda, Maryland, USA.; 2009.

[136] ASTM. D 2584 - 08 - Standard test method for ignition loss of cured reinforced resins. ASTM International; 2008.

[137] Gadelmawla ES, Koura MM, Maksoud TMA, Elewa IM, Soliman HH. Roughness parameters. Journal Of Materials Processing Technology. 2002;123(1):133-45.

[138] Huang H, Talreja R. Effects of void geometry on elastic properties of unidirectional fiber reinforced composites. Compos Sci Technol. 2005;65(13):1964-81.

[139] Ledru Y, Piquet R, Schmidt F, Michel L, Bernhart G. Modelling of void growth mechanisms during the manufacturing of composite lmainates. The 9th International Conference on Flow Processes in Composite Materials Montreal, Canada, 8-10 July 2008.

[140] Olivier P, Cottu JP, Ferret B. Effects of cure cycle pressure and voids on some mechanical-properties of carbon-epoxy laminates. Composites. 1995;26(7):509-15.

[141] Ranganathan S, Advani SG, Lamontia MA. A nonisothermal process model for consolidation and void reduction during in-situ tow placement of thermoplastic composites. Journal of Composite Materials. 1995;29(8):1040-62.

[142] Pitchumani R, Gillespie JW, Lamontia MA. Design and optimization of a thermoplastic tow-placement process with in-situ consolidation. Journal of Composite Materials. 1997;31(3):244-75.

[143] Toso YMP, Ermanni P. Thermal Phenomena in Fiber-reinforced Thermoplastic Tape Winding Process: Computational Simulations and Experimental Validations. Journal of Composite ,Ä¶. 2004.

[144] Sarrazin H, Springer GS. Thermochemical and mechanical aspects of composite tape laying. Journal of Composite Materials. 1995;29(14):1908-43.

[145] Land IB. Design and Manufacture of Advanced Composite Aircraft Structures Using Automated Tow Placement: Massachusetts Institute of Technology; 1996.

[146] Åström BT, Pipes RB, Advani SG. On flow through aligned fiber beds and its application to composites processing. Journal of Composite Materials. 1992;26(9):1351-73.

[147] Hubert P, Poursartip A. A review of flow and compaction modelling relevant to thermoset matrix laminate processing. Journal Of Reinforced Plastics And Composites. 1998;17(4):286-318.

[148] Loos AC, Springer GS. Curing of epoxy matrix composites. Journal of Composite Materials. 1983;17(2):135-69.

[149] Dave R. A unified approach to modeling resin flow during composite processing. Journal of Composite Materials. 1989(24):22-41.

[150] Gutowski TG, Cai Z, Bauer S, Boucher D, Kingery J, Wineman S. Consolidation experiments for laminate composites. Journal of Composite Materials. 1987;21(7):650-69.

[151] Gutowski TG, Dillon G. The elastic deformation of ubricated carbon-fiber bundles - comparison of theory and experiments. Journal of Composite Materials. 1992;26(16):2330-47.

[152] Gutowski TG, Cai Z, Kingery J, Wineman SJ. Resin flow fiber deformation experiments. Sampe Quarterly-Society For The Advancement Of Material And Process Engineering. 1986;17(4):54-8.

[153] Hubert P, Poursartip A. A method for the direct measurement of the fibre bed compaction curve of composite prepregs. Compos Pt A-Appl Sci Manuf. 2001;32(2):179-87.

[154] Gu Y, Li M, Zhang Z, Sun Z. Numerical simulation and experimental study on consolidation of toughened epoxy resin composite laminates. Journal of Composite Materials. 2006.

[155] Kim KS, Hahn HT. Residual-stress development during porcessing of graphite epoxy composites. Composites Science And Technology. 1989;36(2):121-32.

[156] Kim YK, White SR. Viscoelastic analysis of processing-induced residual stresses in thick composite laminates. Mechanics Of Composite Materials And Structures. 1997;4(4):361-87.

[157] Eom Y, Boogh L, Michaud V, Sunderland P, Manson JA. Time-cure-temperature superposition for the prediction of instantaneous viscoelastic properties during cure. Polym Eng Sci. 2000;40(6):1281-92.

[158] Prasatya P, McKenna GB, Simon SL. A viscoelastic model for predicting isotropic residual stresses in thermosetting materials: Effects of processing parameters. Journal of Composite Materials. 2001;35(10):826-48.

[159] Chen Y, Xia ZH, Ellyin F. Evolution of residual stresses induced during curing processing using a viscoelastic micromechanical model. Journal of Composite Materials. 2001;35(6):522-42.

[160] Melo JDD, Radford DW. Viscoelastic characterization of transversely isotropic composite laminae. Journal of Composite Materials. 2003;37(2):129-45.

[161] Zhao LG, Warrior NA, Long AC. A thermo-viscoelastic analysis of process-induced residual stress in fibre-reinforced polymer-matrix composites. Materials Science And Engineering A-Structural Materials Properties Microstructure And Processing. 2007;452:483-98.

[162] Schapery RA. Nonlinear viscoelastic and viscoplastic constitutive equations based on thermodynamics. Mechanics Of Time-Dependent Materials. 1997.

[163] Megnis M, Varna J. Micromechanics based modeling of nonlinear viscoplastic response of unidirectional composite. Composites Science And Technology. 2003;63(1):19-31.

[164] Megnis M, Varna J. Nonlinear viscoelastic, viscoplastic characterization of unidirectional GF/EP composite. Mechanics Of Time-Dependent Materials. 2003;7(3-4):269-90.

[165] Park SW, Schapery RA. Methods of interconversion between linear viscoelastic material functions. Part I - a numerical method based on Prony series. International Journal Of Solids And Structures. 1999;36(11):1653-75.

[166] Ludwik P. On the influence of the speed of deformation in case of enduring deformations with special regard to the after-effects. Physikalische Zeitschrift. 1909;10:411-7.

[167] Imetrum. Imetrum Video Gauge Bristol, United Kingdom, 2011

[168] Langer C-LM. The influence of UD prepreg properties on the non-thermoelastic mechanisms driving manufacturing distortions in composite components [PhD Thesis]. Bristol, UK: University of Bristol; 2005.

[169] Potter K. In-plane and out-of-plane deformation properties of unidirectional preimpregnated reinforcement. Compos Pt A-Appl Sci Manuf. 2002;33(11):1469-77.

[170] Klinkel S, Sansour C, Wagner W. An anisotropic fibre-matrix material model at finite elastic-plastic strains. Computational Mechanics. 2005;35(6):409-17.

[171] Wisnom MR. Nonlinear-analysis of misaligned unidirectional carbon fiber-epoxy compression specimens. Composites Engineering. 1993;3(6):547-56.

[172] Ersoy N, Garstka T, Potter K, Wisnom MR, Porter D, Clegg M, et al. Development of the properties of a carbon fibre reinforced thermosetting composite through cure. Composites Part A: Applied Science and Manufacturing. 2010;41(3):401-9.

[173] Hilton HH, Yi S. The significance of (an)isotropic viscoelastic Poisson ratio stress and time dependencies. International Journal Of Solids And Structures. 1998;35(00007401350006):3081-95.

[174] Dassault Systèmes Simulia Corp. Abaqus 6.9-EF1. Providence, RI, USA2009.

[175] Ersoy N, Garstka T, Potter K, Wisnom MR, Porter D, Clegg M, et al. Development of the properties of a carbon fibre reinforced thermosetting composite through cure. Compos Pt A-Appl Sci Manuf. 2010;41(3):401-9.

[176] Chaboche JL. A review of some plasticity and viscoplasticity constitutive theories. International Journal Of Plasticity. 2008;24(10):1642-93.

[177] Sonmez F, Hahn H, Akbulut M. Analysis of process-induced residual stresses in tape placement. J Thermoplast Compos. 2002;15(6):525-44.

[178] Sonmez FO, Akbulut M. Process optimization of tape placement for thermoplastic composites. Compos Part A-Appl S. 2007;38(9):2013-23.

[179] Offringa A. Thermoplastic composites - rapid processing applications. Compos Part A-Appl S. 1996;27:329-36.

[180] Lamontia MA, Gruber MB. Limitations On Mechanical Properties In Thermoplastic Laminates Fabricated By Two Processes: Automated Thermoplastic Tape Placement And Filament winding. Proceedings of the 26th International SAMPE Conference Paris, France, 5-7 April 2005.

[181] Airbus SAS. Boeing 787 Lessons Learnt - October 2008 2008

[182] Lamontia MA, Gruber MB, Waibel BJ. Conformable Compaction System used in Automated Fiber Placement of Large Composite Aerospace Structures. Proceedings of the 23rd Sampe Conference Paris, France, 9-11 April 2002.

[183] Departement of Defense. Composite materials handbook2002.

[184] Hancox NL. Compression strength of unidirectional carbon-fiber reinforced plastic. J Mater Sci. 1975;10(2):234-42.

[185] Hancox NL. Effects of flaws and voids on shear properties of CFRP. J Mater Sci. 1977;12(5):884-92.

[186] Yoshida H, Ogasa T, Hayashi R. Statistial apporach to the relationship between ILSS and void content of CFRP. Compos Sci Technol. 1986;25(1):3-18.

[187] Harper BD, Staab GH, Chen RS. A note on the effects of voids upon the hygral and mechanical-properties of AS4/3502 graphite epoxy. J Compos Mater. 1987;21(3):280-9.

[188] Wisnom MR, Reynolds T, Gwilliam N. Reduction in interlaminar shear strength by discrete and distributed voids. Compos Sci Technol. 1996;56(1):93-101.

[189] Haberle JG, Matthews FL. An improved technique for compression testing of unidirectional fibre-reinforced platics; development and results. Composites. 1994;25(5):358-71.

[190] Lukaszewicz DH-JA. Methods for evaluating uncured prepreg in processing science. 2011.

[191] Ward C. personal communication. 2011.

[192] Ferry JD. Viscolelastic properties of ploymers. New York: John Wiley & Sons; 1960.